Felismina Teixeira Coelho Moreira
Mestre em Tecnologia Ciência e Segurança Alimentar

Fast screening for diagnostic of heart ischemic episodes

Dissertação para obtenção do Grau de Doutor em
Química Sustentável

Setembro, 2013

Fast screening for early diagnostic of heart ischemic

To my lovely brother and parents,

for the encouragement and love in all moments of my life.

Acknowledgments

First, I want to acknowledge my supervisors Prof. Goreti Sales and Prof. João Paulo Noronha for their support, encouragement and guidance throughout this work. Their scientific knowledge and teaching expertise and their enthusiasm for science contributed to both my professional and personal evolution. Thank both of you for the trust you deposited in me and my work.

I thank Prof. Goreti Sales for the opportunity to develop this new line of work within the BioMark group, for her persistent efforts to provide all the necessary means for the success of this project with international collaborations and my own academic formation.

To all my colleagues in the BioMarK group that, direct or indirectly, contributed to this work. Thank to Joana Guerreiro, Liliana Truta, Helena Gomes, Sofia Teixeira and all others colleagues.

To Prof. Owen Guy for welcoming me in his research laboratory in *College of Engineering, Swansea University*, help in the lab and hospitality during my stay.

To Prof. Rosa Dutra for receive me in her group *Procape, Laped, Universidade Federal de Pernambuco*, for all the knowledge shared in a new area of knowledge and hospitality.

To Prof. Anthony Cass from *Department of Chemistry and Institute of Biomedical Engineering, Imperial College London,* for receive me in his group, for the hospitality and shared knowledge. To Sanjiv Sharma for his help, friendship and encouragement during my stay in Imperial.

To Prof. João C. Salvador Fernandes from *Departamento de Engenharia Química e Biológica, Instituto Superior Técnico* for his help and hospitality during my stay in his group.

To all my friends for their comprehension and support. Specially to Elizabeth Vieira, Joana Guerreiro and Cátia Moreira. For to believe in my work, encouragement and friendship.

To my family: my brother and parents for being beside me in all moments of my life! This important moment of my life is theirs also!

Resumo

As doenças cardiovasculares foram responsáveis, em 2010, por cerca de metade das mortes por doença crónica em toda a Europa (dados Eurostat). Os dados estatísticos mais recentes relativos ao território português confirmam este cenário, no qual as doenças cardiovasculares matam cerca de 11 pessoas por 100000 habitantes.

A redução destes números é urgente e passa necessariamente por um diagnóstico precoce, rápido e eficaz da condição cardíaca.

Neste sentido, o principal objetivo deste projeto foi desenvolver sistemas sensores uma plataforma sensora de baixo custo, baseada em novos biomateriais sintéticos para o rastreio de biomarcadores cardíacos em 'point-of-care'. São considerados neste estudo biomarcardores de interesse clínico convencionais, nomeadamente troponina T (TnT), creatina quinase isoenzima (CK-MB) e mioglobina (Myo). O desenho de novos materiais biossensores baseou-se na síntese dos anticorpos plásticos por novas tecnologias de impressão molecular (MI). No geral, o anticorpo de plástico foi obtido usando o biomarcador cardíaco como obstáculo ao crescimento de um polímero rígido e quimicamente estável. As unidades sensoras nanoestruturadas foram preparadas por modificação de um suporte sólido de carbono ou de ouro com esses biomateriais.

Espera-se, com este trabalho, que as ferramentas desenvolvidas abram novos caminhos para o diagnóstico, não invasivo ou minimamente invasivo, tendo em vista a deteção precoce de doenças crónicas ou um despiste rápido em situações de doença aguda.

Palavras-chave: Biosensores; Biomarcadores cardíacos; Eletroquímica; Polímeros de impressão molecular.

Abstract

Cardiovascular diseases (CVD) are top-killer chronic diseases, accounting for almost half of the European deaths in 2010 (Eurostat data). Most recent statistics in Portuguese territory confirm this scenario, with cardiovascular diseases killing about 11 persons per 100000 inhabitants. Reducing these numbers is urgent and requires early, quick and efficient diagnostic of the specific heart condition.

Thus, the main goal of this proposal is to develop a low cost sensing-devices based on newly synthesized sensory biomaterials for screening cardiac biomarkers in point-of-care. These were applied to screen the conventional biomarkers of clinical interest, all peptides in nature. These include troponin T (TnT), creatine kinase isoenzyme (CK-MB) and myoglobin (Myo). This was achieved by means of novel and low cost biosensing materials that were designed to display good selectivity to each biomarker, assembled on nanostructured sensing units and tested on serum samples. The design of novel biosensing materials consisted on synthesizing plastic antibodies by means of novel molecular imprinting (MI) and enzymatic approaches. Nanostructured sensing units were assembled by modifying the surface of standard conductive materials with the previously indicated biomaterials. Standard conductive supports selected for this purpose were carbon and gold.

Overall, it is expected that the emerging biosensing materials and platforms out coming from this project may contribute for the development of new non-invasive or minimally invasive methods with clinical application in the early screening of chronic diseases and fast-screening in point-of-care (POC) of acute events.

Keywords: Biosensors; Cardiac biomarkers; Surface imprinting; Electrochemistry.

"What distinguishes us from others is not what we are given, but it is what we can do with what we have"

Nelson Mandela (1918 -)

Index

List of figures

List of tables

List of Abbreviations

Symbols

C_{dl}	Capacitance of the double layer
D	Diffusion coefficient specie
E	Applied potential
Epa	Anodic peak potential
Epc	Cathodic peak potential
F	Faraday
K_D	Dissociation Constant
K_M	Michaelis-Menten Constant
Rct	Charge transfer resistance
Rs	Resistance of the solution
W	Warburg diffusion element
Z′	Imaginary component of impedance
Z″	Warburg impedance
ω	Angular frequency
ϕ	Phase angle
Λ	Quantitative measure of the reversibility
ν	Sweep rate
α	Charge transfer coefficient
ΔG	Free energy change

Abbreviations

AAM	Acrylamide

AMPSA	2-Acrylamido-2-methyl-1-propanesulfonic acid sodium salt
Ab	Antibody
AC	Alternating current
ACS	Acute Coronary Syndrome
AES	Aptameric Enzyme Subunit
AEMA	2-aminoethylmethacrylate
AFM	Atomic Force Microscopy
AMI	Acute Myocardial Infarction
AP	Aminophenol
APTES	(3-aminopropyl)triethoxysilane
APTMS	(3-aminopropyl)trimethoxysilane
APS	Ammonium persulphate
APZ	Aminophenoxazone
ATR	Attenuated Total Reflectance
ATP	Adenosine Triphosphate
Au-NP	Gold Nanoparticles
BPO	Benzoyl Peroxide
BSA	Bovine Serum Albumin
Crea	Creatine
Creat	Creatinine
CE	Counter electrode
CNT	Carbon nanotubes
CPE	Constant Phase Element
CRP	C reactive protein
CV	Cyclic Voltammetry

CVD	Cardiovascular Diseases
CK	Creatine Kinase
CK-MB	Creatine Kinase- Isoenzyme MB
Cys	Cysteamine
ConcA	Concavidine A
DHAB	2,2`-dihydroxyazobenzene
DNA	Deoxyribonucleic acid
EDS	Energy Dispersive Spectrometer
EDAC	*N*-ethyl-*N'*-(3-dimethylaminopropyl)carbodiimide hydrochloride
EIS	Electrochemical Impedance Spectroscopy
ELISA	Enzyme Linked Immunosorbent Assay
Emf	Electromotive force
FET	Field Effect Transistors
FRA	Frequency Response Analysis
FTIR	Fourier Transformed Infrared Spectroscopy
GA	Glutaraldehyde
Gat	Galactose
GCE	Glassy-Carbon Electrode
Glu	Glucose
GOx	Glucose oxidase
HEPES	4-(2-Hydroxyethyl)-1-piperazineethanesulfonic acid
Hmb	Hemoglobin
ISE	Ion-Selective Electrode
ITO	Indium Tin Oxide
IUPAC	International Union of Pure and Applied Chemistry

LLLD	Lower Limit of Detection
LOD	Limit of Detection
MES	2-(*N*-morpholino) ethanesulfonic acid
MI	Molecular Imprinting
MIP	Molecularly-Imprinted Polymer
MPM	Matched-Potential Method
MWCNT	Multi-walled Carbon Nanotubes
Myo	Myoglobin
NHS	*N*-hydroxysuccinimide
NI	Non Imprinting
NIP	Non Imprinting Polymer
NIM	Non-imprintted material
NNMBA	*N,N'*-methylenebisacrylamide
NP	Nanoparticles
NPG	Nanoporous Gold
NSPAM	Non- Smart Plastic Antibody
oNPOE	*o*-Nitrophenyloctyl Ether
Oac	Oxalic acid
PBS	Phosphate Buffered Saline
Pcrea	Phosphocreatine
Pa	Anodic Potential
Pc	Cathodic Potential
PIPES	Piperazine-*N,N'*-bis(2-ethanesulfonic acid)
PAP	Polyaminophenol
PDMS	Polydimethlysiloxane
PEG-DA	Poly (ethylene glycol)-diacrylate

POC	Point-of-Care
PTMS	Propyltrimethoxysilane
PVC	Poly(vinyl chloride)
PVC-COOH	Poly(vinyl chloride) carboxilated
QCM	Quartz Crystal Microbalance
RE	Reference Electrode
RMS	Sinusoidal Potential Perturbation
RNA	Ribonucleic Acid
SAM	Self-Assembled Monolayer
SCE	Saturated Calomel Electrode
SELEX	Systematic Evolution of Ligands by Exponential Enrichment
SEM	Scanning Electron Microscopy
SPE	Screen-Printed Electrode
Sac	Sucrose
SPAM	Smart Plastic Antibody
SPR	Surface Plasmon Resonance
SWV	Square Wave Voltammetry
RNA	Ribonucleic Acid
TBA	Thrombin-Binding Aptamer
TEM	Transmission Electron Microscopy
TEGDMA	Tetraethyleneglycoldimethacrylate
THF	Tetrahydrofuran
Thia	Thiamine
TMA	Thiomalic acid
TnT	Troponin T

TnI	Troponin I
TnC	Troponin C
TKClPB	Potassium *tetrakis*(4-chlorophenyl)borate
TRIS	Tris(hydroxymethyl)aminomethane
UV	Ultraviolet
WHO	World Health Organization

1

1. Framework

1.1 Motivation

Heart-related diseases are responsible for more 40% of deaths every year in Portugal (INE, 2013). The initial diagnostic assessment of acute events includes monitoring biochemical markers of cardiac injury, substances that are released into the blood when the heart is damaged. The use of biochemical markers in the diagnosis and management of patients is today fundamental, and has increased continuously in recent decades (Eriksson et al. 2006). It may offer invasive tools for diagnostic of cardiovascular diseases when cardiac biomarkers are found in the blood. The inherent analytical tools should produce a quick response, on-site and at low cost, allowing a quick diagnostic and application over wide screening programs.

The identification of cardiac biomarkers levels is very important to reach a diagnosis. However, conventional assay techniques take about 2 hours *per* marker, therefore much longer than desired. In general, current techniques used to determine biomarkers of cardiovascular diseases rely mostly on immune/antigen reactions, being thus expensive, not portable and requiring long time for a response that may not be accurate. Alternative methods rely on highly sophisticated chromatographic procedures, but these are of even higher cost and unsuitable to carry out analysis in point-of care (POC), at least outside central hospitals. Overall, these handicaps may be eliminated by replacing natural antibodies by synthetic materials that are designed to be as close as possible to the natural ones, and

therefore reveal great affinity for the molecule of interest. Thus, the goal of this project is to develop novel devices for screening cardiac biomarkers in POC with the purpose of reducing diagnostic procedures and enhancing the diagnostic accuracy. Only biomarkers present in biological fluids were considered for this work. The conventional biomarkers selected to monitor acute cardiac injury: are TroponinT (TnT), Creatine Kinase (CK-MB) and Myoglobin (Myo).

Any device meant for screening a biomarker demands the integration of the bioreceptor material in a biosensor unit, a compact analytical apparatus or unit incorporating a biological - or biologically derived - sensitive recognition element integrated or associated with a physico-chemical transducer (Eriksson et al. 2006). This device must be assembled in such a way that a high sensitivity and selectivity are both achieved with the most relevant biomarkers in cardiac diseases.

For this purpose, a nanostructured transducer surfaces are modified and tailored with a suitable bioreceptor (plastic antibodies). The surface where the bioreceptor is immobilized and the nature of the transduced signal are fundamental aspects for a successful sensor. The gap between the transducing surface and the subsequent biorecognition layer is bridged by surface modification. The nanomaterials used as substrate can be tailored with a wide range of small organic ligands and large biomacromolecules (Turner et al. 2006), following quite distinct approaches, such as self-assembled monolayer (SAM) and covalent attachment.

Any biomolecule is typically imprinted by growing a polymeric network around the template and removing it once the network is rigid. The selection of a suitable imprinting technique for each biomarker is a critical step, especially considering the low detection levels required and the nature of the imprinted compounds. Applying traditional bulk imprinting to large biomolecules, especially proteins, has been difficult (Bonini et al. 2007; Turner et al. 2006). The main drawbacks include reduced mass transfer and permanent entrapment of the macromolecule template in the polymer matrix, diminished integrity of the polymer structure, restricted solvent selection, and production of heterogeneous binding sites (Bossi et al. 2001; Ramanaviciene and Ramanavicius 2004). This hindered performance is avoided by surface imprinting. In surface imprinting, molecules with nanoscale dimensions are assembled on a surface, with high structural control,

mimicking Nature's approach to nanostructured materials. Likewise, nanostructured imprinted materials can be assembled instead of the conventional imprinted films and surface-imprinted materials, which offer several advantages. Their small dimension leads to extremely high surface-to-volume ratio, favouring miniaturization (Agasti et al. 2010). They show a higher affinity and sensitivity to the analyte (cardiac biomarker) and a more homogeneous distribution of recognition sites (Guan et al. 2008).

The interaction between each biorecognition element and target analyte is translated by the transducer surface into an analytical electrical signal. Techniques such as Voltammetry, Potentiometry and Electrochemical Impedance Spectroscopy (EIS) are used for this purpose. Some of these are easily adjusted for screening purposes, especially with Screen Printed electrodes (SPE). They enable simple and inexpensive procedures providing selective readings with low concentrations and low sample volumes. Furthermore, they may offer portable versions to carry out tests in POC.

1.2 Structure of the thesis

This thesis is organized in ten chapters.

Chapter 1 the present chapter gives the motivation of the present work, describes the structure and the framework of the thesis and lists the publications and communications associated with the PhD research program.

Chapter 2 presents a brief literature review about the pillars of this work: the target analytes, the recognition elements and the signal transducers, emphasizing those of special relevance to the present research work. It addresses specifically relevant issues of TnT, CK-MB and Myo cardiac biomarkers.

Chapters 3 to 9, present the development, characterization and application of electrochemical assays for TnT, CK-MB and Myo detection.

Chapter 3 reports a novel biomimetic ionophore for the potentiometric transduction of Myo. It was synthesized by molecular imprinting on silica beads. The resulting materials were dispersed in plasticized poly(vinyl chloride) (PVC) selec-

tive membranes and used as ionophores in potentiometric transduction. The analytical application was conducted successfully, showing accurate and precise results. The limit of detection (LOD) is however higher than the level found in biological fluids of patients with ischemic episodes.

In order to improve that feature, a surface imprinting approach on nanosized materials of special electrical properties, carbon nanotubes (CNTs), was developed in **chapter 4**. A novel artificial antibody for TnT was synthesized by MI on the surface of multiwalled carbon nanotubes (MWCNTs). The ability of this material to rebind TnT was confirmed by including it as an electroactive compound in a PVC/plasticizer mixture, coating a wire of silver, gold or titanium in potentiometric transduction. However, although the results obtained were promising, the apparatus employed was not disposable.

Therefore, the elaboration of a simpler and cheaper measurement setup is essential, and was reported in **Chapter 5**. The MI was assembled on a polymeric layer of carboxylated PVC (PVC-COOH) for Myo detection. This polymer was casted on the gold (Au) working area of a SPE, creating a novel disposable device relying on plastic antibodies. The major critical issue in this work came from the PVC membrane. The thickness couldn't be controlled and another approach was explored.

In order to avoid the difficulties found from the thickness control of the membrane, **chapter 6** describes an Au-SPE biosensor for fast screening of Myo obtained by merging molecular imprinting and self-assembly monolayer (SAM) techniques. The analytical features of the resulting biosensor were studied by different electrochemical techniques, including electrochemical impedance spectroscopy (EIS), square-wave voltammetry (SWV) and potentiometry. The biosensor was successfully applied to biological fluids, but only potentiometry assays showed limits of detection lower than the cut-off Myo levels found in patients with ischemic disease.

Novel strategies for improving the binding affinity of the protein to its binding site were implemented. This was tried out by introducing specific modifications on the imprinting process and as shown in **Chapter 7.** In this work the imprinted sites were created with charged monomers while the surrounding environment

was tailored using neutral material, and the protein was removed from its imprinted site using a protease, aiming at preserving the polymeric network of the plastic antibody.

The most challenging task in the imprinting process is the control of the polymer thickness. Electropolymerization allows the film production with thicknesses ranging 10-100 nm due to its self-limiting growth under electrochemical conditions. **Chapter 8** reported therefore an electrosynthesized polyaminophenol (PAP) film imprinted by Myo. This strategy prevents the undesired entrapment of proteins within the polymeric matrix in the surface imprinting approach.

In **Chapter 9,** instead of developing another molecularly imprinted material (MIM), the catalytic properties of the analyte were explored. A simple electrochemical biosensor for a sensitive detection of CK-MB by using SAM techniques on Au-SPE surface was successfully developed. A reverse concept of a catalytic biosensor was explored here, by immobilizing the substrate instead of the enzyme. This approach also accounted the need to measure the enzyme and not its substrate or its by-products.

Chapter 10 summarizes the main results obtained and presents guidelines for future research work.

1.3 List of Publications

1.3.1 Papers published in international scientific journals

1: FTC Moreira, S Sharma, RAF Dutra, JP Noronha, AEG Cass, MGF Sales, A Protein-responsive polymeric material for cardiac biomarker detection in point-of-care. *Submitted.*

2: FTC Moreira, RAF Dutra, JP Noronha, MGF Sales, Electrochemical Biosensor for Creatine Kinase detection in Ischemic Episodes. *Submitted.*

3: FTC Moreira, RAF Dutra, JPC Noronha, MGF Sales, Electrochemical biosensor based on biomimetic material for myoglobin detection, *Electrochimica Acta*, 2013, 107, 481-487.

4: FTC Moreira, RAF Dutra, JPC Noronha, JCS Fernandes, MGF Sales, Novel biosensing device for point-of-care applications with plastic antibodies grown on Au-Screen Printed Electrodes, *Sensors and Actuators B*, 2013, 182, 733-740.

5: FTC Moreira, S Sharma, RAF Dutra, JPC Noronha, AEG Cass, MGF Sales, Smart Plastic Antibody Material (SPAM) tailored on disposable screen printed electrodes for protein recognition: application to Myoglobin detection, *Biosensors and Bioelectronics*, 2013, 15, 237-244.

6: FTC Moreira, RAF Dutra, JPC Noronha, AL Cunha, MGF Sales, Artificial antibodies for troponin T by its imprinting on the surface of multiwalled carbon nanotubes: Its use as sensory surfaces, *Biosensors and Bioelectronics*, 2011, 28(1), 243-250.

7: FTC Moreira, RAF Dutra, JPC Noronha, MGF Sales, Myoglobin-biomimetic electroactive materials made by surface molecular imprinting on silica beads and their use as ionophores in polymeric membranes for potentiometric transduction, *Biosensors and Bioelectronics*, 2011, 26(12), 4760-4766.

1.3.3 Conference Proceedings

1: Moreira FTC, RAF Dutra, JPC Noronha, MGF Sales, Surface Imprinting Approach on Screen Printed Electrodes Coated with Carboxylated PVC for Myoglobin detection with Electrochemical Transduction, *Procedia Engineering*, 2012, 47, 865-868.

1.3.4 Communications presented in national and international scientific conferences

1: FTC Moreira, S Sharma, RAF Dutra, JPC Noronha, AEG Cass, MGF Sales, A Biomimetic biosensor based on poly(o-aminophenol) film for cardiac biomarker detection in point-of-care. III Jornadas de Eletroquímica e Inovação to be presented at Universidade de Trás-os-Montes e Alto Douro, on September 16-17,2013.

2: F.T.C. Moreira, S. Sharma, R.A.F. Dutra, J.P.C. Noronha, A.E.G. Cass, M.G.F. Sales, Smart Plastic Antibody Material (SPAM) tailored on disposable screen printed electrodes for protein recognition: application to Myoglobin detection. 5th Graduate Student Symposium on Molecular Imprinting, Queen's University, in Belfast, on August 15-17, 2013. Oral presentation.

3: FTC Moreira, RAF Dutra, JPC Noronha, MGF Sales, Surface Imprinting Approach on Screen Printed Electrodes Coated with Carboxylated PVC for Myoglobin detection with Electrochemical Transduction, P2258, presented at Eurosensors XXVI, Krakow, Polónia, 9 – 12 September de 2012.

4: FCT Moreira, Z Tehrani, RAF Dutra, JPC Noronha, OJ Guy, MGF Sales, Electrochemicalassay for ischemicepisodesdiagnosis, Poster, presented at European Biomarkers Summit 2011, Londres, Reino Unido, 18 - 19 de May, 2011.

5: FTC Moreira, RAF Dutra, JPC Noronha, MGF Sales, Artificial antibodies for Troponin T by its imprinting on the surface of MWCNT: its use as sensory surfaces, P128, presented at the 2nd International Conference on Bio-Sensing Technology 2011, Amsterdam, The Netherlands, 10 - 12 de October de 2011.

6: FTC Moreira, RAF Dutra,GG Aguilar, JPC Noronha, MGF Sales , Molecular Imprinting of Myoglobin on Silica Surfaces using silanes in Potentiometric Transduction presented at the Ibersensor, 7th Ibero-American Congress on Sensors, Lisbon, 9-11 November 2010.

1.3.5 References

Agasti, S.S., Rana, S., Park, M.H., Kim, C.K., You, C.C., Rotello, V.M., 2010. Nanoparticles for detection and diagnosis. *Advanced Drug Delivery Reviews* 62(3), 316-328.

Bonini, F., Piletsky, S., Turner, A.P.F., Speghini, A., Bossi, A., 2007. Surface imprinted beads for the recognition of human serum albumin. *Biosensors & Bioelectronics* 22(9-10), 2322-2328.

Bossi, A., Piletsky, S.A., Piletska, E.V., Righetti, P.G., Turner, A.P.F., 2001. Surface-grafted molecularly imprinted polymers for protein recognition. *Analytical Chemistry* 73(21), 5281-5286.

Eriksson, S., Wittfooth, S., Pettersson, K., 2006. Present and future biochemical markers for detection of acute coronary syndrome. *Critical Reviews in Clinical Laboratory Sciences* 43(5-6), 427-495.

--Guan, G.J., Liu, B.H., Wang, Z.Y., Zhang, Z.P., 2008. Imprinting of Molecular Recognition Sites on Nanostructures and Its Applications in Chemosensors. *Sensors* 8(12), 8291-8320.

INE, Instituto Nacional de Estatística, http://www.ine.pt, *The People,* http://www.ine.pt/xportal/xmain?xpid=INE&xpgid=ine_publicacoes&PUBLICACOESpub_boui=67053424&PUBLICACOESmodo=2, assessed oby July 2013.

Ramanaviciene, A., Ramanavicius, A., 2004. Molecularly imprinted polypyrrole-based synthetic receptor for direct detection of bovine leukemia virus glycoproteins. *Biosensors & Bioelectronics* 20(6), 1076-1082.

Turner, N.W., Jeans, C.W., Brain, K.R., Allender, C.J., Hlady, V., Britt, D.W., 2006. From 3D to 2D: A review of the molecular imprinting of proteins. *Biotechnology Progress* 22(6), 1474–1489.

2

Literature Review

2.1 Cardiovascular diseases

Cardiovascular diseases (CVD) affect the heart and surrounding blood vessels, assuming many forms, such as high blood pressure, coronary artery disease, valvular heart disease, stroke, or rheumatic heart disease. According to the World Health Organization (WHO), 17.5 million (30%) of all global deaths in 2005 were associated with CVD and it is estimated that by 2015 CVD can be the most important cause of death in developing countries (2007; WHO 2007). European CVD statistics of 2008, point out a striking number of over 4.3 million deaths in Europe alone and 2 million deaths in European Union caused by CVD and it is overall estimated to cost the European Union Economy 192 billion *per* year (S. Allender 2008). The most recent European Statistics of the European Commission, show that CVD are the largest single cause of death and morbility in the EU, accounting 42.4% all deaths in 2010 (EuroStat), http://bec.europa.eu/heath/major_chronic_diseases assessed in the August 2013).

A huge part of deaths originated by chronic diseases can be prevented through population based strategies, and by making cost-effective interventions available

and affordable, both for people with established disease and for those at high risk of developing the disease.

The population is targeted in risk of CVD when abnormal values of lipids and glucose are detected in the blood. The early and quick diagnosis of CVD is really important and crucial, not only for patient survival but also for saving cost and great deal of time in the successful prognosis of the disease.

Early diagnostic and efficient therapeutic protocols are required to improve this public health indicator or to reduce cell injury and subsequent organic damage. Initial assessment of patients with acute heart-injury symptoms is based on clinical presentation, physical examination, electrocardiogram (ECG), and measurement of biochemical markers of cardiac injury, substances that are released into the blood when the heart is damaged (Yang and Zhou 2006) .

ECG is an important tool for guiding therapy (Foy et al. 1991; Yusuf et al. 1984), but it is inappropriate for CVD diagnosis, since about half of the CVD patients in emergency conditions do not show ECG alterations (Foy et al. 1991; Kost and Tran 2005; Stubbs and Collinson 2001; Yusuf et al. 1984). On the contrary, monitoring cardiac biochemical markers in POC context improves diagnosis and management of patients, a practice that has been increasing continuously in recent years.

Sensitive and rapid devices are consequently needed to achieve quick diagnosis requirements in CVD (early) detection. The construction of biosensors is undoubtedly one of the most promising ways to solve some of the problems concerning fast, sensitive, and cost effective measurements (Mascini and Tombelli 2008). Biosensors allow rapid diagnosis, providing better health care and reducing the waiting time for result dissemination, benefiting patients and clinicians.

Thus this thesis is meant to establish novel strategies for screening cardiac biomarkers in patients with acute myocardial infarction (AMI) episodes. Some considerations about the general topics around these will be presented next, starting by cardiac biomarkers.

2.1.1 Cardiac Biomarkers

Biomarkers are biomolecules of deoxyribonucleic acid (DNA), ribonucleic acid (RNA), protein and glycol derivatives present in biological fluids, such as blood, urine or saliva. Because proteins are the main executioner biomolecules in cells, protein-based markers are more important biomarkers than DNA- or RNA-based markers (Ravichandran et al. 2004; Srivastava et al. 2005). Protein molecules influence the molecular pathways both in normal and transformed cells; therefore, proteomic markers are closer and more relevant to the disease state initiation and progression. Several biomarkers have been found and associated to each pathophysiology state and risk factors. However, not all of these molecules are appropriate to this aim but should fulfil certain conditions (Ravichandran et al. 2004) .

There are several characteristics that biomarkers should exhibit include: (i) high sensitivity or high concentration in myocardium after myocardial injury, rapid release for early diagnosis and long half-life in blood for late diagnosis; (ii) high specificity, or absent in non-myocardial tissues and not detectable in blood of non-diseased subjects; (iii) analytical suitability, or measurable by cost-effective assay, simple to perform, rapid turnaround time and sufficient precision and trueness; and (iv) clinical suitability, or ability to influence therapy and to improve patient outcome (Martin-Ventura et al. 2009).

Table 1: A summary of primary clinically used cardiac biomarkers, highlighting their respective cut-off values (Qureshi et al. 2012).

Cardiac Biomarker	Cardiac biomarker Disease	Cut-off levels	Specificity	MW (kDa)	Initial elevation	Type of peak	Return normal
TnI	Detection of AMI	0.01 – 0.1 ng/mL	High	23.5	4-6h	12-24h	6-8 days
TnT	Detection of AMI	0.05 – 0.1 ng/mL	High	37	4-6h	12-24h	7-10 days
Myo	Early detection of AMI	70 – 200 ng/ mL	Low	18	1-3h	6-12h	24-48 days
C- reactive protein (CRP)	Early detection of inflammation/cardiac risk Factor	< 103 ng/ mL low risk 1 – 3×10^3 ng/mL intermediate risk >3 – 15 $\times10^3$ ng/mL high	High	125	ND	ND	ND
CK-MB	Early detection of AMI	10 ng/ mL	Medium	85	4-6h	12-24h	3-4days
B-type natriuretic peptide	Acute coronary syndromes/diagnosis of heart failure/ventricular overload	—	High	3.4	ND	ND	ND

Table 1: A summary of primary clinically used cardiac biomarkers, highlighting their respective cut-off values(Qureshi et al. 2012)values (cont.).

Cardiac Biomarker	Cardiac biomarker disease	Cut-off levels	Specificity	MW (kDa)	Initial elevation	Type of peak	Return normal
N-terminal pro-B-typenatriuretic peptide	Acute coronary, syndromes/diagnosis of heart failure/ventricular overload	0.25 – 2 ng/mL	High	8.5	ND	ND	ND
Myeloperoxidase	Detection of inflammation	> 350 ng/mL	Medium	150	ND	ND	ND
Heart fatty acid binding protein	Myocardial necrosis	≥ 6 ng/mL stratification risk	Low	15	2-3h	8-10h	18-30h
Tumor necrosis factor α (TNF)	Inflammation/cardiac risk factor	< 0.0036 ng/mL low risk ≥ 0.0036 ng/mL high risk	ND	ND	ND	ND	ND
Interlukin-6 (IL-6)	Inflammation/cardiac risk factor	Low < 0.0013 ng/mL Mid 0.00138–0.002 ng/mL High > 0.002 ng/mL	ND	ND	ND	ND	ND

The selection of a specific marker for the diagnosis of CVD is a challenging task. Thus, a variety of biomarkers can potentially be analysed simultaneously for accurate disease diagnosis (Anderson 2005; Kost and Tran 2005; Martin-Ventura et al. 2009; McDonnell et al. 2009; Stubbs and Collinson 2001; Vasan 2006). Anderson et al. described a set of 177 candidate biomarkers that are potential plasma markers for CVD and stroke (Anderson 2005).

Several cardiac biomarkers have been found so far and presented in (

Table 1) heart disease. Although not a very specific marker, Myo is the first marker released after damage of the myocardial muscle cells, and it has to be increased in the first hours after the cardiac event. B-type natriuretic peptide (BNP), cardiac TnI, and C reactive protein (CRP) are released after Myo, but they are specific markers for coronary events. BNP is useful for the emergency diagnosis of heart failure and for the prognosis in patients with acute coronary syndrome (ACS) (Tang and Kang 2006). CRP is an important predictor of cardiovascular risk and acute coronary syndrome. Troponin is considered as a gold standard marker for the detection of AMI. During the heart infarction, TnT is immediately released to the bloodstream. Elevated concentrations of these cardiac markers in biological samples are related with recurrent CVD events.

Overall, the simultaneous monitoring of these biomarkers allows clinicians to diagnose CVD quickly and/or to accurately design a patient care strategy. A fast and reliable detection of these proteins, correlated to the life-span of the cardiac even, will also help medical professionals to differentiate diseases among those showing similar symptoms.

2.1.2 Cardiac biomarkers in acute myocardial infarction

Monitoring biomarkers is absolutely fundamental to the (re)definition and diagnosis of AMI. In this context, several biomarkers for the assessment of myocardial necrosis have been given special attention over last half century. The earliest biomarkers include aspartate aminotransferase and lactate dehydrogenase, prior to the use of CK-MB and particularly cardiac TnT. Myo is also relevant in this

context, because although it offers low sensitivity for AMI diagnosis, it has an increased value for risk stratification.

Some characteristics of the main cardiac biomarker for AMI diagnostic are described below. These include TnT, CK and Myo (see fig Figure 1)

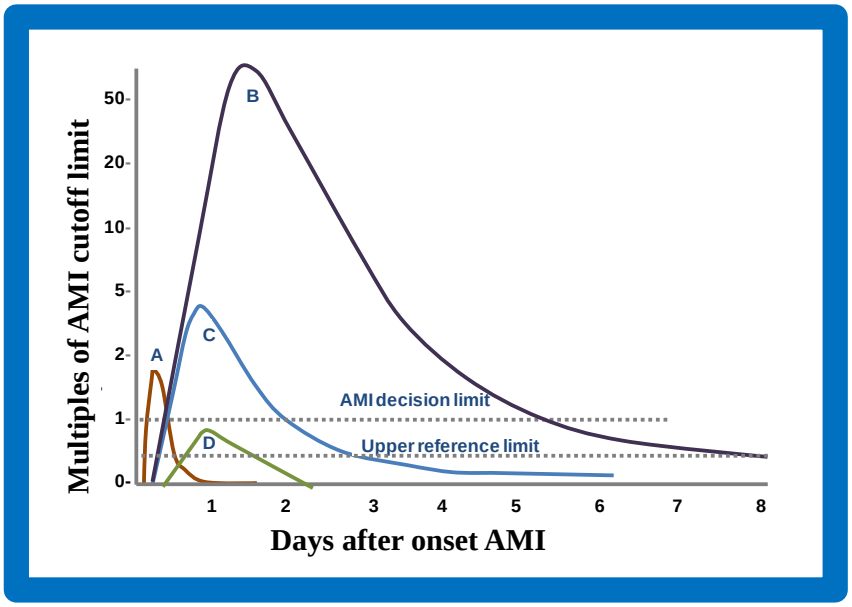

Figure 1: Plot of the appearance of cardiac markers in blood vs. time after onset of symptoms Peak A, early release of Myo or CK-MBisoforms after AMI; peak B, cardiac TnT after AMI; peak C, CK-MB after AMI; peak D, cardiac TnT after unstable angina. Data are plotted on a relative scale, where 1.0 is set at the AMI cut-off concentration (Panteghini et al. 2004).

2.1.2.1 Troponin

The troponin complex has three protein subunits and is located on the thin filament of striated muscle. The three subunits are TnT, TnI and TnC. TnT is a binding protein that attaches the troponin complex to tropomyosin; TnI modulates the interaction of actin and myosin by acting as an inhibitor of actomyosin adenosine triphosphatase activity; and TnC is the calcium-binding subunit of the troponin complex. After stimulation for contraction, excess calcium enters into cells and binds to TnC. This binding causes a change in the conformation of tropomyosin, exposing the binding site on actin and leading to muscle contraction. TnC has an identical amino acid sequence in both skeletal and cardiac tissues and,

thus, has no potential as a cardiac-specific marker (Aldous 2013). However, TnT and TnI have different isoforms in cardiac and skeletal muscle, encoded by separate genes (Christenson and Azzazy 1998). Until now, TnT and TnI release has not been attributed to a tissue source other than myocardium, and except for rare analytical false positives, detection of TnT or TnI in the blood is indicative of heart injury (Jaffe 2001). TnT and TnI are structural biomarkers of cardiac necrosis whose kinetics require several hours after the onset of acute ischemia before they can be detected. For this reason, TnT and TnI are not considered early biomarkers of necrosis. High diagnostic sensitivity and specificity require specimen collection at patient presentation, 6–9 h later, and at 12–24 h if clinical suspicion is high and earlier results are negative (Rosalki et al. 2004). The increase in concentration of TnI and TnT after necrosis is extended compared with that of other biomarkers of necrosis. The exact pattern of TnT and TnI release diverges among individuals and is unpredictable. So, TnT and TnI may be less useful for assessing reocclusion or for infarct sizing compared to CK-MB mass (Morrow and Braunwald 2003). It is important that all efforts done in terms of diagnostics and therapeutics should focus on phase of myocardial ischemia, during which injury is reversible and the myocardial save can be maximized.

Biomarkers as Myo and CK-MB can be used simultaneously with TnT and TnI for risk stratification and clinical decision, improving the outcomes, of patients with ACS (Morrow and Braunwald 2003).

In the myocardial necrosis, TnI and TnT measurements are fundamental for the diagnosis of AMI. Therefore, identifying biomarkers that will improve the tissue specificity and clinical performance taken by cardiac troponin for AMI is a significant undertaking. Also essential is the progression on the detection of specific patterns of modification of cardiac troponin that might improve the early detection of myocardial necrosis, regarding the specific mechanism of myocardial injury. As well, proteomics and modelling can improve the ability to detect and diagnosis of myocardial necrosis (Morrow and Braunwald 2003).

2.1.2.2 Myoglobin

Myo is a heme protein that is abundant in the cytoplasm of cardiac and skeletal muscle cells, being responsible for the transport of intracellular oxygen (Romic et al. 2009). When necrosis of the plasma tissue occurs, Myo is released and blood levels of Myo increase. Myo is considered as an earliest biomarker that is currently available for assessment of patients with ACS (Balk et al. 2001).

Research work, has shown that the sensitivity in diagnostic specificity in the emergency medicine population of Myo is about 90% (Balk et al. 2001). The diagnostic sensitivity of the biomarker has led to recommendations by the National Academy for Clinical Biochemistry and the American College of Cardiology/European Society of Cardiology that the biomarker is useful as an early marker (Alpert et al. 2001; Maron et al. 2003; Wu et al. 1999).

In order to improve sensitivity for the detection of AMI, researchers have been focused on the increase in Myo after cardiac injury. These efforts have given rise to strategies in which differences between measurements at presentation and 60 to 120 min later are compared as an early indicator of AMI (Balk et al. 2001). Although several studies have suggested that elevated levels of Myo are associated with adverse outcomes (Apple and Jaffe 2001; de Lemos et al. 2002), Overall, low levels of Myo may confirm the absence of an AMI condition. To access and accurate diagnosis, cardiac troponin and CK-MB should be evaluated in combination with Myo.

2.1.2.3 Creatine kinase

CK is a protein displaying catalytic activity against creatine (crea, enzyme EC 2.7.3.2), being expressed by several tissues and cell types. It is crea phosphokinase or phospho-CK, catalysing the conversion of crea to phosphocreatine while consuming adenosine triphosphate (ATP). This enzymatic reaction is reversible and thus ATP can be generated from it.

CK and its isoenzymes have long been used for the diagnosis of myocardial infarction. CK is an enzyme present in many parts of the body and can be fractionated into three (Keffer 1996; Owen 1995) isoenzymes, MM, MB and BB. The CK-

MB isoenzyme conserves an adequate supply of high energy phosphorylated creatine, which is used to renovate ATP levels depleted during muscle contraction. CK is composed by 2 subunits, each with a molecular weight of 43 KDa. The three isoenzymes result from the pairing of two different subunits (B for brain and M for muscle). CK-MM predominates in the skeletal muscle and CK-MB is most prevalent in heart muscle. After AMI, elevated CK-MB levels appear within 3-8 hours, peaking within 9-30 hours and returning to normal level after 48-72 hours. Even though CK-MB has been an important biomarker the gold standard for detecting myocardial necrosis, it does have several limitations and is not an ideal marker. The limitations include inability to act as early marker, chances of false diagnosis of AMI and lack of cardiac specificity. Several determinations of CK-MB enhance its efficiency for the diagnosis of AMI and for assessing (Keffer 1996) reperfusion following thrombolytic therapy. The complementars test of others cardiac biomarkers is also important for accurate diagnosis.

2.1.3 Monitoring cardiac biomarker

Several conventional methods have been employed to detect and quantify cardiac biomarkers (Heeschen et al. 1999; Huang et al. 1998; Luo et al. 2012). These include enzyme linked immunosorbent assay (ELISA) (Crivellente et al. 2011; Huang et al. 1998; Liu et al. 2011b; Nishida et al. 1985; Porika et al. 2011), and chromatographic (Crimmins and Kao 2011; Liu et al. 2012; Zhao et al. 2012) or spectrophotometric methods (Modi et al. 1989; Schuder et al. 1979; Shiomi et al. 2005). In general, these methods lack the required specificity and/or involve several steps, are time consuming and require very expensive reagents.

Biosensors are a challenging alternative to these methods providing faster analysis with a direct read-out without the need to transport samples to a laboratory. These can be integrated into a portable analyser system, allowing POC testing of biomarkers in clinical context (Mohammed and Desmulliez 2011). The biorecognition element may be integrated in electronic transducers where the interactions between biological target molecules, such as proteins (Moreira et al. 2011a; Moreira et al. 2011b), enzymes (Albareda-Sirvent et al. 2000), sugars (Chen et al.

2008; Egawa et al. 2011) or DNA fragments (Cai et al. 2002; Chang et al. 2008), are transformed into electronic signal. The physicochemical transducer can be optical (Chen et al. 2011a; Lee et al. 2010), electrochemical (Moreira et al. 2011b; Tweedie et al. 2006), piezoelectric (Loo et al. 2011) or magnetic (Ma et al. 2011). Artificial receptors may act as recognition elements in biosensors, and this has become a fast-growing area for research. These receptors offer several advantages compared to their natural analogues, including greater long-term storage stability, potential re-usability, robustness, versatility, and ease of preparation (Andersson 2000; Zayats et al. 2011). Apart from the present work,of artificial receptors have not been employed in this context.

2.2. Recognition elements in biosensors

But biosensor technology faced great improvements in other fields of application in the past years. Leading to the development of new generations of biosensing devices, used in a wide range of practical applications. Medical, environmental, agricultural, drug detection and food safety are the mostly explored fields for biosensors. Most applications require the detection/identification of ligands or molecules with particular binding properties, and biosensors can be the perfect tool for molecular screening regarding their features.

Biosensor research was also carried out regarding constant demand level throughout the years, aiming at high speed, good precision, and feasibility to carry out analysis in POC or on-site. Highlighted characteristic of biosensors include high selectivity resulting from the possibility to tailor the specific interaction of compounds by immobilizing recognition elements on the sensor substrate that have a specific binding affinity to the desired molecule (Singhal et al. 2002b). The recognition element is indeed a fundamental key at the selectivity provided by biosensors.

Many biological molecules and artificial materials have been used so far as recognition elements in biosensors. These include enzymes, antibodies, cells, DNA, oligonucleotide, aptamers, dendrimers, and molecularly- imprinted materials (MIP), and so on (see Figure 2). Biological elements are widely used due to their

similarity with biological systems and high/specific molecular affinity. They present, however, poor stability, complex production methods, and high cost. Moreover, some biological elements may not be yet commercially available. The artificial elements emerged to overcome these disadvantages, being more robust, resistant to high temperatures and pressures and usually less expensive. Overall, each recognition element has advantages and disadvantages, and the selection should be made according to the analytical method under development and intended application.

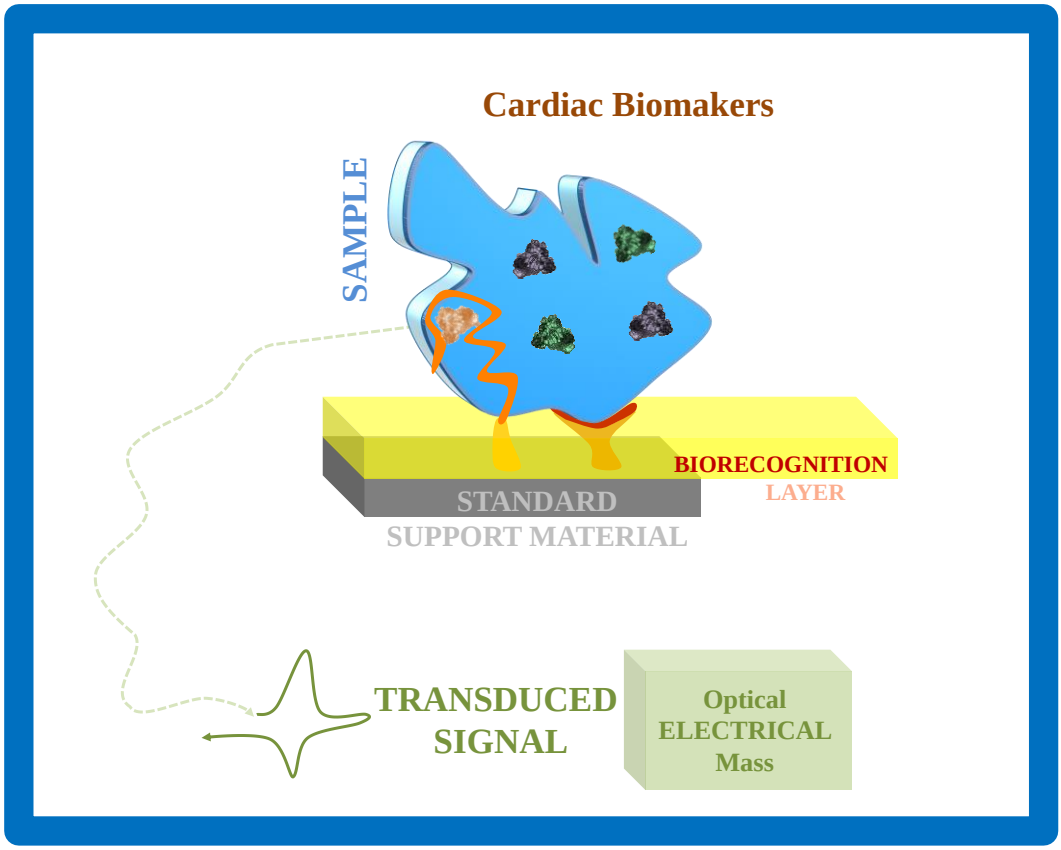

Figure 2: Schematic representation of a biosensing device.

The development of a biosensor with good operating features also requires that a suitable biorecognition element is immobilized on a suitable receptor surface. A wide variety of different materials have been developed for this purpose, varying in agreement with the measuring mode used, including gold, silver, diamond, graphene, carbon nanotubes, etc.

However, the construction of the biosensors not only relies on the recognition element or surface but also with the design strategy. Hereby, a brief overview of biosensors regarding the construction perspective in terms of the biorecognition elements, the materials and the assembly strategy, for both biological and artificial materials is intended.

2.2.1 Enzymatic approach

Enzymatic biosensors are proven powerful tools for qualitative and quantitative analysis of several target analytes in biomedicine, environmental, and food quality control, agricultural, and pharmaceutical industry (Ispas et al. 2012). In the clinical sector, enzymatic approach offers advantages in terms of rapid response, reduced extra-laboratorial analysis with substantial decrease of cost *per* sample (Ispas et al. 2012). Enzymatic biosensors also display considerable benefits over conventional analytical methodologies in terms of high specificity and sensitivity, no need of sample preparation, high throughput and portability.

But the immobilization step is crucial for the efficiency of the biosensor. The biomolecules bound to the surface must be stable and keep their structure and functionality in order to hold their biological activity after the immobilization stage. These are important features to reach accuracy of measurements, reproducibility and operational lifetimes.

Overall, the analytical performance of the biosensor in terms of selectivity, reproducibility, sensitivity, response time and stability are strongly affected by the immobilization process. Thus, intensive efforts have been done to develop successful immobilization strategies, being the most suitable approach correlated with the enzyme nature, transducer and associated transduction method. Each immobilization method presents advantages and drawbacks where reproducibility, cost and difficulty of the immobilization process need to be considered at the selection (Sassolas et al. 2012).

The sensitivity decreases if immobilization causes enzyme denaturation or significant conformational changes especially when the active site is involved. Oriented immobilizations on the transducer surface allows better results in terms of

sensitivity due the correct exposure of the active site to the solution phase. Many immobilization techniques involve random distribution or poor orientation of enzyme molecules inducing partial or total loss of activity due to enzyme denaturation of the active site and/or hindered substrate accessibility (Sassolas et al. 2012). SAM-based immobilization reduces the number of random orientations, generates uniform, reproducible and stable structures with high coverage (Sassolas et al. 2012) (Figure 3).

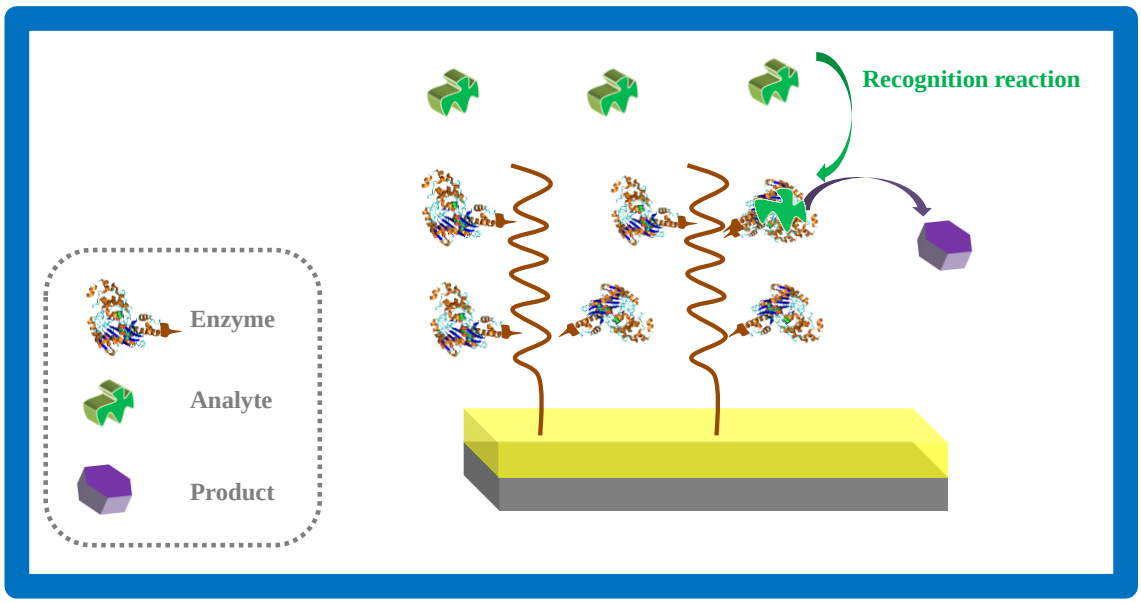

Figure 3: Schematic representation of an enzymatic approach of biosensors.

Different immobilization approaches of enzymes on the transducer surface have been reported in the literature, including: i) entrapment; ii) adsorption; iii) covalent immobilization and cross linking; iv) and affinity along with a combination of the previous approaches.

2.2.1.1 Entrapment

In this method the enzymes are immobilized in a three-dimensional matrix such as: an electropolymerized film, an amphiphilic network, a photopolymer, silica gel, polysaccharide and/or carbon paste.

The electrochemical polymerization consists in the application of a suitable potential or current in a transducer that is submerged in an aqueous solution of enzyme and monomers. Mostly conductive polymers are used, including polyaniline (Bossi et al. 2002; Langer et al. 2004; Mathebe et al. 2004; Morrin et al. 2005; Mu 1994; Mu and Xue 1996) polypyrrole (Sohail and Adeloju 2008; Uang and Chou 2003; Wang and Musameh 2005; Zhu et al. 2007) or polythiophene (Sharma et al. 2004; Singhal et al. 2002b). One of the most important features of these polymers is the reproducible thickness of the film. It can be easily controlled and is not restricted to thin films contrary to non-conducting polymers. The conducting polymers allow/enhance electron transfer and have been considered as a promising tool for enzyme-immobilization (Sassolas et al. 2012).

Non-conducting polymers display high resistivity and have permselective properties preventing interference from the species in the samples displaying good selectivity, high sensitivity, fast response time and good reproducibility (Faridbod et al. 2008; Sassolas et al. 2012; Yuqing et al. 2004). Insulating electropolymerized films like polyphenol, poly(*o*-phenylenediamine) (Centonze et al. 1994; Reyes-De-Corcuera et al. 2005), poly(*o*-aminophenol) (Ekinci et al. 1996; Pan et al. 2004) and overoxidized polypyrrole (Reyes De Corcuera et al. 2004; Zane et al. 2011) have also been largely used in enzymatic biosensors (Sassolas et al. 2012; Yuqing et al. 2004). Usually, the enzyme is incorporated in an amphiphilic polymer (Bruns and Tiller 2005; Hanko et al. 2006a; Hanko et al. 2006b), however the incorporation of the target is made in a hydrophilic matrix of (poly(2-hydroxyethylacrylate) and hydrophobic phases of polydimethlysiloxane (PDMS) (Bruns and Tiller 2005), according to several authors.

Another important technique that is entrapment-based is the immobilization by photopolymerization. Some researchers have used water soluble poly(vinyl alcohol)-bearing styrylpyridinium groups and azide-unit pendant water-soluble

photopolymer for this purpose. The insoluble matrix was obtained with photopolymerization process, initiated by light exposure (Leca et al. 1995a, b; Tsafack et al. 2000).

Sol-gel process has also been used for entrapping enzymes. Sol-gel is based on the ability to form solid metal or semimetal oxides via the aqueous processing at low temperatures of hydrolytically labile precursors (Gill and Ballesteros 2000). Combination of sol-gel with optical (Choi 2004; Hanko et al. 2006b) and electrochemical (Alhitti et al. 1984; Bartlett and Whitaker 1987a, b) transduction methods were developed and good results in terms of sensitivity and stability were obtained.

Enzymes were also entrapped in a polysaccharide-based gel (Kofuji et al. 2009; Schneider et al. 2012) including alginate (Qin et al. 2012), chitosan (Colak and Gencer 2012; Yadav et al. 2012) and agarose (Tu et al. 2011). These matrices provide a natural environment to the enzymes due to their features in terms of biocompatibility, also promoting the access of electrons between the enzyme and transducer.

Carbon paste has been largely used as well for the preparation of several electrodes and detectors (Svancara et al. 2009). The enzyme is entrapped in the matrix and allows the contact between the biological compound, mediator and the sensing sites, increasing the electron transfer. The method is versatile, reproducible and the surface can be renewed (Boujtita et al. 1996; Zhu et al. 2007). Other inorganic host matrix, such as silica or clays, were also an alternative to organic polymers and have been extensively used for immobilizing enzymes in biosensing (Sassolas et al. 2012).

Overall, enzyme immobilization by entrapment is easy to perform. Enzyme, mediators and additives can be simultaneously deposited in the same sensing layer. There is no modification of the biological element so that the activity of the enzyme is preserved during the immobilization process. Biosensors based on physically entrapped enzymes are often characterized by increased operational and storage stability. However, limitations such as leaching of biocomponent and possible diffusion barriers can restrict the performance of these systems.

2.2.1.2 Adsorption

Adsorption methods are largely used due to the easy protocol of immobilization. The enzyme solution just needs to be in contact with the support for certain period of time. The adsorption mechanisms are based on weak bonds such as Van der Waal's forces, electrostatic and/or hydrophobic interactions.

Several adsorption methods have been described based on i) physical adsorption (Mu and Xue 1996), ii) electrostatic interactions (Liu and Sun 2007) through layer-by-layer deposition, electrochemical doping and pre-immobilization in ion-exchanger beads and iii) retention in a lipidic microenvironment (Sharma et al. 2004; Singhal et al. 2002a). These techniques do not require functionalization of the support and in this regard the activity of the enzyme is not affected. However, changes of temperature, pH and ionic strength can result in desorption of the enzyme from the support surface due to its week bond to the surface. Poor operational features and storage stability are also factors of concern. Another drawback is the non-specific adsorption of other proteins or side-substances, namely other proteins within the sample matrix (Sassolas 2012).

2.2.1.3 Cross-linking and covalent immobilization

Enzymes can also be immobilized by cross-linking with bifuntional reagents such as glutaraldehyde (GA) (Hernandez-Cazares et al. 2011), glyoxal or hexamethylenediamine (Portaccio et al. 2007). Several methods have been reported so far with conductimetric readings, where the enzyme is entrapped in a gel co-reticuled with GA for detection of some metals (Zhang et al. 2009b) nitrite (Bean et al. 2005) or pollutants (Gogol et al. 2000). An amperometric glucose biosensor was developed by immobilizing glucose oxidase (GOx) onto zinc oxide (ZnO) nanotube-modified electrode by crosslinking (Kong et al. 2009). A needle-type biosensor (developed for monitoring blood glucose in fish (Yonemori et al. 2009), by employing a cross-linking between GOx and bovine serum albumin (BSA) induced by addition of GA. Its main drawback was the possibility of activity losses due to the distortion of the active enzyme conformation and the chemical modifications of the active site during cross-linking (A. Sassolas et al., 2012).

2.2.1.4 Affinity

Affinity methods enable the production of oriented and site-specific immobilized enzymes. Several affinity methods have been described to immobilize enzymes by including compounds with strong affinity such as: i) biotin/streptavidin (Andreescu and Marty 2006; Esseghaier et al. 2008; Hsiao and Heller 2012), ii) metal ion–chelator and (Andreescu et al. 2003) iii) lectin-carbohydrate (Pei et al. 2005).

A self-assembly composed of alternating layers of biotin nanoparticles and streptavidin-/avidin-conjugated enzymes was developed on a microelectrode array device with GOx, horseradish peroxidase (HRP), and alkaline phosphatise (Hsiao and Heller 2012). In a similar way, an impedimetric biosensor for H_2O_2 detection was developed. HRP conjugated with streptavidin was immobilized on a mixed SAM formed by 1,2-dipalmitoyl-sn-glycero-3-phosphoethanolamine-*N*-(biotinyl) and 16-mercaptohexadecanoic acid previously grafted on a gold electrode (Esseghaier et al. 2008).

The strong affinity between a metal cation and a chelator such as nitrilotriacetic acid (NTA), imidodiacetic acid or tag poly(histidine) can also be used to develop enzymatic biosensors. Some authors reported in the literature polyaniline-polyacrylate films formed on the electrode and then loaded with Ni^{2+} ions, which acted as coordination sites for histidine residues present on histidine-tagged lactate dehydrogenase. NTA was also frequently used as chelator for selective enzyme attachment. In this case, four of six coordinations of Ni^{2+} ions were occupied by the four ligands of the NTA chelate, while the other two positions were occupied by water or buffer molecules which could be selectively replaced by the histidine tag that were incorporated in the enzyme sequence (Andreescu et al. 2001). This strategy also allowed immobilizing His-tagged acetylcholinesterase on functionalized graphite used for SPE fabrication (Andreescu et al. 2003).

Affinity immobilization was also described between a sugar moiety naturally present in some enzymes such as acetylcholinesterase and concanavalin A deposited onto a surface. Concanavalin A is a lectin with multiple sites of high affinity for carbohydrates (Andreescu and Marty 2006). First, the lectin was immobilized on a support and then glycosidic enzyme was bound to specific lectins

(Sassolas et al. 2012). Enzymes, such as HRP (Liu et al. 2008) or GOx (Anzai et al. 2000) have also been incorporated into multilayers without any chemical modification. The response of the electrode modified by the Con A/enzyme multilayers was related to the number of assembled bilayers of Con A/enzyme (Yang et al. 2006).

Overall, and considering specifically the biomarkers of interest in this work, there is no work reported in the literature so far that uses a biosensor with an enzyme acting as biorecognition element for Myo, TnT and CK-MB detection.

2.2.2 Immunoassay approach

Immunosensors prospect the interaction between an antibody and its antigen and have the ability to effectively capture the target and spread this information as a measureable signal. Antibodies are proteins found within the blood of vertebrates and are produced by white blood cells. They are typically associated to a "Y" structure that contains two antigen binding sites on the upper tips of the protein. The recognition site at the antigen is known as epitope. An antigen may contain many epitope regions, but an antibody binds only to one specific epitope site, which is responsible for the antigen/antibody recognition in complex samples with different proteins.

There are two types of antibodies, the polyclonal and monoclonal. Polyclonal antibodies are produced in result of the immune response against an antigen, involving the activation of multiple B-cells. Each of these cells targets a specific epitope region to which they display a specific binding affinity. As a result, polyclonal antibodies include a large number of antibodies with different specificities and epitope affinities. Monoclonal antibodies are, on the contrary, technically identical because they are produced in the laboratory from clones of a single B lymphocyte immune cell (Llames et al. 1999). In result of this, monoclonal antibodies display high specificity for a single epitope region at the antigen, being indifferent to other possible epitope regions, which in turn may lead to a decreased sensitivity. For this reason, the selection of antibodies is a challenging issue when optimizing a given assay, and depends mostly of the main purpose of the method under development.

Overall, biosensors relying in immunoassays comprise different binding formats for antigen identification, as illustrated in Figure 4, and may operate in a labelled or non-labelled basis. Most of these are based in non-competitive reactions using two binding sites, also called sandwich assays. Their selectivity and sensitivity are high and based on the specific recognition of an antibody with an antigen, but their use is limited by the availability of paired antibodies (Figure 4). . Due to the numerous published works in immunoassay based biosensors, the description of these methods was not exhaustive, but aimed to focus the prominent biosensor configuration in a tutorial style approach.

The direct interaction between antibody/antigen is the most simple format. Suprun et al. (Suprun et al. 2011) described an electrochemical immunosensor based on metal nanoparticles (NPs) of gold, silver, and copper for cardiac Myo detection in human-blood plasma. The detection of cardiac Myo was based on direct electron transfer between the Fe(II)-heme and the metal NP-modified electrode surface. Although the method did not require signal enhancement or amplification, it involved a 15-min immunoreaction time with the target-Myo sample, followed by further 5-min incubation in phosphate buffered saline (PBS) and washing of non-specifically binding molecules before electrochemical measurement. Billah et al. (Billah et al. 2008) used a different approach for assembling a Myo immunosensor. This work employed a mixed SAM of biotinyl-phospholipid and mercaptohexadecanoic acid, for subsequent neutravidin functionalization and further attachment of biotinyl anti-Myo antibodies. This time biological levels were achieved but the immunosensor design was rather complex. Sandwich immunoassay consists of a sensor reaction substrate functionalized with immobilized primary reaction antibodies, complementary to the target analyte. Some of the labelled and non-labelled approaches are described next, focusing on screening cardiac biomarkers

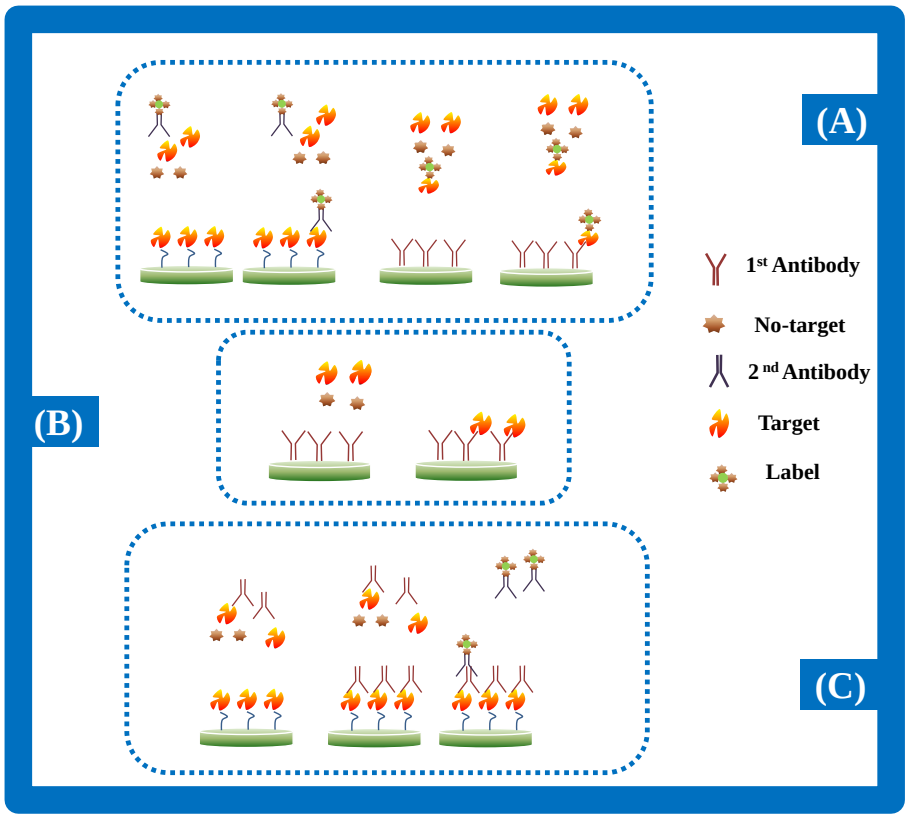

Figure 4: Main immunoassay formats. (A): competitive indirect format; (B): competitive direct format; (C): Non-competitive assay.

2.2.2.1 Labelled sandwich immunoassay

The generation of an immunosensor signal is several times made by some kind of label placed at a secondary antibody. This includes fluorescents labels (Caulum et al. 2007; Gul et al. 2007; Joensson et al. 2008; Plowman et al. 1999; Wolf et al. 2004; Ziegler et al. 2008), enzymes producing/consuming compounds that are easily detected (Campbell et al. 2008; Cho et al. 2009; Hatakeyama et al. 2009; Kurita et al. 2006; Mohammed et al. 2009; SiegmannThoss et al. 1996), paramagnetic particles (Enpuku et al. 2005; Eveness et al. 2009; Kiely et al. 2007; Luxton et al. 2004; Richardson et al. 2001) and metallic colloids as Surface Enhanced Raman Spectroscopy probes (Mulvaney et al. 2003; Ni et al. 1999; Xu et al. 2004). Silva and co-authors (Silva et al. 2010) prepared a new modified sensor

using graphite-epoxy silver composite followed by streptavidin-micro sphere integration and its binding to the anti-TnT biotinylated monoclonal antibody for TnT detection. In this work, it was observed that streptavidin microspheres enhanced the analytical sensitivity by 8.5 times, showing as linear response 0.1-10 ng/mL of TnT and limit of detection of 0.2 ng/mL. Also, Zhou et al. (Zhou et al. 2010) reported clinical applications of a newly TnI and CRP immunosensor, based on a composite poly(dimethylsiloxane)-gold nanoparticle (Au-NP) composite. This work described an approach to the simultaneous electrochemical detection of these biomarkers in the previous composite, integrating the immunosensor in a microfluidic system. In other work by Ahmmad et al., (Ahammad et al. 2011), Au-NPs were electrodeposited on indium-tin oxide (ITO) and applied to detect molecular interaction between human cardiac TnI and specific antibody. The open circuit potential was generated due to an enzyme-based immune catalytic reaction, providing linear ranges of 1-100 ng/mL TnI.

Rajesh et al. (Rajesh et al. 2010) reported an electrochemical immunosensor based on a thin gold wire with a mixed SAM of a small-chain alkanethiol and a long-chain alkanethiol for Myo detection. In another approach and , in order to enhance the stability and the loading of the antibody molecules at the transducer surface, large surface-areas of ZnS-NPs modified with 3-Mercaptopropionic acid for protein-immobilizing conjugates of Myo have been proposed (Mishra et al. 2012). This was done by synthesis of ZnS nanocrystals and subsequent modification with 3-mercaptopropionic acid and covalent binding to a SAM of 3-aminopropyltriethoxysilane (APTES) on ITO glass plates. This surface was after made react with *N*-(3-dimethylaminopropyl)-*N*-ethyl carbodiimide hydrochloride (EDAC)/*N*-hydroxysuccinimide (NHS) for carboxylic function activation and subsequent reaction with Myo antibody. The resulting immunosensor exhibited an electrochemical impedance response to Myo in a linear range of 10 ng/mL to 1 μg/mL.

Luxon and co–authors reported an interesting and rapid immunoassay system based on antibody coated micrometer-sized paramagnetic particle (Luxton et al. 2004) for the detection of CRP and CK-MB. In this original work, the proposed assay did not require sample preparation or washing step, and results could be

obtained in less than 3 min after introducing the sample into the vessel with sensitivities in the standard clinical range.

An alternative to this approach is based in label-free detection methods, where the target protein is not labelled, and detected in its native form. This type of detection is cheap and easy to perform. In general, these strategies for the detection of cardiac biomarkers are carried out by monitoring the changes in the interfacial or electronic performance caused by antibody protein interaction.

2.2.2.2 Label-free sandwich immunoassay

Literature review shows that one of the best immunosensors for cardiac biomarkers involve label-free immunodetectors which offer many advantages including the omission of a second reaction incubation phase, the decrease in the complexity of both the acquisition of the biosensor signal and the overall reaction chemistry, and the reduction of the cost *per* assay as antibodies and fluorophores contribute to the bulk of the cost for single assay.

Recently, Bhalla et al., (Bhalla et al. 2012) proposed a new immunosensing method for detecting low-level TnI concentrations. In this work, citrate-capped Au-NPs were deposited in SPEs using one step electrochemical technique. The subsequent interaction of TnI with its corresponding antibody was studied with respect to electrical capacitance changes. The sensor showed a LOD of 4.3 ng/mL.

Suprun et al. (Suprun et al. 2012) described a novel direct antibody-free electrochemical approach for AMI diagnosis. In this work, SPEs modified with didodecyldimethylammonium bromide were used for plasma characterization by cyclic voltammetry (CV) and SWV. Also, the applicability of the electrochemical testing for AMI diagnostics was confirmed by statistical methods. The authors concluded that the proposed approach could be considered as one of the first steps towards the ''electrochemical profiling'' of the samples of healthy and diseased donors, similar to proteomic approaches. Zhou et al. (Zhuo et al. 2012) reported a new strategy for application of polyaniline for electrochemical immunosensing of CK. The CK immunosensor had a LOD of 0.5 pg/mL. Which may account the use of a highly conductive film such as polyaniline.

Overall, in the immunosensing approach there are several proprieties that should be carefully optimized in order to improve the sensitivity, selectivity and the reactivity of the antibody-antigen pair. In order to improve current immunosensor technology, the task will involve not only innovation on the part new sensor technologies and material, but also in creating new immunoreactions formats, maximizing reaction efficiencies and applicability to biosensing purposes. Immunosensor technology is indeed gold standard for cardiac biomarker detection and allowed for clinically applicable detection sensitivities from a variety of novel detection format.

However, natural antibodies display some limitations in terms of i) robustness, ii) reusability (antibody/antigen binding is mostly irreversible) and iii) solvent compatibility (natural antibody are denatured in the presence of organic solvents). These materials can be replaced by other kind of biorecognition elements, including synthetic materials displaying high selectivity towards an intended target.

2.2.3 Aptamer aproach

Aptamers are artificial biomaterials for recognition of antigens consisting of oligonucleotides, such as RNA or single-strand DNA. Aptamers present high stability at elevated temperatures, allowing their use over a wide range of conditions and may also offer reusability. Compared to antibodies, aptamers are not dependent of immune systems meaning that they can be produced to identify non-immunogenic or toxic targets. They also have high affinities to their targets, with dissociation constants at the low-picomolar level (Auger et al. 2005).

Aptamers are typically selected and amplified *in vitro*, aiming to achieve high specificity and affinity with a specific target that can range from small ions, single molecules, to proteins or even cells. This is done by systematic evolution of ligand by exponential enrichment (SELEX), which identifies the biomolecule from a random library containing 1013–1016 single-strendeed DNA or RNA sequences (Keefe et al. 2010).

Aptamers can be targeted to recognize an entire molecule or only a specific region of it (Song et al. 2008). The kind of nucleotide, the nucleotide sequence and

the folding pattern of the aptamer may be considered at the time of selection. Regarding folding pattern, aptamers hold the ability to form stem-loop arrangements leading to proper three-dimensional structures that facilitate binding specificity. Overall, the physical and chemical properties of aptamers make these efficient at the segregation of closely related peptides or viral sub-types, making them ideal candidates as biorecognition elements.

Sensors developed with aptamers as biorecognition elements are called "aptasensors". To use an aptamer as recognition element, it is necessary to immobilize it or part of it in a support. Depending on the approach taken for the analyte determination, immobilization can be carried out through chemical or biological entities and should account different edification conditions, such as: the aptamer binding site (attach to the 5'or 3' end), the type of chemistry used, the molecule orientation and spacer length. The immobilization may be conducted through covalent or electrostatic interactions mainly hydrogen bonding or van der Waals forces. Electrostatic interactions allow a rapid, simple and cheaper immobilization, but the use of covalent binding offers a more stable surface modification. This covalent binding is easily achieved because aptamers may be modified with suitable linkers that may present different functional groups. The covalent attach of the aptamer to a receptor surface may be achieved by SAM-modification, which allows close nanostructural control over the aptasensor under development.

Once the aptamer is bond, the aptasensor shall provide the target recognition and subsequent signal transduction, in the form of optical, electrical or mass response. Although aptasensors may adopt different designs, the molecular recognition using aptamer should involve suitable conditions for the formation of the complex aptamer-ligand on a surface (Figure 5). Small target molecules are typically more difficult to detect when compared to big size particles and, according to their position in the target and aptamer complexes two binding paths are possible: embedded or outside binding. The aptamer can embed the target on itself through special oligonucleotides sequences or can lead to outside binding, which is usually associated with macromolecules with complex special structures.

Four different strategies can be followed for using aptamer as recognition elements, namely: i) target-induced response; ii) sandwich or sandwich mode; iii)

target-induced dissociation; iv) competitive replacement mode, and v) aptamer-based enzyme.

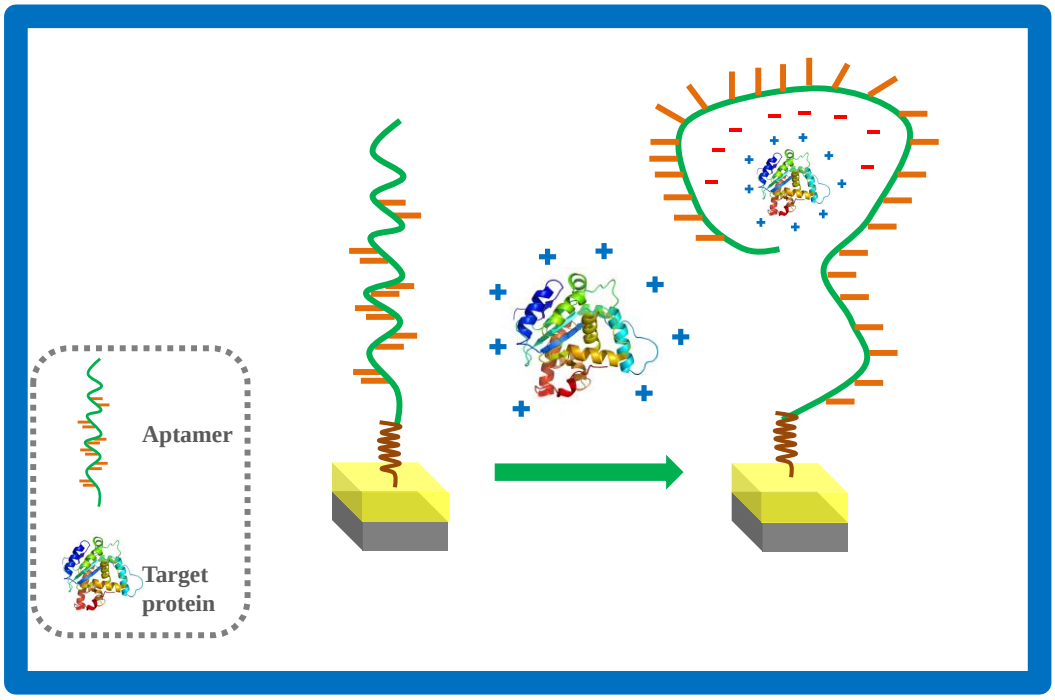

Figure 5: Schematic representation of the aptamer approach of biosensors.

2.2.3.1 Target-induced response

The target molecules may complex directly with the aptamer leading to conformational or specific physico-chemical changes at the aptamer, thus allowing target-induced specific response. Usually, the aptamer attached to the surface is labelled and this label changes in result of the conformational transition of the aptamer thus acting as signal generator.

There are several kinds of labels that may be used in aptasensors, including a quencher, a fluorophore, a nanomaterial or a redox species. Depending on the kind of label, the signal obtained can be translated by several forms. These in-

clude a signal change due to a variation on the distance of the label and the transducer, the interaction of the target with the fluorescence or quencher label (Jhaveri et al. 2000), changing some properties of the nanomaterials and so on. The previous situation, but now label free aptamer was also described. The aptamer with a duplex or hairpin structure where the 5'-end fluorescent signal moiety was quenched by the guanine bases at the 3'-end of the aptamer or the 3'-end of complementary sequence, and therefore no fluorescent signal was present. In the presence of the analyte, the aptamer conformation changed annulling the quenching effect from the guanine promoting a fluorescent signal (Lerga and O'Sullivan 2008).

The direct interaction between the aptamer and the target molecule can be achieved as previously described, but also through more complex approaches regarding the chemical modification of the surface transducer before aptamer attachment, enhancing its ratio on the surface. In some cases, using an aptamer with single-stranded oligonucleotides is not enough to eliminate background noise.

2.2.3.2 Sandwich or sandwich mode

Another format adopted for the aptasensor design is having three monolayers on the surface: aptamer-target-modified aptamer or aptamer-target-antibody. This format is only possible if the target possess dual binding sites for the aptamer or both aptamer and antibody.

Typically, the common approach is based on the immobilization of the aptamer by self-assembly, followed by the interaction with the target molecule, forming the first part of the complex and ready to react with the modified aptamer. The modification can incorporate different molecules or even nanomaterials as previously described to act as electrochemical (Wang et al. 2009b) or optical (Fang et al. 2008) labels.

Alternatives with antibody were also established by immobilizing on the aptamer an anti-adenosine aptamer sequence. The DNA subsequently loaded with Au-NPs was bound to the surface through hybridization. In the presence of the

target, the aptamer part of the linker DNA formed a target-aptamer complex, releasing the probes modified with nanoparticles (Wang et al. 2009a).

2.2.3.3 Target-induced dissociation

Approaches based on the target inducing dissociation of aptamer from its complementary sequence were also used, where the complementary sequences of the aptamers are normally immobilized on the surface. This design allowed several variations, such as: i) immobilizing the complementary sequences of the aptamers and using a labelled-aptamer sequence, where the presence of the target lead to the formation of target-aptamer complexes, occurring the liberation of the complex and subsequent signal generation (Radi 2011); ii) and a similar approach to the previous one, but without labelling the aptamer because the detection enables label-free assays (Babu et al. 2013; Chen et al. 2013; Xiao et al. 2013). Depending on the signal expected, the complementary sequence can also be hybridized with another modified DNA, producing a response or simply detect the complex released(Song et al. 2008).

2.2.3.4 Competitive replacement mode

Assays carried out through competitive replacement are another alternative using the aptamers as recognition elements. This consists in the conventional way of anchoring the aptamer to a specific surface and establishing its binding with one specific target molecule labelled, in the present of the targets to be quantified. The label free competition for the aptamer binding starts and the label free target replaces the labelled ones. According to the detection mode selected, the signal can be generated by the species released from the surface or the labelled molecules released after the competition. This strategy may also involve the combination of different aptamers on the surface, detecting two targets at the same time (Fang et al. 2008).

2.2.3.5 Aptamer-Based enzyme

The properties of aptamers and enzymes were also used in combination. The system is known by Aptameric Enzyme Subunit (AES). The AES consists of two aptamers: an enzyme-inhibiting aptamer and a target molecule-binding aptamer. In the absence of target molecule, the enzyme does not generate signals because the AES inhibits enzymatic activity. However, once the target molecule binds to the AES, the AES changes its conformation, which results in a loss of enzyme inhibitory activity. Then the target molecule can be measured via enzyme activity measurements. Aptamers can also be joined to nucleic acid enzymes (e.g., ribozymes and deoxy-ribozymes) to create allosteric enzymes or so-called aptazymes (Tang and Breaker 1997). Some aptamers show enzymatic activity after binding their analyte and adopt other configuration promoting a response. Thus, aptazymes possess allosteric properties that transduce the recognition of target analytes into catalytically generated observable signals.

Until now no report of the construction of aptasensors for Myo, TnT and CK-MB was found in the literature. Only aptamer-based sensors for thrombin cardiac biomarker have been reported so far and are described next.
Qiu et al. (Qiu et al. 2010) developed a nanoporous gold (NPG)-based electrochemical aptasensor with a sandwich mode, connecting the aptamer modified NPG and the aptamer-modified Au-NPs. The LOD of this aptasensor for thrombin was 30 fM. Polsky et al. (Polsky et al. 2006) reported a thrombin sensor by employing aptamer-functionalized platinum NPs as catalytic labels for amplified electrochemical detection. Zheng et al. (Zheng et al. 2007) also described an ultrasensitive electrochemical sensor for thrombin detection based on network-like thiocyanuric acid/Au-NPs. This type of electrochemical immunosensor based on nanomaterials was further improved by Wang et al., who introduced an aptamer/quantum-dot-based immunosensor for the detection of thrombin (Wang et al. 2007).
New nanomaterial-based schemes coupling multiple amplification units and processes on the surface were also explored for meeting the high sensitivity of electrochemical aptasensor in the detection of proteins. Liu et al. (Liu et al. 2010) reported a new electrochemical aptasensor for the detection of thrombin based

on MWCNTs as carriers of the electrochemical capture probe and thrombin-binding aptamer (TBA) as a molecular recognition element. The results demonstrated that a MWCNT-modified glassy carbon electrode (GCE) could offer a promising platform for electrochemical capture probe immobilization and greatly enhance the sensitivity of the electrochemical aptasensor due largely to the specific area of the MWCNTs, which capture a lot of molecular recognition elements. The LOD of this aptasensor for thrombin was 0.5 pM.
In general, aptasensors have attracted the attention of many researchers due to their intrinsic selectivity and sensitivity. The introduction of aptamers in biosensing devices has become a powerful tool due to its simple operation and suitability for miniaturization. However, these biomaterials may not be reusable, are sensitive to temperature, solvent, and pH of operation, and turn out expensive for screening programs. Costs will be significantly reduced once these are replaced by plastic counterparts, suitably attached to a platform that allows detection of very low concentrations.

2.2.4 Molecularly Imprinted material

Molecular recognition by molecularly-imprinted polymers (MIPs) is a challenging area in supramolecular chemistry and a promising alternative to natural materials, such as antibodies, enzymes or other biological receptors displaying selective affinity to specific targets. These natural biological receptors are used in a multiplicity of applications, ranging from analytical and preparative chemistry to nanomedicine, including diagnostics, drug development, and drug delivery. The stability of such biomolecules is however limited, which is coupled to a high cost, leading to a booming number of research works aiming at more stable synthetic systems mimicking, highly selective and sensitive recognition processes occurring in nature. Although nature selectivity and sensitivity have not yet been matched, steady progresses are being made in creating synthetic systems for molecular recognition (Ravelet and Peyrin 2006).

MI is typically the 3-D imprint of a certain molecule in a rigid polymeric matrix. The overall process may be seen in Figure 6, and consists in a pre-arrangement between target compound and selected monomers, followed by suitable

polymerization procedures that lead to the formation of a rigid matrix. The template molecule is after removed, eventually without disturbing the geometry of the solid. The resulting material keeps the ability to rebind the template because of its 3-D functional arrangement (Ravelet and Peyrin 2006).

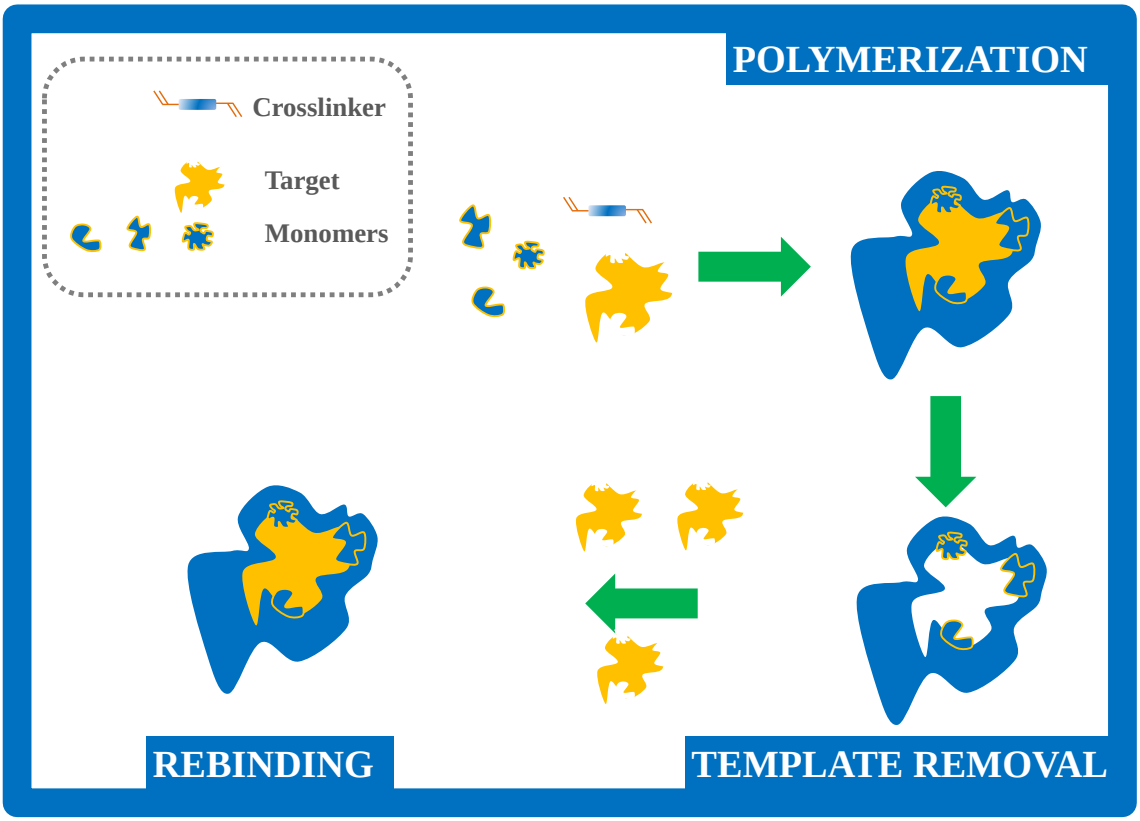

Figure 6: Molecular imprinting approach.

While the imprinting of target compounds of low molecular weight is today reasonably established, protein imprinting is still a challenge due to the typical flexibility and instability of proteins. Proteins change their 3-D structure (due to conformational changes) depending on the surrounding environment, which typically leads to a mismatched imprint. Special care must be taken at the time of selecting the experimental conditions, including the way the MIP is integrated at the transducer surface.

The integration of protein MI materials in biosensors has been achieved so far by many different approaches. These approaches may vary from the target to be imprinted (total compound or only epitope region) and the way the polymerization is conducted (*in situ* – bulk – or surface, being photochemically or thermally initiated) (Henry et al. 2008). Each of these presents advantages and drawbacks. Bulk protein imprinting is easier to achieve, using fairly simple experimental procedures, but surface-imprinting methods provide a controlled modification of the imprinted surface within thin films of specific polymers. The template removal is here much easier to achieve, allowing good access to the imprinted sites, and providing lower non-specific binding, while bulk approach could suffer from poor template extraction, slow binding kinetics, template entrapment and bleeding. The main drawback of surface imprinting is the number of binding sites, which is limited by the reduced surface available. Consequently, the suitable choice of the application of the material and the signal transduction method used should be carefully studied.

Several methods for imprinting cardiac biomarker have been presented so far in the literature. This includes mostly bulk or surface imprinting of the entire protein target molecule, but few works also report epitope imprinting, which can also include bulk or surface techniques. These works are detailed next.

2.2.3.1 Bulk imprinting

Bulk imprinting has been successful for small molecular weight MI, is the most straight forward approach to macromolecular imprinting. The advantages to this approach are that 3-D binding sites are formed for the entire protein and that there are a multitude of facile procedures already presented in the literature (Kryscio and Peppas 2012).

Several strategies have been reported in the literature with bulk protein approach, including acrylate, hydrogel, and/or sol-gel chemistry (Jeong et al. 2012).

2.2.3.1.1 Acrylate

Acrylate imprinting has been the most widely used approach for small molecule imprint, but it is of little application in protein imprinting. Turan et al., reported a bulk imprinted material prepared with 2-acrylamido-2-methyl-propanosulfonic acid as monomer that also included isopropylacrylamide due to the good biocompatibility of acrylamide (AAM) environments for proteins. This was done by free-radical cross-linking copolymerization in aqueous solution at three different temperatures. The effects of the initial concentration and adsorption time over the Myo adsorption capacity of the materials have been analysed and found strongly dependent on the preparation temperature. The imprinted materials displayed better features in terms of rebinding and selectivity than the non-imprinted (NI) material (Turan et al. 2009).

Overall, a major limitation of acrylate approach is that it is carried out using solvents in which proteins are largely insoluble. Additionally, the dissolution or dispersion of protein in nonaqueous media commonly results in protein conformational arrangements that are different from that of the native form. This may have strong implications at the efficiency of the resulting MI material because the shape of the protein being imprinted differs from the shape of the protein to be detected. The use of high temperatures in the polymerization process hinders in a similar way the quality of imprinting. Other polymerization approaches enabling mild environments regarding protein stability include the formation of hydrogels.

2.2.3.1.2 Hydrogel/Sol Gel

Hydrogels can substitute conventional polymeric materials in MI due to their peculiar characteristics. A hydrogel is a porous polymeric network that may react to external stimulus (mainly pH, ionic strength or temperature) with a change in its structure or dimension. This change can be used to control the uptake and release of the templates with a slight effect on the polymeric network which memorizes the imprinting shape.

Hdjertén group described imprinting gels for several proteins such as hemoglobin (Hmg), cytochrome C and transferrin in AAM with low level of cross-linker.

The MI materials so obtained were relatively soft material owning pores large enough for proteins to diffuse through the polymer, being similar in composition to polyacrylamide gels used in protein separation. The resulting sensor also showed selective binding of the template proteins from the mixtures. High selectivity was also demonstrated by the ability to adsorb Myo from horse, but not whale Myo on the horse Myo-imprinted column, demonstrating selectivity for these two proteins with similar sequences and 3-D structures (Hjerten et al. 1997).

A similar approach to the previous one has also been used to prepare imprinted gel within the pores from a more rigid gel prepared from end-linked poly(ethylene glycol)-diacrylate (PEG-DA). The polymeric matrix was prepared via photopolymerization from PEG-DA macromonomer solutions with three initial solid contents with different amount of PEG. This work studied only diffusion coefficients for Myo travelling across the hydrogel membrane for all PEG network compositions (Engberg and Frank 2011), and no application to biosensing was tried out.

An artificial gel antibody prepared by the same approach has been developed by Liao et al. The authors optimized the formation of Myo imprinted polymer and developed a mass spectrometry-based profiling system for assessing the binding selectivity of the artificial antibodies. Experimental results showed that Myo and albumin were bound/absorbed onto Myo-MI chips and not to NI chips. Other proteins, such as histidine-rich glycoprotein, immunoglobulins, proapolipoprotein, and leech-derived tryptase inhibitor, were also tested, but provided less reproducible chip signals (Liao et al. 2009).

Sol-gel template synthesis employs colloidal suspensions of silica particles that are polymerized to form a solid gel (Buckley and Greenblatt 1994). The starting materials (the precursors) used in the preparation of sol are usually inorganic metal salts or metal organic compounds such as metal alkoxides. The hydrolysis of precursor reagents begins when they are mixed with water in the presence of an acid or a base catalyst, but the addition of a mutual solvent (usually alcohol) is not necessarily required. Hydrolysis of precursors leads to the formation of

silanol groups (≡Si–OH), followed by progressive condensation reactions producing siloxane bonds (≡Si–O–Si≡), alcohol and water as by-products. During the sol-gel phase transition, the viscosity of the solution gradually increases as colloidal sol becomes interconnected to form a rigid, porous gel. Thus, sol-gel process provides a simple way to incorporate numerous organic, organometallic and biological molecules into a microporous matrix of sol-gel (Hench and West 1990).

Sol-gel materials offer a combination of advantages over many other polymers for protein imprinting. These include: i) the mild preparation conditions allow entrapped protein to retain much of its physical and chemical properties inside the polymer matrix, ii) the rigid property of sol-gel cross-linking network favours retaining the shape of the cavities after removal of the templates, iii) sol-gel glasses are electro-, photo- and chemically stable and can be optically transparent. The thickness, porosity and surface area of the material are also easily controlled (Lahav et al. 2001; Marx and Liron 2001). In addition, there is a wide range of possibilities to obtain well-controlled properties of the materials by varying the chemical composition of the precursors and the ratio of inorganic to organic components (Tripathi et al. 2006). A drawback of the method might be that the fragile polymer network could be less robust than a simple surface or bulk imprinted material.

Few researchers described some research work based on sol-gel imprinting of cardiac biomarkers. Schirò et al. described the effect of hydration on the dynamics of encapsulated material in a porous silica matrix. They used an elastic neutron scattering to investigate the temperature dependence of the mean square displacements of non-exchangeable hydrogen atoms of sol-gel (Schiro et al. 2008). Other work was described for Wang, the studing a direct electrochemical and electrocatalytic behaviour of Myo immobilized on carbon paste electrode by a silica sol-gel film derived from tetraethyl orthosilicate was investigated for the first time. This work based on Myo/sol-gel film modified electrode provided a convenient way to perform electrochemical research having protein as a target element (Wang et al. 2004).

2.2.3.2 *Surface imprinting*

Surface imprinting of proteins is widely used as imprinting strategy (Turner et al. 2006), requiring a smaller amount of target than the conventional bulk MI approaches. It consists on immobilizing the template on a nanostructured surface with subsequent polymerization around it, thus creating binding sites close to the surface (Figure 7). These binding sites are more accessible than in bulk based approaches and target/polymer interactions are not hindered by diffusion (Mirsky et al. 1999). Generally, this decreases the equilibrium time and increases binding kinetics.

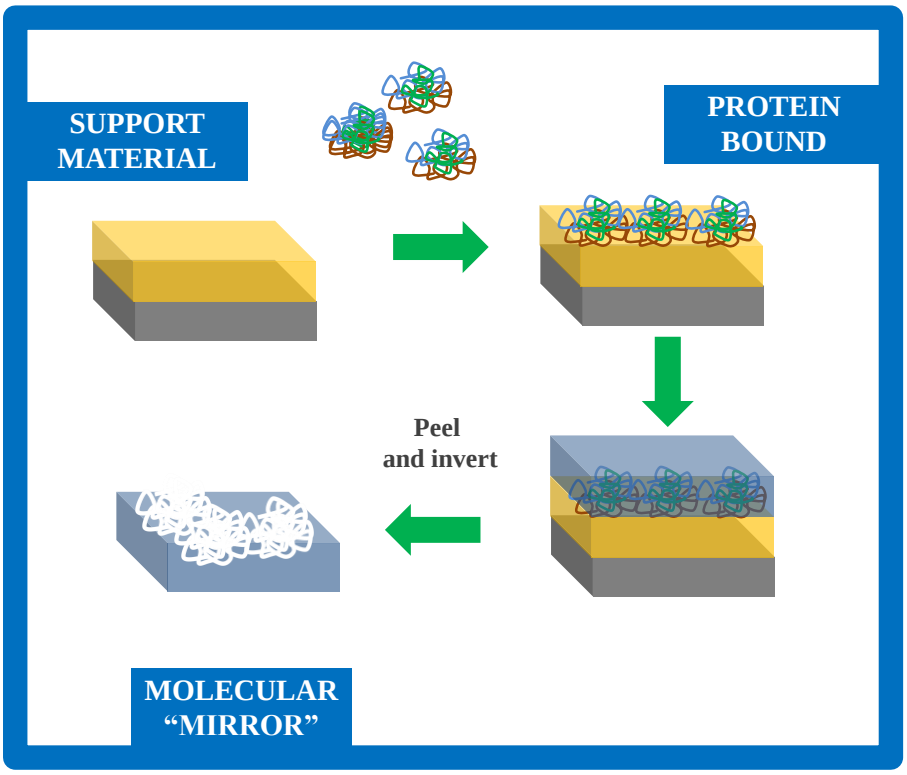

Figure 7: Surface imprinting approach. Formation of "molecular mirrors" by casting replicas of protein molecules adsorbed on mica surfaces.

As mentioned before, the imprinting of small molecules is today a well-established technique while the imprinting of protein is still a challenging field of research. Small molecules may be successfully imprinted through many approaches, but for mimicking proteins, surface imprinting is a more suitable technique. Though the more promising details around this technique are yet to be discovered, surface imprinting is always made on a suitable receptor surface acting as support of the MI material. Different technical approaches can be used for this purpose, such as stamp-coating/micro-contact, polymer-brush imprinting, surface grafting and electropolymerization.

2.2.3.2.1 Stamp-coating/micro-contact

The micro-contact approach to protein imprinting uses only a minimal mass of protein, which is effectively present as a monolayer to the recognition substrate in which the imprint is formed (see Figure 8).

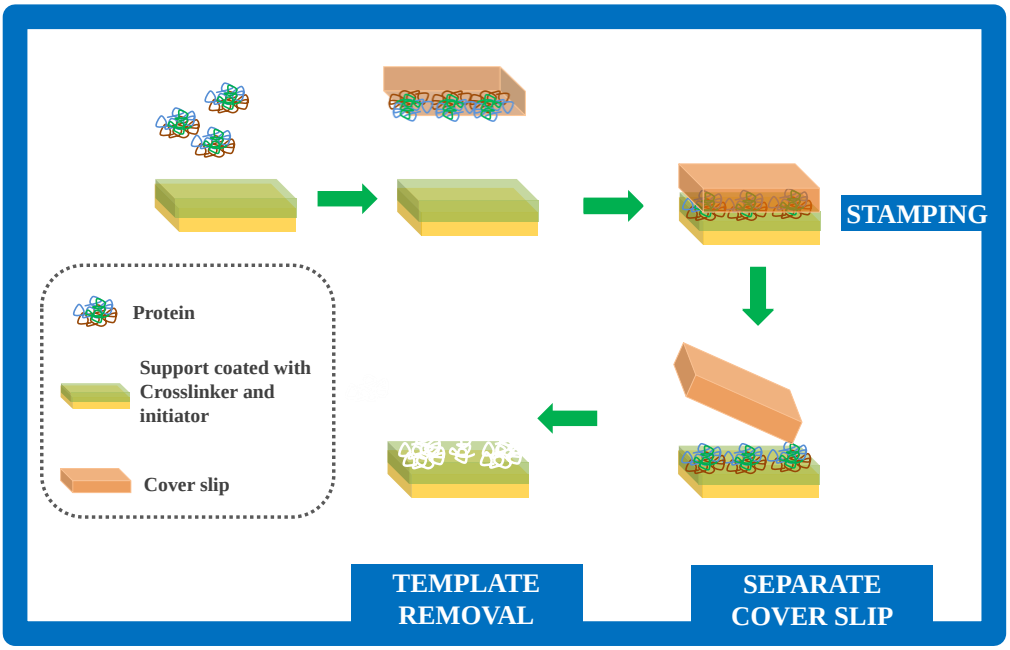

Figure 8: Surface micro-contact imprinting method.

Some researchers have employed the use of a stamp to physically position the template moiety during the imprinting process (Bernard et al. 1998; Piletsky et al. 2000). Chou et al., described a C-reactive protein thin-film molecularly imprinted polymers formed using a micro-contact approach. In this study they formed a single layer of protein on a microscope cover glass, together with a functional monomer, and then contacted this on a glass support carrying the cross-linking agent. After UV induced polymerization the cover glass was able to be easily removed to allow surface washing of the polymer and evaluation of its affinity in subsequent rebinding protocols (Chou et al. 2005).

A systematic approach to forming micro-contact imprints of CK was described by Chen et al, where PEG dimethacrylate was selected as crosslinker. The functional monomer, methacrylic acid, was chosen from a panel of six candidates by showing the highest differential affinity with respect to a NI polymer. The resulting polymer showed excellent imprint recognition, with CK intensive binding to the imprinted sites (Chen et al. 2009).

Another work based on thin-film Myo MIP produced using a micro-contact approach was reported by Lin and co-authors (Lin et al. 2007b), combining MI and micro-contact printing techniques to prepare a polymer thin-film as an artificial antibody (Lin et al. 2006b). Several proteins including lysozyme, ribonuclease A and Myo were adsorbed on cover glasses that were pre-treated with hexamethyldisilazane. These protein stamps were then contacted with different monomer solutions on a glass slide substrate. Photopolymerization yielded the MI layer. This technique, analogous to micro-contact printing, allowed the rapid, parallel synthesis of MI of different compositions, and required very small volumes of monomer solution. It also avoided potential solubility problems with the molecular targets. Of several cross-linking monomers screened, tetraethyleneglycoldimethacrylate (TEGDMA) gave the most selective lysozyme binding, while PEG dimethacrylate were most selective for ribonuclease A and Myo (Lin et al. 2006b).

Blinka et al., demonstrated that a porous silica surface modification, combined with micro-contact printing, could be an effective method for enhanced protein patterning and adsorption on arbitrary surfaces (Blinka et al. 2010). Compared to

conventional chemical treatments, this approach offered scalability and long-term device stability without requiring complex chemical activation. Two chemical surface treatments using functionalization with the commonly used APTES and GA were compared with the nanoporous silica surface on the basis of protein adsorption. The deposited thickness and uniformity of porous silica films were evaluated for fluorescein isothiocyanate-labelled rabbit immunoglobulin G protein printed on substrates via patterned PDMS stamps. A more complete transfer of proteins was observed on porous silica substrates compared to chemically functionalized substrates (Blinka et al. 2010).

Liao et al. reported a new approach for assessing the binding selectivity of MIP by mass spectrometry-based profiling system. The imprinting process presented for this purpose consisted in three steps: i) Myo adsorption on glass surface, by van der Waals' force, ii) protein stamp brought into contact with the substrate and UV irradiation application to initiate polymerization, and (iii) protein template removal from the MI film. The imprinting sensor exhibited good results in terms of selectivity for Myo resulting in a successful imprinting of Myo. However, the limited selectivity with respect to albumin limited its immediate application (Liao et al. 2009).

Micro-contact printing technique was also developed by Chou et al. to form MI thin-films for recognition of several biomarkers, such as CRP, ribonuclease, lysozyme and Myo. Micro-contact imprinting polymers were formed between two glass surfaces. The nanocavity sensing layer was synthesized by UV polymerization and the resulting imprinted surface reflected the topographic features of the template molecules. The authors found the nanocavities by optimizing the composition ratio between the lowest affinity cross-linker and the highest affinity functional monomer. This way, highly selective recognition sites for a wide variety of template proteins were able to be formed (Chou et al. 2007).

2.2.3.2.2 Polymer-brush imprinting

Zdyrko et al. described an original approach for a surface protein imprinting employing grafting of polymer brushes. Protein molecules were first chemically bound to an ultrathin polyglycidylmethacrylate reactive polymer layer and later

removed by protease treatment. Unlike the PEG-coated surface, the imprinted surfaces were able to absorb the protein template. Additionally, they were able to differentiate between bovine serum fibrinogen and BSA (Zdyrko et al. 2009).

2.2.3.2.3 Surface grafting

Yildirim et al. described the construction of Myo imprinted films by grafting from silicon surface. MI films on silicon wafers were prepared by surface-initiated atom transfer polymerization. 2-Hydroxyethyl methacrylate and ethylene glycol dimethacrylate were used as functional monomer and cross-linking agent, respectively. The MI films exhibited higher rebinding capacity than the NIP films at all solution concentrations of Myo (Yildirim et al. 2012).

Wang et al., showed a potentiometric protein sensor based on the surface MI technique using SAMs of alkanethiol with hydroxyl terminal groups as the matrix material, and target protein molecules as the template. The sensing layer was created on the surface of the gold-coated silicon chip, acting as an electrochemical transducer. Potentiometric measurement demonstrated that the sensor could selectively detect Myo or Hmg molecules, either with or without the presence of other protein molecules in the same solution (Wang et al. 2008). The Figure 9 shows an example of surface grafting process on the surface of silica beads.

2.2.3.2.4 Electropolymerization

The electropolymerization (Syritski et al. 2008) is a helpful technique once it allows to control the thickness of the film (by controlling the number of cycles or the applied current) and its morphology (by suitable selection of the solvent). The mechanism behind the polymer formation involves the generation of a radical by electro-oxidation reaction, with subsequent polymerization reaction (Figure 10). The formation of thin polymers with molecular recognition directly on the transducer surface usually follows the electrochemical polymerization (Sharma et al. 2012). The electropolymerization typically requires a functional monomer, a porogenic solvent, the template and sometimes a cross-linking monomer in contact with the transducer surface. Moreover it is not necessary an initiator, UV light or heat.

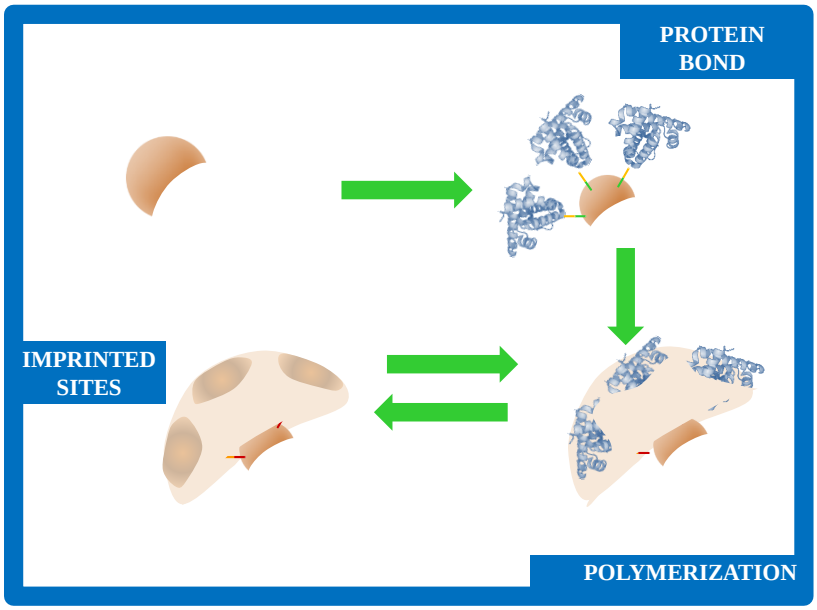

Figure 9: Surface grafting of polymer around template molecules.

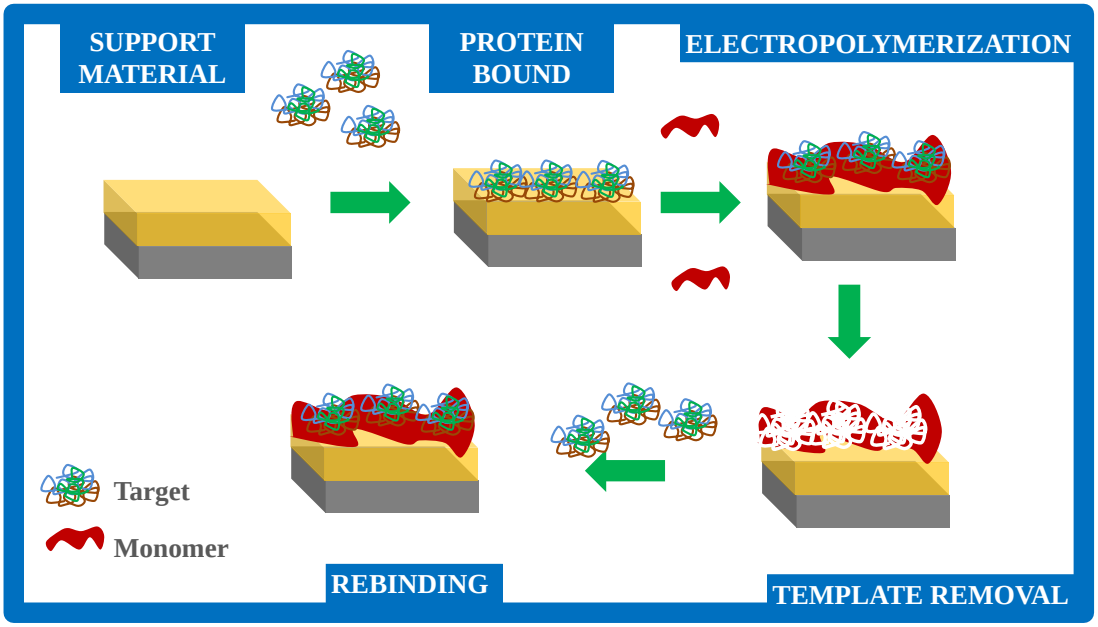

Figure 10: Schematic synthesis of by electropolymerization.

The factor responsible for the initiation of the polymerization defines its. The electrochemical polymerization, is initiated by the electro- oxidation of the radical (Zhang et al. 2009a); the thermo polymerization initiated by a thermally generated radical (Gao et al. 2012); and photopolymerization, initiated with a light source (Fuchs et al. 2011). Other procedures to construct imprinted polymeric

thin films directly at the transducer surface consist in the drop coating where a thin imprinted polymer film is obtained by depositing a certain volume of polymerization mixture (Pesavento et al. 2009).

These surface imprinting approaches are in the basis of biorecognition methods that but there are still some limitations as difficulty in integrating them with a transducer or converting the binding event into a signal. These disadvantages may be reduced with the use of imprinted nanomaterials that present higher affinity and sensitivity to target analyte, more homogeneous distribution of recognition sites and an increase of tuneable flexibility of shapes and sizes. The use of imprinted nanomaterials also provide better dispersibility in analyte solutions reducing greatly part of the resistance mass transfer and exhibiting a fast binding kinetics, greater surface-to-volume ratio (Xie et al. 2008).

Until now, no research work was reported with biomimetic materials produced by electropolymerization for CK-MB or Myo cardiac biomarkers. The only specific work in this context is that of Karimian et al. (Karimian N 2013), most recently published for troponin T. The authors report a successful electropolymerised imprinted film for troponin, by mixing the cardiac biomarker in the solution with o-phenylenediamine, acting as monomeric parts of the film.

2.2.3.3 Epitope imprinting

In epitope MI, only a peptide sequence on the surface of the protein acting as epitope region is isolated and imprinted in the material. When the original protein is exposed to that imprint, the small peptide on its surface that was imprinted recognizes its spatial and chemical mimic in the polymer and binds. In this approach, only a portion of the entire molecule is needed for preferential binding, which shows potential for optimization of protein immobilization. A few approaches of epitope imprinting have been presented in the literature.

Nishino et al. (Nishino et al. 2006) used epitope sequences from several target proteins (cytochrome C, alcohol dehydrogenase, and BSA) to create mixtures with C-terminal-imprinted AAM/*N,N'*-methylenebisacrylamide (NNMBA) polymer thin films. This was done by stamp coating, in which the N-terminal of the

epitope peptide sequence was immobilized on a silanized silicon surface functioning as the stamp. The authors demonstrated that terminal peptides created better imprinting targets because their structure was unambiguously defined. In contrast to other regions of the target protein, these regions have fewer interactions with the protein secondary structure, which may hinder or disturb binding. According to the authors, the minimum length of peptide necessary to create a unique recognition for target protein was around 9 aminoacids. An exposed C-terminal seemed favourable, because this site was less prone to post-translational modifications (Polevoda and Sherman 2000).

Bossi et al., described the synthesis of a fingerprint-imprinted polymer for rational selection of peptide epitope templates for the determination of NT-proBNP biomarker by MI. Good results were obtained in terms of imprinting factor, binding capacity and ability to rebind the template in a complex sample, composed of the whole digests of NT-proBNP (Bossi et al. 2012).

A quantitative method using artificial antibody to detect CKs was developed by Tai co-workers. A linear epitope sequence was selected based on an artificial-epitope mapping strategy. Nine different MIs corresponding to the selected peptides were developed on quartz crystal microbalance (QCM) chips. Good results were obtained in terms of linear range and LOD for CK-MB (Tai et al. 2011).

Overall, the epitope approach seems to present some advantages, compared to the previous MI approaches. Most importantly, the conformation of the whole protein does not need to be retained and the selectivity in protein recognition can be controlled by the choice of epitope and its length. Also, template removal from the imprinted matrix is more easily achieved than with whole protein. The main disadvantage of this approach is that a good knowledge of the protein structure is required and the custom synthesis may be required in order to prepare the templates which may be relatively costly and time-consuming. In addition, the sensitivity of the material may not be as high as when the complete protein is imprinted, mostly because only one epitope region is used for binding.

Regardless of the approach used for imprinting proteins for biosensing applications, the practical use of such principle is strongly correlated to the signal being

generated after the antigen interaction (cardiac biomarker), which is turn depends of the selected transducer system.

2.3 Transducers

The nature of the transducing surface and of the detection are fundamental aspects for a well succeeding biosensor. The gap between the transducing surface and imprinted layers is bridged by surface modification. The nanomaterials used as substrate can be fashioned with a wide range of small organic ligands and large biomacromolecules (Turner et al. 2006), following quite distinct approaches, such as SAM and covalent attachment.

Different sensor platforms for detection of CVD with electrochemical, optical (Cho et al. 2009; Dutra and Kubota 2007; Heyries et al. 2009; Hill and Martins 2006; Wolf et al. 2004) or magnetic nature (Ibraimi et al. 2006; Monson et al. 2009) have been reported in the literature. These have been presented in Table 2, highlighting the transduction, the biorecognition element, the concentration levels involved in the analytical response, the target biomarker and the ability to carry out single or multi-analyte detection, in conventional or microfluidic conditions.

In general, fluorimetric and chemiluminometric methods allow reaching quite low LODs, which is quite interesting especially for TnT that has a very low cut-off level. These experiments are typically simple, rather quick and inexpensive, but not suitable for use in emergency situation because it employs mixing several reagents, may require heat and some time before reading. Surface Plasmon Ressonance (SPR) methods are more sensitivity than the conventional luminometric ones, but the equipment involved is too expensive to be used in POC context.

Table 2: Cardiac biomarkers detection with different transducers and their detection range reported in the literature.

Target Biomarker	Transduction platform	Concentration Response Range	Assay type	Biorecognition element	Reference
Myo	Fluorescence	—	Microfluidic with multi-analyte	Antibody	(Wolf et al. 2004)
TnI	Fluorescence	—	Microfluidic with multi-analyte	Antibody	(Wolf et al. 2004)
TnI	Fluorescence	0.1–100 ng/mL	Single analyte	Antibody	(Song et al. 2011)
TnT	ELISA	0.1–100 ng/mL LOD: 0.027 ng/mL	Single analyte	–	(Heyries et al. 2009)
Myo	ELISA	20–230 ng/mL LOD: 16 ng/mL	Single analyte	–	(Wu et al. 2010b)
TnI	ELISA	4.3×10^4 to 4.3×10^6 ng/mL	Single analyte	–	(Torabi et al. 2007)
Myo; CK-MB; TnI; Fatty acid-binding Protein (H-FABP)	Chemiluminescence	Myo: 1.2 ng/mL; CK-MB: 0.6 ng/mL TnI: 5.6 ng/mL FABP: 4 ng/mL	Multi-analyte	–	(Cho et al. 2009)
TnI	Colorimetric; PDMS- gold nanoparticle composite film	10^4 to 4.3×10^6 ng/mL	Single analyte		(Leung et al. 2005)
TnI	Electrochemiluminescence	0.002 ng/mL	Single analyte	–	(Park et al. 2010)

Table 2 Cardiac biomarkers detection with different transducers and their detection range reported in the literature **(cont.).**

Target/biomarker	Transduction platform	Concentration Response Range	Assay type	Biorecognition element	Reference
TnT	SPR	0.03 – 6.5 ng/mL LOD: 0.01 ng/mL	Single analyte	Antibody	(Dutra and Kubota 2007)
TnT	SPR	0.05 – 5.5 ng/mL LOD: 0.05 ng/mL	Single analyte	Antibody	(Dutra et al. 2007)
Myo and TnT	SPR	LOD: below 1 ng/mL	Multi-analyte	Antibody	(Hoa et al. 2009)
TnT	SPR	100 ng/mL	Single analyte	Antibody	(Liu et al. 2011a)
TnI	SPR	0.068 ng/mL	Single analyte	Antibody	(Kwon et al. 2011)
TnI, Myo	Optical fiber	TnI: 7×10^{-3} ng/mL Myo:70 ng/mL	Multi-analyte	Antibody	(Tang and Kang 2006)
TnT	Optamagnetic	0.03 ng/mL	Single analyte	Antibody	(Dittmer et al. 2010)
TnT	Optamagnetic	0.0039 – 3.9 ng/mL LOD: 0.0117 ng/mL	Single analyte	Antibody	(Bruls et al. 2009)

Table 2: Cardiac biomarkers detection with different transducers and their detection range reported in the literature **(cont.).**

Target Biomarker	Transduction platform	Concentration Response Range	Assay type	Biorecognition element	Reference
Myo	Faradaic, Impedance/interdigitated electrodes	100 ng/mL	Single analyte	Antibody	(Tweedie et al. 2006)
TnT	Non-Faradaic, impedance/ interdigitated electrodes	0.07– 6.83 ng/mL	Multi-analyte	Antibody	(Ruan et al. 2004)
TnI	Faradaic, nanostrutural gold and carbon nanotubes composite	0.01 ng/mL	Microfluidic with single analyte	Antibody	(Zhou et al. 2010)
TnT	Faradaic, streptavidin-microsphere modified screen printed electrodes	0.2 ng/mL	Single analyte	Antibody	(Silva et al. 2010)
Myo	Faradaic, nanoparticles modified electrodes	17.8– -1780 ng/mL	Single analyte	Antibody	(Shumiantseva et al. 2010)
TnI	Faradaic, gold nanoparticles modified ITO electrodes	1 – 100 ng/mL	Single analyte	Antibody	(Ahammad et al. 2011)

Table 2: Cardiac biomarkers detection with different transducers and their detection range reported in the literature **(cont.).**

Target Biomarker	Transduction platform	Concentration Response Range	Assay type	Biorecognition element	Reference
Myo	Faradaic, nanoparticles modified Fe graphite electrodes	5 ng/mL	Single analyte	Antibody	(Suprun et al. 2011)
TnT	Conductance, metal-oxide semiconductor-compatible silicon nanowire	In buffer solution - 10^{-6} ng/mL Undiluted human serum – $3x10^{-6}$ ng/mL	Single analyte	Antibody	(de Vasconcelos et al. 2009)
Myo	Polyaniline nanowires/ conductance	1.4 ng/mL	Single analyte	Aptamer	(Qureshi et al. 2010)
TnI	SnO_2 nanobelt, field-effect transistor (FET) sensor/IV curve	2 ng/mL	Single analyte	Antibody	(Arakaki et al. 2004)
CK-MB	Magnetometer sensing coil/ coated paramagnetic particles	1 – 15 ng/mL	Multianalyte	Antibody	(Ibraimi et al. 2006)
TnI	Magnetic tweezer /magnetic beads	0.368 ng/mL	Single analyte	Antibody	(Monson et al. 2009)

The electrochemical studies using EIS seem to be a fair alternative to these optical approaches, also offering the possibility to carry out *on-site* analysis and adjust the technique to disposable devices.

2.3.1 Electrochemical

Electrochemical biosensors are affinity-based biosensors, using an immobilized recognition element that binds selectively to the target molecule. When the target binds to the recognition element at the surface of the biosensor, it generates current and/or voltage changes at that surface.

Based on their operating principle, electrochemical biosensors can employ potentiometric, amperometric and impedimetric transducers, converting the chemical information into a measurable electrical output signal. Due to their low cost and simple miniaturization, electrochemical biosensors hold great promise for POC applications, where minimizing size and cost are crucial. Potentiometric-based methods are amongst the oldest ones, usually correlated by all to the conventional pH glass electrode.

2.3.1.1 Potentiometry

Potentiometry is an electro-analytical tool in which the potential of an electrochemical cell is measured under conditions of no current flow (or near zero current) (Christopher. Brett 1993). The potentiometric electrochemical cell is composed by an anode and a cathode, and their potential difference is indeed the potential being measured at the electrochemical cell.

The developed potential at the electrochemical cell results from the free energy change (ΔG) that occurs if the chemical were to proceeds until the equilibrium condition (Equation1) has been reached.

$$\Delta G = -nFE \qquad \textbf{Equation1}$$

In this equation, E is the maximum potential difference between two electrodes, *F* is Faraday's constant (96,485 C mol^{-1}) and *n* is the number of electrons exchanged.

When the reaction takes place in non-standard conditions, the Nernst equation (Equation 2) to determine the cell potential should be used.

$$E = E_0 + \frac{2{,}303RT}{z_A F}\log\left[a_A + \sum_{i=1}^{n} K_{A,B_i}^{pot}\left(a_{B_i}\right)^{z_A/z_{B_i}}\right] \qquad \textbf{Equation 2}$$

In this, E_0 is the cell potential at standard conditions, *R* is the universal gas constant (8.314 J/(Kmol)), T is the temperature (in Kelvin), *n* is the charge of the ion or number of electrons participating in the reaction and *K* is the selectivity coefficient.

A simple example of the potentiometric potential generated at the cell would be assisting the ion concentration gradients across a semi-permeable membrane. This system is indeed the basis of measurements carried out with ion-selective electrodes (ISEs) (Buck and Lindner 1994). ISEs contain a selective membrane that enables a selective discrimination towards the targeted ionic species, and thus acts like a "semi-permeable" membrane. This selective membrane is separating the compartments of reference and to the potentiometer sample solutions, or it is casted over a solid conductive support that transmits all electrical changes occurring at the membrane (Amemiya 2007).

An ISE is always combined with a reference electrode in order to obtain a potential difference that is also known as electromotive force (emf). Both reference and indicator electrodes are immersed in the test solution and connected through a salt bridge. The reference consists in an aqueous bridge electrolyte in contact with the sample solution via liquid junction. The potential of the reference electrode

should be constant and stable along the experiments, in order to promote a stable potential independent of the environmental conditions. The Ag/AgCl reference electrode is the one most widely used due to its simplicity and inexpensive design. The Ag/AgCl reference electrode is composed by a silver wire with an electrolytic coating of a thin layer of silver chloride. The wire is immersed in a solution of potassium chloride (KCl) of known concentration, saturated with AgCl.

Compared to other analytical systems, potentiometry with ISEs displays several advantages including: i) high signal stability over time and respond over a wide range of concentrations; ii) good selectivity; iii) easy operation; iv) easy construction in the laboratory; v) low cost of the detectors and the equipment involved; vi) short time; vii) and low cost of each analytical determination.

The selective membrane of an ISE is at the core of its analytical response, also displaying low solubility, electrical conductivity and selective reactions with the target analyte (Buck and Lindner 1994). Membranes with mobile local exchangers are used often, being named as non-crystalline. They consist of three basic components: an ion-exchanger/ionophore, a mediator solvent and a polymer matrix. The exchanger/ionophore is the material responsible for the electrochemical response of the electrode and can be positive or negatively charged or neutral. The polymer matrix is the body of the selective membrane and should join all ingredients inside it. It should display rubbery properties at room temperature in order to enable/enhance ion-exchange processes. Most of the polymer matrices used display rubbery properties because they have been added of a plasticizer, also known as the mediator solvent.

The electrode body using solid-conducive supports for casting the selective membrane is typically very simple. A typical construction procedure of such device is presented in Figure 11. In this, the solid conductive support made of carbon was introduced in a Perspex tube over a copper contact connected to an electrical wire. Solid contact electrodes are among the most used potentiometric sensors due to simplicity of construction and operation and the longer lifespan, be-

cause leaching the electroactive materials from the selective membrane by osmotic pressure of the reference solution does not take place in these solid contact supports.

Overall, ISEs most often used are based on selective PVC membranes that include a suitable ionophore for analyte recognition, being this material at the core of the electrode performance. No such device was reported for the cardiac biomarkers of interest in this work.

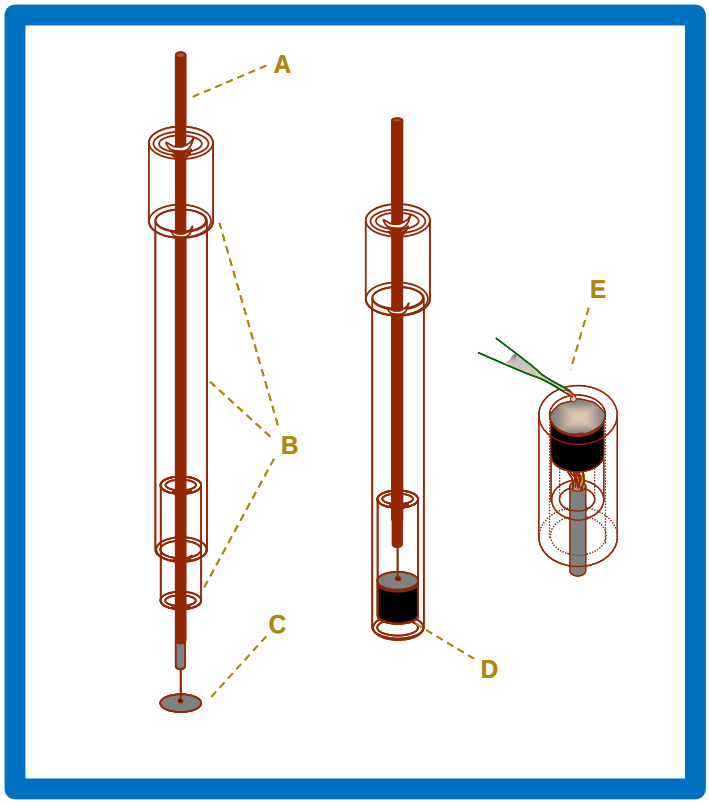

Figure 11: Scheme of the ion- selective electrode construction. A: electrical wire; B: Perspex tube; C: copper circle; D: carbon paste: E: membrane.

2.3.1.2 Cyclic voltammetry

CV is a simple, fast and straightforward electroanalytical technique providing qualitative and quantitative information about any electroactive species. It consists in applying a linear potential (E) sweep at a steady scan-rate (the rate of change of potential with time, $\nu=\Delta E/\Delta t$) to the working electrode (WE), leading to sequential linear potential increases or decreases between minimum and maximum potential limits. The CV plot measures the resulting electrical current at the electrode surface (I) against applied the potential. The application of this potential sweep is controlled by a reference electrode and has a triangular waveform when plotted against time (Borges), 2013), with minimum and maximum potential limits (E_{min} and E_{max}, respectively) established within the procedure (Figure 12).

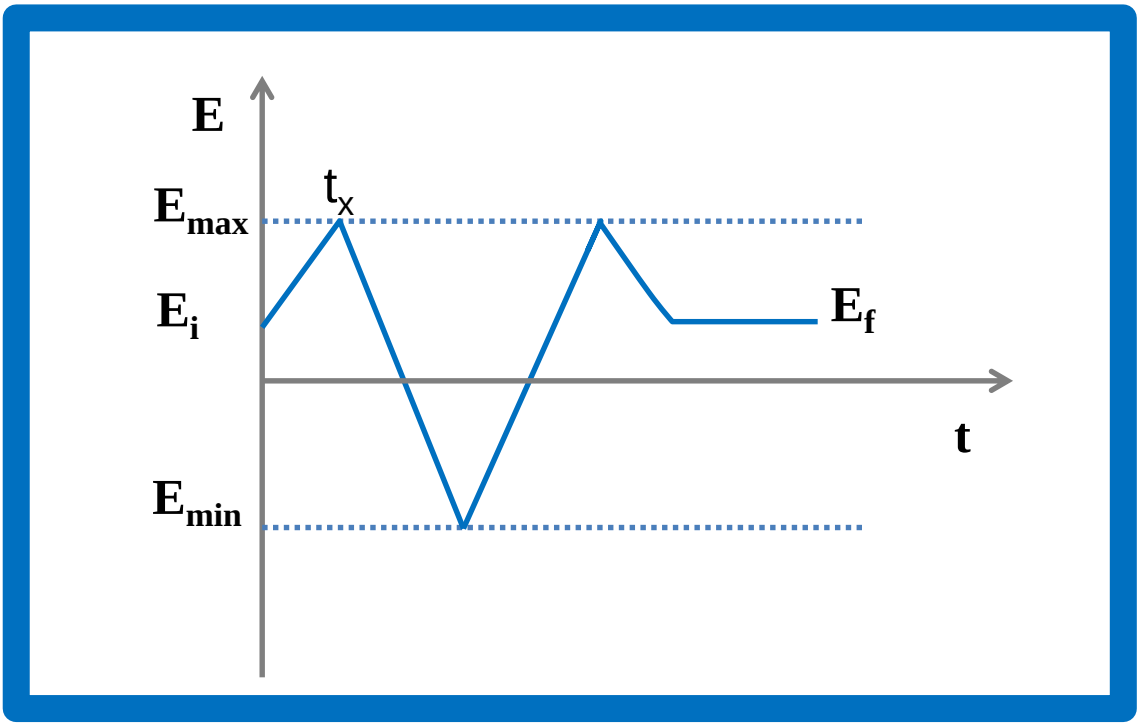

Figure 12: Variation of the applied potential to the WE with the time in CV: E_i- Initial potential; E_f- final potential; E_{min}– minimum potential; E_{max} - maximum potential, t_x- time for the reverse scan.

The electrical current response of the electrode *versus* the applied potential is named as cyclic voltammogram and has different characteristics according to the type of redox system involved. The shape of the observed voltammogram depends on the reversibility of the redox couple (O/R), and/or the electrostatic repulsive or attractive forces between the redox centres. Regarding the redox couple features, mostly these can be subdivided in reversible, quasi-reversible and irreversible.

2.3.1.2.1 Reversible systems

When the kinetics of couple O/R is fast enough to keep the electron transfer process in equilibrium, the product of the initial oxidation or reduction is oxidized or reduced, on reversing the scan direction. The typical response of such reversible redox process may be seen in Figure 13.

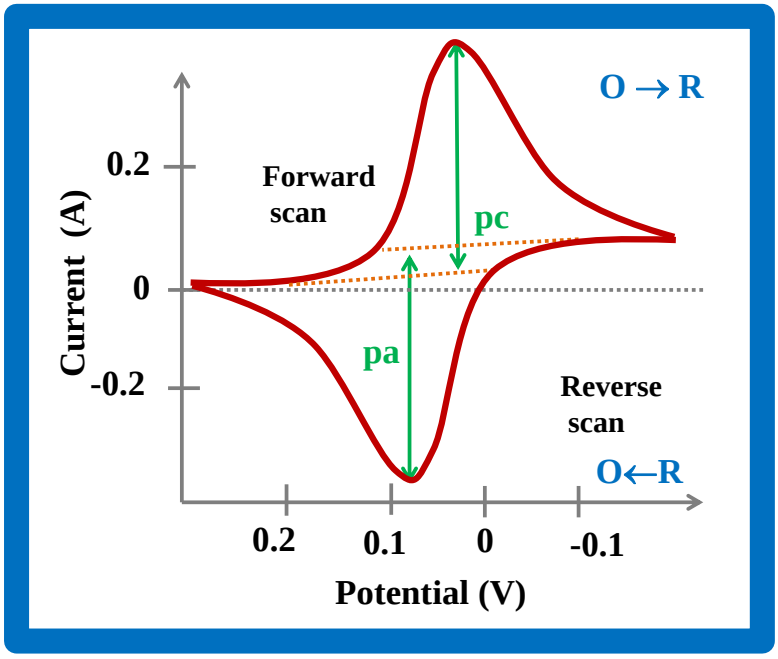

Figure 13: Typical voltammogram for a reversible system when Pa and Pc are the anodic and cathodic potential, respectively.

Assuming that the scan begun at a potential well positive for the reduction to occur, when the electrode potential reaches the vicinity of formal potential (E^0) of the redox couple O/R, the reduction begins and current starts flowing. As the potential shifts to more negative values, the surface concentration of oxidized species drops; hence the flux to the surface (and the current) increases. As the potential moves past E° towards more negative values, the concentration of the oxidized species at the surface drops to nearly zero, mass transfer of species to the surface reaches a maximum rate, and then it declines as the depletion effect sets in, thus generating a peak. A similar but opposite peak may be observed in the reverse scan, prevented that a reversible redox system is present. The reduced species generated in the forward half-cycle are re-oxidized and the anodic peak appears (Yuan et al., 2010).

The first theoretical analysis of the wave shape for a reversible system was achieved by Randles and Sevcik (Randles 1948). The Randles-Sevcik equation allows obtaining the peak current (I_p) as indicated in Equation 3.

$$Ip = (2.69\times10^5)n^{3/2}ACD^{1/2}\nu^{1/2} \qquad \textbf{Equation 3}$$

In this equation, n is the number of electrons involved in the reaction, A is the electrode surface area (cm^2), D is the diffusion coefficient of the species ($cm^2\ s^{-1}$), C is the bulk concentration of the species (mol dm^{-3}), ν is the scan-rate ($V\ s^{-1}$), and I_p is the peak current (A). Overall, the information provided by the Randles-Sevcik equation can be presented in the form of a diagnostic tool for cyclic voltammograms of reversible systems (Bard and Faulkner 2001; Brett 1993) where the following equations are involved:

$$I_p \alpha \upsilon^{1/2}\ ;\ E_p \text{ independent from } \upsilon;\ \ |E_p - E_{p/2}| = (1RT/\ nF) \qquad \textbf{Equation 4}$$

$$\Delta E_p = \left| E_{Pa} - E_{Pc} \right| \neq 0 = (2.3RT/nF) = 59.0/n \quad \textbf{Equation 5}$$

$$\left| Ipa / Ipc \right| \neq 1 \quad \textbf{Equation } 6$$

When all these conditions are verified simultaneously, the peak separation can be used to determine the number of electrons involved in the electron transfer process of reversible systems. If one of the above conditions is missing, the system cannot be considered reversible, and should be considered *as quasi-irreversible*, or irreversible depending on the extension of the irreversibility (Yuan et al., 2010)..

2.3.1.2.2 Irreversible and quasi-reversible systems

In irreversible processes the electron transfer kinetics is very slow-moving compared to the time-scale of the sweep. In such condition, concentrations of the oxidized and reduced species do not follow the Nernst equation and the individual O/R peaks are reduced in size and widely separated. This means that totally (O/R) irreversibility is characterized by a shift of the peak potential with sweep rate and peak intensity (Borges 2013). In irreversible systems the linear potential sweep and CV lead to the same voltammetry profile, since no reverse peaks appear on changing the sweep direction, which means that re-reduction or re-oxidation cannot occur (Figure 14).

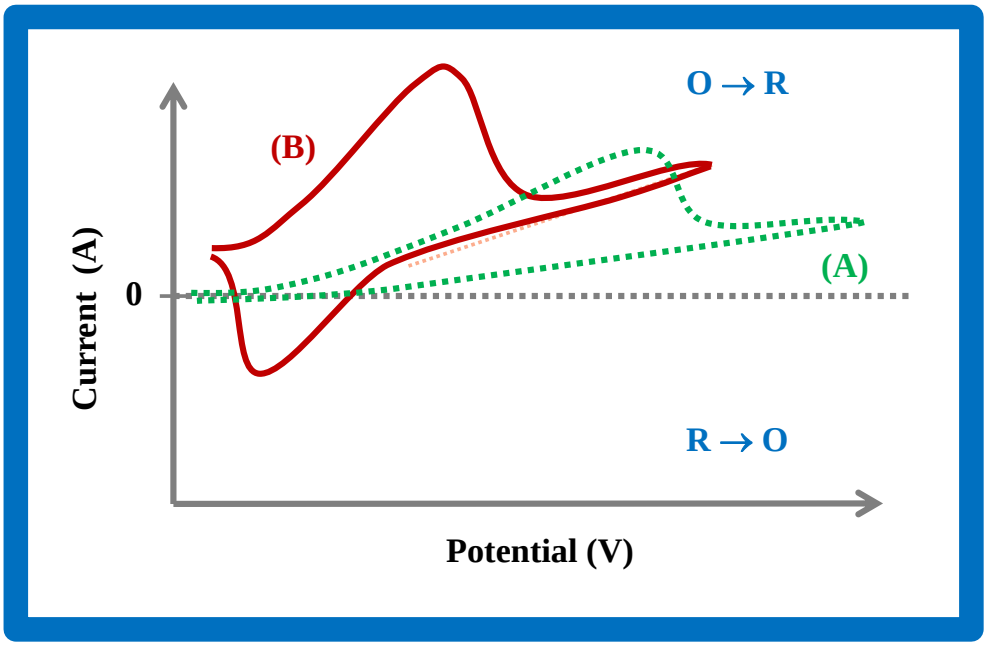

Figure 14: Typical voltammogram for *irreversible* (A) and *quasi-reversible* (B) systems.

In order to observe the net current, the forward process must be so strongly activated, by application of overpotential, that the reverse reaction is virtually completely inhibited (Bard and Faulkner 2001; Brett 1993)

In completely irreversible processes the peak current (I_p) is given by:

$$Ip = (2.99\times10^{5})\alpha^{1/2}n^{3/2}ACD^{1/2}\nu^{1/2} \quad \textbf{Equation 7}$$

From the Equation 7 it is clear that the peak current (I_P) for the oxidized or reduced species is still directly proportional to the concentration of the specie (C) and to the square root of the scan rate ($\nu^{1/2}$), but is lower in height when compared with reversible systems.

From the information provided by this equation it can be deduced the following diagnostic criteria for cyclic voltammograms of totally irreversible systems:

$I_p \alpha \upsilon^{1/2}$; E_p independent from υ;

$$\left| E_p - E_{p/2} \right| = 47.7/an(mV) \quad \textbf{Equation 8}$$

$$\Delta E_p = \left| E_{Pa} - E_{Pc} \right| \geq 59.0/n \quad \textbf{Equation 9}$$

$$\left| Ipa/Ipc \right| = 1 \quad \textbf{Equation 10}$$

However, the electrode processes are not always easy and fast or very sluggish, and sometimes we must consider the whole voltammogram characteristics. In such case the net current, which is controlled by both the charge transfer and mass transport, involves appreciable activated components from the forward and reverse charge transfers. In these systems the reverse appears but is smaller than the forward peak, which means that $\Delta Ep = \left| E_{pa} - E_{pc} \right|$. These are called *a quasi-reversible or quasi-Nernstian system* for electrochemically quasi reversible reactions, the surface concentration is controlled both by kinetics and diffusion processes (Yuan et al., 2010).

The peak shape and associated parameters can be expressed by a parameter, Λ, which is a quantitative measure of the reversibility, being effectively defined as the ratio kinetics/transport:

$$\Lambda = \frac{k_0}{(D_o^{\alpha_a} D_R^{\alpha_c} \alpha)^{1/2}} = \frac{k_0}{(D_o^{1-\alpha^c} D_R^{\alpha_c} \alpha)^{1/2}} \quad \textbf{Equation 11}$$

$$\sigma = \nu(nF/RT).$$

When the diffusion coefficients of the oxidized and reduced species are equal $D_o = D_R = D$ the equation can be rewritten:

$$\Lambda = k_o D^{-1/2} \sigma^{-1/2} \quad \textbf{Equation 12}$$

Showing that when scan rate (ν) increases, when σ is high, the reversibility degree is low Λ is small.

The parameter Λ can be estimated by using the parameter ψ, which expresses the relation between the separation of the anodic and cathodic peaks with the degree of reversibility (Equation 13).

$$\psi = \Lambda \pi^{1/2} = \frac{K_0}{(D\pi\nu\frac{nF}{RT})^{1/2}} \quad \textbf{Equation 13}$$

This parameter can be found in the literature (Christopher M. A. Brett 1993), assuming that α = 0.5 ψ allows obtaining information about the different type of systems involved in the electrodes.

As general conclusion, when ψ increases, at very slow sweep rate (ν), the system approaches the reversibility. For small values of ψ, at very fast sweep rate, the system exhibits an irreversible behaviour in which there is a decrease in the peak current relative to the reversible case and increasing separation between the anodic and cathodic peaks (Yuan et al., 2010)...

2.3.1.3 Electrochemical impedance spectroscopy

EIS is one of the electroanalytical techniques used for analysing electrochemical processes occurring at the interface electrode/solution. It measures the impedance of a system over a range of frequencies, and therefore the frequency response of the electrochemical system, being related to the electrical resistance.

The electrical resistance is a very well-known concept, corresponding to the ability of a circuit element to resist the flow of electrical current. Ohm`s law (Equation 14) defines resistance (R) in terms of ratio between voltage (E) and current (I), as follow:

$$R = \frac{E}{I} \quad \textbf{Equation 14}$$

This equation is applied to only one circuit element, the ideal resistor. The ideal resistor displays several simplifying proprieties including: i) it follows Ohm´s law at all current and voltage levels; ii) its resistance value is independent of frequency; iii) AC (alternating current) and voltage signals though a resistor are in phase with each other.

Impedance is a measure of the ability of a circuit to resist the flow of electrical current, but it is not limited by the simplifying proprieties listed above. The impedimetic approach consists in the application of a small sinusoidal excitation signal to the WE of the electrochemical system under investigation and measure the subsequent response of the system in steady-state (Yuan et al., 2010)..

In EIS, the current signal can be analysed as a sum of sinusoidal functions. The potential and the current changes with the time are represented by a sinusoidal function. Figure15 shows a typical graph that illustrates the relationship between two related sinusoidal signals, such as AC and E signals rotating at the same angular frequency (ω).

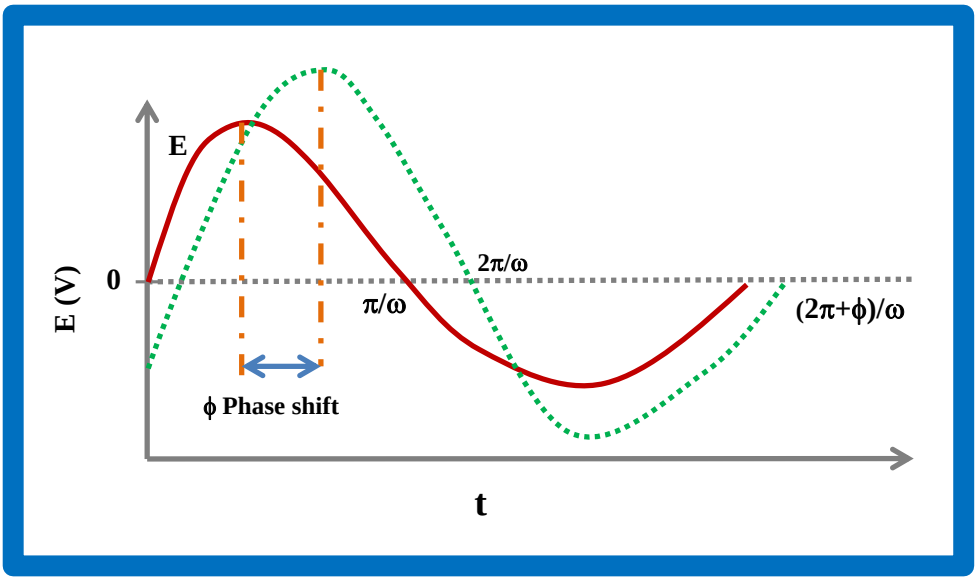

Figure15: Sinusoidal current response in a linear system after applying an alternating current

Normally, in a linear system, as shown in Figure15, the current response to a sinusoidal potential applied perturbation is sinusoidal at the same frequency but differs in phase and amplitude from the applied signal. Consequently, their phases will be separated by a certain phase angle (ϕ). The measurement of the electrode process is related to the contributions of diffusion, kinetics, double layer and coupled homogeneous reactions (Yuan et al., 2010)..

The EIS measurements can take from some minutes to hours, depending on the selected frequency range. As well, the system being measured must be at steady state throughout the time required to measure the EIS, otherwise EIS analysis tools may give inaccurate results due the growth of an oxide layer, adsorption of solution impurities, coating degradation, temperature changes, and so on. If the system is at the steady-state, it allows the study of the processes with the time constants that vary throughout several orders of magnitude (Borges 2013).

The application of a purely sinusoidal voltage to the electrode/electrolyte solution interface, expressed as a function of time, has the form:

$$E(t) = E_0 \sin(\omega t)$$ **Equation 15**

Where $E(t)$ is the applied voltage at a time t, E_0 is the oscillation amplitude of the excitation signal, and ω is the angular frequency of the sinusoidal excitation (rad s^{-1}). ω is 2π times higher than the conventional frequency (Hz) in agreement with equation:

$$\omega = 2\pi f$$ **Equation16**

In linear systems, the current response (I), which has different oscillation amplitude (I_0) and is shifted in phase (ϕ) relatively to the excitation signal, is expressed by:

$$I(t) = I_0 \sin(\omega t + \phi)$$ **Equation 17**

The electrical impedance of the system (Z) is defined as the proportionality factor between the applied potential perturbation and the current response. Using an expression analogous to the Ohm´s law, one calculates the impedance of sinusoidal system as follows:

$$Z = \frac{E(t)}{I(t)} = \frac{E_0 \sin(\omega t)}{I_0 \sin(\omega t + \phi)} = Z_0 \frac{\sin(\omega t)}{\sin(\omega t + \phi)}$$ **Equation 18**

Where the impedance (Z) is characterized by the magnitude (Z_0) and phase angle (ϕ). Remember Euler´s equation:

$$\exp(j\phi) = \cos(\phi) + j\sin(\phi)$$ **Equation 19**

It is possible to express the impedance as a complex function. In this way, the potential is described as:

$$E(t) = E_0 \exp(j\omega t)$$ **Equation 20**

Where *j* is the imaginary number defined as j = $(-1)^{1/2}$. In the same way, the current response is defined as:

$$I(t) = I_0 \sin(j\omega t - \phi)$$ **Equation 21**

Thus, the impedance can be represented as a complex number:

$$Z = Z_0 \frac{\exp(j\omega t)}{\exp[j(\omega t - \phi)]} = |Z|\exp(j\phi) = |Z|(\cos\phi + j\sin\phi)$$ **Equation 22**

Equation 22 states that in the complex plane, the impedance is composed of real $(Z' = Z_0 \cos\phi)$ and imaginary $(Z'' = Z_0 \sin\phi)$ parts, at any value of ω, as follow:

$$Z = Z' + j\,Z''$$ **Equation 23**

The Nyquist plot is obtained by plotting the real part on the X-axis and the imaginary part on the Y-axis of a chart (Figure 16). In this plot the Y-axis is negative and each point is the impedance at the specific angular frequency (ω).

As it has been indicated in the Figure 16, low frequency data are on the right side of the plot and higher frequencies are on the left. However, this criterion is only valid for electric circuits in EIS data where the impedance usually falls as frequency rises. Furthermore, on the Nyquist plot the impedance can be represented as a vector of length $|Z|$. The angle between this vector and the X-axis, generally called as a phase angle, is defined as $\phi = \arg Z$ (Yuan et al., 2010).

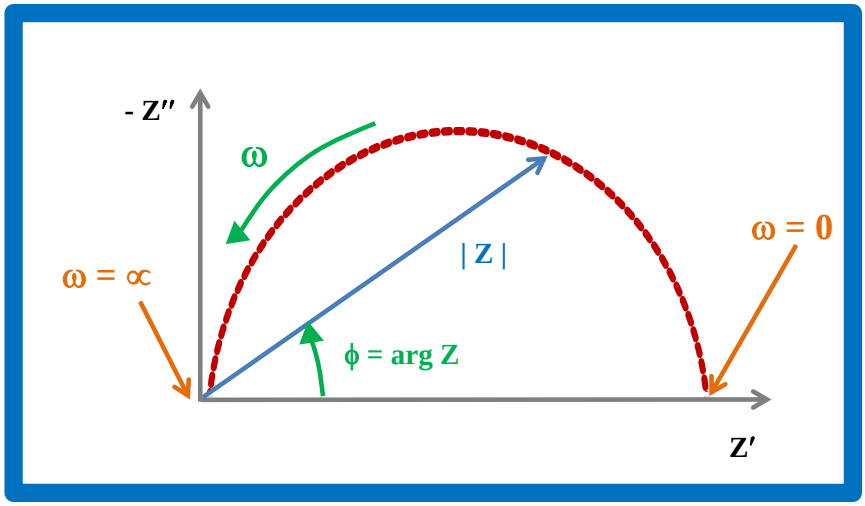

Figure 16 Nyquist plot that illustrates both real (Z′) and imaginary (Z″) components of impedance at each ω.

Nyquist plot gives a fast overview of the EIS data, allowing making some qualitative interpretations. The semicircle presented in Figure 16 is characteristic of a simple equivalent electrical circuit with a single time constant (τ), even though electrochemical impedance plots often contain several semicircles.

A more complete way of presenting impedance data involves the use of Bode plots in which the impedance is plotted with logarithm of the frequency on the X-axis and both the absolute values of the logarithm of the impedance ($\log|Z| = \log Z_0$) and the phase-shift on the Y-axis. The Bode modulus and the Bode phase plots for a simple equivalent electrical circuit with a single time constant are shown in Figure 17. Unlike the Nyquist plot, Bode plots clearly show the frequency values at each point (Yuan et al., 2010).

Randle's equivalent circuit was adopted to model the physiochemical process occurring at the electrode surface. The Randles simple circuit elements comprised mainly solution resistance (R_S), constant phase element (CPE) that accounts for the double layer capacitance, (R_{ct}) and Warburg diffusion element (W). Of these, Rct and capacitance depend on the dielectric and insulating features at the electrode/solution interface, and is controlled by the immobilization steps taking place at electrode surface (Billah et al. 2008).

Electrical-based devices are also suitable as transduction element mostly considering the low cost and portability features. Thus, the following charpters report new approaches meeting these targets for TnT, Myo, and CK-MB cardiac biomarkers.

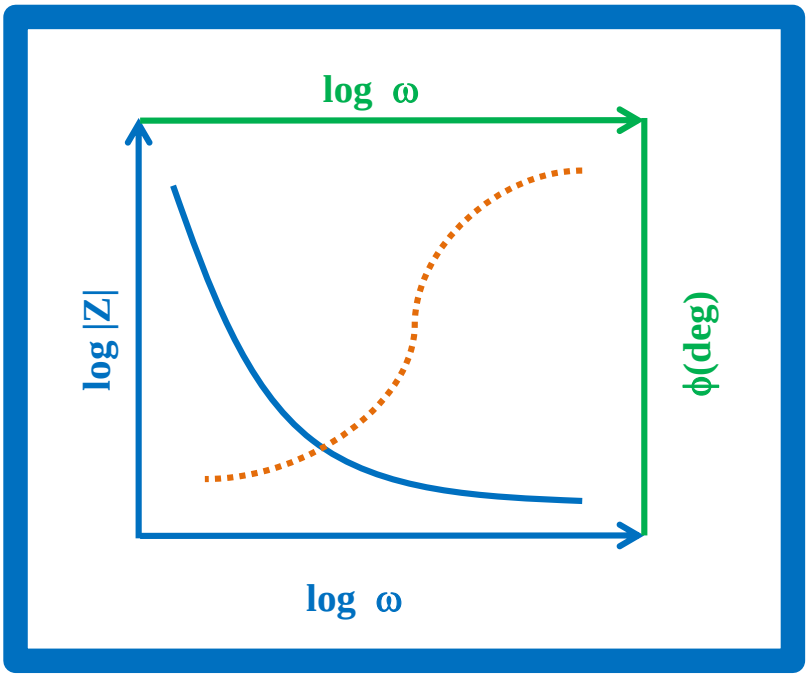

Figure 17: Typical Bode modulus (blue straight line) and Bode phase (orange dashed line) plots of an electric circuit equivalent time constant.

2.5 Final considerations

The brief review of the current methods and technologies applied for the assessment of cardiac biomarkers shows the need to establish new methods for screening cardiac biomarkers in POC. From all biorecognition elements, it seems logical that synthetic material acting like natural antibodies would be highly appreciated. New approaches are however required in order to achieve the desired selectivity compared to the natural receptors.

2.6 References

Bard A.J., Faulkner L.R., 2001. Electrochemical Methods: Fundamentals and Applications. p. 427. John Wiley and Sons, INC: New York.

Ahammad, A.J.S., Choi, Y.-H., Koh, K., Kim, J.-H., Lee, J.-J., Lee, M., 2011. Electrochemical Detection of Cardiac Biomarker Troponin I at Gold Nanoparticle-Modified ITO Electrode by Using Open Circuit Potential. *International Journal of Electrochemical Science* 6(6), 1906-1916.

Albareda-Sirvent, M., Merkoci, A., Alegret, S., 2000. Configurations used in the design of screen-printed enzymatic biosensors. A review. *Sensors and Actuators B-Chemical* 69(1-2), 153-163.

Alhitti, I.K., Moody, G.J., Thomas, J.D.R., 1984. Immobilization of enzymes in membranes for use with electrochemical sensors. *Journal of Biomedical Engineering* 6(3), 178-180.

Aldous, S.J.,2013. Cardiac biomarkers in acute myocardial infarction. *International Journal of Cardiology* 164(3), 282-294.

Alpert, J.S., Thygesen, K., Antman, E., Bassand, J.P., 2001. Myocardial infarction redefined - A consensus document of the Joint European Society of Cardiology American College of Cardiology Committee for the Redefinition of Myocardial Infarction. *Journal of the American College of Cardiology* 37(3), 973-973.

Amemiya, S., 2007. Potentiometric Ion-Selective Electrodes, Elsevier Science, Amsterdam, The Netherlands, 261-292.

Anderson, L., 2005. Candidate-based proteomics in the search for biomarkers of cardiovascular disease. *Journal of Physiology-London* 563(1), 23-60.

Andersson, L.I., 2000. Molecular imprinting for drug bioanalysis - A review on the application of imprinted polymers to solid-phase extraction and binding assay. *Journal of Chromatography B* 739(1), 163-173.

Andreescu, S., Fournier, D., Marty, J.L., 2003. Development of highly sensitive sensor based on bioengineered acetylcholinesterase immobilized by affinity method. *Analytical Letters* 36(9), 1865-1885.

Andreescu, S., Magearu, V., Lougarre, A., Fournier, D., Marty, J.L., 2001. Immobilization of enzymes on screen-printed sensors via an histidine tail. Application to the detection of pesticides using modified cholinesterase. *Analytical Letters* 34(4), 529-540.

Andreescu, S., Marty, J.L., 2006. Twenty years research in cholinesterase biosensors: From basic research to practical applications. *Biomolecular Engineering* 23(1), 1-15.

Anzai, J., Kobayashi, Y., Nakamura, N., Hoshi, T., 2000. Use of Con A and mannose-labeled enzymes for the preparation of enzyme films for biosensors. *Sensors and Actuators B-Chemical* 65(1-3), 94-96.

Apple, F.S., Falahati, A., Paulsen, P.R., Miller, E.A., Sharkey, S.W., 1997. Improved detection of minor ischemic myocardial injury with measurement of serum cardiac troponin I. *Clinical Chemistry* 43(11) 2047-2051.

Apple, F.S., Jaffe, A.S., 2001. Bedside multimarker testing for risk stratification in chest pain units: The chest pain evaluation by creatine kinase-MB, myoglobin, and troponin I (CHECKMATE) study. *Circulation* 104(22), E125-E125.

Arakaki, A., Hideshima, S., Nakagawa, T., Niwa, D., Tanaka, T., Matsunaga, T., Osaka, T., 2004. Detection of biomolecular interaction between biotin and streptavidin on a self-assembled monolayer using magnetic nanoparticles. *Biotechnology and Bioengineering* 88(4), 543-546.

Auger, C., Rouanet, J.M., Vanderlinde, R., Bornet, A., Decorde, K., Lequeux, N., Cristol, J.P., Teissedre, P.L., 2005. Polyphenols-enriched Chardonnay white wine and sparkling Pinot Noir red wine identically prevent early atherosclerosis in hamsters. *Journal of Agricultural and Food Chemistry* 53(25), 9823-9829.

Balk, E.M., Ioannidis, J.P.A., Salem, D., Chew, P.W., Lau, J., 2001. Accuracy of biomarkers to diagnose acute cardiac ischemia in the emergency department: A meta-analysis. *Annals of Emergency Medicine* 37(5), 478-494.

Bartlett, P.N., Whitaker, R.G., 1987a. Electrochemical immobilization of enzymes .1. Theory. *Journal of Electroanalytical Chemistry* 224(1-2), 27-35.

Bartlett, P.N., Whitaker, R.G., 1987b. Electrochemical immobilization of enzymes.2. Glucose-oxidase immobilized in poly-n-methylpyrrole. *Journal of Electroanalytical Chemistry* 224(1-2), 37-48.

Bean, L.S., Heng, L.Y., Yamin, B.M., Ahmad, M., 2005. Photocurable ferrocene-containing poly(2-hydroxyl ethyl methacrylate) films for mediated amperometric glucose biosensor. *Thin Solid Film*s 477(1-2), 104-110.

Bernard, A., Delamarche, E., Schmid, H., Michel, B., Bosshard, H.R., Biebuyck, H., 1998. Printing patterns of proteins. *Langmuir* 14(9), 2225–2229.

Bhalla, V., Carrara, S., Sharma, P., Nangia, Y., Suri, C.R., 2012. Gold nanoparticles mediated label-free capacitance detection of cardiac troponin I. *Sensors and Actuators B-Chemical* 161(1), 761-768.

Billah, M., Hays, H.C.W., Millner, P.A., 2008. Development of a myoglobin impedimetric immunosensor based on mixed self-assembled monolayer onto gold. *Microchimica Acta* 160(4), 447-454.

Blinka, E., Loeffler, K., Hu, Y., Gopal, A., Hoshino, K., Lin, K., Liu, X., Ferrari, M., Zhang, J.X.J., 2010. Enhanced microcontact printing of proteins on nanoporous silica surface. *Nanotechnology* 21(41), 415302.

Borges, J., Adsorption of Proteins on Au Surfaces modified with SAMs and Biopolymeric Materials, Department of Chemistry and Biochemistry, 2013.

Bossi, A., Piletsky, S.A., Piletska, E.V., Righetti, P.G., Turner, A.P.F., 2001. Surface-grafted molecularly imprinted polymers for protein recognition. *Analytical Chemistry* 73(21), 5281-5286.

Bossi, A., Piletsky, S.A., Turner, A.P.F., Righetti, P.G., 2002. Repartition effect of aromatic polyaniline coatings on the separation of bioactive peptides in capillary electrophoresis. *Electrophoresis* 23(2), 203-208.

Bossi, A.M., Sharma, P.S., Montana, L., Zoccatelli, G., Laub, O., Levi, R., 2012. Fingerprint-Imprinted Polymer: Rational Selection of Peptide Epitope Templates

for the Determination of Proteins by Molecularly Imprinted Polymers. *Analytical Chemistry* 84(9), 4036-4041.

Boujtita, M., Chapleau, M., ElMurr, N., 1996. Biosensors for analysis of ethanol in food: Effect of the pasting liquid. *Analytica Chimica Acta* 319(1-2), 91-96.

Bruls, D.M., Evers, T.H., Kahlman, J.A.H., van Lankvelt, P.J.W., Ovsyanko, M., Pelssers, E.G.M., Schleipen, J.J.H.B., de Theije, F.K., Verschuren, C.A., van der Wijk, T., van Zon, J.B.A., Dittmer, W.U., Immink, A.H.J., Nieuwenhuis, J.H., Prins, M.W.J., 2009. Rapid integrated biosensor for multiplexed immunoassays based on actuated magnetic nanoparticles. *Lab on a Chip* 9(24), 3504-3510.

Bruns, N., Tiller, J.C., 2005. Amphiphilic network as nanoreactor for enzymes in organic solvents. Nano Letters 5(1), 45-48.

Buck, R.P., Lindner, E., 1994. Recommendations for nomenclature of ion-selective electrodes - (iupac recommendations 1994). Pure and *Applied Chemistry* 66(12), 2527-2536.

Buckley, A.M., Greenblatt, M., 1994. The sol-gel preparation of silica-gels. *Journal of Chemical Education*, 71(7)599.

Bucur, B., Danet, A.F., Marty, J.L., 2004. Versatile method of cholinesterase immobilisation via affinity bonds using Concanavalin A applied to the construction of a screen-printed biosensor. *Biosensors & Bioelectronics* 20(2), 217-225.

Cai, H., Wang, Y.Q., He, P.G., Fang, Y.H., 2002. Electrochemical detection of DNA hybridization based on silver-enhanced gold nanoparticle label. *Analytica Chimica Acta* 469(2), 165-172.

Campbell, F.M., Ingram, A., Monaghan, P., Cooper, J., Sattar, N., Eckersall, P.D., Graham, D., 2008. SERRS immunoassay for quantitative human CRP analysis. *Analyst* 133(10), 1355-1357.

Casas, J.P., Shah, T., Hingorani, A.D., Danesh, J., Pepys, M.B., 2008. C-reactive protein and coronary heart disease: a critical review. *Journal of Internal Medicine* 264(4), 295-314.

Casey, B.J., Kofinas, P., 2008. Selective binding of carcinoembryonic antigen using imprinted polymeric hydrogels. *Journal of Biomedical Materials Research Part A* 87A(2), 359-363.

Caulum, M.M., Murphy, B.M., Ramsay, L.M., Henry, C.S., 2007. Detection of cardiac biomarkers using micellar electrokinetic chromatography and a cleavable tag immunoassay. *Analytical Chemistry* 79(14), 5249-5256.

Centonze, D., Malitesta, C., Palmisano, F., Zambonin, P.G., 1994. Permeation of solutes through an electropolymerized ultrathin poly-o-phenylenediamine film used as an enzyme-entrapping membrane. *Electroanalysis* 6(5-6), 423-429.

Chang, Z., Pan, H., Zhao, K., Chen, M., He, P., Fang, Y., 2008. Electrochemical DNA biosensors based on palladium nanoparticles combined with carbon nanotubes. *Electroanalysis* 20(2), 131-136.

Chen, C.-S., Kuan, S., Chang, T.-H., Chou, C.-C., Chang, S.-W., Huang, L.-S., 2011. Microcantilever biosensor: sensing platform, surface characterization and multiscale modeling. *Smart Structures and Systems* 8(1), 17-37.

Chen, Y.-W., Rick, J., Chou, T.C., 2009. A systematic approach to forming micro-contact imprints of creatine kinase. *Organic & Biomolecular Chemistry* 7(3), 488-494.

Chen, Z., Xi, F., Yang, S., Wu, Q., Lin, X., 2008. Development of a bienzyme system based on sugar-lectin biospecific interactions for amperometric determination of phenols and aromatic amines. *Sensors and Actuators B-Chemical* 130(2), 900-907.

Cho, I.-H., Paek, E.-H., Kim, Y.-K., Kim, J.-H., Paek, S.-H., 2009. Chemiluminometric enzyme-linked immunosorbent assays (ELISA)-on-a-chip biosensor based on cross-flow chromatography. *Analytica Chimica Acta* 632(2), 247-255.

Choi, M.M.F., 2004. Progress in enzyme-based biosensors using optical transducers. *Microchimica Acta* 148(3-4), 107-132.

Chou, P.C., Rick, J., Chou, T.C., 2005. C-reactive protein thin-film molecularly imprinted polymers formed using a micro-contact approach. *Analytica Chimica Acta* 542(1), 20-25.

Chou, T.-C., Rick, J., Weng, Y.-C., Ieee, 2007. Nanocavity Protein Biosensor - Fabricated by Molecular Imprinting. 2007 7th Ieee Conference on Nanotechnology, Vol 1-3, 16-20.

Christenson, R.H., Azzazy, H.M.E., 1998. Biochemical markers of the acute coronary syndromes. *Clinical Chemistry* 44(8), 1855-1864.

Christopher M. A. Brett, A.M.O.B., 1993. Electrochemistry: Principles, Methods, and Applications. 427. Oxford University Press, Incorporated.

Colak, U., Gencer, N., 2012. Immobilization of paraoxonase onto chitosan and its characterization. Artificial cells, blood substitutes, and immobilization biotechnology 40(4), 290-295.

Crimmins, D.L., Kao, J.L.F., 2011. A 68 residue N-terminal fragment of pro-atrial natriuretic peptide is a monomeric intrinsically unstructured protein. *Journal of Biochemistry* 150(2), 157-163.

Crivellente, F., Tontodonati, M., Fasdelli, N., Casartelli, A., Dorigatti, R., Faustinelli, I., Cristofori, P., 2011. NT-proBNP as a biomarker for the assessment of a potential cardiovascular drug-induced liability in beagle dogs. *Cell Biology and Toxicology* 27(6), 425-438.

de Lemos, J.A., Morrow, D.A., Gibson, C.M., Murphy, S.A., Sabatine, M.S., Rifai, N., McCabe, C.H., Antman, E.M., Cannon, C.P., Braunwald, E., 2002. The prognostic value of serum myoglobin in patients with Non-ST-segment elevation acute coronary syndromes - Results from the TIMI 11B and TACTICS-TIMI 18 studies. *Journal of the American College of Cardiology* 40(2), 238-244.

de Vasconcelos, E.A., Peres, N.G., Pereira, C.O., da Silva, V.L., da Silva, E.F., Jr., Dutra, R.F., 2009. Potential of a simplified measurement scheme and device structure for a low cost label-free point-of-care capacitive biosensor. *Biosensors & Bioelectronics* 25(4), 870-876.

Dittmer, W.U., Evers, T.H., Hardeman, W.M., Huijnen, W., Kamps, R., de Kievit, P., Neijzen, J.H.M., Nieuwenhuis, J.H., Sijbers, M.J.J., Dekkers, D.W.C., Hefti, M.H., Martens, M.F.W.C., 2010. Rapid, high sensitivity, point-of-care test for cardiac troponin based on optomagnetic biosensor. *Clinica Chimica Acta* 411(11-12), 868-873.

Dou, Y.-H., Haswell, S.J., Greenman, J., Wadhawan, J., 2012. Voltammetric Immunoassay for the Detection of Protein Biomarkers. *Electroanalysis* 24(2), 264-272.

Dutra, R.F., Kubota, L.T., 2007. An SPR immunosensor for human cardiac troponin T using specific binding avidin to biotin at carboxymethyldextran-modified gold chip. *Clinica Chimica Acta* 376(1-2), 114-120.

Dutra, R.F., Mendes, R.K., da Silva, V.L., Kubota, L.T., 2007. Surface plasmon resonance immunosensor for human cardiac troponin T based on self-assembled monolayer. *Journal of Pharmaceutical and Biomedical Analysis* 43(5), 1744-1750.

Egawa, Y., Seki, T., Takahashi, S., Anzai, J.-i., 2011. Electrochemical and optical sugar sensors based on phenylboronic acid and its derivatives. *Materials Science & Engineering C-Materials for Biological Applications* 31(7), 1257-1264.

Ekinci, E., Karagozler, A.A., Karagozler, A.E., 1996. The preparation and sensor application of poly(p-aminophenol). *Electroanalysis* 8(6), 571-574.

Engberg, K., Frank, C.W., 2011. Protein diffusion in photopolymerized poly(ethylene glycol) hydrogel networks. *Biomedical Materials* 6(5) 055006.

Enpuku, K., Inoue, K., Soejima, K., Yoshinaga, K., Kuma, H., Hamasaki, N., 2005. Magnetic immunoassays utilizing magnetic markers and a high-T-C SQUID. *Ieee Transactions on Applied Superconductivity* 15(2), 660-663.

Eriksson, S., Wittfooth, S., Pettersson, K., 2006. Present and future biochemical markers for detection of acute coronary syndrome. *Critical Reviews in Clinical Laboratory Sciences* 43(5-6), 427-495.

Esseghaier, C., Bergaoui, Y., ben Fredj, H., Tlili, A., Helali, S., Ameur, S., Abdelghani, A., 2008. Impedance spectroscopy on immobilized streptavidin horseradish peroxidase layer for biosensing. *Sensors and Actuators B-Chemical* 134(1), 112-116.

Eveness, J., Kiely, J., Hawkins, P., Wraith, P., Luxton, R., 2009. Evaluation of paramagnetic particles for use in a resonant coil magnetometer based magneto-immunoassay. *Sensors and Actuators B-Chemical* 139(2), 538-542.

Fang, L., Lv, Z., Wei, H., Wang, E., 2008. A electrochemiluminescence aptasensor for detection of thrombin incorporating the capture aptamer labeled with gold nanoparticles immobilized onto the thio-silanized ITO electrode. *Analytica Chimica Acta* 628(1), 80-86.

Faridbod, F., Ganjali, M.R., Dinarvand, R., Norouzi, P., 2008. Developments in the field of conducting and non-conducting polymer based potentiometric membrane sensors for ions over the past decade. *Sensors* 8(4), 2331-2412.

Fellahi, J.L., Piriou, V., Longrois, D., 2011. Cardiac biomarkers in perioperative risk stratification. *Annales Francaises D Anesthesie Et De Reanimation* 30(2), 126-140.

Fesmire, F.M., Christenson, R.H., Fody, E.P., Feintuch, T.A., 2004. Delta creatine kinase-MB outperforms myoglobin at two hours during the emergency department identification and exclusion of troponin positive non-ST-segment elevation acute coronary syndromes. *Annals of Emergency Medicine* 44(1), 12-19.

Foy, S.G., Kennedy, I.C.S., Ikram, H., Low, C.J.S., Shirlaw, T.M., Crozier, I.G., 1991. The early diagnosis of acute myocardial-infarction. *Australian and New Zealand Journal of Medicine* 21(3), 335-337.

Fuchs, Y., Linares, A.V., Mayes, A.G., Haupt, K., Soppera, O., 2011. Ultrathin Selective Molecularly Imprinted Polymer Microdots Obtained by Evanescent Wave Photopolymerization. *Chemistry of Materials* 23(16), 3645-3651.

Gao, N., Dong, J., Liu, M., Ning, B., Cheng, C., Guo, C., Zhou, C., Peng, Y., Bai, J., Gao, Z., 2012. Development of molecularly imprinted polymer films used for detection of profenofos based on a quartz crystal microbalance sensor. *Analyst* 137(5), 1252-1258.

Gill, I., Ballesteros, A., 2000. Bioencapsulation within synthetic polymers (Part 1): sol-gel encapsulated biologicals. *Trends in Biotechnology* 18(7), 282-296.

Gogol, E.V., Evtugyn, G.A., Marty, J.L., Budnikov, H.C., Winter, V.G., 2000. Amperometric biosensors based on nafion coated screen-printed electrodes for the determination of cholinesterase inhibitors. *Talanta* 53(2), 379-389.

Gornall, D.A., Roth, S.N.L., 1996. Serial myoglobin quantitation in the early assessment of myocardial damage: A clinical study. *Clinical Biochemistry* 29(4), 379-384.

Guan, G.J., Liu, B.H., Wang, Z.Y., Zhang, Z.P., 2008. Imprinting of Molecular Recognition Sites on Nanostructures and Its Applications in Chemosensors. *Sensors* 8(12), 8291-8320.

Gul, O., Calay, E., Sezerman, U., Basaga, H., Gurbuz, Y., 2007. Sandwich-type, antibody microarrays for the detection and quantification of cardiovascular risk markers. *Sensors and Actuators B-Chemical* 125(2), 581-588.

Hanko, M., Bruns, N., Rentmeister, S., Tiller, J.C., Heinze, J., 2006a. Nanophase-separated Amphiphilic conetworks as versatile matrixes for optical chemical and biochemical sensors. *Analytical Chemistry* 78(18), 6376-6383.

Hanko, M., Bruns, N., Tiller, J.C., Heinze, J., 2006b. Optical biochemical sensor for determining hydroperoxides in nonpolar organic liquids as archetype for sensors consisting of amphiphilic conetworks as immobilisation matrices. *Analytical and Bioanalytical Chemistry* 386(5), 1273-1283.

Hatakeyama, K., Tanaka, T., Sawaguchi, M., Iwadate, A., Mizutani, Y., Sasaki, K., Tateishi, N., Matsunaga, T., 2009. Microfluidic device using chemiluminescence and a DNA-arrayed thin film transistor photosensor for single nucleotide polymorphism genotyping of PCR amplicons from whole blood. *Lab on a Chip* 9(8), 1052-1058.

Heeschen, C., Goldmann, B.U., Langenbrink, L., Matschuck, G., Hamm, C.W., 1999. Evaluation of a rapid whole blood ELISA for quantification of troponin I in patients with acute chest pain. *Clinical Chemistry* 45(10), 1789-1796.

Hench, L.L., West, J.K., 1990. The sol-gel process. *Chemical Reviews* 90(1), 33-72.

Henry, O.Y.F., Piletsky, S.A., Cullen, D.C., 2008. Fabrication of molecularly imprinted polymer microarray on a chip by mid-infrared laser pulse initiated polymerisation. *Biosensors & Bioelectronics* 23(12), 1769-1775.

Hernandez-Cazares, A.S., Aristoy, M.C., Toldra, F., 2011. An enzyme sensor for the determination of total amines in dry-fermented sausages. *Journal of Food Engineering* 106(2), 166-169.

Heyries, K.A., Mandon, C.A., Ceriotti, L., Ponti, J., Colpo, P., Blum, L.J., Marquette, C.A., 2009. "Macromolecules to PDMS transfer" as a general route for PDMS biochips. *Biosensors & Bioelectronics* 24(5), 1146-1152.

Hill, H.R., Martins, T.B., 2006. The flow cytometric analysis of cytokines using multi-analyte fluorescence microarray technology. *Methods* 38(4), 312-316.

Hjerten, S., Liao, J.L., Nakazato, K., Wang, Y., Zamaratskaia, G., Zhang, H.X., 1997. Gels mimicking antibodies in their selective recognition of proteins. *Chromatographia* 44(5-6).

Hoa, X.D., Kirk, A.G., Tabrizian, M., 2009. Enhanced SPR response from patterned immobilization of surface bioreceptors on nano-gratings. *Biosensors & Bioelectronics* 24(10), 3043-3048.

Hsiao, A.P., Heller, M.J., 2012. Electric-field-directed self-assembly of active enzyme-nanoparticle structures. *Journal of Biomedicine &Biotechnology*, 2012, 178487.

Hsu, C.-Y., Lin, H.-Y., Thomas, J.L., Wu, B.-T., Chou, T.-C., 2006. Incorporation of styrene enhances recognition of ribonuclease A by molecularly imprinted polymers. *Biosensors & Bioelectronics* 22(3), 355-363.

Huang, Q.J., Tang, Y.C., Liu, W.P., Yu, S.X., Lan, X.P., Xu, B., Wu, Y.S., Li, L., Zhu, Z.Y., 1998. Qualitative bedside assay of increased human serum myoglobin by sandwich dot-immunogold filtration for the diagnosis of acute myocardial infarction. *Clinica Chimica Acta* 273(2), 119-130.

Ibraimi, F., Kriz, D., Lu, M., Hansson, L.O., Kriz, K., 2006. Rapid one-step whole blood C-reactive protein magnetic permeability immunoassay with monoclonal antibody conjugated nanoparticles as superparamagnetic labels and enhanced sedimentation. *Analytical and Bioanalytical Chemistry* 384(3), 651-657.

Ispas, C.R., Crivat, G., Andreescu, S., 2012. Review: recent developments in enzyme-based biosensors for biomedical analysis. *Analytical Letters* 45(2-3), 168-186.

Jaffe, A.S., 2001. Elevations in cardiac troponin measurements: false false-positives: the real truth. *Cardiovascular toxicology* 1(2), 87-92.

Jegourel, D., Delepee, R., Breton, F., Rolland, A., Vidal, R., Agrofoglio, L.A., 2008. Molecularly imprinted polymer of 5-methyluridine for solid-phase extraction of

pyrimidine nucleoside cancer markers in urine. *Bioorganic & Medicinal Chemistry* 16(19), 8932-8939.

Jhaveri, S.D., Kirby, R., Conrad, R., Maglott, E.J., Bowser, M., Kennedy, R.T., Glick, G., Ellington, A.D., 2000. Designed signaling aptamers that transduce molecular recognition to changes in fluorescence intensity. *Journal of the American ChemicalSociety* 122(11), 2469-2473.

Joensson, C., Aronsson, M., Rundstroem, G., Pettersson, C., Mendel-Hartvig, I., Bakker, J., Martinsson, E., Liedberg, B., MacCraith, B., Oehman, O., Melin, J., 2008. Silane-dextran chemistry on lateral flow polymer chips for immunoassays. *Lab on a Chip* 8(7), 1191-1197.

Keefe, A.D., Pai, S., Ellington, A., 2010. Aptamers as therapeutics, *Nature Reviews Drug Discovery* 9(8). 537.

Keffer, J.H., 1996. Myocardial markers of injury - Evolution and insights. American J*ournal of Clinical Pathology* 105(3), 305-320.

Kiely, J., Hawkins, P., Wraith, P., Luxton, R., 2007. Paramagnetic particle detection for use with an immunoassay based biosensor. *Iet Science Measurement & Technology* 1(5), 270-275.

Kofuji, K., Isobe, T., Murata, Y., 2009. Controlled release of alpha-lipoic acid through incorporation into natural polysaccharide-based gel beads. *Food Chemistry* 115(2), 483-487.

Kong, T., Chen, Y., Ye, Y., Zhang, K., Wang, Z., Wang, X., 2009. An amperometric glucose biosensor based on the immobilization of glucose oxidase on the ZnO nanotubes. *Sensors and Actuators B-Chemical* 138(1), 344-350.

Kost, G.J., Tran, N.K., 2005. Point-of-care testing and cardiac biomarkers: The standard of care and vision for chest pain centers. *Cardiology Clinics* 23(4), 467-490.

Kryscio, D.R., Peppas, N.A., 2012. Critical review and perspective of macromolecularly imprinted polymers. *Acta Biomaterialia* 8(2), 461-73.

Kurita, R., Yokota, Y., Sato, Y., Mizutani, F., Niwa, O., 2006. On-chip enzyme immunoassay of a cardiac marker using a microfluidic device combined with a portable surface plasmon resonance system. *Analytical Chemistry* 78(15), 5525-5531.

Kwon, Y.-C., Kim, M.-G., Kim, E.-M., Shin, Y.-B., Lee, S.-K., Lee, S.D., Cho, M.-J., Ro, H.-S., 2011. Development of a surface plasmon resonance-based immunosensor for the rapid detection of cardiac troponin I. *Biotechnology Letters* 33(5), 921-927.

Lahav, M., Kharitonov, A.B., Katz, O., Kunitake, T., Willner, I., 2001. Tailored chemosensors for chloroaromatic acids using molecular imprinted TiO2 thin films on ion-sensitive field-effect transistors. *Analytical Chemistry* 73(3), 720-723.

Langer, J.J., Filipiak, M., Kecinska, J., Jasnowska, J., Wlodarczak, J., Buladowski, B., 2004. Polyaniline biosensor for choline determination. *Surface Science* 573(1), 140-145.

Leca, B., Morelis, R.M., Coulet, P.R., 1995a. Design of a choline sensor via direct coating of the transducer by photopolymerization of the sensing layer. *Sensors and Actuators B-Chemical* 27(1-3), 436-439.

Leca, B., Morelis, R.M., Coulet, P.R., 1995b. Direct biosensor coating with a photopolymerised microlayer through a controllable step-procedure. *Mikrochimica Acta* 121(1-4), 147-154.

Lee, M.H., Chen, Y.C., Ho, M.H., Lin, H.Y., 2010. Optical recognition of salivary proteins by use of molecularly imprinted poly(ethylene-co-vinyl alcohol)/quantum dot composite nanoparticles. *Analytical and Bioanalytical Chemistry* 397(4), 1457-1466.

Lerga, T.M., O'Sullivan, C.K., 2008. Rapid determination of total hardness in water using fluorescent molecular aptamer beacon. *Analytica Chimica Acta* 610(1), 105-11.

Leung, W.M., Chan, C.P., Leung, M.F., Renneberg, R., Lehmann, K., Renneberg, I., Lehmann, M., Hempel, A., Glatz, J.F.C., 2005. Novel "digital-style" rapid test simultaneously detecting heart attack and predicting cardiovascular disease risk. *Analytical Letters* 38(3), 423-439.

Liao, P.-C., Tyan, Y.-C., Wang, C.-Y., Hsu, J.-F., Chou, T.-C., Lin, H.-Y., 2009. Assessing the binding selectivity of molecularly imprinted polymer artificial antibodies by mass spectrometry-based profiling system. *Journal of Biomedical Materials Research Part A* 91A(2), 597-604.

Lin, H.-Y., Hsu, C.-Y., Thomas, J.L., Wang, S.-E., Chen, H.-C., Chou, T.-C., 2006. The microcontact imprinting of proteins: The effect of cross-linking monomers for lysozyme, ribonuclease A and myoglobin. *Biosensors & Bioelectronics* 22(4), 534-543.

Lin, H.-Y., Rick, J., Chou, T.-C., 2007. Optimizing the formulation of a myoglobin molecularly imprinted thin-film polymer-formed using a micro-contact imprinting method. *Biosensors & Bioelectronics* 22(12), 3293-3301.

Liu, J.T., Chen, C.J., Ikoma, T., Yoshioka, T., Cross, J.S., Chang, S.-J., Tsai, J.-Z., Tanaka, J., 2011a. Surface plasmon resonance biosensor with high anti-fouling ability for the detection of cardiac marker troponin T. *Analytica Chimica Acta* 703(1), 80-86.

Liu, L., Chen, Z., Yang, S., Jin, X., Lin, X., 2008. A novel inhibition biosensor constructed by layer-by-layer technique based on biospecific affinity for the determination of sulfide. *Sensors and Actuators B-Chemical* 129(1), 218-224.

Liu, Q., Han, M., Bao, J., Jiang, X., Dai, Z., 2011b. CdSe quantum dots as labels for sensitive immunoassay of cancer biomarker proteins by electrogenerated chemiluminescence. *Analyst* 136(24), 5197-5203.

Liu, R., Lv, Y., Hou, X., Yang, L., Mester, Z., 2012. Protein Quantitation Using Ru-NHS Ester Tagging and Isotope Dilution High-Pressure Liquid Chromatography-Inductively Coupled Plasma Mass Spectrometry Determination. *Analytical Chemistry* 84(6), 2769–2775.

Liu, S., Sun, Y., 2007. Co-immobilization of glucose oxidase and hexokinase on silicate hybrid sol-gel membrane for glucose and ATP detections. *Biosensors & Bioelectronics* 22(6), 905-911.

Llames, L., Goyache, J., Domenech, A., de Avila, A., Suarez, G., Gomez-Lucia, E., 1999. Rapid detection of specific polyclonal and monoclonal antibodies against bovine leukemia virus. *Journal of Virological Methods* 82(2), 129-136.

Loo, L., Wu, W., Shih, W.Y., Shih, W.-H., Borghaei, H., Pourrezaei, K., Adams, G.P., 2011. A Rapid Method to Regenerate Piezoelectric Microcantilever Sensors (PEMS). *Sensors* 11(5), 5520–5528.

Luo, Y., Zhang, B., Chen, M., Jiang, T., Zhou, D., Huang, J., Fu, W., 2012. Sensitive and rapid quantification of C-reactive protein using quantum dot-labeled microplate immunoassay. *Journal of Translational Medicine* 10, 24.

Luxton, R., Badesha, J., Kiely, J., Hawkins, P., 2004. Use of external magnetic fields to reduce reaction times in an immunoassay using micrometer-sized paramagnetic particles as labels (magnetoimmunoassay). *Analytical Chemistry* 76(6), 1715-1719.

Ma, L., Wang, C., Zhang, M., 2011. Detecting protein adsorption and binding using magnetic nanoparticle probes. *Sensors and Actuators B-Chemical* 160(1), 650-655.

Martin-Ventura, J.L., Blanco-Colio, L.M., Tunon, J., Munoz-Garcia, B., Madrigal-Matute, J., Moreno, J.A., Vega de Ceniga, M., Egido, J., 2009. Biomarkers in Cardiovascular Medicine. *Revista Espanola De Cardiologia* 62(6), 677-688.

Marx, S., Liron, Z., 2001. Molecular imprinting in thin films of organic-inorganic hybrid sol-gel and acrylic polymers. *Chemistry of Materials* 13(10), 3624-3630.

Mascini, M., Tombelli, S., 2008. Biosensors for biomarkers in medical diagnostics. *Biomarkers* 13(7-8), 637-657.

Mathebe, N.G.R., Morrin, A., Iwuoha, E.I., 2004. Electrochemistry and scanning electron microscopy of polyaniline/peroxidase-based biosensor. *Talanta* 64(1), 115-120.

McDonnell, B., Hearty, S., Leonard, P., O'Kennedy, R., 2009. Cardiac biomarkers and the case for point-of-care testing. *Clinical Biochemistry* 42(7-8), 549-561.

Mir, M., Vreeke, M., Katakis, L., 2006. Different strategies to develop an electrochemical thrombin aptasensor. *Electrochemistry Communications* 8(3), 505-511.

Mishra, S.K., Kumar, D., Biradar, A.M., Rajesh, 2012. Electrochemical impedance spectroscopy characterization of mercaptopropionic acid capped ZnS nanocrystal based bioelectrode for the detection of the cardiac biomarker-myoglobin. *Bioelectrochemistry* 88, 118-126.

Modi, S., Shedbalkar, V.P., Behere, D.V., 1989. Spectrophotometric measurements on verdo-myoglobin - relevance to the oxidation of ferri-myoglobin by chlorite ion. *Indian Journal of Biochemistry & Biophysics* 26(2), 84-86 .

Mohammed, M.-I., Desmulliez, M.P.Y., 2011. Lab-on-a-chip based immunosensor principles and technologies for the detection of cardiac biomarkers: a review. *Lab on a Chip* 11(4), 569-595.

Mohammed, M.-I., Sills, G.J., Brodie, M.J., Ellis, E.M., Girkin, J.M., 2009. A complete miniaturised genotyping system for the detection of single nucleotide polymorphisms in human DNA samples. *Sensors and Actuators B-Chemical* 139(1), 83-90.

Monson, C.F., Driscoll, L.N., Bennion, E., Miller, C.J., Majda, M., 2009. Antibody-Antigen Exchange Equilibria in a Field of an External Force: Design of Reagentless Biosensors. *Analytical Chemistry* 81(17), 7510-7514.

Montague, C., Kircher, T., 1995. Myoglobin in the early evaluation of acute chest pain. *American Journal of Clinical Pathology* 104(4), 472-476.

Moreira, F.T.C., Dutra, R.A.F., Noronha, J.P.C., Cunha, A.L., Sales, M.G.F., 2011a. Artificial antibodies for troponin T by its imprinting on the surface of multiwalled carbon nanotubes: Its use as sensory surfaces. *Biosensors & Bioelectronics* 28(1), 243-250.

Moreira, F.T.C., Dutra, R.A.F., Noronha, J.P.C., Sales, M.G.F., 2011b. Myoglobin-biomimetic electroactive materials made by surface molecular imprinting on silica beads and their use as ionophores in polymeric membranes for potentiometric transduction. *Biosensors & Bioelectronics* 26(12), 4760-4766.

Morrin, A., Ngamna, O., Killard, A.J., Moulton, S.E., Smyth, M.R., Wallace, G.G., 2005. An amperometric enzyme biosensor fabricated from polyaniline nanoparticles. *Electroanalysis* 17(5-6), 423-430.

Morrow, D.A., Braunwald, E., 2003. Future of biomarkers in acute coronary syndromes - Moving toward a multimarker strategy. *Circulation* 108(3), 250-252.

Mu, S.L., 1994. Bioelectrochemical response of the polyaniline galactose-oxidase electrode. *Journal of Electroanalytical Chemistry* 370(1-2), 135-139.

Mu, S.L., Xue, H.G., 1996. Bioelectrochemical characteristics of glucose oxidase immobilized in a polyaniline film. *Sensors and Actuators B-Chemical* 31(3), 155-160.

Mulvaney, S.P., Musick, M.D., Keating, C.D., Natan, M.J., 2003. Glass-coated, analyte-tagged nanoparticles: A new tagging system based on detection with surface-enhanced Raman scattering. *Langmuir* 19(11), 4784-4790.

Ni, J., Lipert, R.J., Dawson, G.B., Porter, M.D., 1999. Immunoassay readout method using extrinsic Raman labels adsorbed on immunogold colloids. *Analytical Chemistry* 71(21), 4903-4908.

Nishida, Y., Kawai, H., Nishino, H., 1985. A sensitive sandwich enzyme-immunoassay for human myoglobin using fab-horseradish peroxidase conjugate - methods and results in normal subjects and patients with various diseases. *Clinica Chimica Acta* 153(2), 93-104.

Nishino, H., Huang, C.S., Shea, K.J., 2006. Selective protein capture by epitope imprinting. *Angewandte Chemie-International Edition* 45(15), 2392-2396.

Ou, S.H., Wu, M.C., Chou, T.C., Liu, C.C., 2004. Polyacrylamide gels with electrostatic functional groups for the molecular imprinting of lysozyme. *Analytica Chimica Acta* 504(1), 163-166.

Owen, A., 1995. Tracking the rise and fall of cardiac enzymes. *Nursing* 25(5), 34-45.

Pakapongpan, S., Palangsuntikul, R., Surareungchai, W., 2011. Electrochemical sensors for hemoglobin and myoglobin detection based on methylene blue-multiwalled carbon nanotubes nanohybrid-modified glassy carbon electrode. *Electrochimica Acta* 56(19), 6831-6836.

Pan, D.W., Chen, J.H., Nie, L.H., Tao, W.Y., Yao, S.Z., 2004. An amperometric glucose biosensor based on poly(o-aminophenol) and Prussian blue films at platinum electrode. *Analytical Biochemistry* 324(1), 115-122.

Panteghini, M., Linsinger, T., Wu, A.H.B., Dati, F., Apple, F.S., Christenson, R.H., Mair, J., Schimmel, H., 2004. Standardization of immunoassays for measurement of myoglobin in serum. Phase 1: Evaluation of candidate secondary reference materials. *Clinica Chimica Acta* 341(1-2), 65-72.

Park, J.P., Cropek, D.M., Banta, S., 2010. High Affinity Peptides for the Recognition of the Heart Disease Biomarker Troponin I Identified Using Phage Display. *Biotechnology and Bioengineering* 105(4), 678-686.

Pei, Z.C., Anderson, H., Aastrup, T., Ramstrom, O., 2005. Study of real-time lectin-carbohydrate interactions on the surface of a quartz crystal microbalance. *Biosensors & Bioelectronics* 21(1), 60-66.

Pesavento, M., D'Agostino, G., Biesuz, R., Alberti, G., 2009. Molecularly Imprinted Polymer-Based Sensors for Amperometric Determination of Nonelectroactive Substances. *Electroanalysis* 21(3-5), 604-611.

Piletsky, S.A., Piletska, E.V., Chen, B.N., Karim, K., Weston, D., Barrett, G., Lowe, P., Turner, A.P.F., 2000. Chemical grafting of molecularly imprinted homopolymers to the surface of microplates. Application of artificial adrenergic receptor in enzyme-linked assay for beta-agonists determination. *Analytical Chemistry* 72(18), 4381-4385.

Pinto, R., Carvalho, A.S., Conze, T., Magalhaes, A., Picco, G., Burchell, J.M., Taylor-Papadimitriou, J., Reis, C.A., Almeida, R., Mandel, U., Clausen, H., Soderberg, O., David, L., 2012. Identification of new cancer biomarkers based on aberrant mucin glycoforms by in situ proximity ligation. *Journal of Cellular and Molecular Medicine* 16(7), 1474-1484.

Plowman, T.E., Durstchi, J.D., Wang, H.K., Christensen, D.A., Herron, J.N., Reichert, W.M., 1999. Multiple-analyte fluoroimmunoassay using an integrated optical waveguide sensor. *Analytical Chemistry* 71(19), 4344-4352.

Polevoda, B., Sherman, F., 2000. N alpha-terminal acetylation of eukaryotic proteins. *Journal of Biological Chemistry* 275(47), 36479-36482.

Polsky, R., Gill, R., Kaganovsky, L., Willner, I., 2006. Nucleic acid-functionalized Pt nanoparticles: Catalytic labels for the amplified electrochemical detection of biomolecules. *Analytical Chemistry* 78(7), 2268-2271.

Porika, M., Tippani, R., Bollam, S.R., Panuganti, S.D., Thamidala, C., Abbagani, S., 2011. Serum human telomerase reverse transcriptase: a novel biomarker for breast cancer diagnosis. *International Journal of Clinical Oncology* 16(6), 617-622.

Portaccio, M., Durante, D., Viggiano, A., Di Martino, S., De Luca, P., Di Tuoro, D., Bencivenga, U., Rossi, S., Canciglia, P., De Luca, B., Mita, D.G., 2007. Amperometric glucose determination by means of glucose oxidase immobilized on a cellulose acetate film: Dependence on the immobilization procedures. *Electroanalysis* 19(17), 1787-1793.

Qin, C., Chen, C., Xie, Q., Wang, L., He, X., Huang, Y., Zhou, Y., Xie, F., Yang, D., Yao, S., 2012. Amperometric enzyme electrodes of glucose and lactate based on poly(diallyldimethylammonium)-alginate-metal ion-enzyme biocomposites. *Analytica Chimica Acta* 720, 49-56.

Qureshi, A., Gurbuz, Y., Kallempudi, S., Niazi, J.H., 2010. Label-free RNA aptamer-based capacitive biosensor for the detection of C-reactive protein. *Physical Chemistry Chemical Physics* 12(32), 9176-9182.

Qureshi, A., Gurbuz, Y., Niazi, J.H., 2012. Biosensors for cardiac biomarkers detection: A review. *Sensors and Actuators B-Chemical* 171, 62-76.

Rachkov, A., Minoura, N., 2001. Towards molecularly imprinted polymers selective to peptides and proteins. The epitope approach. Biochimica Et Biophysica Acta-Protein *Structure and Molecular Enzymology* 1544(1-2), 255-266.

Rajesh, Sharma, V., Tanwar, V.K., Mishra, S.K., Biradar, A.M., 2010. Electrochemical impedance immunosensor for the detection of cardiac biomarker Myogobin (Mb) in aqueous solution. *Thin Solid Films* 519(3), 1167-1170.

Ramanaviciene, A., Ramanavicius, A., 2004. Molecularly imprinted polypyrrole-based synthetic receptor for direct detection of bovine leukemia virus glycoproteins. *Biosensors & Bioelectronics* 20(6), 1076-1082.

Randles, J.E.B., 1948. A cathode ray polarograph .2. The current-voltage curves. *Transactions of the Faraday Society* 44(5), 327-&.

Ravelet, C., Peyrin, E., 2006. Recent developments in the HPLC enantiomeric separation using chiral selectors identified by a combinatorial strategy. Journal of *Separation Science* 29(10), 1322-1331.

Ravichandran, V., Vasquez, G.B., Srivastava, S., Verma, M., Petricoin, E., Lubell, J., Sriram, R.D., Barker, P.E., Gilliland, G.L., 2004. Data standards for proteomics: mitochondrial two-dimensional polyacrylamide gel electrophoresis data as a model system. *Mitochondrion* 3(6), 327-336.

Reyes De Corcuera, J.I., Cavalieri, R.P., Powers, J.R., 2004. Simultaneous determination of film permeability to H2O2 and substrate surface area coverage of overoxidized polypyrrole. *Synthetic Metals* 142(1-3), 71-79.

Reyes-De-Corcuera, J.I., Cavalieri, R.P., Powers, J.R., Tang, J.M., Kang, D.H., 2005. Enzyme-electropolymer-based amperometric biosensors: An innovative platform for time-temperature integrators. *Journal of Agricultural and Food Chemistry* 53(23), 8866-8873.

Richardson, J., Hill, A., Luxton, R., Hawkins, P., 2001. A novel measuring system for the determination of paramagnetic particle labels for use in magneto-immunoassays. *Biosensors & Bioelectronics* 16(9-12), 1127-1132.

Romic, E., Unic, A., Derek, L., Pehar, M., 2009. Biochemical markers in the diagnosis of acute coronary syndrome. *Acta medica Croatica: časopis Hravatske akademije medicinskih znanosti* 63(1), 15-19.

Rosalki, S.B., Roberts, R., Katus, H.A., Giannitsis, E., Ladenson, J.H., Apple, F.S., 2004. Cardiac biomarkers for detection of myocardial infarction: Perspectives from past to present. *Clinical Chemistry* 50(11), 2205-2213.

Ruan, C.M., Zeng, K.F., Varghese, O.K., Grimes, C.A., 2004. A staphylococcal enterotoxin B magnetoelastic immunosensor. *Biosensors & Bioelectronics* 20(3), 585-591.

S. Allender, P.S., V. Peto, M. Rayner,, 2008. European Cardiovascular Disease Statistics 2008, http://www.heartstats.org/datapage.asp?id=7683., 1–112.

Sassolas, A., Blum, L.J., Leca-Bouvier, B.D., 2012. Immobilization strategies to develop enzymatic biosensors. *Biotechnology Advances* 30(3), 489-511.

Schneider, K.P., Gewessler, U., Flock, T., Heinzle, A., Schenk, V., Kaufmann, F., Sigl, E., Guebitz, G.M., 2012. Signal enhancement in polysaccharide based sensors for infections by incorporation of chemically modified laccase. *New Biotechnology* 29(4), 502-509.

Schuder, S., Wittenberg, J.B., Haseltine, B., Wittenberg, B.A., 1979. Spectrophotometric determination of myoglobin in cardiac and skeletal-muscle - separation from hemoglobin by subunit-exchange chromatography. *Analytical Biochemistry* 92(2), 473-481.

Sharma, P.S., Pietrzyk-Le, A., D'Souza, F., Kutner, W., 2012. Electrochemically synthesized polymers in molecular imprinting for chemical sensing. *Analytical and Bioanalytical Chemistry* 402(10), 3177-3204.

Sharma, S.K., Singhal, R., Malhotra, B.D., Sehgal, N., Kumar, A., 2004. Lactose biosensor based on Langmuir-Blodgett films of poly(3-hexyl thiophene). *Biosensors & Bioelectronics* 20(3), 651-657.

Shiomi, T., Matsui, M., Mizukami, F., Sakaguchi, K., 2005. A method for the molecular imprinting of hemoglobin on silica surfaces using silanes. *Biomaterials* 26(27), 5564-5571.

Shumiantseva, V.V., Bulko, T.V., Vagin, M.I., Suprun, E.V., Archakov, A.I., 2010. Electrochemical immunoanalysis of cardiac myoglobin. *Biomeditsinskaia khimiia* 56(6), 758-768.

SiegmannThoss, C., Renneberg, R., Glatz, J.F.C., Spener, F., 1996. Enzyme immunosensor for diagnosis of myocardial infarction. *Sensors and Actuators B-Chemical* 30(1), 71-76.

Silbiger, V.N., Luchessi, A.D., Crespo Hirata, R.D., Lima Neto, L.G., Pastorelli, C.P., Ueda, E.K.M., dos Santos, E.S., Pereira, M.P., Ramos, R., Sampaio, M.F., Armaganijan, D., Paik, S.H., Murata, Y., Ooi, G.T., Ferguson, E.W., Hirata, M.H., 2011. Time course proteomic profiling of human myocardial infarction plasma samples: An approach to new biomarker discovery. *Clinica Chimica Acta* 412,11-12.

Silva, B.V.M., Cavalcanti, I.T., Mattos, A.B., Moura, P., Sotomayor, M.D.P.T., Dutra, R.F., 2010. Disposable immunosensor for human cardiac troponin T based on streptavidin-microsphere modified screen-printed electrode. *Biosensors & Bioelectronics* 26(3), 1062-1067.

Singhal, R., Takashima, W., Kaneto, K., Samanta, S.B., Annapoorni, S., Malhotra, B.D., 2002. Langmuir-Blodgett films of poly(3-dodecyl thiophene) for application to glucose biosensor. *Sensors and Actuators B-Chemical* 86(1), 42-48.

Sohail, M., Adeloju, S.B., 2008. Electroimmobilization of nitrate reductase and nicotinamide adenine dinucleotide into polypyrrole films for potentiometric detection of nitrate. *Sensors and Actuators B-Chemical* 133(1), 333-339.

Song, S., Wang, L., Li, J., Zhao, J., Fan, C., 2008. Aptamer-based biosensors. *Trac-Trends in Analytical Chemistry* 27(2), 108-117.

Song, S.Y., Han, Y.D., Kim, K., Yang, S.S., Yoon, H.C., 2011. A fluoro-microbead guiding chip for simple and quantifiable immunoassay of cardiac troponin I (cTnI). *Biosensors & Bioelectronics* 26(9), 3818-3824.

Srivastava, S., Verma, M., Gopal-Srivastava, R., 2005. Proteomic maps of the cancer-associated infectious agents. *Journal of Proteome Research* 4(4), 1171-1180.

Steinfeld, U., Palm, B., Lee, H.H.,Molecularly imprinted polymer matrix with specific binding affinity for a cell surface epitope or receptor, useful for isolating cells or for diagnostic or therapeutic purposes. Kist Euro Forschungsges Mbh.

Stubbs, P., Collinson, P.O., 2001. Point-of-care testing: a cardiologist's view. *Clinica Chimica Acta* 311(1), 57-61.

Suprun, E.V., Saveliev, A.A., Evtugyn, G.A., Lisitsa, A.V., Bulko, T.V., Shumyantseva, V.V., Archakov, A.I., 2012. Electrochemical approach for acute myocardial infarction diagnosis based on direct antibodies-free analysis of human blood plasma. *Biosensors & Bioelectronics* 33(1), 158-164.

Suprun, E.V., Shilovskaya, A.L., Lisitsa, A.V., Bulko, T.V., Shumyantseva, V.V., Archakov, A.I., 2011. Electrochemical Immunosensor Based on Metal Nanoparticles for Cardiac Myoglobin Detection in Human Blood Plasma. *Electroanalysis* 23(5), 1051-1057.

Svancara, I., Vytras, K., Kalcher, K., Walcarius, A., Wang, J., 2009. Carbon Paste Electrodes in Facts, Numbers, and Notes: A Review on the Occasion of the 50-Years Jubilee of Carbon Paste in Electrochemistry and Electroanalysis. *Electroanalysis* 21(1), 7-28.

Syritski, V., Reut, J., Menaker, A., Gyurcsanyi, R.E., Oepik, A., 2008. Electrosynthesized molecularly imprinted polypyrrole films for enantioselective recognition of L-aspartic acid. *Electrochimica Acta* 53(6), 2729-2736.

Tai, D.-F., Ho, Y.-F., Wu, C.-H., Lin, T.-C., Lu, K.-H., Lin, K.-S., 2011. Artificial-epitope mapping for CK-MB assay. *Analyst* 136(11).

Tang, J., Breaker, R.R., 1997. Rational design of allosteric ribozymes. *Chemistry & Biology* 4(6), 453-459.

Tang, J., Tang, D., Niessner, R., Knopp, D., Chen, G., 2012. Hierarchical dendritic gold microstructure-based aptasensor for ultrasensitive electrochemical detection of thrombin using functionalized mesoporous silica nanospheres as signal tags. *Analytica Chimica Acta* 720, 1-8.

Tang, L., Kang, K.A., 2006. Preliminary study of fiber optic multi-cardiac-marker biosensing system for rapid coronary heart disease diagnosis and prognosis. Oxygen Transport to Tissue Xxvii 578, 101-106.

Titirici, M.M., Sellergren, B., 2006. Thin molecularly imprinted polymer films via reversible addition-fragmentation chain transfer polymerization. *Chemistry of Materials* 18(7), 1773-1779.

Torabi, F., Far, H.R.M., Danielsson, B., Khayyami, M., 2007. Development of a plasma panel test for detection of human myocardial proteins by capillary immunoassay. *Biosensors & Bioelectronics* 22(7), 1218-1223.

Tripathi, V.S., Kandimalla, V.B., Ju, H.X., 2006. Preparation of ormosil and its applications in the immobilizing biomolecules. *Sensors and Actuators B-Chemical* 114(2), 1071-1082.

Tsafack, V.C., Marquette, C.A., Pizzolato, F., Blum, L.J., 2000. Chemiluminescent choline biosensor using histidine-modified peroxidase immobilised on metal-chelate substituted beads and choline oxidase immobilised on anion-exchanger beads co-entrapped in a photocrosslinkable polymer. *Biosensors & Bioelectronics* 15(3-4), 125-133.

Tu, X., Luo, S., Luo, X., Zhao, Y., Feng, L., Li, J., 2011. Metal chelate affinity to immobilize horseradish peroxidase on functionalized agarose/CNTs composites for the detection of catechol. *Science China-Chemistry* 54(8), 1319-1326.

Turan, E., Ozcetin, G., Caykara, T., 2009. Dependence of Protein Recognition of Temperature-Sensitive Imprinted Hydrogels on Preparation Temperature. *Macromolecular Bioscience* 9(5), 421-428.

Turner, N.W., Jeans, C.W., Brain, K.R., Allender, C.J., Hlady, V., Britt, D.W., 2006. From 3D to 2D: A review of the molecular imprinting of proteins. *Biotechnology Progress* 22(6), 1474-1489.

Tweedie, M., Subramanian, R., Lemoine, P., Craig, I., McAdams, E.T., McLaughlin, J.A., Maccraith, B., Kent, N., 2006. Fabrication of impedimetric sensors for label-free point-of-care immunoassay cardiac marker systems, with passive microfluidic delivery. Conference proceedings: International Conference of the IEEE Engineering in Medicine and Biology Society. IEEE Engineering in Medicine and Biology Society. Conference 1.

Uang, Y.M., Chou, T.C., 2003. Fabrication of glucose oxidase/polypyrrole biosensor by galvanostatic method in various pH aqueous solutions. *Biosensors & Bioelectronics* 19(3), 141-147.

Vasan, R.S., 2006. Biomarkers of cardiovascular disease - Molecular basis and practical considerations. *Circulation* 113(19), 2335-2362.

Wang, H., Yang, R., Yang, L., Tan, W., 2009a. Nucleic Acid Conjugated Nanomaterials for Enhanced Molecular Recognition. *Acs Nano* 3(9), 2451-2460.

Wang, J., Meng, W., Zheng, X., Liu, S., Li, G., 2009b. Combination of aptamer with gold nanoparticles for electrochemical signal amplification: Application to sensitive detection of platelet-derived growth factor. B*iosensors & Bioelectronics* 24(6), 1598-1602.

Wang, J., Musameh, M., 2005. Carbon-nanotubes doped polypyrrole glucose biosensor. *Analytica Chimica Acta* 539(1-2), 209-213.

Wang, Y., Zhou, Y., Sokolov, J., Rigas, B., Levon, K., Rafailovich, M., 2008. A potentiometric protein sensor built with surface molecular imprinting method. *Biosensors & Bioelectronics* 24(1), 162-166.

Whitcombe, M.J., Chianella, I., Larcombe, L., Piletsky, S.A., Noble, J., Porter, R., Horgan, A., 2011. The rational development of molecularly imprinted polymer-based sensors for protein detection. *Chemical Society Reviews* 40(3), 1547-1571.

WHO, 2007. WHO, Facts About Cardiovascular Diseases, World Health Organization, ttp://www.who.int/mediacentre/factsheets/fs317/en/index.html.,

Wolf, M., Juncker, D., Michel, B., Hunziker, P., Delamarche, E., 2004. Simultaneous detection of C-reactive protein and other cardiac markers in human plasma using micromosaic immunoassays and self-regulating microfluidic networks. *Biosensors & Bioelectronics* 19(10), 1193-1202.

Wu, A.H.B., Apple, F.S., Gibler, W.B., Jesse, R.L., Warshaw, M.M., Valdes, R., 1999. National Academy of Clinical Biochemistry standards of laboratory practice: Recommendations for the use of cardiac markers in coronary artery diseases. *Clinical Chemistry* 45(7), 1104-1121.

Wu, W.-Y., Bian, Z.-P., Wang, W., Zhu, J.-J., 2010. PDMS gold nanoparticle composite film-based silver enhanced colorimetric detection of cardiac troponin I. *Sensors and Actuators B-Chemical* 147(1), 298-303.

Xie, C., Liu, B., Wang, Z., Gao, D., Guan, G., Zhang, Z., 2008. Molecular imprinting at walls of silica nanotubes for TNT recognition. *Analytical Chemistry* 80(2), 437-443.

Xu, S.P., Ji, X.H., Xu, W.Q., Li, X.L., Wang, L.Y., Bai, Y.B., Zhao, B., Ozaki, Y., 2004. Immunoassay using probe-labelling immunogold nanoparticles with silver staining enhancement via surface-enhanced Raman scattering. *Analyst* 129(1), 63-68.

Yadav, S., Devi, R., Bhar, P., Singhla, S., Pundir, C.S., 2012. Immobilization of creatininase, creatinase and sarcosine oxidase on iron oxide nanoparticles/chitosan-g-polyaniline modified Pt electrode for detection of creatinine. *Enzyme and Microbial Technology* 50(4-5), 247-254.´

Yuan X., Wang H, Song C., Zhang J. , 2010. Electrochemical Impedance Spectroscopy in PEM Fuel Cells. Fundamentals and Applications. Springer London Dordrecht Heidelberg New York.

Yang, R., Tang, Z., Yan, J., Kang, H., Kim, Y., Zhu, Z., Tan, W., 2008. Noncovalent assembly of carbon nanotubes and single-stranded DNA: An effective sensing

platform for probing biomolecular interactions. *Analytical Chemistry* 80(19), 7408-7413.

Yang, S., Chen, Z., Jin, X., Lin, X., 2006. HRP biosensor based on sugar-lectin biospecific interactions for the determination of phenolic compounds. *Electrochimica Acta* 52(1), 200-205.

Yang, Y.-N., Lin, H.-I., Wang, J.-H., Shiesh, S.-C., Lee, G.-B., 2009. An integrated microfluidic system for C-reactive protein measurement. *Biosensors & Bioelectronics* 24(10), 3091-3096.

Yang, Z., Zhou, D.M., 2006. Cardiac markers and their point-of-care testing for diagnosis of acute myocardial infarction. *Clinical Biochemistry* 39(8), 771-780.

Yildirim, E., Turan, E., Caykara, T., 2012. Construction of myoglobin imprinted polymer films by grafting from silicon surface. *Journal of Materials Chemistry* 22(2), 636-642.

Yonemori, Y., Takahashi, E., Ren, H., Hayashi, T., Endo, H., 2009. Biosensor system for continuous glucose monitoring in fish. *Analytica Chimica Acta* 633(1), 90-96.

Yuqing, M., Jianrong, C., Xiaohua, W., 2004. Using electropolymerized non-conducting polymers to develop enzyme amperometric biosensors. *Trends in Biotechnology* 22(5), 227-231.

Yusuf, S., Pearson, M., Sterry, H., Parish, S., Ramsdale, D., Rossi, P., Sleight, P., 1984. The entry ecg in the early diagnosis and prognostic stratification of patients with suspected acute myocardial-infarction. *European Heart Journal* 5(9), 690-696.

Zane, D., Appetecchi, G.B., Bianchini, C., Passerini, S., Curulli, A., 2011. An Impedimetric Glucose Biosensor Based on Overoxidized Polypyrrole Thin Film. *Electroanalysis* 23(5), 1134-1141.

Zayats, M., Kanwar, M., Ostermeier, M., Searson, P.C., 2011. Molecular Imprinting of Maltose Binding Protein: Tuning Protein Recognition at the Molecular Level. *Macromolecules* 44(10), 3966-3972.

Zdyrko, B., Hoy, O., Luzinov, I., 2009. Toward protein imprinting with polymer brushes. *Biointerphases* 4(2), FA17-FA21.

Zhang, J., Xu, L., Wang, Y.Q., Lu, R.H., 2009a. Electrochemical Sensor for Bisphenol A Based on Molecular Imprinting Technique and Electropolymerization Membrane. *Chinese Journal of Analytical Chemistry* 37(7), 1041-1044.

Zhang, Z., Xia, S., Leonard, D., Jaffrezic-Renault, N., Zhang, J., Bessueille, F., Goepfert, Y., Wang, X., Chen, L., Zhu, Z., Zhao, J., Almeida, M.G., Silveira, C.M., 2009b. A novel nitrite biosensor based on conductometric electrode modified with cytochrome c nitrite reductase composite membrane. *Biosensors & Bioelectronics* 24(6), 1574-1579.

Zhao, X.-Y., Qu, F., Dong, M., Chen, F., Luo, A.-Q., Zhang, J.-H., 2012a. Separation of Proteins by Aqueous Two-phase Extraction System Combined with Liquid Chromatography. *Chinese Journal of Analytical Chemistry* 40(1), 38-42.

Zhao, Y.-P., Ruan, C.-P., Wang, H., Hu, Z.-Q., Fang, M., Gu, X., Ji, J., Zhao, J.-Y., Gao, C.-F., 2012b. Identification and assessment of new biomarkers for colorectal cancer with serum N-glycan profiling. *Cancer* 118(3), 639-650.

Zheng, J., Feng, W., Lin, L., Zhang, F., Cheng, G., He, P., Fang, Y., 2007. A new amplification strategy for ultrasensitive electrochemical aptasensor with network-like thiocyanuric acid/gold nanoparticles. *Biosensors & Bioelectronics* 23(3), 341-347.

Zhou, F., Lu, M., Wang, W., Bian, Z.-P., Zhang, J.-R., Zhu, J.-J., 2010. Electrochemical Immunosensor for Simultaneous Detection of Dual Cardiac Markers Based on a Poly(Dimethylsiloxane)-Gold Nanoparticles Composite Microfluidic Chip: A Proof of Principle. *Clinical Chemistry* 56(11), 1701-1707.

Zhu, L., Yang, R., Zhai, J., Tian, C., 2007. Bienzymatic glucose biosensor based on co-immobilization of peroxidase and glucose oxidase on a carbon nanotubes electrode. *Biosensors & Bioelectronics* 23(4), 528-535.

Zhuo, Y., Yi, W.-J., Lian, W.-B., Yuan, R., Chai, Y.-Q., Chen, A., Hu, C.-M., 2011. Ultrasensitive electrochemical strategy for NT-proBNP detection with gold nanochains and horseradish peroxidase complex amplification. *Biosensors & Bioelectronics* 26(5), 2188-2193.

Ziegler, J., Zimmermann, M., Hunziker, P., Delamarche, E., 2008. High-performance immunoassays based on through-stencil patterned antibodies and capillary systems. *Analytical Chemistry* 80(5), 1763-1769.

3

Myoglobin-Biomimetic Electroactive Materials made by Surface Molecular Imprinting on Silica Beads and their used as Ionophores in Polymeric Membranes for Potentiometric Transduction

3.1 Introduction

Molecules with nanoscale dimensions can be assembled on a surface, with high structural control, mimicking nature's modular approach to nanostructured materials. This is the case of surface imprinting, lead to higher binding capacity and faster mass transfer/binding kinetics than traditional bulk processes. In general, surface imprinting involves 4 steps: (i) attachment of the template to the surface (ii) selection of functional monomers showing a special ability to interact with the functional groups of the template molecule; (iii) a pre-polymerization stage where these monomers are allowed to bind to the template molecule, followed by a polymerized step; (iv) and template removal, leaving behind cavities that constitute the templates comprising of empty rebinding sites. Most of the imprinted sites obtained are near or in the surface, with most templates being removed from the highly cross-linked matrix.

In surface imprinting the nanostructured support where the imprinted material is being formed should be carefully selected.

Typical examples include superparamagnetic nanosized particles for magnetic separation, gold (Moreira et al. 2013) and silica beads (Shiomi et al. 2005). Silica beads demonstrated good mechanical strength and large surface area which offer great potential for their application in biosensors and chromatography. In addition, it can be included in biosensors as a support of biomaterials and be applied as a part of optical, electrical, mass or thermal platforms (Hua et al. 2009). Thus regarding the transduction, several possibilities arise in this context. Considering specifically that this is intended for diagnosis in POC, portability, low cost, high selectivity and small size are required features. This may be achieved by potentiometric readings with PVC-based sensory surfaces, employing the plastic antibodies as electroactive materials designed on silica beads. Potentiometric biosensors offer the advantage of selectivity and portability for use in point-of-care and have been widely recognized as potential analytical tools in this field. The inherent method is simple, precise, accurate and inexpensive regarding reagent consumption and equipment involved. Washing steps are not required before the signal can be read and the analyte can be captured from complex mixtures without prior purification. In terms of environmental "impact", they are called a green analytical approach for avoiding the use of organic solvents and discharging wastewaters of small concern with regard to volume and composition.

Thus, a potentiometric sensor selective to Myo is proposed. Here having as electroactive material the surface imprint of Myo on silica beads. The corresponding MI particles are after included in a polymeric membrane. The imprinting effect is tested by carrying out the same procedure without Myo. NI particles so obtained were similarly included in polymeric membranes and used as control.

3.2. Experimental Section

3.2.1 Apparatus

Emf was measured in a Crison GPL 22 decimilivoltammeter (±0.1 mV sensitivity), at room temperature, and under constant stirring. The output signal was reconnected to a commutation point with six ways out, enabling the simultaneous reading of six selective electrodes.

The potentiometric cell was assembled as conductive contact of epoxy-graphite | Myo selective membrane | buffered sample solution, (4-(2-hydroxyethyl)-1-piperazineethanesulfonic acid, HEPES, 1.0×10^{-3} mol/L, pH 4.5) || electrolyte solution, KCl | AgCl(s) | Ag. The reference was an Ag/AgCl double-junction electrode (Orion 90-02-00).

When necessary, the pH was measured by a Crison CWL/S7 combined glass electrode connected to the same decimelivoltimeter.

3.2.2 Reagents

All chemicals were of analytical grade and de-ionized water (conductivity <0.1 µS/cm) was employed. Aminopropyl silica (particle size 15-40 µm, mean pore size 75 Å), Myo, Sodium salt buffer grade (3-(*N*-morpholino)propanesulfonic acid) (MOPS), HEPES, piperazine-*N,N*'-bis(2-ethanesulfonic acid) (PIPES), *o*-nitrophenyloctylether (*o*NPOE), PVC of high molecular weight, 3-aminopropyltrimethoxysilane (APTMS), propyltrimethoxysilane (PTMS), GA , oxalic acid (Oac), and sodium chloride (NaCl) were purchased from Fluka. Tetrahydrofuran (THF) was obtained from Riedel-deHäen.

3.2.3 Solutions

Stock solutions of 1.0×10^{-4} mol/L Myo were prepared in water. Less concentrated Myo standards were prepared by accurate dilution of the previous solution in buffer. Buffer solutions were 1.0×10^{-2} mol/L HEPES. The pH of this solution was altered by adding suitable volumes of either concentrated hydrochloric acid or saturated sodium hydroxide solution freshly prepared.

The interference of other chemicals was evaluated for 1.0×10^{-6} mol/L Myo prepared in pH 4.5 buffer. Solutions of interfering species were of variable concentrations and prepared in the same buffer. Creatinine (Creat, 1.04×10^{-3} mol/L), sucrose (Sac, 1.61×10^{-5} mol/L), fructose (Fru, 9.34×10^{-4} mol/L), galactose (Gat, 5.58×10^{-5} mol/L), sodium glutamate (Glt, 7.61×10^{-5} mol/L), thiamine (Thia, 2.13×10^{-5} mol/L), alanine (Ala, 6.17×10^{-5} mol/L), and glucose (Glu, 4.19×10^{-5} mol/L) solutions were prepared for this purpose.

3.2.4 Surface analysis of the host-tailored polymers

The surface of the MI and NI modified silica bead was analysed by SEM (with X-Ray Microanalysis, JEOL JSM 35C/Noran Voyager. SEM observation was conducted with metal coating at 33 Pa and room temperature by using low vacuum mode. Energy Dispersive Spectrometer (EDS) analysis was carried out in several points of each material.

Fourier Transformed Infrared Spectroscopy (FTIR) analysis was conducted in a Nicolet 6700 FTIR spectrometer. Infrared spectra were collected under room temperature/humidity control after background correction. The number of scans was 32 for both sample and background. X-axis was wavenumber, ranging 525 to 4000 cm^{-1}, and Y-axis was % transmittance. Resolution was 4000.

3.2.5 Synthesis of host-tailored polymers

About 100 mg of aminopropyl silica was suspended in 1 mL of 10 mM pipes buffer (pH 5.0) and the mixture was then degassed for 10 min. at room temperature. The supernatant was removed after and 1 mL of 10 mmol/L PIPES buffer (pH 5.0) containing 1% of GA was added to the wet aminopropyl silica. The resulting mixture was incubated for 12 h at room temperature. The silica particles were then repeatedly washed with distilled water and incubated next in 1 mL of 2.5 mg/mL Myo solution (pH 7, 10 mmol/L MOPS, 1 mol/L NaCl) for 3 h at 4 ^{o}C. The resulting supernatant was replaced by 10 mmol/L MOPS buffer (pH7). After that, 2.5 mL of 3-APTMS and 25 mL of PTMS were added and the subsequent polymerization was carried out at room temperature, for 36 h. The Myo-imprinted silica was rinsed with water until the supernatant was clear. Then, 1.0 mL of 1.0 mol/L Oac was added to remove the template. This step was carried out at room temperature and the incubation lasted 12 h. Finally, the product was repeatedly washed with distilled water and dried in a desiccator. The synthesis of the NIM was made by the same process as that of the imprinted material but without the template molecule.

3.2.6 Preparation of the potentiometric sensors

Myo selective membranes were prepared by mixing 210 mg of PVC, 350 mg of plasticizer *o*NPOE and 15 mg of MI and NI modified silica beads. The mixture was stirred until the PVC was well moistened, and dispersed in 2.5 mL THF. These membranes were applied over the solid conductive supports and let dry for 24 h. After that they were conditioned in a 1×10^{-7} mol/L Myo solution. The electrodes were kept in this solution when not in use.

3.2.7 Potentiometric procedures

All potentiometric measurements were carried out at room temperature and under constant stirring. Increasing concentrations of Myo were obtained by transferring 0.0200 to 2.5 mL aliquots of 1.0×10^{-4} mol/L Myo aqueous solution to a 100 mL beaker containing 20.0 mL of 1.0×10^{-3} mol/L of suitable buffer, of fixed pH and ionic strength. The potential readings of the stirred Myo solutions were measured at room temperature and recorded after stabilization to ± 0.2 mV. Between assays, the sensors were conditioned in 1.0×10^{-5} mol/L Myo solution.

3.2.8 Selectivity

Potentiometric selectivity coefficients were assessed by the Matched Potential Method (MPM). The initial concentration of primary ion was set to 1.0×10^{-6} mol/L (a_A) and the activity of the primary ion solution added into this was 4.0×10^{-6} mol/L ($a_{A'}$). The corresponding potential change was about 10 mV. The interference of Crea, Sac, Fru, Gat, Glt, Thia, Ala, and Glu was assessed by add ing small aliquots of the corresponding solutions into the primary ion solution of a_A until the same potential change was observed, i.e., until the increment of 10 mV was reached, ensuring that the final concentration of primary ion was not altered by more than 5 %.

3.2.9 Determination of binding capacities of molecularly imprinted materials

Binding experiments were carried out by placing 5.0 mg of MI washed particles in contact with 3.5 mL Myo aqueous solutions ranging 0.02 – 2.0 mol/L. The mixtures were oscillated for 20 h at room temperature and the solid phase separated by centrifugation (3000 rpm, 10 min). Myo concentrations in the supernatant

were measured by UV/vis spectrophotometry (at 410 nm) against calibration graph with Myo standard solutions.

3.3. Results and Discussion

3.3.1 Myoglobin artificial antibody assembly

In MI the template recognition capability is defined by the kind(s) of sites or functional groups present in the polymerizable materials employed for their generation. Considering specifically the protein imprint, their hydrophobic interactions with silane surfaces may an play important role, as supported by previous observations (Cha et al. 1999; Venton and Gudipati 1995). On the other hand, surface imprint is much more effective than bulk procedures when sensory surfaces are to be prepared.

Thus, aminopropyl silica was employed as physical support to assemble the Myo artificial antibody. Nanopored silica was selected for this purpose because it has a large surface area and known capacity to adsorb Myo (Wu and Walters 1988).

The surface of the silica beads was modified following the scheme presented in (Figure 18). It consisted of three different stages: (i) template immobilization on the bead surface; (ii) filling vacant places with suitable functionalities and hard material; and (iii) template removal, leaving behind its imprinted site with rebinding properties.

Myo was immobilized by reaction between its amine groups and the aldehyde function on the surface of the beads, with subsequent formation of an imine bond. Aldehyde groups were introduced on the external surface of the beads by reacting aminopropyl silica with GA. The organic silane monomers APTMS and PTMS were selected to fill the free space around the template. These polymerize under mild conditions, which contributed to preserve the template configuration unaltered.

Myo imprinted material resulted from the template removal (Wang et al. 2008). Strong acids had to be used to break the silica-protein covalent bonds. Thus, the material was incubated in 1.0 mol/L Oac for 12 hours (Shiomi at al., 2005). Several washing steps were made after with 10 mmol/L MOPS buffer to remove the protein fragments adsorbed to the beads and increase the inherent pH from 1.2 to 8.0. The modified beads were conditioned in this buffer before carrying out binding experiments.

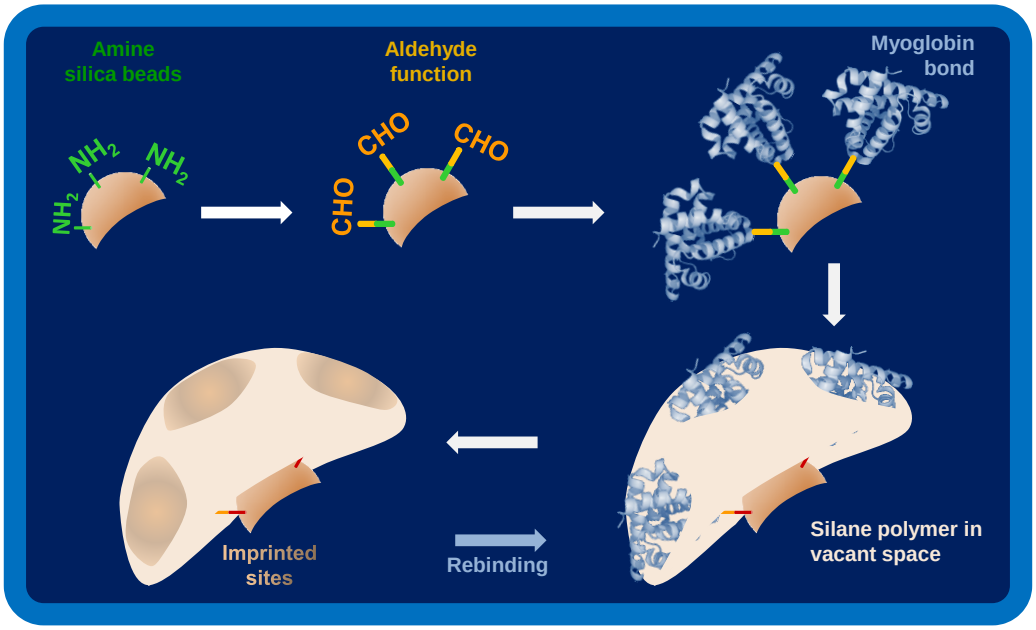

Figure 18: Assembly of the molecularly-imprinted.

3.3.2 Surface analysis of the host-tailored polymers.

3.3.2.1 Scanning Electron Microscopy Energy Dispersive Spectrometer analysis

The silica beads had an average diameter of 15-40 nm and were mainly composed by Si and O, before surface modification. Clearly, the imprinting effect could not

be proven by means of SEM, because MI and NI materials were similar. However, the chemical modification of the surface was easily detected. The diameter of the beads increased up to 125.6 nm, measured when the original material was magnified by 400,000 times. This was consistent with the EDS spectra in Figure 19. Both MI and NI materials showed similar composition, with N and C (besides Si and O). These atoms came from the APTMS and PTMS monomers used for the sol-gel based imprint

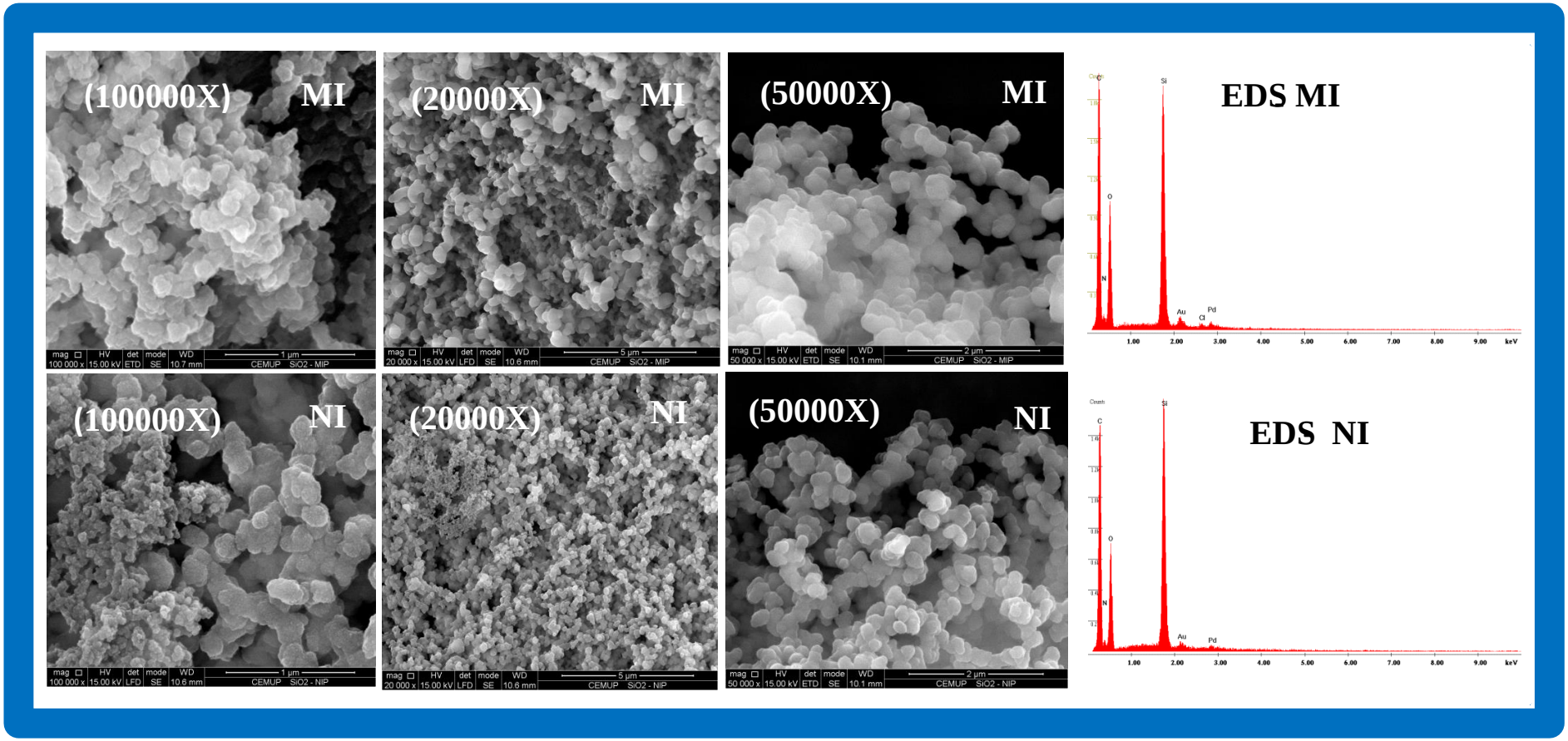

Figure 19: SEM and EDS analysis of MI (A) and NI (B) modified silica beads immobilized in tape carbon.

3.3.2.2 Fourier Transformed Infrared Spectroscopy analysis

Structural changes of the silica beads and its composites were confirmed by FTIR spectra (Figure 20). The IR spectrum for non-modified silica beads showed significant bands at 920 and 1075 cm^{-1}, revealing the medium intensity absorption bands from the Si-OH and Si-O-Si vibrations, respectively.

Since the chemical modification of the silica beads also employed sol-gel based materials, the above peaks were also in the spectra of FTIR surface analysis of the MI and NI modified beads. These spectra also pointed out a small increase of the C=O band, approximately at 1620 cm^{-1}. Since the carbonyl bears a highly absorbing bond, it is likely that only a very small part of the surface had unreacted C=O groups. The broad absorption low intensity band lying between 3000 and 3500 cm^{-1} was probably a combined result of the N-H stretch of the amine groups (introduced through polymerization of APTMS and the O-H stretch of the a small number of alcohol groups (generated by alcoxide hydrolysis).

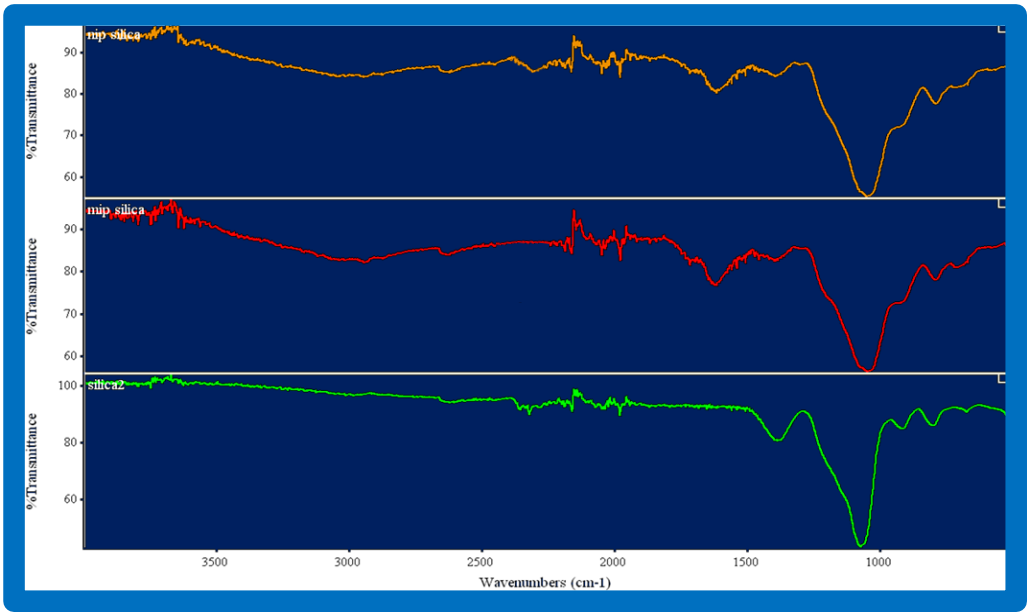

Figure 20: FTIR spectra of modified MI and NI and unmodified silica beads.

3.3.3 Rebinding properties of the imprinted materials

In practical terms, the MI materials should have a high affinity for the template to which they were designed. This may be assessed by rebinding experiments. For this purpose, fixed amounts of MI materials were incubated with different concentrations of Myo until the equilibrium was reached (Connors 1987; Shea et al. 1993). The resulting binding capacity was calculated by equation 24:

$$Q = \frac{\mu mol(Myo\ bound)}{g(MIP)} = \frac{(C_i - C_f)V_s \times 1000}{M_{MIP}} \qquad \textbf{Equation 24}$$

where Q was binding capacity of MI (μmol/g), C_i the initial Myo concentration (μmol/mL), C_f the final Myo concentration (μmol/mL), V_s the volume of solution tested (mL), MIP the mass of dried polymer (mg).

The binding capacities were plotted against Myo initial concentration in the incubation medium (Figure 21). The resulting adsorption data showed that the binding capacity of imprinted polymer increased with the increasing of the initial concentration of Myo, but it reached to saturation when high concentrations of template were present. The binding data was used to carry out Scatchard analysis, providing important information on binding properties of the imprinted particles (Sellergren 1994). The Scatchard equation,

$$Q/C_{free} = (Q_{max} - Q)/K_d \qquad \textbf{Equation 25}$$

was applied for this purpose, where Q is the binding capacity; C_{free} the free analytical concentration at equilibrium (μmol/L); Q_{max} is the maximum apparent binding capacity; and K_D is the dissociation constant at binding site. The equilib-

rium dissociation constant was calculated from the slopes and the apparent maximum number of binding sites from the *y*-intercepts in the linear plot of Q/C_{free} *versus* Q.

Scatchard plot of the MI consisted of two distinct straight lines (Figure 21), inferring the existence of high and low affinity populations of binding sites (Sellergren, 2001). K_{d1} and Q_{max} were, respectively, 0.21 µmol/L and 49 µmol/g for the high affinity binding sites, and 12 µmol/L and 163 µmol/g for the low affinity binding sites. The lower affinity binding behaviour resulted from non-specific interactions while the higher affinity came from the interaction between specific sites of the artificial antibody and the template, leading to stereochemical recognition of the analyte.

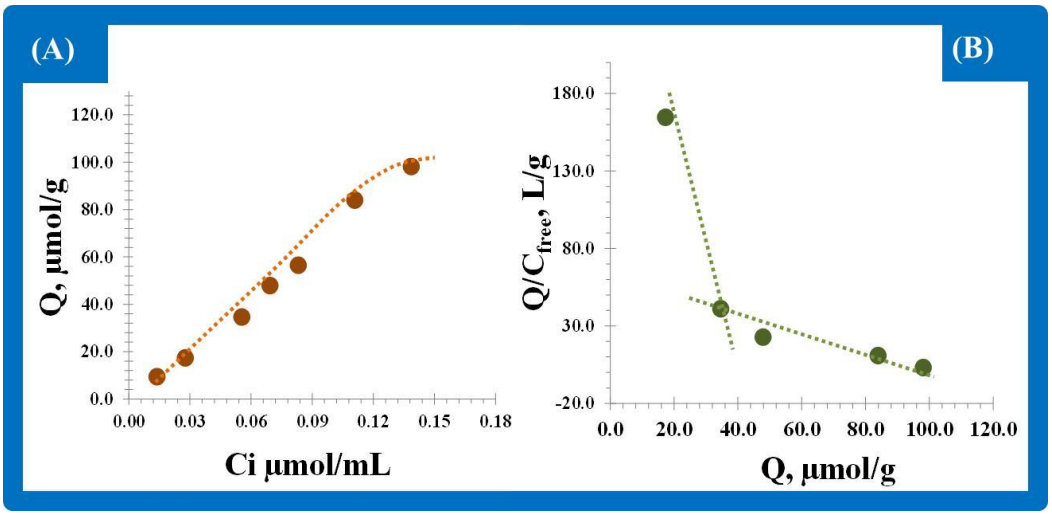

Figure 21: Binding isotherm (left) and Scatchard plot (right) for Myo imprinted materials.

3.3.4 Imprinted and non-impronted materials acting as ionophores

Myo sensors were prepared by dispersing the active ingredients (MI or NI particles) in a high dielectric constant plasticizer and PVC. Evaluation of their main

analytical features followed the International Union of Pure and Applied Chemistry (IUPAC) recommendations (Umezawa et al. 2000), and was carried out in batch conditions.

For NI sensors, the emfs changed linearly with log[Myo] for concentrations down to 1.0 x 10^{-6} mol/L, displaying detection limits within the 10^{-7} mol/L decade. On the contrary, the potentiometric sensor prepared with NI particles was unable to produce a linear response, no matter the pH of the test solution (Figure 22). These results indicated that the non-specific places of interaction (the only kind that exists on NI particles) between the template and the polymer were not leading the potentiometric response. Only monomers polymerized in the presence of a template could have imprinted cavities, enabling the specific interaction between the template and the sensor. Therefore, the potentiometric response observed for the MI electroactive materials was mainly due to a topographic recognition of the analyte at the imprinted cavities.

3.3.5 Effect of pH

Electrodes with MI particles were calibrated in different pH conditions (3, 4, 5, 6 and 9). The results obtained are presented in (Figure 22). Linear behavior was observed down to 3.5 × 10^{-6}, 1.2 × 10^{-6}, 1.2 × 10^{-6}, 1.2 × 10^{-6}, and 3.8 × 10^{-6} mol/L of Myo, with slopes of -178.7, -65.9, -25.5, -12.5, and +8.2 mV/decade and detection limits of 81.3, 13.5, 10.7, 2.2, and 5.4 µg/mL, respectively. The squared correlation coefficients were always > 0.990. The electrodes were also tested in pH 7.5 but there was no linear response observed.

Essentially, the slopes were anionic below pH<7.5 and turned out cationic for pH 9.0. These results suggested that Myo was negatively charged below 7.5 pH and positively charged above that value. However, this is the opposite behaviour expected from the isoelectric point for Myo, equal to 7.2. Myo has many ionizable functional groups on the outer surface that may interact with the membrane. The closest idea to explain the negative behaviour of these selective electrodes under acidic media is that the protein is approaching the membrane by its negatively

charged groups, which is favoured by the positively charged H^+ hanging close to the membrane and creating a positive environment. Apparently, it seems that the exceeding H^+ in acidic medium is binding to the electrode surface and contributing to the detection of a negatively charged portion of Myo.

In terms of analytical application, a pH of 4.0 was selected for further studies. This was the only condition where the sensor displayed a near-Nernstian behaviour, assuming that Myo was singly charged under this condition (see Figure 22).

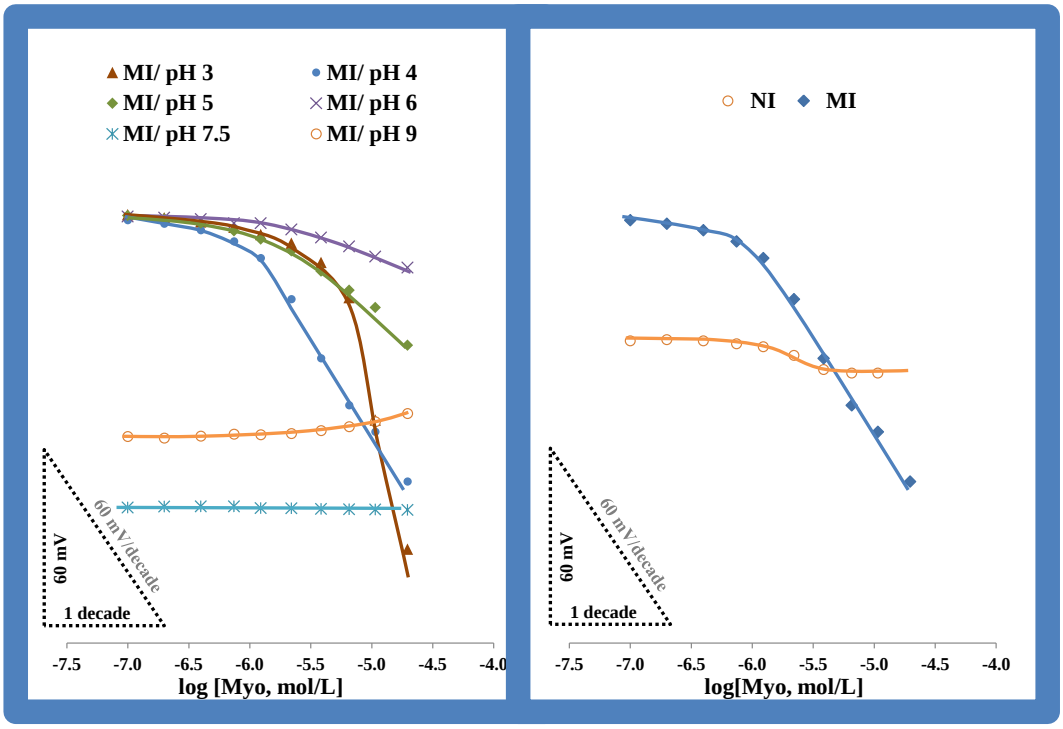

Figure 22: Calibration curve of imprinted based sensors in different pHs (A) and imprinted and non-imprinted sensors in pH 4.5.

3.3.6 Response time and lifetime

The time required to achieve a steady potential response (± 3 mV) in 1.0×10^{-3} mol/L Myo solutions with a rapid 10-fold increase in concentration was < 15 s. Low potential drift and long-term stability were observed within calibrations made in consecutive days. In general, detection limits, response times, linear

range and calibration slopes were reproducible within ± 5% of their original values over a period of at least 5 weeks.

3.3.7 Sensor selectivity

The selectivity of an ISE depends on the selectivity of the template/ionophore binding and on the standard free energies of the respective ions in the aqueous and organic phases (Bakker and Pretsch 2001). Thus, a high selectivity suggests the use of ligands that strongly bind the preferred ion and only weakly all the others.

The selectivity behaviour of Myo ISEs was observed by calculating logarithmic potentiometric selectivity coefficients, $\log K_{pot}$. These coefficients defined the ability of an ISE to differentiate a particular (primary) ion from others (interfering species). The MPM was used for this study (Umezawa et al. 2000), where K_{pot} is defined as the activity (concentration) ratio of primary and interfering ions that give the same potential change under identical conditions (Equation 26). A known activity ($a_{A'}$) of the primary ion solution is added first into a reference solution that contains a fixed activity (a_A) of primary ions, and the corresponding potential change (ΔE) is recorded. Next, a solution of an interfering ion is added (a_B) to the reference solution until the same potential change (ΔE) is observed. The change in potential produced at the constant background of the primary ion must be the same in both cases.

$$K_{A,B}^{POT} = \frac{(a_{A'} - a_A)}{a_B} \qquad \textbf{Equation 26}$$

Creat, Sac, Fru, Gal, Glu, Glt, Ala, and Thia were tested as possible interfering species in biological samples. Overall, $\log K_{pot}$ ranged from -0.69 to -2.50 and the lowest value (-2.5) was obtained for Creat, a biological metabolite. Different

amino acids interfered in a similar way, leading to log $K_{pot} \approx$ - 1.3. The relative selectivity degree of sugar interference was Fru < Gal < Glu < Sac, with log K_{pot} varying from -2.45 to -0.69. The interference from Thia that is vitamin B_1, a sulfur-containing vitamin, was negligible, with log K_{pot} = -0.8.

In general, the recorded values reported negligible interference for all species tested (Table 3). The interference of Hmg was also tested for concentrations ranging from 700 to 70000 ng/mL and found negligible.

Table 3: Potentiometric selectivity coefficients of non- imprinted Myo sensors.

Interfering species	log Kpot
Creatinine	-2.50
Sucrose	-0.69
Fructose	-2.45
Galactose	-1.24
Sodium glutamate	-1.37
Alanine	-1.27
Glucose	-1.11
Thiamine	-0.81

3.3.8 Myoglobin Assay

A real application requires previous pre-concentration procedures that can reach up to 1000 times the concentration in the sample. This has been already tested and described in the literature (Nesbitt, 2005). Thus, the present method has presumably applied to those concentrated samples.

The method was applied to determine Myo in spiked samples ranging from 107.9 – 321.8 µg/mL Myo. A good agreement was found between added and found amounts of Myo. Results of the potentiometric analysis conducted in steady state

showed recoveries ranging 93.8 – 107.5 % with an average relative standard deviation of 1.8%. The relative error ranged 5.70 – 6.96% with an average relative standard deviation of 0.02%.

3.3.9 Impedimetric analysis

Detection capability may be improved by changing the technique and the electrode design. Since the potentiometric sensitivity is regulated by the Nernst equation, no further improvements may be obtained by this technique, and impedance was selected to improve the present proposal. SPE modified by the same imprinting procedure were used in order to improve signal/noise ratio.

Impedimetric analysis was conducted on modified gold-screen printed electrodes. The electrode modification was made by applying the same PVC membrane over the gold surface. Impedance measurements were performed in buffer (pH 7.4) including 5.0 mmol/L $[Fe(CN)_6]^{3-}$ and 5.0 mmol/L $[Fe(CN)_6]^{4-}$ at a standard potential of 0.225V. The frequency range was 0.5–1000 Hz. The impedance data were fitted to an equivalent circuit using the implemented ANOVA software. The sensor displayed better features in terms of linear range compared to the graphite electrodes, decreasing the lower limit for linear response from 1.24 x 10^{-6} mol/L to 3.71 x 10^{-7} mol/L.

3.4. Conclusions

MI technology was successfully employed to produce biomimetic Myo sensors for potentiometric transduction with similar to host-guest interactions. The shape of Myo was tailored by attaching it covalently to a silane surface and filling the surroundings by polymerization of 3-APTMS and PTMS monomers. The covalent bond to Myo was broken and the corresponding site showed rebinding capabilities, indicating that the template was stereochemically recognized.

Only imprinted organic materials were capable to discriminate Myo from other organic compounds in aqueous media in potentiometric assays. The corresponding sensors offered simplicity in designing low response time, good precision, high accuracy, low limit of detection and good selectivity. The proposed method is simple, of low cost, precise, accurate and inexpensive, and may turn out, in a near future, an alternative method for screening Myo in POC.

Further improvements may be however achieved by introducing alterations at the imprinting stage as well as the nanostructured support, as described in the following charpter.

3.5. References

Bakker, E., Pretsch, E., 2001. Potentiometry at trace levels. Trac-Trends in *Analytical Chemistry* 20(1), 11-19.

Cha, J.N., Shimizu, K., Zhou, Y., Christiansen, S.C., Chmelka, B.F., Stucky, G.D., Morse, D.E., 1999. Silicatein filaments and subunits from a marine sponge direct the polymerization of silica and silicones in vitro. *Proceedings of the National Academy of Sciences of the United States of America* 96(2), 361-365.

Connors, K., 1987. Binding constants. The measurement of molecular complex stability. John Wiley & Sons, New York.

Hua, Z., Zhou, S., Zhao, M., 2009. Fabrication of a surface imprinted hydrogel shell over silica microspheres using bovine serum albumin as a model protein template. *Biosensors & Bioelectronics* 25(3), 615-622.

Moreira, F.T.C., Sharma, S., Dutra, R.A.F., Noronha, J.P.C., Cass, A.E.G., Sales, M.G.F., 2013. Smart plastic antibody material (SPAM) tailored on disposable screen printed electrodes for protein recognition: Application to myoglobin detection. *Biosensors & Bioelectronics* 45, 237-244.

Sellergren, B., 1994. Imprinted dispersion polymers - a new class of easily accessible affinity stationary phases. *Journal of Chromatography A* 673(1), 133-141.

Sellergren, B., 2001. Molecularly Imprinted Polymers. Elsevier.

Shea, K.J., Spivak, D.A., Sellergren, B., 1993. Polymer complements to nucleotide bases - selective binding of adenine-derivatives to imprinted polymers. *Journal of the American Chemical Society* 115(8), 3368-3369.

Shiomi, T., Matsui, M., Mizukami, F., Sakaguchi, K., 2005. A method for the molecular imprinting of hemoglobin on silica surfaces using silanes. *Biomaterials* 26(27), 5564-5571.

Umezawa, Y., Buhlmann, P., Umezawa, K., Tohda, K., Amemiya, S., 2000. Potentiometric selectivity coefficients of ion-selective electrodes Part I. Inorganic cations - (Technical report). *Pure and Applied Chemistry* 72(10), 1851-2082.

Venton, D.L., Gudipati, E., 1995. Entrapment of enzymes using organo-functionalized polysiloxane copolymers.*Biochimica Et Biophysica Acta-Protein Structure and Molecular Enzymology* 1250(2), 117-125.

Wang, Y., Zhou, Y., Sokolov, J., Rigas, B., Levon, K., Rafailovich, M., 2008. A potentiometric protein sensor built with surface molecular imprinting method. *Biosensors & Bioelectronics* 24(1), 162-166.

Wu, D.L., Walters, R.R., 1988. Protein immobilization on silica supports - a ligand density study. *Journal of Chromatography* 458, 169-174.

4

Artificial antibodies for Troponin T by its imprinting on the surface of Multiwalled Carbon Nanotubes: its use as sensory surfaces

4.1 Introduction

A high number of imprinted sites, may be achieved on top of nanostructured materials, favouring miniaturization (Agasti et al. 2010) and providing a more homogeneous distribution of the recognition sites (Guan et al. 2008). The selection of a support to carry out such modification may also lead to additional advantages, especially by selecting materials that display special electrical features.

The use of MWCNTs for this purpose is a possibility. They display one hundred times the tensile strength of steel, excellent thermal conductivity and electrical conductivity similar to copper but with the ability to carry much higher currents (Merkoci 2006). They have been included in biosensors as biorecognition elements as single probes (Ishikawa et al. 2009) as support of biomaterials (Mao et al. 2011) or individually attached onto a proper transducing surface after synthesis (Li et al. 2005). They may also be used for surface modification or integrated in polymeric matrices, in both oriented and non-oriented configurations (Merkoci et al. 2005). Several applications of these

materials, as part of electrochemical platforms, have also been reported (Lu et al. 2008; Shumyantseva et al. 2005).

Thus, the design of new MI materials interacting selectively with the cardiac biomarker TnT on the surface of MWCNT and subsequent potentiometric transduction are presented.

TnT is linked to the surface of carboxylated MWCNTs. Then, functional monomer, cross-linker, initiator are reacted under mild conditions to create a rigid structure around the template. After, the template is removed by chemical treatment. A similar procedure is carried out without template (TnT) and considered as non-imprinted (NI) control (Jiang et al. 2004).

4.2. Experimental

4.2.1 Apparatus

Potentials were measured by a Crison pH-meter GLP 21 (± 0.1 mV sensitivity), at room temperature, and under constant stirring. The output signal was transferred to a commutation unit and reconnected to one of six ways out, enabling the simultaneous reading of sensing surfaces.

Infrared spectra were collected by a Nicolet 6700 FTIR spectrometer coupled to an ATR (Attenuated Total Reflectance) sampling accessory of diamond contact crystal from Nicolet. A SEM with X-Ray Microanalysis, JEOL JSM 35C/Noran Voyager, was used for microscopy analysis.

4.2.2 Reagents

All chemicals were of analytical grade and de-ionized water (conductivity <0.1 μS/cm) was employed throughout. Carboxylated MWCNTs were bought to Dropsens, Spain. TnT, HEPES, PIPES, oNPOE, PVC, AAM, NNMBA, ammonium persulphate (APS), Oac, NHS, EDAC, and NaCl were purchased to Fluka. THF was obtained from Riedel-deHäen.

4.2.3 Synthesis of biomimetic materials

4.2.3.1 Activation of the carboxylic acid in the multi-wall carbon nanotubes

About 3.0 mg of carboxylated MWCNTs were suspended in 1.0 mL of deionized water by sonication of the mixture for about 1 minute. Then, 1.0 mL of an aqueous solution containing 5 mmol/L NHS and 2 mmol/L EDAC were added to the above suspension and the mixture was continuously stirred at room temperature for 45 min. The suspension was then filtered with filter paper whatman and the solid material rinsed thoroughly with deionized water to remove unreacted reagents.

4.2.3.2 Imprinting step

The modified CNT were redispersed in 1 mL of 10 µmol/L PIPES buffer solution (pH 7.0) containing 8.0 µmol/L TnT and 0.1 mol/L NaCl for 4 hours at 4 °C to bind the template. The MWCNTs were then incubated in 1 mol/L Tris for 30 minutes, in order to block the un-reacted ester groups. Several washes with deionised water followed and finally 1 mL of 50 mmol/L AAM and 50 mmol/L NNMBA, PIPES solution (pH 7.0) was added to the MWCNTs. After 60 min incubation, 1 mL of 50 mmol/L APS solution in pH 7.0 was added to start the polymerization. The polymerization was carried out at room temperature for 1 h, after which the sensor was thoroughly washed with deionised water. Finally, 1 mL of 1.0 mol/L Oac was added to remove the template. This step was carried out at room temperature for 12 h. The imprinted MWCNTs were washed and conditioned in 10 mM phosphate buffer, pH 8.0, in order to increase the pH and remove the peptide fractions produced by Oac treatment.

4.2.3 Scanning Electron Microscopy/ Energy Dispersive Spectrometer analysis

SEM analysis was conducted over the dried MMWCNTs, NMWCNTs and MWCNT materials, at room temperature and in low vacuum mode. EDS analysis was conducted on several sampling points for each biomaterial.

4.2.4 Fourier Transformed Infrared Spectroscopy analysis

Infrared spectra were collected after background correction and under room temperature/humidity control. The number of scans was 32 for both sample and background. X-axis was wavenumber, ranging 525 to 4000 cm^{-1}, and Y-axis was % transmittance. Resolution was 4000.

4.2.5 Preparation of sensory membranes

About 100 mg of PVC, 75 mg of plasticizer oNPOE and 3.0 mg of each sensing polymer MI-MWCNT, NI-MWCNT or MWCNT were mixed. The mixture was stirred until the PVC was well moistened, and dispersed in 3.5 mL THF. These membranes were used to coat conductive wires of different metals and let dry during 48 h. After drying, the electrodes were kept in 1.0 x 10^{-4} mol/L TnT solution.

4.2.6 Potentiometric procedures.

All potential measurements were made by a Crison µpH 2002 decimilivoltammeter (±0.1 mV sensitivity), at room temperature, and under constant stirring, by means of a Crison, micro ST 2038. The output signal in steady state evaluations was transferred to a commutation unit and reconnected to one of six ways out, enabling the simultaneous reading of ISEs. The assembly of the potentiometric cell was as follows: different metals | TnT selective membrane | buffered

sample solution (HEPES pH 7.0) |AgCl/Ag|. The reference electrode was an Ag/AgCl metal wire.

Decreasing concentrations in TnT were obtained by transferring 0.0200 to 1.0 mL aliquots of HEPES solution pH 7.0 to a 5.0 mL beaker containing 0.200 mL of 7.0 x 10^{-8}mol/L TnT solution prepared in HEPES buffer.

The potential readings of the stirred TnT solutions were measured at room temperature and recorded after 10 seconds stabilization to ±0.2 mV. Each calibration curve was done 3 times. Selectivity studies followed the MPM, (Umezawa et al. 2000). The initial concentration of TnT was set to 1 x 10^{-7}mol/L and it was added of 4 x 10^{-7}mol/L TnT, changing the potential in 10 mV. Solutions of interfering species were added until the same potential change was observed.

4.3. Results and discussion

4.3.1. Design of plastic antibodies

The plastic antibodies were designed by surface imprinting on MWCNTs in order to improve the number of effective binding sites. MWCNTs were selected because of its large surface area, recognized capacity to adsorb the template (TnT), and compatibility with a wide range of transducers.

The overall process for synthesizing the plastic antibody consisted on linking the protein to the surface of the CNT (Figure 23), filling the vacant places around it with a suitable rigid structure and removing the protein after this (Figure 24) Almost all steps were carried out under mild conditions to ensure that the protein TnT remained unaltered in terms of 3-dimensional distribution and electrostatic environment.

An overview of the reactions carried out for the covalent attachment of TnT to the MWCNTs is shown in (Figure 23) The carboxylic acid groups on the surface

of the MWCNTs were activated by EDAC. This reaction forms a highly reactive *O*-acylisourea intermediate that reacts quickly with NHS to form a more stable ester (succinimidyl intermediate). This ester undergoes nucleophilic substitution with any readily available amine group on TnT, resulting in the formation of an amide bond between the MWCNTs and TnT.

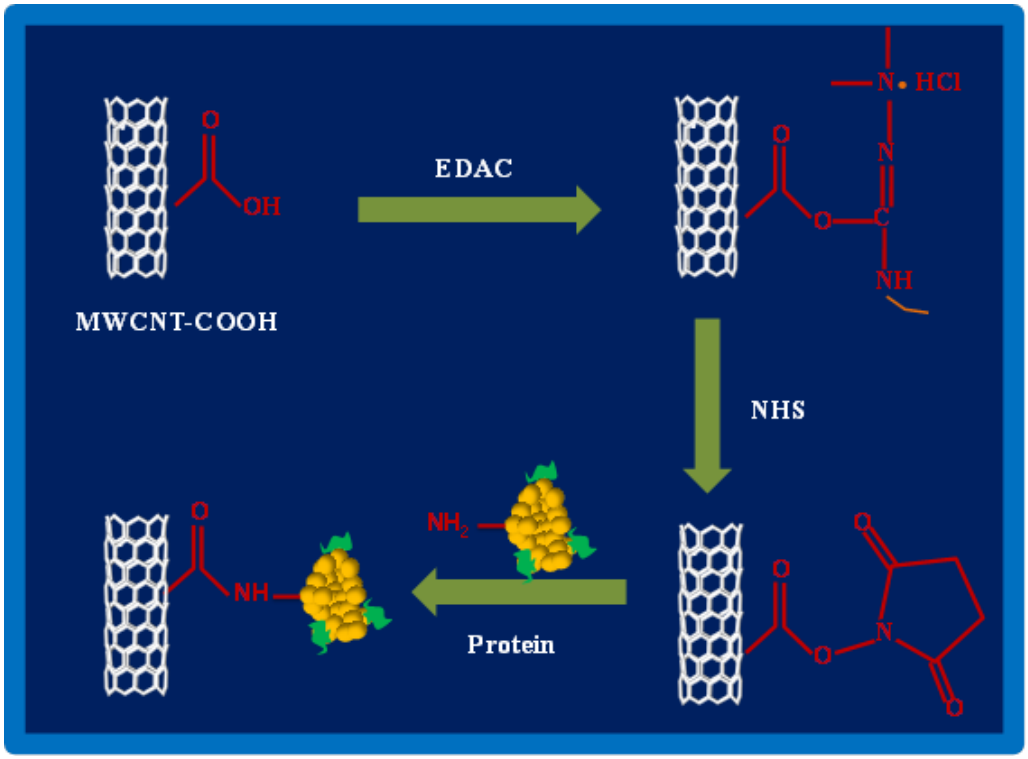

Figure 23: Protein attach to carbon nanotubes via a two-step process of diimide-actived amidation.

TnT-MWCNTs were then incubated in Tris solution for 30 min to block un-reacted ester groups. The resulting material was washed with PIPES solution (pH 7.0) and let stand during 45 min first in AAM (vinyl monomer) and after in NNMBA (cross-linker), both prepared in the same buffer (Figure 24). After an incubation period to allow the orientation of monomers and cross-linkers

around the template following electrostatic interactions, APS was added to start the polymerization. This polymerization was carried out at room temperature for 5 h to avoid any alterations of the protein conformation. The modified MWCNTs were washed again. The attached protein was after removed by reaction with Oac. Subsequently, several washing steps were performed to remove the released peptide fractions from the surface of the modified nanotubes. At this stage, the pH was increased from 1.2 to 8.0 to facilitate peptide/amino acid removal.

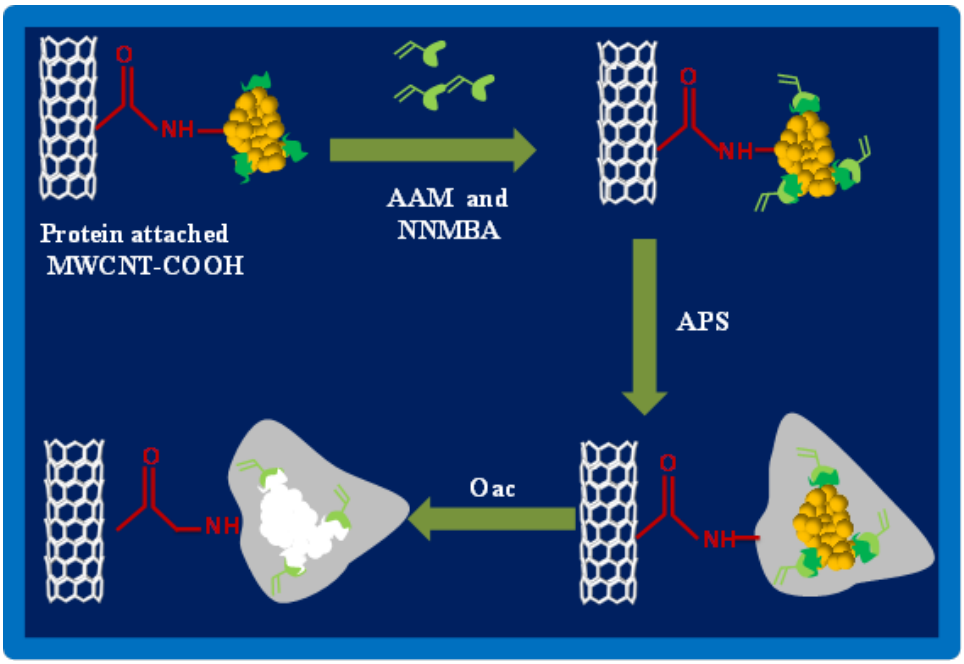

Figure 24: Schematic process of the TnT imprinting.

4.3.2 Scanning Electron Microscopy / Transmission Electron Microscopy analysis

The SEM images of the carboxylated MWCNT are shown in the first line of Figure 25. The multi-walled tubes of carbon had an average thickness of 12-13 nm.

This was confirmed by magnifying the original biomaterial by 400,000 and 800,000 times. As expected, the EDS spectra confirmed the presence of C and O, this last atom coming from the carboxyl functions.

The surface modification increased the thickness of the carbon rods up to 15-19 nm (Figure 25, second line). It also reduced significantly the conductivity of the biomaterial. This was made clear by the poorer resolution of the SEM image of MI-MWCNTs and NI-MWCNTs biomaterials obtained with 800,000 times magnification, especially when compared to those of the non-modified MWCNTs.

The chemical modification of the MWCNTs introduced Na, S, and Cl in the overall structure (EDS spectra Figure 25). This was common in both MI-MWCNTs and NI-MWCNTs biomaterials. MI structures displayed, however, higher levels of these atoms, which probably resulted from prevailing peptide structures sequestered inside the imprinted layer.

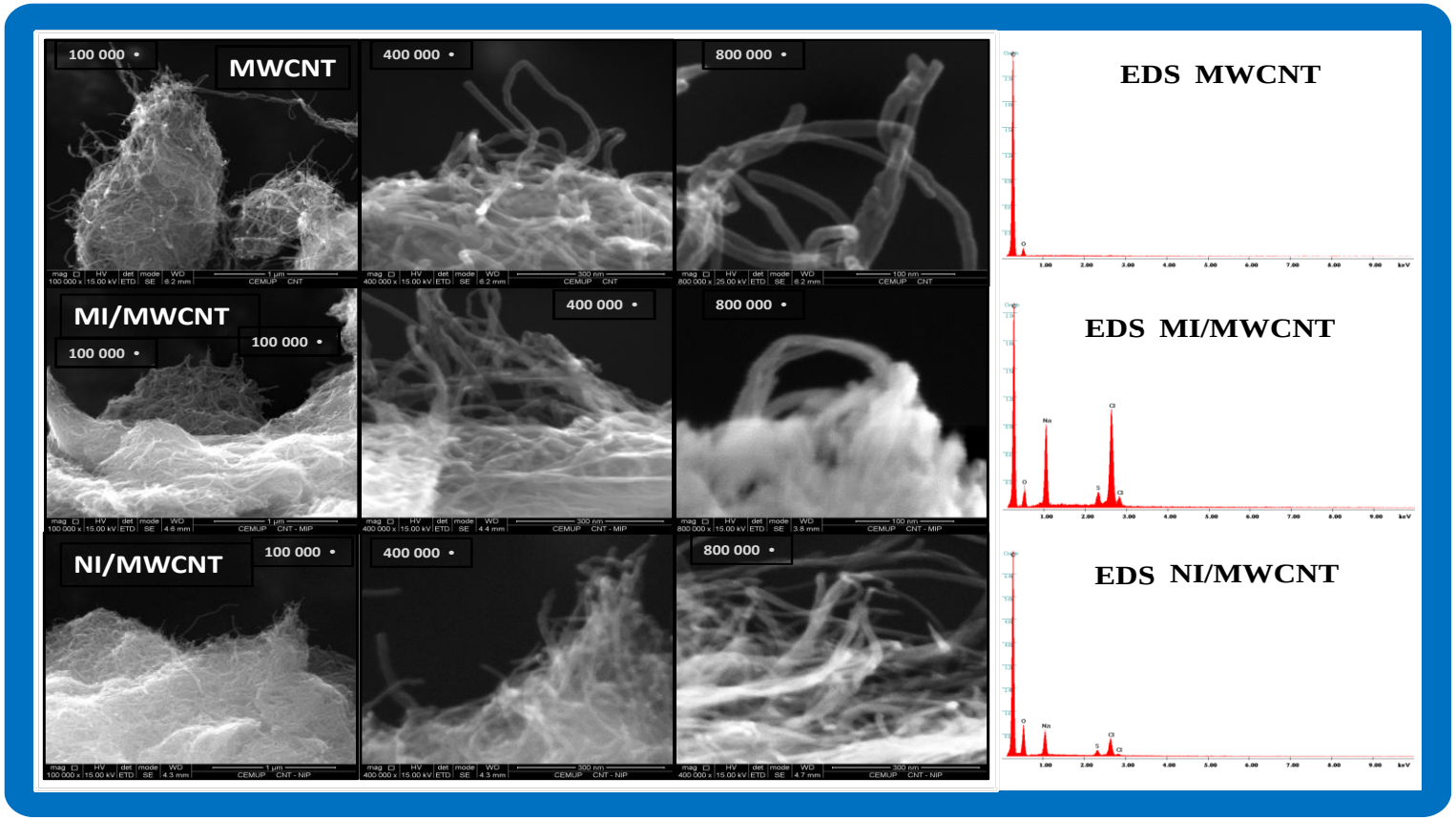

Figure 25: SEM and Energy Dispersive Spectrometer images of plain MWCNT (first line) and modified MWCNT by MI (second line) or by NI (third line) technologies.

The (Transmission Electron Microscopy) TEM images of the carboxylated MWCNT, MI-MWCNTs and NI-MWCNTs are shown in Figure 26. Although there was no protein label, several points of higher density were found at the wall of the CNTs. This has been attributed to protein structures bound to the tubes.

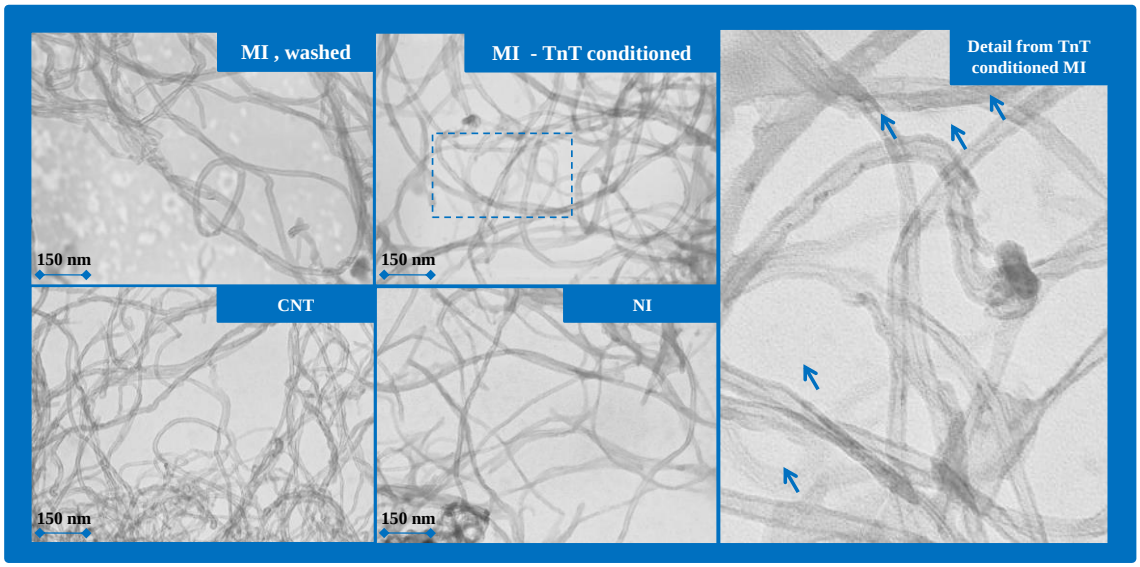

Figure 26: TEM images of MI washed, non-imprinting - TnT conditioned, CNT, NI and detail from TnT conditioned molecular imprinting.

4.3.3 Rebinding properties on sensory surfaces

The spectra of non-modified and MI/NI carboxylated MWCNTs are presented in Figure 27. The FTIR spectrum of the non-modified biomaterials (MWCNT-COOH) confirmed the presence of a carbonyl function (C=O) by a strong absorption near 1650 cm^{-1}.

The surface modification of MI and NI biomaterials was confirmed by the presence of amide functions in both monomer and cross-linker structures. Both bi

omaterials displayed a strong absorption band near 3400 cm^{-1} that was assigned to N-H stretching vibration. The C-N stretching vibrations could also be observed near 1300 and 1000 cm^{-1}. This C=O group was the major responsible for the strong adsorption around 1750 cm^{-1}.

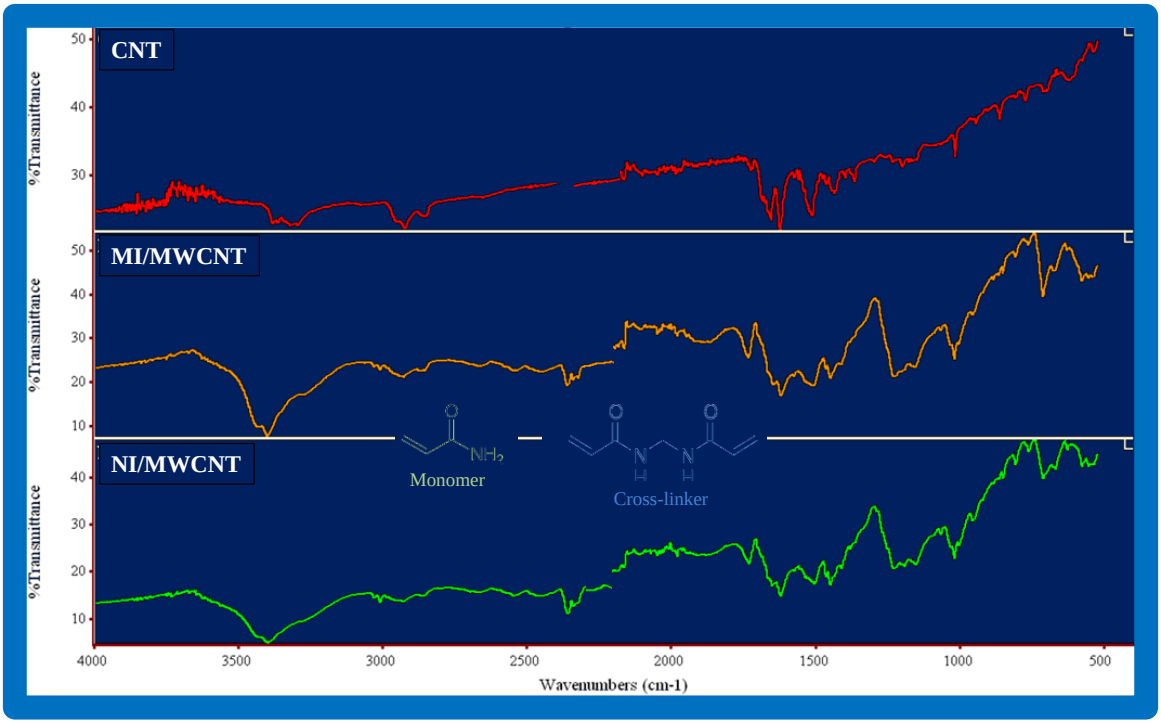

Figure 27: FTIR images of plain MWCNT (first line) and modified MWCNT by MI (second line) or by NI (third line) technologies.

4.3.4 Rebinding proprieties of the sensory surfaces

The rebinding ability of the MI-MWCNTs and NI-MWCNTs was tested by using these biomaterials as electroactive ingredients. They were dispersed in a high dielectric constant plasticizer and PVC for this purpose. Non-modified MWCNTs were also employed as control. The obtained membrane was used to coat wires of different metals: silver, gold and titanium. This particular configuration (coated-wire) was selected for allowing further miniaturization.

Their main analytical features were evaluated following the IUPAC recommendations (Umezawa et al. 2000). All potentiometric measurements were carried out at room temperature. Emf values of each electrode were measured in solutions of fixed pH and ionic strength. Increasing concentration levels of TnT were obtained by transferring 0.0200-1.000 mL aliquots of HEPES buffer pH 7.0 aqueous solutions to a 0.15 mL $7.0x10^{-8}$ mol/L TnT. Potential readings were recorded after stabilization to ±0.2 mV and emf was plotted as a function of logarithm TnT concentration. Calibration graphs were used for subsequent determination of unknown TnT concentrations.

As a potentiometric sensor detects ionic species, the net charge of TnT in solution must be controlled. This feature is highly dependent on the pH. The pH of its isoelectric point (8.8) ensures equal contribution of positive and negatively charges and the net charge on the protein surface is zero, while in lower pHs the protein is predominantly positively charged. In this work the pH selected was 7.0. It is near physiological conditions and ensured positively charged species.

The analytical parameters of the calibrations are presented in Table 4. In most NI-MWCNT and MWCNT materials producing immeasurable responses, the potential values of NI-MWCNT and MWCNT materials were unstable and no linear response were obtained in all concentration range of readings, their calibrations are also depicted in Figure 28.

In general, the sensor with MI as electroactive biomaterial showed the best analytical features (Figure 29). Linear behaviour with MI sensing polymer with coated-wire (silver, gold and titanium) electrodes was observed from 9.0×10^{-9}, 4.2×10^{-9} and 2.8×10^{-8} mol/L TnT, cationic slopes were 53.7, 49.6 and 36.3 mV $decade^{-1}$ and detection limits were 0.259, 0.157 and 0.435 µg/mL respectively. The gold-based electrodes displayed the lowest concentration for linear range, which is of utmost importance for a practical application of the proposed biomaterials; their sensitivity was also suitable for this purpose.

Table 4: Membrane composition of TnT PVC membrane sensors and their analytical features in 1.0 x 10^{-2} M Hepes buffer of pH 7.0.

Characteristic	**ISE I**	**ISE II**	**ISE III**	**ISE IV**	**ISE V**	**ISE VI**	**ISE VII**	**ISE VIII**	**ISE IX**
(Ionophore)	*MI/Ag*	*NI/Ag*	*CNT/Ag*	*MI/Ti*	*NI/Ti*	*CNT/Ti*	*MI/Au*	*NI/Au*	*CNT/Au*
Slope, (mV/log([TPN]/mol/L)	53.7 ± 1.6	59.1	n.d.	38.3 ± 5.3	n.d.	n.d.	49.6 ± 0.3	45.9 ± 7.1	n.d.
r^2 (n = 2)	0.993	0.951	n.d.	0.992	n.d.	n.d.	0.991	0.997	n.d.
LOD, mol/L	0.259	0.304	n.d.	0.435	n.d.	n.d.	0.157	0.234	n.d.
LLLR, mol/L	9.0×10^{-9}	9.1×10^{-9}	n.d.	2.8×10^{-8}	n.d.	n.d.	4.2×10^{-9}	9.1×10^{-9}	n.d.
Response time/s	< 15	Unstable	Unstable	< 15	Unstable	Unstable	< 15	< 15	< 15
S, mV	12.3	5.3	9.89	16.3	1.62	14.0	4.45	1.27	n.d.
Repeatability, (%) mV	13.2	12.4	36.8	26.1	1.4	14.0	5.1	1.75	n.d.

LLLR: Lower Limit of Linear Range.

Using NI biomaterial as sensor, only silver and gold conductive supports displayed potential changes against TnT concentration. These were the most conductive and inert supports. The reported signals were however highly unstable. All potentiometric sensors prepared with the corresponding MWCNTs particles (ISEs III, VI and IX) displayed no linear response (Figure 28).

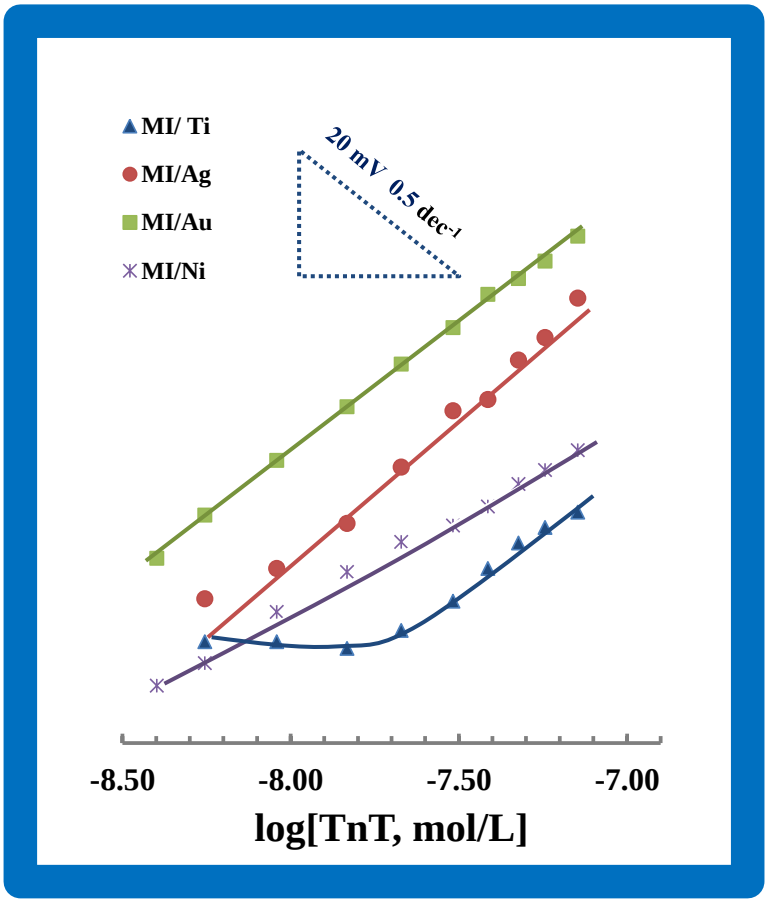

Figure 28: Potentiometric response of the several TnT PVC membrane sensors under static mode of operation at pH 7.0 with different coated-wire metal.

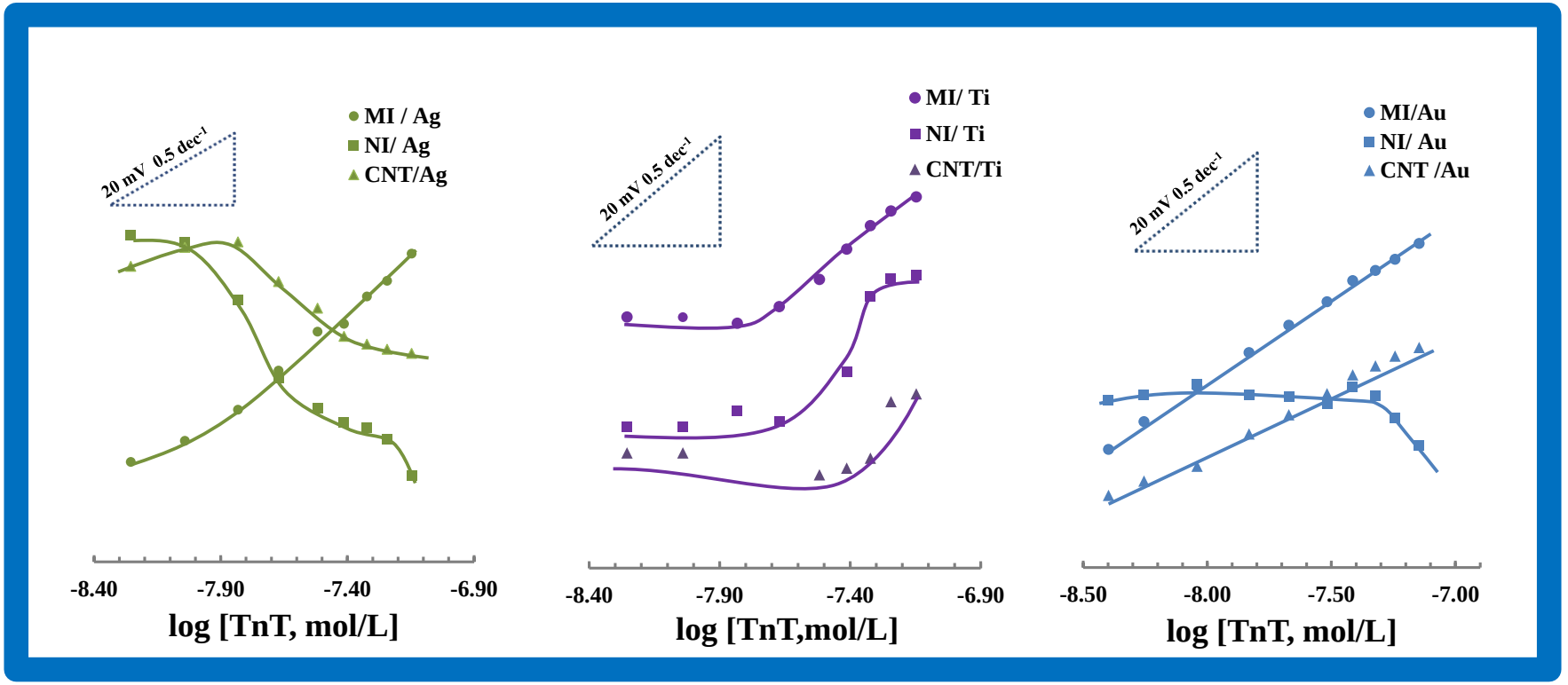

Figure 29: Potentiometric response of molecular imprinting /TnT PVC membrane sensors under static mode of operation at pH 7.0 with different coated-wire metals.

These results indicated that the non-specific places of interaction (the only kind that exists on NI-MWCNTs or MWCNTs particles) between the template and the polymer were not the main responsible for the potentiometric response. Only monomers polymerized in the presence of a template may have imprinted cavities, enabling the specific interaction between the template and the sensor. Therefore, the potentiometric response observed for the MI electroactive biomaterials is mainly due to a topographic recognition of the analyte at the imprinted cavities.

4.3.5 Sensor selectivity

The selectivity behaviour of potentiometric sensor is defined by the ion exchange constants between electroactive biomaterial and TnT (Bakker and Pretsch 2007). This suggests the use of ligands that strongly bind the preferred ion and only weakly all the others. Thus, the use of MI-MWCNTs should induce higher selectivity behaviour, than both NI-MWCNTs and MWCNTs materials.

The selectivity behaviour was assessed by calculating the potentiometric selectivity coefficients. The MPM was used for this purpose, as it is closer to a practical application of the sensor; it tests main and interfering ion together and does not require Nernstian behaviour of the electrode against each interfering species. In this method, the potentiometric selectivity coefficient, calculated by Equation 26.

As possible interfering compounds, several organic species that are common in biological samples, such as proteins, sugars, aminoacids and metabolites, were selected. Creat, Suc, Fru, Myo, Sodium Glut, Ala, Thia and urea were considered for this purpose. Their interference was found negligible. Almost all logarithm selectivity coefficients were below -3.0

Table 5). Below this limit any interference under study could have been a result of the dilution effect caused by the addition of the interfering ion, despite the use of highly concentrated interfering solutions. Only MWCNT and NI-MWCNT

showed logarithm selectivity coefficients above this limit, ranging from -2.77 to -1.08.

In many cases, the interfering species were unable to reach the potential change obtained by the main ion, as may be seen by the missing values in table 5. This may indicate very low interfering effect, in the case of the electrodes that were working properly, or very small sensitivity, such as that observed for MI-MWCNT or MWCNT based membranes.

4.3.5 Application

The MI-based sensors were applied to determine TnT in serum samples ranging 1.41 – 20.86 µg/mL. A good agreement was found between added and found amounts of TnT. Results of the potentiometric analysis conducted in steady state showed recoveries ranging 94.4 – 105.5% with an average relative standard deviation of 2.6%. The relative error ranged from -5.65 to 5.83% with an average relative standard deviation of 0.07%.

Table 5: Potentiometric selectivity coefficients assessed by the matched- potential method.

$\log K_{A,B}^{POT}$	**ISE I** MI/Ag	**ISE II** NI/Ag	**ISE III** CNT/Ag	**ISE IV** MI/Ti	**ISE V** NI/Ti	**ISE VI** CNT/Ti	**ISE VII** MI/Au	**ISE VIII** NI/Au	**ISE IX** CNT/Au
Creatinine	-3.31	-3.45	n.d.	-3.45	-3.45	n.d.	-3.62	n.d.	-3.45
Sucrose	-3.62	-3.62	n.d.	-3.83	-2.37	-2.37	n.d.	n.d.	n.d.
Fructose	-3.04	-3.04	n.d.	-3.31	-3.45	-3.45	-3.67	-3.31	n.d.
Myoglobin	-3.67	-3.55	n.d.	-3.55	-3.55	-3.45	n.d.	n.d.	n.d.
Sodium Glutamate	n.d.	n.d.	n.d.	n.d.	n.d.	-2.36	n.d.	n.d.	-1.08
Thiamine	n.d.	n.d.	n.d.	n.d.	n.d.	n.d.	n.d.	n.d.	-2.77
Urea	-3.04	-2.37	-3.35	n.d.	-3.35	-2.66	n.d.	-3.55	n.d.

4.4. Conclusions

Surface molecular imprinting technique was employed successfully to produce biomimetic TnT tailored sensors for potentiometric transduction making use of host-guest interactions. Nanostructured materials of MWCNTs were selected as support biomaterial to increase the number of imprinted sites and results suggest this material may have contributed to an improved analytical performance.

The results pointed out that membranes should be casted over an Au wire for an improved performance.

In general, the sensors offered the simplicity in designing, short measuring time, good precision, high accuracy, high analytical throughput, low limit of detection and good selectivity. The proposed method is simple, of low cost, precise, accurate and inexpensive regarding reagent consumption and equipment involved.

Further improvements are however required because the cut-off of the TnT are quite below the LOD obtained in the present study.

4.5. References

Agasti, S.S., Rana, S., Park, M.H., Kim, C.K., You, C.C., Rotello, V.M., 2010. Nanoparticles for detection and diagnosis. *Advanced Drug Delivery Reviews* 62(3), 316-328.

Bakker, E., Pretsch, E., 2007. Modern Potentiometry. *Angewandte Chemie-International Edition* 46(30), 5660-5668.

Guan, G.J., Liu, B.H., Wang, Z.Y., Zhang, Z.P., 2008. Imprinting of Molecular Recognition Sites on Nanostructures and Its Applications in Chemosensors. *Sensors* 8(12), 8291-8320.

Ishikawa, F.N., Stauffer, B., Caron, D.A., Zhou, C., 2009. Rapid and label-free cell detection by metal-cluster-decorated carbon nanotube biosensors. *Biosensors & Bioelectronics* 24(10), 2967-2972.

Jiang, K.Y., Schadler, L.S., Siegel, R.W., Zhang, X.J., Zhang, H.F., Terrones, M., 2004. Protein immobilization on carbon nanotubes via a two-step process of diimide-activated amidation. *Journal of Materials Chemistry* 14(1), 37-39.

Li, J., Wang, Y.B., Qiu, J.D., Sun, D., Xia, X.H., 2005. Biocomposites of covalently linked glucose oxidase on carbon nanotubes for glucose biosensor. *Analytical and Bioanalytical Chemistry* 383(6), 918-922.

Lu, X., Zhou, J., Lu, W., Liu, Q., Li, J., 2008. Carbon nanofiber-based composites for the construction of mediator-free biosensors. *Biosensors & Bioelectronics* 23(8), 1236-1243.

Mao, Y., Bao, Y., Gan, S., Li, F., Niu, L., 2011. Electrochemical sensor for dopamine based on a novel graphene-molecular imprinted polymers composite recognition element. *Biosensors & Bioelectronics* 28(1), 291-297.

Merkoci, A., 2006. Carbon nanotubes in analytical sciences. Microchimica Acta 152(3-4), 157-174.

Merkoci, A., Pumera, M., Llopis, X., Perez, B., del Valle, M., Alegret, S., 2005. New materials for electrochemical sensing VI: Carbon nanotubes. T*rac-Trends in Analytical Chemistry* 24(9), 826-838.

Shumyantseva, V.V., Carrara, S., Bavastrello, V., Riley, D.J., Bulko, T.V., Skryabin, K.G., Archakov, A.I., Nicolini, C., 2005. Direct electron transfer between cytochrome P450scc and gold nanoparticles on screen-printed rhodium-graphite electrodes. *Biosensors & Bioelectronics* 21(1), 217-222.

Umezawa, Y., Buhlmann, P., Umezawa, K., Tohda, K., Amemiya, S., 2000. Potentiometric selectivity coefficients of ion-selective electrodes Part I. Inorganic cations - (Technical report). *Pure and Applied Chemistry* 72(10), 1851-2082.

5

Electrochemical biosensor based on biomimetic material for myoglobin detection

5.1 Introduction

SPE can be easily applied to the mass production of inexpensive, reproducible and sensitive disposable electrodes, (Silva et al. 2010) and have been applied in POC. The SPE microfabrication technology is nowadays used for production of thick-film electrochemical transducers. Additional important feature that these electrodes exhibit is related to the miniaturization of the corresponding device, easy handling and manipulation in a disposable way (Silva et al. 2010).

SPE are also disposable devices that can act as support of SAM in order to produce the desired MI for a cardiac biomarker. When the metal support of the WE area is not suitable for carry out such modification, it can be changed polymeric film deposition. Furthermore electrical transduction can be generated and measured by amperometric/voltammetric biosensors, potentiometric biosensors, conductimetric biosensors, EIS biosensors and Field Effect Transistors (FET) biosensors. (Ahammad et al. 2011; Billah et al. 2008; Chu et al. 2011; Gogol et al. 2000; Jena and Raj 2006; Kamel et al. 2008).

The CV is voltammetric method where the information about an analyte is obtained by varying a potential and then measuring the resulting current. CV offers information about the redox potential and electrochemical reaction rates of analyte solutions. The voltage is swept between two values at a fixed rate.

EIS allows investigating immobilized organic films on surfaces (Billah et al. 2008) can giving information on the impedance changes of the electrode surface in the modification process. In EIS, the semicircle diameter of EIS equals the electron transfer resistance, (R_{ct}). This resistance controls the electron transfer kinetics of the redox-probe at the electrode interface. A small alternating current voltage perturbations cause variations in impedance in a way that is related to the properties of the liquid or solid under investigation. Thus, EIS is constantly used as a non-destructive technique for providing accurate and repeatable measurements regarding surface conditions such as adsorption and desorption processes at electrode surfaces. Due its proprieties electrochemical EIS and CV is an appropriate tool for to apply in POC diagnosis.

Thus, a new disposable biomedical device for monitoring Myo in POC designed by coating the conductive working area of a SPE with a PVC-COOH film and assembling the plastic antibody on top of it was developed. The MI/Au-SPE features towards the quantitative estimation of the Myo concentration was investigated by EIS and SWV.

5.2. Experimental Section

5.2.1 Apparatus

The electrochemical measurements were carried out using a Metrohm-autolab potentiostat/galvanostat Autolab PGSTAT302N interfaced to computer. The SPEs were purchased from Dropsens, Spain (DRP-C220AT). Gold working electrode diameter was 4 mm with pseudo reference Ag/AgCl electrode. Infrared spectra were collected by a Nicolet 670 FTIR spectrometer. Measurements were conducted in ATR mode by a Nicolet ATR sampling accessory of diamond contact crystal. When necessary, the pH was measured by a Crison CWL/S7 combined glass electrode connected to a decimilivoltammeter Crison, pH meter, GLP 22.

5.2.2 Reagents

All chemicals were of analytical grade and de-ionized water (conductivity <0.1 μS/cm) was employed. Myo from cardiac muscle, PVC-COOH, HEPES, EDAC,

Oac and NNMBA, BSA and CK-MB were obtained from Fluka. APS from JPV, KCl, Tris and potassium di-hydrogenphosphat (KH_2PO_4) from Panreac, AAM from Fisher Bio Reagents and NHS from Acros. 2-(N-morpholino) ethanesulfonic acid monohydrate 98% (MES) , THF, $[Fe(CN)_6]^3$, NaCl, sodium phosphate dibasic dehydrate $[Fe(CN)_6]^{4-}$ trihydrate and sodium hydrogen phosphate dihydrate was obtained from Riedel-deHäen.

5.2.3 Solutions

Buffer solutions were 1.0×10^{-1} mol/L PBS, 1.0×10^{-1} mol/L Tris or 1.0×10^{-2} mol/L HEPES. The pH of the buffer solution was adjusted to the desired value by adding suitable volumes of either concentrated hydrochloric acid or saturated sodium hydroxide solution freshly prepared.
Stock standard solutions of Myo were 5.0×10^{-7} mol/L and prepared in buffer. Less concentrated solutions were prepared by accurate dilution of the previous solution in the same buffer.

5.2.4 Synthesis of biomimetic materials

The working area of the SPE (gold) was cleaned by washing three times with ethanol. The PVC-COOH layer was obtained by casting on the working area about 15 µL of a solution of 0.021 g of PVC-COOH dissolved in 2.5 mL THF. The complete dissolution of the polymer was achieved by magnetic stirring inside a fume hood. About 15 µL of this solution was casted. This solution was let dry for 4 h, at room at temperature. To activate the –COOH groups, the dry polymer layer was incubated for 3h in an aqueous solution of 50 mmol/L EDAC and 25 mmol/L NHS. The electrode was then rinsed thoroughly with distilled water to remove un-reacted species.
The imprinting stage started by incubating the activated polymer layer in $5x10^{-6}$ M Myo solution, prepared in 0.1 mol/L PBS buffer of pH 7.4. The incubation time was set to 4 h, at 4°C. After, the electrode was washed twice with PBS buffer (pH 7.4) to remove any exceeding Myo that remained unbound. The sensor was then incubated in 0.5 mol/ L Tris for 30 minutes, in order to block any activated group left over in the surface. Several washes with deionised water followed this

procedure. The polymerization stage started by adding 1 mL of a solution containing 1.0 mol/L AAM and 0.07 mol/L NNMBA, in PBS buffer, pH 7.4, and 1 mL of 0.06 mol/L APS solution, in the same buffer. This polymerization was carried out at room temperature for 5 h, after which the sensor was thoroughly washed with deionised water several times.

The sites displaying complementary features to Myo were obtained by extracting the template from the polymer strong acids have the ability to break the protein covalent bonds, 0.5 mol/L solution of Oac was added to the sensory surface. This was done at room temperature, for 3 h. The MIP was finally washed and conditioned in phosphate buffer, pH 7.4, in order to increase the pH and remove the peptide fractions produced by Oac treatment. The MIP-SPE was ready to use after washing thoroughly with water.

5.2.5 FTIR analysis

FTIR analysis were made without previous sample pre-treatment. The spectra were collected under room temperature/humidity control after background correction. The number of scans was 32 for both sample and background. X-axis was wavenumber, ranging 600 to 4000 cm^{-1}, and Y-axis was % transmittance. Resolution was 4000.

5.2.6 Electrochemical measurements

CV and SW measurements were performed in a solution of 5.0 mmol/L $[Fe(CN)_6]^{3-}$, 5.0 mmol/L $[Fe(CN)_6]^{4-}$, 0.1 mol/L KCl, prepared in HEPES buffer and with pH 5.0. The potential was scanned between –0.2 and +0.4 V, at 30 mV/s. EIS analysis was conducted on the SPE-MIP electrodes. Impedance readings were performed in the same solution as indicated for CV and SW, under a standard potential of 0.225 V, a number of frequencies equal to 50 and amplitude of 0.01 V. The frequency range was 0.1–100 kHz. The impedance data was fitted to a Randles equivalent circuit using the implemented ANOVA software.

5.2.7 Selectivity study

Selectivity studies were conducted by competitive assay between Myo, with a 4.0 µg/mL concentration, and TnT (0.22 ng/mL), BSA (1 mg/mL) and CK-MB (5ng/mL) solutions. All these were prepared in HEPES buffer pH 5. These concentration values were selected according to their relative concentration to Myo in biological fluids.

5.2.8 Serum samples analysis

The performance of the sensor was carried out using synthetic serum samples spiked with Myo. The serum was 1:10 diluted in MES buffer. The measurements were performed by SWV measurements.

5.3. Results and Discussion

5.3.1 Chemical assembly of molecular imprinting polymer

The MIP was assembled on a polymeric film (Figure 30). This was the most simple and cheap way of binding the protein to a sensory material enabling a signal transduction. PVC-COOH was selected for this purpose because carboxylic groups enable the covalent binding of proteins under mild conditions after carboxylic activation via carbodiimide chemistry. Furthermore, it is a readily available and cheap material. The polymer film was obtained by dissolving the solid polymer in THF and casting 15 µL of this solution over the WE of a commercial SPE. This electrode was made of gold, although any other conductive material would suite this purpose.

Carboxylic acid groups were activated by EDAC, forming a highly reactive O-acylisourea intermediate that follows immediate reaction with NHS. The obtained product undergoes easy nucleophilic substitution by any amine group in the outer surface of Myo, resulting in the formation of an amide function binding Myo to the polymer film. The protein molecules remaining in the surface by electrostatic interaction were removed by thorough washing with PBS, pH 7.0.

Any carboxylic acid function remaining active was subsequently inactivated by reaction with Tris.

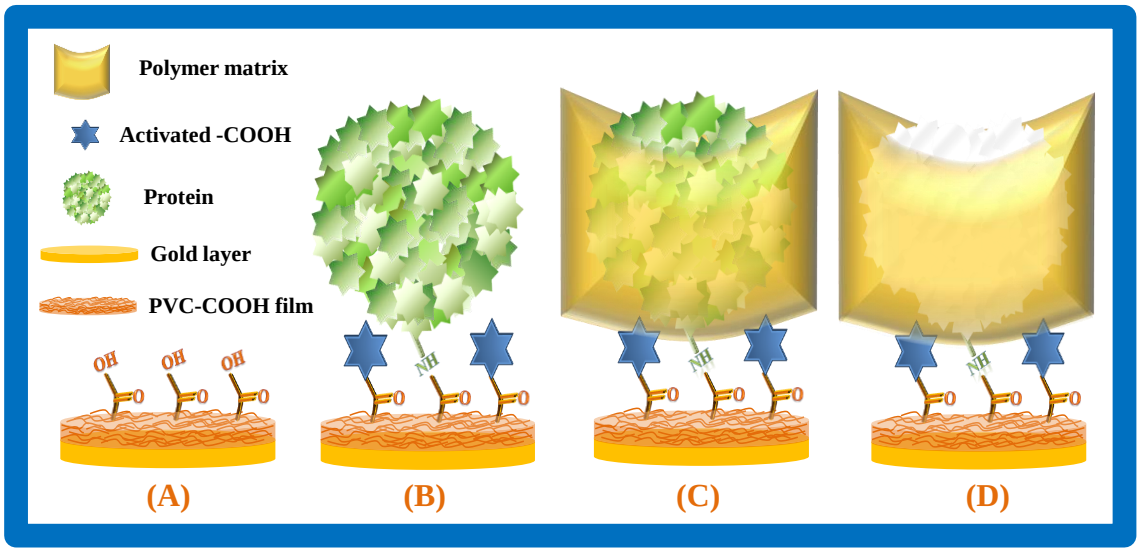

Figure 30: Schematic representation of the molecular imprinting polymer.

The binding sites where designed by filling the vacant space around the protein with a suitable polymer. A careful choice of monomers is crucial for a successful imprinting. In general, any protein has a complex structure and many potential recognition sites at their surface, with hydrophobic/hydrophilic regions. Charged sites, hydrogen bonding and hydrophobic interactions are all possible in a single protein. Furthermore, the great flexibility of the protein structure means that it should be polymerized under almost-native conditions so that its shape would be preserved and the binding site accurately designed. AA matrices meet these criteria (Guo et al. 2004; Pang et al. 2006; Wang et al. 2010; Wu et al. 2010a). They polymerize under mild conditions and carry uncharged functions that establish hydrogen bonds and dipole-dipole interactions with Myo. Thus, AAM monomers were selected for this purpose. These monomers were let interact with the protein prior to polymerization. This procedure allowed the orientation of the amide groups towards the sites of the protein with which they would interact more favourably, thus allowing subsequent oriented binding after template removal. A cross-linker of the same chemical nature (NNMBA) was also used in order to create a highly reticulated matrix. This would reduce the

flexibility of the polymer and preserve the protein site (as seen Figure 30). APS was added to start the polymerization and the monomers were let react for 5 h. The binding site (MI, Figure 30) was obtained after removing the protein from the imprinted cavity. At this stage, the polymer was a rigid and stable structure, for which the protein could be extracted by more or less aggressive treatments. Many approaches may be followed in the literature for this purpose. In this work, extraction was succeeded by incubation in Oac, for 3 h (Tong et al. 2001). After the sensor was washed with PBS buffer, pH 7.4, a condition that ensured a more efficient removal of oligopeptides and free amino acids. After thorough washing with water, the material was ready for rebinding with Myo

5.3.2 Control of the surface modification

All modification steps in the preparation of the MIP were followed by FTIR analysis. EIS and CV studies were also used in parallel as they allowed investigating the integrity and proprieties of immobilized organic films at the polymer and interfacing surfaces.

5.3.3 FTIR analysis

The FTIR spectra were taken at all stages of surface modification (Figure 31). This included measuring the typical absorption profile of the PVC-COOH (A) film casted the gold surface, the subsequent modification with Myo (B) and finally MIP (C) itself. The spectrum of gold was not included here because it does not provide relevant information and it is only used as support of the polymer film. The spectrum of Myo was also evaluated because if provides significant insight into the presence of Myo in the polymer.

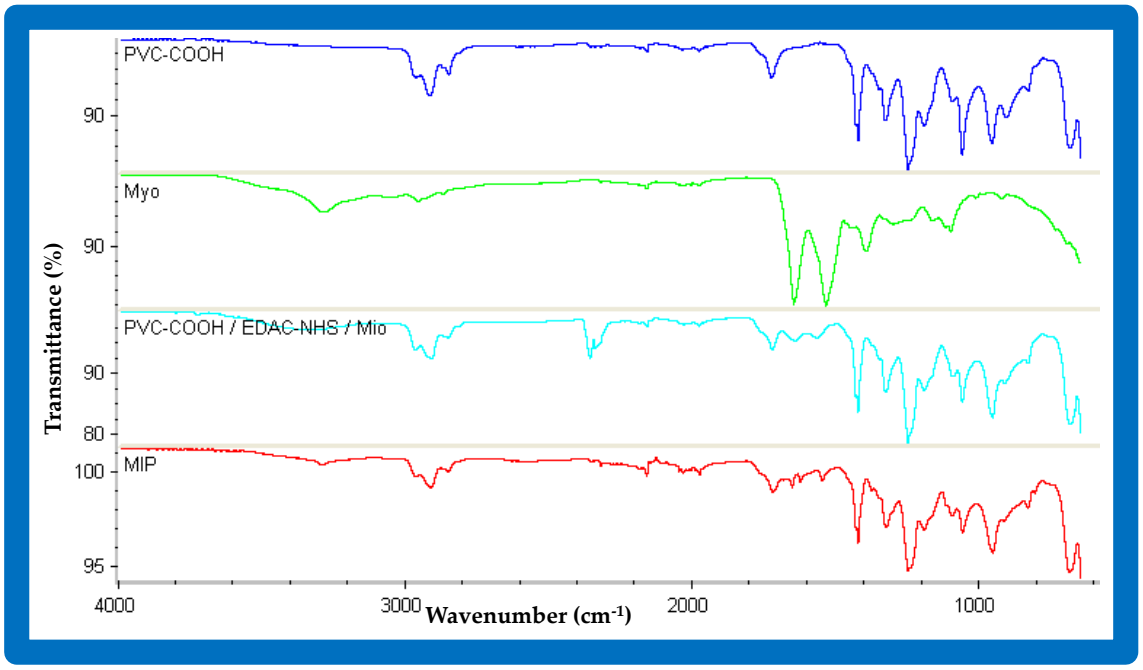

Figure 31: FTIR analysis of PVC-COOH; Myo; Protein attach and MIP.

The presence of carbonyl groups (C=O) in PVC-COOH was evidenced by a strong absorption peak at 1727.8 cm^{-1}. The C–H stretch coming from methylene ($–CH_2–$) groups in the central carbon chain was evident at 2918.9 cm^{-1}. The rocking absorption from having more than four methylene in a row was also marked at about 720 cm^{-1}.

The most evident absorption bands in Myo were at 3284.2, 1538.2 and 1651.4 cm^{-1}. These could be correlated to the many functional groups among the side chains of each amino acid. Considering the wave number at which these occur, it is quite probable that they come from alcohol, amine and/or amide groups in the protein. The band at 1398 cm^{-1} correlates well with the hydroxyl (–OH) function and that at 1062 cm^{-1} with the C–N stretching.

The presence of protein species attached to the polymeric film was quite evident by combining the spectra of PVC-COOH and Myo. Almost all bands belonged to PVC-COOH, with the exception of the three most significant bands from Myo. The large band centered at 3342 cm^{-1} suggested the presence of amide groups from the protein ($–CONH_2–$). The two bands at about 1540 and 1650 cm^{-1} were also from Myo but of less intensity, a consequence of being in lower concentration than in the pure solid.

The polymerization step imputed slight alterations in the FTIR profile of the material. These alterations were not significant because only amide functions were introduced, both by monomer and cross-linker structures, and they were already there, coming from the protein. Overall, the biomaterial displayed an absorption band near 3294 cm^{-1} that was assigned to N–H stretching vibration. The C–N stretching vibrations could also be observed at 1000 cm^{-1}. Still, as the protein had been removed from the polymeric structure, it is quite likely that these typical bands of the amide groups were not from the same source as previously.

5.3.4 Electrochemical Impedance Spectroscopy

The organic modification of a gold SPE surface is expected to change the electrical output of the solid-state probe. These changes can be observed by monitoring the alterations in the electrical transfer of a well known redox system, such as $[Fe(CN)_6]^{4-}/[Fe(CN)_6]^{3-}$. Several electrochemical approaches may be used for this purpose, being EIS one of the most sensitive.

EIS evaluates the changes in resistance of the polymer surface along each modification step. The Randle's equivalent circuit was adopted to model the process in the gold surface. Typical plots may include a semicircle region lying on the real axis followed by a straight line. The semicircle is observed at high frequency range and implies a charge-transfer controlled process. The diameter of this semicircle equals the R_{ct}, and this resistance controls the electron transfer kinetics of the redox-probe at the electrode interface (Panagopoulou et al. 2010).

The EIS spectra by this Randle's equivalent circuit were recorded for every step of the gold SPE surface modification and the results were presented as Nyquist plots (Figure 32A). The gold SPE coated with a PVC-COOH membrane displayed high electron transfer resistance due the PVC-COOH layer casted on the gold. This behaviour was already expected, owing the absence/weak electrostatic interactions between the uncharged carboxylic acid groups (-COOH) of the polymeric layer and the negatively charged redox probe. It was also likely that the PVC backbone of the polymer film acted like an insulating layer, thus reducing the electrical transfer across the Au surface. The subsequent activation of the carboxyl group produced a neutral ester intermediate. This newly formed

neutral surface acted similarly to the previously mentioned neutral carboxylic functions: the absence of electrostatic interactions hindered the electron transfer process mediated by the negatively charged redox probe. The next stage was protein binding that also hindered the electrical transfer, reflected here by the increasing impedance values of the EIS spectra. Although Myo is positively charged under the pH condition of the redox probe solution (its isoelectric point is ~7.0), its size and packing over the surface must have contributed to this observation. This stage was followed by the polymerization reaction, producing again an additional barrier for the redox probe access to the gold SPE modified electrode. This resulted in an extra increase in the electron transfer resistance, reflected by further substantial increase in R_{ct}. This subsequent increase in charge transfer resistant is consistent with the several modification steps imposed to the Au SPE surface.

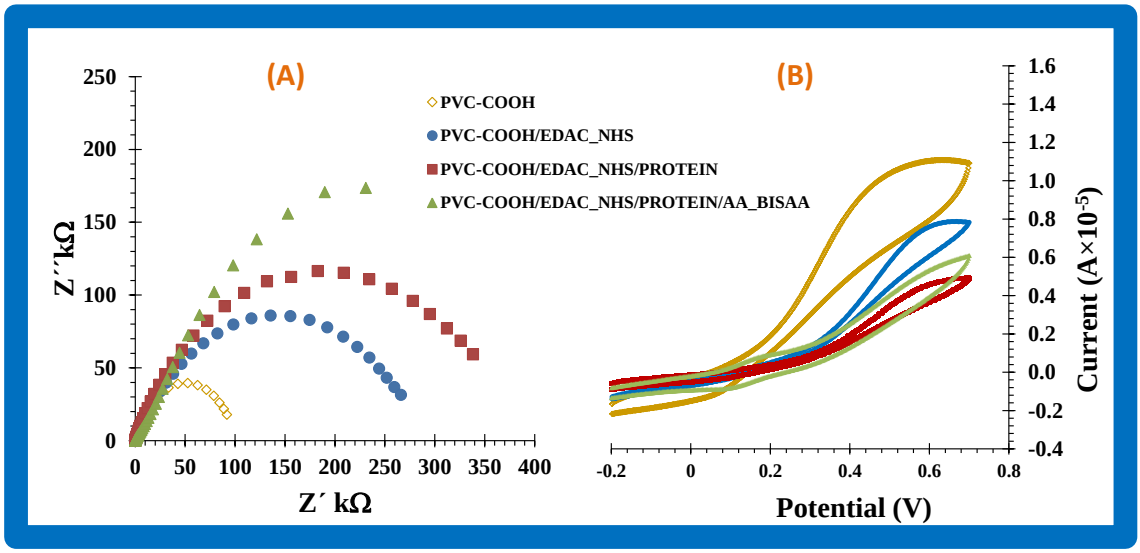

Figure 32: (A) Nyquist plot of sequential immobilization steps on SPE /PVC-COOH towards functional molecular imprinting sensor in 5.0 mM [Fe $(CN)_6]^{3-}$ and 5.0 mM $[Fe(CN)_6]^{4-}$ in HEPES buffer pH 5.0 at a frequency range of 0.1–100 kHz. (B) CV of sequential immobilization steps onto SPE towards functional molecular imprinting sensor in 5.0 mM $[Fe(CN)_6]^{3-}$ and 5.0 mM $[Fe(CN)_6]^{4-}$ in HEPES buffer pH 5.0.

5.3.5 Cyclic voltammetry

CV assays are not as sensitive as EIS but may serve as an additional confirmation of the chemical modification introduced on a gold surface. Overall, the results obtained supported the previous electrochemical studies (Figure 32B). The application of PVC-COOH on gold resulted in a more irreversible electron transfer process due to the small current intensity and the high peak-to-peak potential separation of a typical iron redox probe over a clean Au surface. All the subsequent immobilization steps on the PVC-COOH film decreased or annulled the anodic/cathodic peaks of the redox probe and promoted further increase in peak-to-peak separation (when they existed), reducing the overall area of the voltammograms and accounting for the increased charge-transfer resistance on the gold surface. In the voltammograms where the catholic and anodic peaks or the redox probe are not present, the reaction of the redox probe was of irreversible character.

5.3.6 Analytical features

Nyquist plots and the corresponding calibration curves obtained from MIP/Au-SPE devices with different concentrations of Myo are shown in (Figure 33). The EIS assays were conducted in HEPES buffer, pH 5, with 5.0 mmol/L $[Fe(CN)_6]^{4-}/[Fe(CN)_6]^{3-}$, at a standard potential of 0.225 V, with a number of frequencies equal to 50 and an amplitude of 0.01 V. The frequency range was 0.1–100 kHz.

The Rct controlled the electron transfer kinetics of the redox probe at the electrode interface, which was relative to the concentration of Myo. The diameter of the semicircle increased with the increasing of Myo concentration, meaning that Myo was bound to the imprinted material at the gold SPE/PVC-COOH surface. The results showed a linear behaviour resistance versus Myo concentration, of positive slope 6.50 ± 1.48 kΩ/ (µg/mL). This linear response was observed from 0.852 to 4.26 µg/mL. The LOD was 2.25 µg/mL.

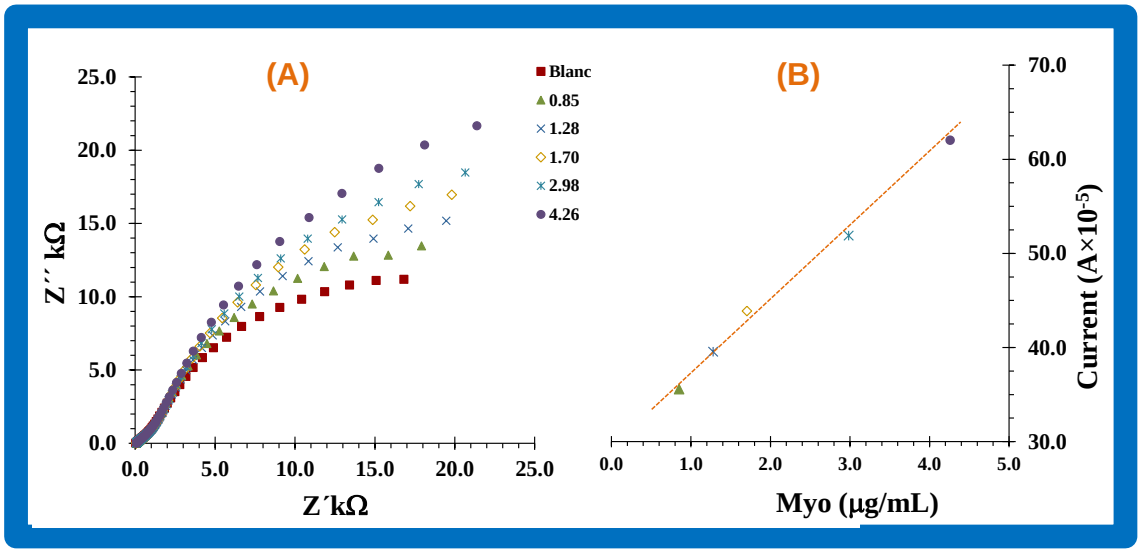

Figure 33: Calibration curve and Nyquist plot obtained in 5.0 mM $[Fe(CN)_6]^{3-}$ and 5.0 mM $[Fe(CN)_6]^{4-}$ in HEPES buffer pH 5.0 with different concentrations of Myo solutions (in µg/mL).

As an alternative electrochemical approach to EIS, SW was chosen this time instead of CV. SW is much more sensitive than CV, enabling the detection of much lower concentrations. These assays were conducted in the same solution as that in EIS studies. Readings were carried out with amplitude of 0.15 V and scan rate of 30 mV/s. The maximum peak of the blank was located at 0.139 V, and corresponded to the oxidation potential of Fe(II). This peak shifted slightly to higher potentials as the concentration of Myo increased. This was consistent with the existence of a more difficult electrical transfer through probe when an increased concentration of Myo is present. Results showed linear slope -0.28 ± 0.038 µA (µg/mL) decreased proportionally to Myo concentration, between 1.1 and 2.98 µg/mL (Figure 34). In all measurements the repeatability was always less than 5%. The biosensor is stable during 4 weeks and is reusable after with 3 consecutive calibrations curves, after rinsed with buffer several times along 30 minutes.

5.3.7 Selectivity

The interfering species tested were proteins that coexist with Myo in serum and their concentrations were selected according to their relative levels in biological

fluids (Kertai et al. 2004; Landesberg et al. 2003; Lewandrowski et al. 2002; McCann et al. 2008). Cardiac biomarkers such as TnT and CK-MB and a protein present in a biological fluids BSA were selected. A competitive assay was used to test their interference in the response of the sensor to a Myo level lying within the linear response range. A concentration of Myo equal to 4.0 µg/mL was selected for this purpose. This test was carried out along time, in order to reach the equilibrium between the binding sites of the sensory surface and the competition between Myo and interfering species for these binding sites. Each assay was conducted in a different Au-SPE/MI sensor, avoiding a cross contamination from adsorbed Myo or interfering compound. The time and % error found for each interfering species were, respectively, 5 minutes and 7% for TnT, 15 minutes and 11% for BSA and 15 min and 2% for urea respectively. In all measurements the repeatability was always less than 5%.

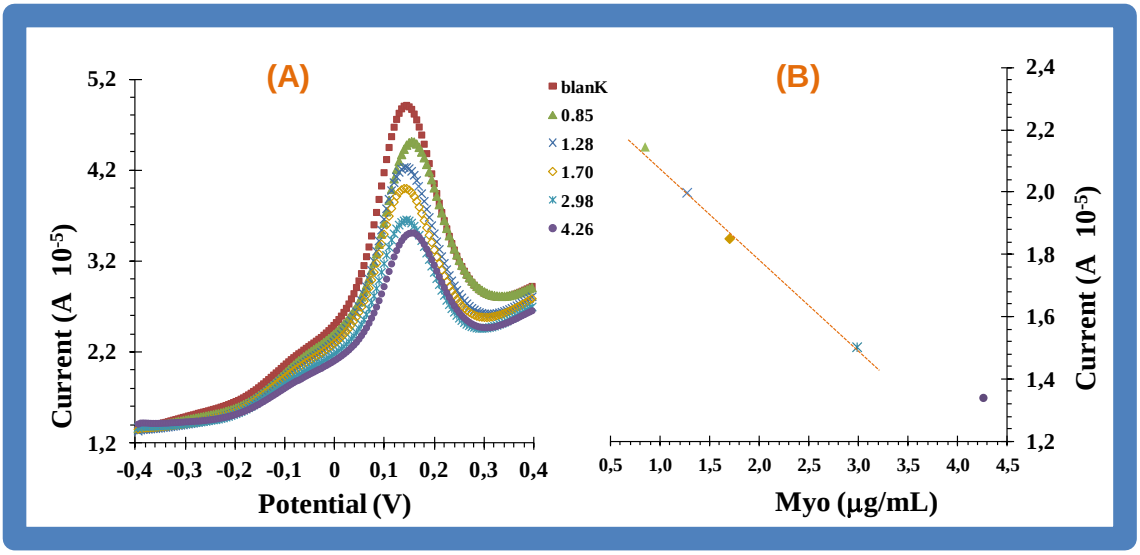

Figure 34: Calibration curve and SWV obtained in 5.0 mMmol/L $[Fe(CN)_6]^{3-}$ and 5.0 mmol/L $[Fe(CN)_6]^{4-}$ in MES buffer pH 5 with different concentrations of Myo solutions (in µg/mL).

5.3.8 Sensor response to synthetic serum samples

Myo was determined in spiked diluted (1:10) synthetic serum samples. The measurements were performed by SWV measurements. The sensor exhibited linear behaviour in range from 1.16 µg/mL to 3.86 µg/mL (Y = 3.345 – 0.1372X).

The response time of the sensor was obtained in <120 seconds. In all measurements the repeatability was always less than 5%.

5.4. Conclusions

A new sensory MI material was presented and allowed the preparations of a disposal biomedical device for Myo screening. The use of a polymer film to assemble the MIP allowed the use of this concept to any other conductive material of any other commercial size/configuration SPE. The biosensor was based on electrochemical transduction: EIS and SW offered simplicity in designing; low response time, good precision, high accuracy, and low limit of detection.

Compared to other biosensors made with natural antibodies, the MI/Au-SPE showed similar analytical features especially concerning the ability to show linear ranges within the biological levels of Myo and good selectivity against other concomitant proteins. Furthermore, MI/Au-SPE showed excellent proprieties in terms of robustness, reusability, response time and stability and these characteristics were incomparable with the natural sensing materials.

Overall, this method is considered simple, of low cost, and inexpensive and a suitable alternative for fast screening Myo in point-of-care. The major critical step of the step this work comes from the PVC membrane. The thickness cannot be controlled and other approach could be explored.

5. 5 References

Ahammad, A.J.S., Choi, Y.-H., Koh, K., Kim, J.-H., Lee, J.-J., Lee, M., 2011. Electrochemical Detection of Cardiac Biomarker Troponin I at Gold Nanoparticle-Modified ITO Electrode by Using Open Circuit Potential. *International Journal of Electrochemical Science* 6(6), 1906-1916.

Billah, M., Hays, H.C.W., Millner, P.A., 2008. Development of a myoglobin impedimetric immunosensor based on mixed self-assembled monolayer onto gold. *Microchimica Acta* 160(4), 447-454.

Chambers, J.P., Arulanandam, B.P., Matta, L.L., Weis, A., Valdes, J.J., 2008. Biosensor recognition elements. *Current Issues in Molecular Biology* 10, 1-12.

Chu, Y.-M., Lin, C.-C., Chang, H.-C., Li, C., Guo, C., 2011. TiO(2) nanowire FET device: Encapsulation of biomolecules by electro polymerized pyrrole propylic acid. *Biosensors & Bioelectronics* 26(5), 2334-2340.

Gogol, E.V., Evtugyn, G.A., Marty, J.L., Budnikov, H.C., Winter, V.G., 2000. Amperometric biosensors based on nafion coated screen-printed electrodes for the determination of cholinesterase inhibitors. *Talanta* 53(2), 379-389.

Guo, T.Y., Xia, Y.Q., Hao, G.J., Song, M.D., Zhang, B.H., 2004. Adsorptive separation of hemoglobin by molecularly imprinted chitosan beads. *Biomaterials* 25(27), 5905-5912.

Heyrovsky, J., 1956. The development of polarographic analysis. *Analyst* 81(961), 189-&.

Jena, B.K., Raj, C.R., 2006. Electrochemical biosensor based on integrated assembly of dehydrogenase enzymes and gold nanoparticles. *Analytical Chemistry* 78(18), 6332-6339.

Kamel, A.H., Moreira, F.T.C., Almeida, S.A.A., Sales, M.G.F., 2008. Novel potentiometric sensors of molecular imprinted polymers for specific binding of chlormequat. *Electroanalysis* 20(2), 194-202.

Katz, E., Willner, I., 2003. Probing biomolecular interactions at conductive and semiconductive surfaces by impedance spectroscopy: Routes to impedimetric immunosensors, DNA-Sensors, and enzyme biosensors. *Electroanalysis* 15(11), 913-947.

Kertai, M.D., Boersma, E., Klein, J., van Urk, H., Bax, J.J., Poldermans, D., 2004. Long-term prognostic value of asymptomatic cardiac troponin T elevations in patients after major vascular surgery. *European Journal of Vascular and Endovascular Surgery* 28(1), 59-66.

Landesberg, G., Shatz, V., Akopnik, I., Wolf, Y.G., Mayer, M., Berlatzky, Y., Weissman, C., Mosseri, M., 2003. Association of cardiac troponin, CK-MB, and postoperative myocardial ischemia with long-term survival after major vascular surgery. *Journal of the American College of Cardiology* 42(9), 1547-1554.

Lewandrowski, K., Chen, A., Januzzi, J., 2002. Cardiac markers for myocardial infarction. A brief review. *American journal of clinical pathology* 118 Suppl.

Lin, H.-Y., Hsu, C.-Y., Thomas, J.L., Wang, S.-E., Chen, H.-C., Chou, T.-C., 2006. The microcontact imprinting of proteins: The effect of cross-linking monomers for lysozyme, ribonuclease A and myoglobin. *Biosensors & Bioelectronics* 22(4) 534-543.

McCann, C.J., Glover, B.M., Menown, I.B.A., Moore, M.J., McEneny, J., Owens, C.G., Smith, B., Sharpe, P.C., Young, I.S., Adgey, J.A., 2008. Novel biomarkers in early diagnosis of acute myocardial infarction compared with cardiac troponin T. *European Heart Journal* 29(23), 2843-2850.

Panagopoulou, M.A., Stergiou, D.V., Roussis, I.G., Prodromidis, M.I., 2010. Impedimetric Biosensor for the Assessment of the Clotting Activity of Rennet. *Analytical Chemistry* 82(20), 8629-8636.

Pang, X.S., Cheng, G.X., Lu, S.L., Tang, E.J., 2006. Synthesis of polyacrylamide gel beads with electrostatic functional groups for the molecular imprinting of bovine serum albumin. *Analytical and Bioanalytical Chemistry* 384(1), 225-230.

Silva, B.V.M., Cavalcanti, I.T., Mattos, A.B., Moura, P., Sotomayor, M.D.P.T., Dutra, R.F., 2010. Disposable immunosensor for human cardiac troponin T based on streptavidin-microsphere modified screen-printed electrode. *Biosensors & Bioelectronics* 26(3), 1062-1067.

Tong, D., Hetenyi, C., Bikadi, Z., Gao, J.P., Hjerten, S., 2001. Some studies of the chromatographic properties of gels ('artificial antibodies/receptors') for selective adsorption of proteins. *Chromatographia* 54(1-2), 7-14.

Wang, Y., Zhang, Z., Jain, V., Yi, J., Mueller, S., Sokolov, J., Liu, Z., Levon, K., Rigas, B., Rafailovich, M.H., 2010. Potentiometric sensors based on surface molecular imprinting: Detection of cancer biomarkers and viruses. *Sensors and Actuators B-Chemical* 146(1), 381-387.

Wu, S., Tan, W., Xu, H., 2010. Protein molecularly imprinted polyacrylamide membrane: for hemoglobin sensing. *Analyst* 135(10), 2523-2527.

6

Novel biosensing device for point-of-care applications with plastic antibodies grown on Au\-Screen Printed Electrodes

6.1 Introduction

Improving the previous work may be achieved by removing the polymeric film and using a different chemical approach.

Furthermore, two special requirements are needed for a successful plastic antibody based device for Myo determination in POC: (i) it should be disposable to allow a direct and easy handling (Zhao et al. 2008) of biological fluids in hospitals; and (ii) it should allow the covalent link of the plastic antibody to the biosensing surface, in order to ensure that it remains there after its contact with a liquid phase. The first requirement may be achieved by using SPE technology. The huge developments of this field originated a massive production of inexpensive, reproducible and sensitive disposable electrodes. The second requirement may be fulfilled by selecting gold surfaces. Over the past decades (Silva et al. 2010), many biosensors have used SAMs as a way to immobilize, in an ordered manner, organic molecules on gold surfaces (Arya et

al. 2009). This organic thin-film material layer may turn out a successful and highly controlled way to link the imprinting layer to the gold surface.
Therefore, the main goal of this work is to develop a biosensing device with plastic antibodies imprinted on Au-SPE modified by self-assembly for POC applications. The analytical features of the resulting biosensor were studied by different electrochemical techniques, including EIS, SWV and potentiometry.

6.2 Experimental Section

6.2.1 Apparatus

The electrochemical measurements were conducted in a potentiostat/galvanostat from Metrohm Autolab/PGSTAT302N, with a FRA2 module and controlled by ANOVA 7.0 software. Au-SPEs were purchased from DROPSENS (DRP-C220AT), having working and counter electrodes (CE) made of gold and pseudo reference electrode and electrical contacts made of silver. The diameter of the WE was 4 mm.
For electrochemical assays, the SPEs were place in a switch box from DROPSENS, interfacing the electrical contacts of the Au-SPE with the electrical connections of the potentiostat/galvanostat. In potentiometric assays a Crison, GLP 21 pH meter (±0.1 mV sensitivity) was used with an Ag wire covered by a layer of AgCl acting as reference electrode. Readings were made at room temperature and under constant stirring.

6.2.2 Reagents

All chemicals were of analytical grade and de-ionized water (conductivity <0.1 μS/cm) was employed. $K_3[Fe(CN)_6]$ and $K_4[Fe(CN)_6]$ trihydrate were obtained from Riedel Haen; KCl, Tris from Panreac; MES, from Alfa Aesar; sodium chloride, GA) 25%, Cys 95% hydrogen peroxide 30%, ethanol 99.5%, Myo, AAM, NNMBA, APS, Oac, and NaCl from Fluka. Crea, Hmg, BSA, Glt and urea were tested as interfering species and obtained from Fluka.

6.2.3 Solutions

Stock solutions of 5.0×10^{-6} mol/L Myo were prepared in MES buffer (1.0×10^{-3} mol/L, pH 4.5). Less concentrated standards were prepared by accurate dilution of the previous solution in buffer.

Electrochemical assays were performed with 5.0×10^{-3} mol/L $K_3[Fe(CN)_6]$ and $K_4[Fe(CN)_6]$ in MES 1.0×10^{-3} mol/L, pH 7. The selectivity study used 1.0×10^{-6} mol/L Myo solutions prepared in buffer. Solutions of interfering species were of variable concentrations and prepared in the same buffer. Creat (5.25×10^{-5} mol/L), Hmg (5.0×10^{-6} mol/L), BSA (5.1×10^{-6} mol/L), Glt (7.61×10^{-5} mol/L) and urea (5.4×10^{-5} mol/L) solutions were prepared for this purpose.

6.2.4 Design of the plastic antibody on the screen printed electrode

The gold surface of the WE was incubated in 25 mmol/L ethanolic solutions of Cys for 4 h, at 25 °C. The resulting Cys/Au-SPE was washed with distilled water and incubated for 50 min. in Glu 2.5%, prepared in 0.1 mol/L PBS, pH 7.0, at 4 °C. The Glu/Cys/Au-SPE was washed with PBS and kept in 1.0×10^{-6} mol/L Myo prepared in PBS buffer, pH 7.0, for 4 h, at 4 °C. The electrode was thoroughly washed again with PBS buffer to remove adsorbed Myo. The Myo/Glu/Cys/Au-SPE was then incubated in 0.5 mol/L Tris for 30 min. and thoroughly washed with deionized water. The imprinting

stage started by adding 10 µL of 1.0 mol/L AAM and 0.07 mol/L NNMBA, prepared in PBS, pH 7.0, to the modified gold. This was followed by the addition of 10 µL of 0.06 mol/L APS solution in PBS pH 7.0. The polymerization was carried out at 25 °C, for 4 h. The sensor was thoroughly washed with deionized water and incubated in diluted Oac for 12 h. This acid is able to break the peptide bond, removing the protein from the modified surface (Bonini et al. 2007). The imprinted sensor was washed and conditioned in 10 mmol/L PBS buffer, pH 7.4.

6.2.5 Atomic Force Microscopy analysis

The morphological analysis of the final MI, the MI with protein, and the negative control NI were performed by Atomic Force microscopy (AFM) in tapping mode. The equipment used was (Veeco Metrology Multimode Nanoscope IVA) and Nanoscope software was used to analyse the AFM images.

6.2.6 Electrochemical assays

CV and SWV measurements were conducted in 5.0 mmol/L of $[Fe(CN)_6]^{3-}$ and 5.0 mmol/L of $[Fe(CN)_6]^{4-}$, prepared in MES buffer, pH 7.0. For CV assays the potential was scanned from -0.5 to +0.7 V, at 30 mV/s. In SWV studies potentials were changed from -0.4 to +0.7 V, at a 0.125 V/s, corresponding to a frequency of 20 Hz and step height of 150 mV.

EIS assays were conducted with the same redox couple $[Fe(CN)_6]^{3-/4-}$ at a standard potential of 0.225V, using a sinusoidal potential perturbation with amplitude 0.01 V (RMS) and a number of frequencies equal to 50, logarithmically distributed over a frequency range of 0.1-100 kHz. The impedance data were fitted to a Randles equivalent circuit using the implemented ANOVA software.

Potentiometric measurements were made at room temperature and under constant stirring, after stabilization to ± 0.2 mV. Increasing concentrations of Myo were obtained by transferring 0.0100 to 0.200 mL aliquots of 7.2×10^{-6} mol/L Myo aqueous solution to a 10 mL beaker containing 5.00 mL of 1.0×10^{-3} mol/L of MES, of fixed pH and ionic strength. Between assays, the sensors were conditioned in 1.0×10^{-5} mol/L Myo solution.

6.2.7 Selectivity

Potentiometric selectivity coefficients were calculated by the MPM, using (Equation26). The initial concentration of primary ion was set to 2.0×10^{-7} mol/L (a_A) and an aliquot of a primary ion solution of 5.0×10^{-6} mol/L,

changing the concentration $a_{A'}$, was added, increasing the potential in ~16 mV. The interference of Crea, Hmg, BSA, Glt, and Urea was assessed by adding small aliquots (a_B) of the corresponding solutions into the primary ion solution (of a_A),

until the same potential change was observed, i.e., until an increment of ~16 mV was reached, ensuring that the final concentration of primary ion was not altered by more than 5%.

6.2.7 Urine sample analysis

The single standard addition method Equation 27 was used following the next equation, where c_0 and V_0 are the unknown analyte concentration and the initial volume of the analyte sample, respectively; c and V are the concentration of the standard reference solution and the volume of its addition; and E_0 and E are the electrode potentials before and after adding the reference solution. The V_0 and c values were 5.0 mL and 5×10^{-6} mol/L respectively.

$$c_0 = \frac{c(V_2 - V_1)}{V_0(10^{(E_2 - E_0/S)} - 10^{(E_1 - E_2)/S})} \quad \textbf{Equation 27}$$

6.3 Results and Discussion

6.3.1 Design of the biosensor

The WE of the Au-SPE was modified by following the scheme in Figure 35. It consisted of six different stages, starting in (A) the formation of an amine layer, (B) made reactive in order to (C) bind the protein. The imprinting step was started by (D) self-organizing the monomeric structures around the template and (E) polymerizing with cross-linker and initiator. The imprinted sites were obtained (F) once the protein was removed.

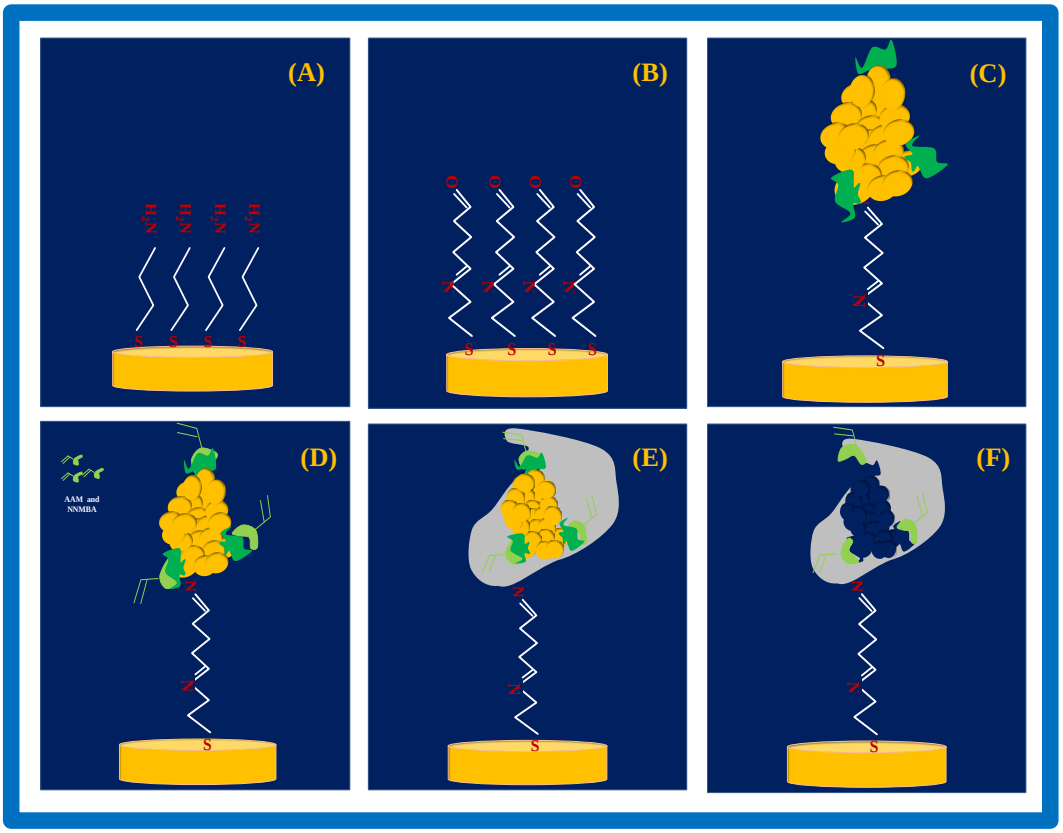

Figure 35: Assembly of the Au-SPE imprinted device.

The amine layer (Figure 35A) was formed by incubating the gold surface in Cys. It contacts with a gold substrate, leading to the spontaneous formation of a closely packed monolayer via a strong gold-sulfur interaction between the -SH (thiol) groups and the gold. This monolayer has a standing-up configuration with the amine groups ($-NH_2$) exposed to the surrounding environment.

The external layer of primary amines was modified by reaction with GA (Figure 35) GA carries two terminal aldehyde functions (-CHO) to which amines react under mild conditions by means of a nucleophilic addition mechanism. The typical product is an imine (-C=N-), ensuring a covalent attach of GA to the amine layer. Of course, the existence of two aldehyde functions in the same reactant (GA) suggests great care in the selection of time, temperature, pH and concentration of GA. One unaltered aldehyde function is expected to remain as an outer layer (Figure 35B) and any deviation from the intended course leads to the reduction of the number of active carbonyls for subsequent binding of Myo. In the present work, the reaction took place with a diluted solution of Glu, at 4 ^{o}C, for 50 minutes. The pH was kept in 7.0, adjusting the surface conditions of the biosensor to receive a protein.

This new aldehyde layer is ready to react with Myo (Figure 35C). Myo has both polar and nonpolar amino acid side-chains directed to the external surface of the protein. The exact amount and nature of these residues are however difficult to identify because proteins are not rigid objects as their biological function is controlled by conformational changes of different magnitudes (Brunori et al. 2004). Therefore, it is reasonable to assume the existence of some external function in Myo that will be able to react with the previous aldehyde layer. Any aliphatic amine or alcohol will be able to carry out this reaction. Of course the pH of this assay must be equal to that in physiological conditions, ensuring the same degree of protonation in each side-chain. The aldehyde functions that remained unaffected after binding Myo were blocked with Tris to prevent unexpected reactions.

The imprinting stage started by incubating the Au-SPE with Myo in AAM allowing their self-organization around the protein (Figure 35D). NNMBA was added after, along with the initiator, producing a radical polymerization (Figure 35E). The time and monomer/cross-linker concentrations given in this stage were of particular importance because if the polymer layer becames too thick it may entrap the protein irreversibly. The temperature at which this polymerization reaction took place was also important because the imprinted conformation should match that of Myo in the samples. Ambient temperature was selected in this stage considering that the sample analysis is also carried under this temperature condition. Finally, the attached protein was after removed later by reaction with Oac to empty the imprinted sites (Figure 35F). Subsequently, several washing steps were performed to remove the released peptide fractions from the sensory surface.

6.3.2 Control of the Surface modification

The immobilization of organic films on metal surfaces produces global modifications in the electrical features of the solid-state probe. This can be measured by monitoring the changes in the electron transfer capability of well-known redox systems, such as $[Fe(CN)_6]^{4-}/[Fe(CN)_6]^{3-}$ by EIS and CV. EIS studies were used to follow the Au-SPE modification after each chemical change. Randle's equivalent circuit was adopted to model the physiochemical process occurring at the gold electrode surface (Figure 36A), as it is often used to interpret simple electrochemical systems (Suni 2008). The elements of this circuit include the uncompensated R_S, C_{dl}, and R_{ct} which is inversely proportional to the rate of electron transfer, and capacitance of double layer (W), accounting for the diffusion of ions from bulk electrolyte to the electrode interface.

The EIS spectra of this Randle's equivalent circuit were recorded for every step of the Au-SPE surface modification and the results were presented as Nyquist plots (Figure 36A). The typical plots may include a semicircle region lying on the real axis followed by a straight line. The semicircle was observed at high

frequency range and indicated a charge-transfer controlled process. The diameter of this semicircle equalled the R_{ct}, controlling the electron transfer kinetics of the redox-probe at the electrode interface (Panagopoulou et al. 2010). The linear range was given at the low frequency range and showed diffusion-controlled process from mass-transfer.

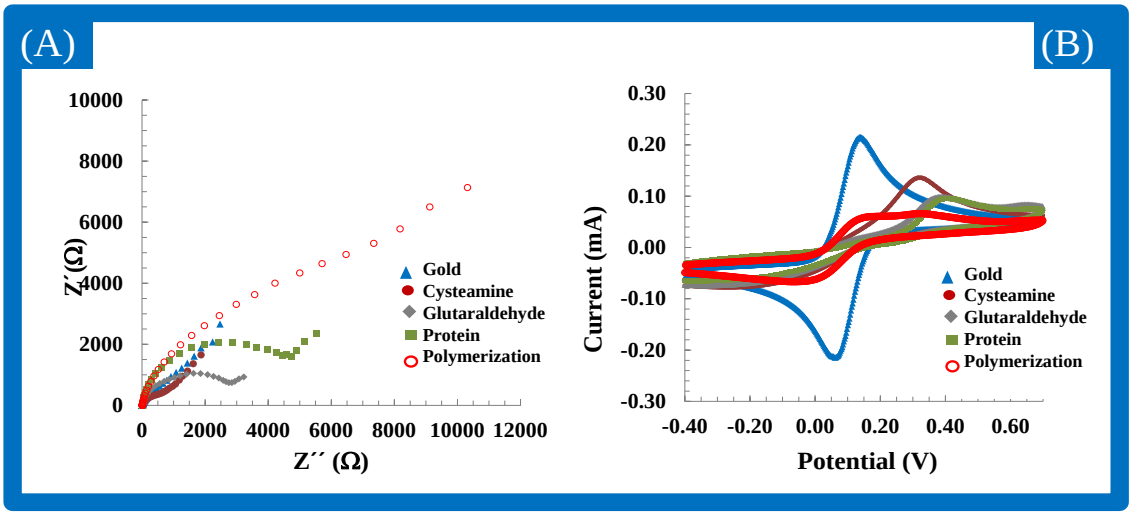

Figure 36: Electrochemical controls of the subsequent modification steps of the Au-SPE in 5.0 mM $[Fe(CN)_6]^{3-}$ and 5.0 mM $[Fe(CN)_6]^{4-}$, in buffer pH 7.0, carried out by of (A, Nyquist plot) and (B, cyclic voltammograms) assays.

The bare gold electrode showed a very small semicircle domain, suggesting a very fast electron-transfer process with a diffusional limiting step (Figure 36A). The consecutive attachment of the Cys and GA gave rise to subsequent increases in the electron transfer resistance, resulting in increases in the semicircular section of the Nyquist plot. The linkage of Myo followed by the polymerization reaction produced an additional barrier for the redox probe access to the Au-SPE modified electrode. This resulted in an extra increase in the electron transfer resistance, reflected by further substantial increase in R_{ct}.

CV assays are shown in Figure 36B and supported the previous studies of EIS. When compared to the redox probe in the bare gold, the subsequent modification steps of the Au-SPE increased the peak-to-peak potential separation in the voltammograms, accounting for the increased charge-transfer resistance. The

anodic peak decreased with additional modification steps and the cathodic peak tended to disappear, attributing a similar-to-irreversible character to the reaction of the redox probe. This irreversibility was curiously reversed after the polymerization step, although the anodic and cathodic peak currents were much lower than that of the redox probe on the bare gold.

6.3.3 Atomic Force Microscopy analysis

The morphological analysis of the MI with protein (A), the final MI (B) and the negative control NI (C) were performed by AFM measurements (Figure 36). Morphological differences were observed between all materials. The MIP material before removing the protein (A) in smother than of the MIP material after Oac treatment (B), evidencing the exit of the protein for the polymeric layer. The rugosity in B may be attributed to the vacant places created by the protein removal. The "cavities" observed in this roughness ranged ~10 nm, suggesting that Myo was imprinted in monomeric or dimeric states (a single Myo molecule is 4.5 nm × 3.5 nm × 2.5 nm) (Lin et al. 2007a).

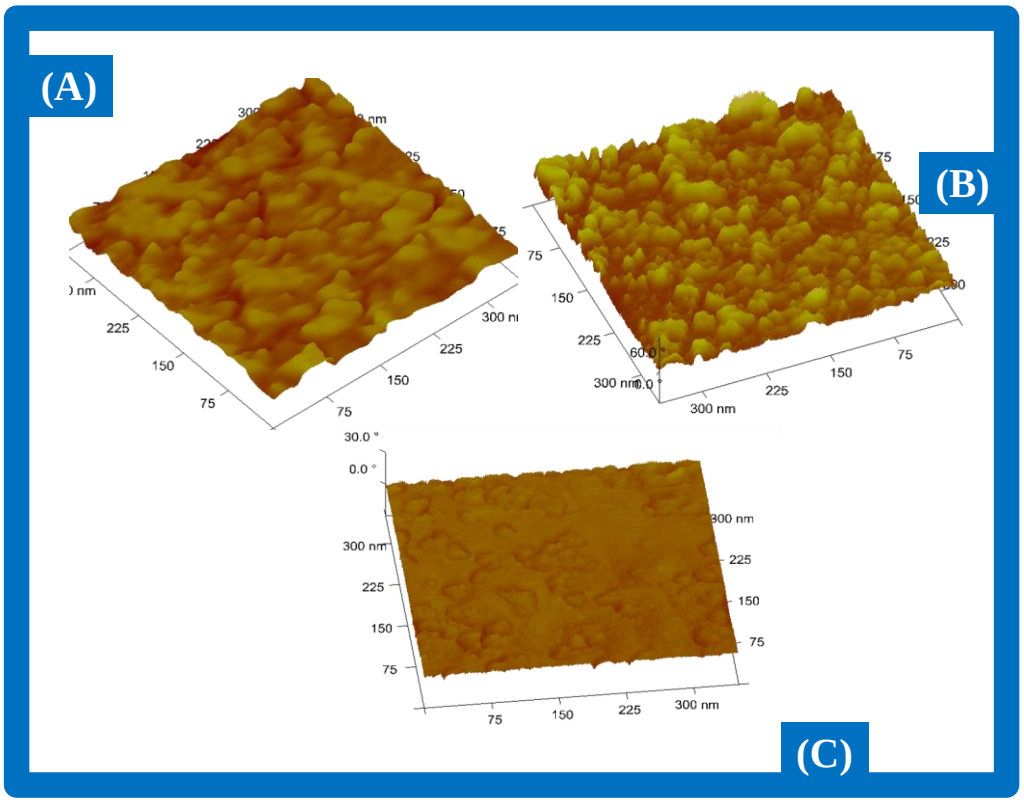

Figure 36: AFM tapping mode images showing 300 nm × 300 nm scan of (A) MI, (B) MI after protein removal and (C) NI surfaces. AFM images processed using Nanorule program to show the 3-dimensional topography.

6.3.4 Selection of the Transducer

Many biosensors in POC employ electrochemical detection (Ronkainen et al. 2010; Soper et al. 2006), where the monitored event changes a specific electrical property of the electrochemical cell, involving, in many cases, a measurable current over a potential range scanning (voltammetry), a measurable charge accumulation or potential at near-zero current (potentiometry), or a measurable resistive and capacitive properties upon perturbation of a system by a small amplitude sinusoidal AC excitation (impedance spectroscopy). These were the technical approaches taken in the present study.

The calibration of the modified Au-SPE in EIS assays checked the effect of Myo on the charge-transfer resistance of a redox probe. Comparing to the spectrum of the redox probe alone, Nyquist plots showed that diameter of the semicircles decreased gradually with increasing concentration of Myo. So, Myo reduced the charge-transfer resistance of the probe once bound to the imprinted sensory layer (Figure 37). This effect was checked for a concentration range of Myo varying from 0.16 to 48.6 µg/mL. Plots of $\log(R_{ct})$ against log[Myo] showed linear behaviour from 9.0 to 36.0 µg/mL, with a limit of detection of 2.25 µg/mL.

SWV was selected among other voltammetric methods for displaying high sensitivity to surface-confined electrode reactions, with suitable detection capabilities and rapidity. In general, the presence of Myo in the redox probe decreased its typical anodic peak current observed without Myo by the imprinted modified Au-SPE (Figure 38). In terms of overall analytical performance, it was possible to observe that this effect of Myo was consistent for all concentrations tested, ranging from 0.16 to 48.6 µg/mL. The electrochemical

response resulted in a negative slope calibration (Figure 38) showing a linear behaviour from 9.0 to 36 µg/mL of Myo. The limit of detection was 8.5 µg/mL.

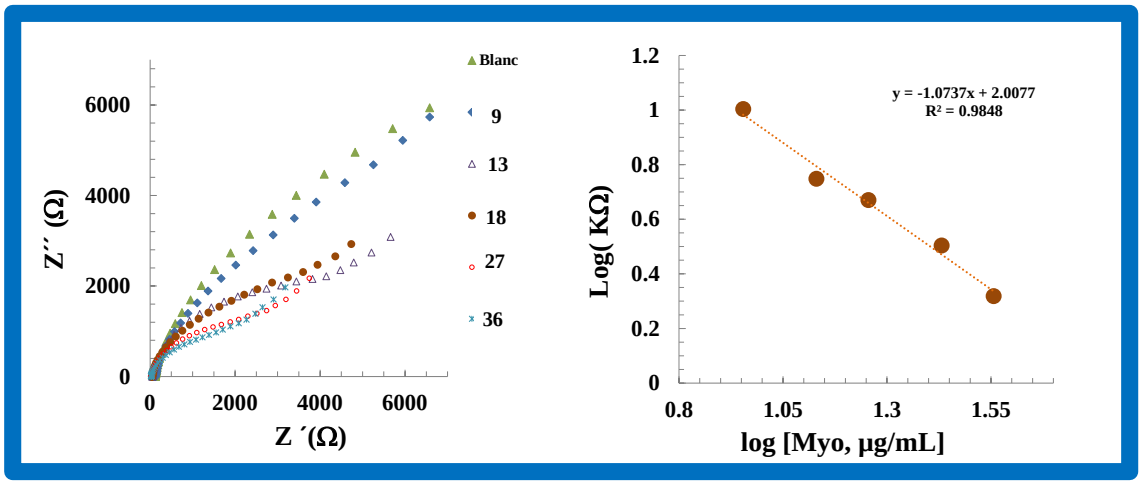

Figure 37: EIS Nyquist plot (left) of modified Au-screen printed electrode and the corresponding calibration curve (right) in 5.0 mmol/L$[Fe(CN)_6]^{3-}$ and 5.0 mmol/L $[Fe(CN)_6]^{4-}$, in buffer pH 7.0, with different concentrations of Myo.

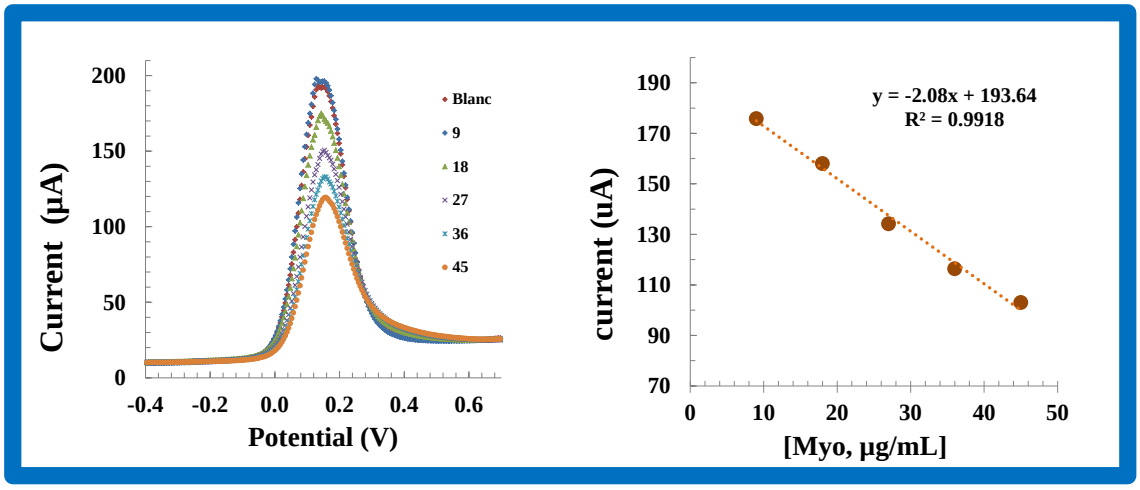

Figure 38: SWV (left) of modified Au- SPE and the corresponding calibration curve (right) in 5.0 mmol/L $[Fe(CN)_6]^{3-}$ and 5.0 mmol/L $[Fe(CN)_6]^{4-}$, in MES buffer pH 7.0, with different concentrations of Myo.

Potentiometric measurements were conducted by calibrating the cell with Myo concentrations ranging from 0.10 to 46 µg/mL. Tests carried out in a pH of 7.4

were unable to produce enough potential changes against concentration, and other pH conditions were tested. In general, the presence of Myo in pH 4.5

increased the potential change against concentration by decreasing the cell potential (Figure 39).

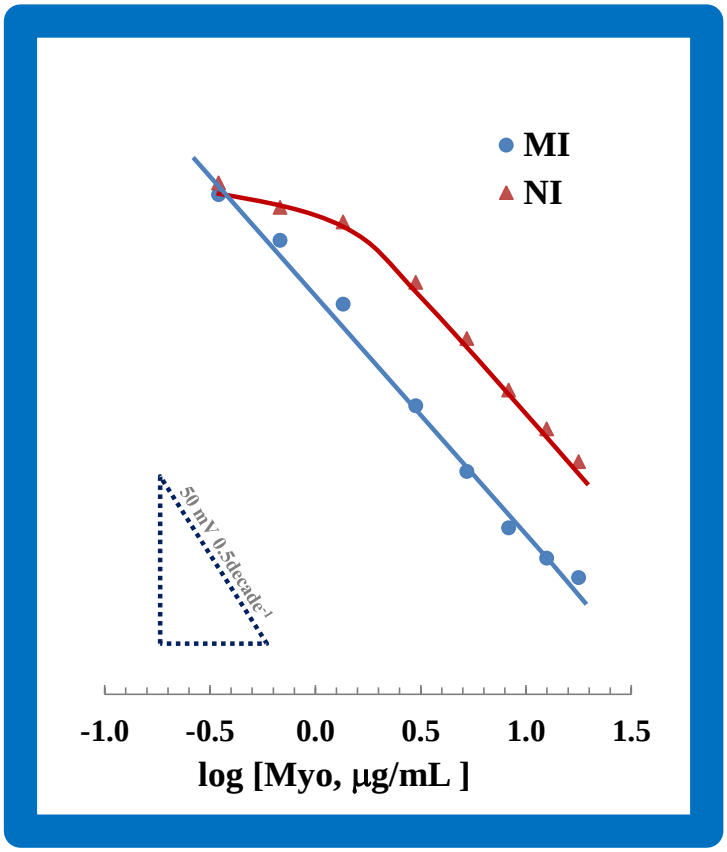

Figure 39: Potentiometric calibration curves of imprinted and non-imprinted Au- SPE in buffer pH 4.5.

That behaviour is typically attributed to negatively charged species, which was not as expected: Myo will be neutral in solutions matching its isoelectric point (7.2), positive in solutions of lower pH, and negative in solutions of higher pH. So, in a solution of pH 4.5 the net charge of Myo is positive. However, it is important to consider the protein great dimensions and its polyionic nature, carrying many positive and negatively-charged side chains. These conditions

may imply non-equilibrium ion-exchange processes between the protein in the aqueous phase and sensory imprinted material in the solid-state electrode that

may cause a large potential change, resulting in a non-equilibrium super-Nernstian response. This would be consistent with the anionic slopes of -70.3 mV/decade. Furthermore, the use of APS as initiator may attribute the sensory surface positive charges, repealing the negative charged sites of the protein and attracting the positively charged ones. The linear behaviour was observed within 0.348 and 24 µg/mL, with detection limit of 0.13 µg/mL. The squared correlation coefficients were always >0.992. The device also offered quick responses, with each standard requiring < 30 s to reach a potential stability of ±1 mV.
Overall, the widest linear range and the lower limit of detection were obtained for the potentiometric assays (Table 6). In terms of POC applications for Myo analysis in biological fluids, this approach was the only one reaching cut-off levels. Thus, potentiometric transduction was selected as transducer in subsequent studies, including its selectivity against other biological species and its behaviour under practical application. The MI biosensor was reused 3 times after several washes with buffer, and was stable for at least 3 weeks in solution

6.3.4 Selectivity study

The selectivity of a membrane electrode is of major importance for a successful analytical application. It is governed mostly by the equilibrium that exists at the membrane-solution interface, and can be determined experimentally by calculating potentiometric selectivity coefficients, K_{POT}. These coefficients define the ability of an electrode to differentiate a primary ion from species that interfere in the analytical reading (Umezawa et al. 2000). The lower the K_{pot} the smaller the interference.
The MPM was selected in this study, because it does not require that the biosensors exhibit Nernstian behaviour for the primary ion and interfering ions, nor that the ions are of equal charge (thus avoiding the difficulties in accuracy coming from the conventional methods)(Horvai 1997; Umezawa et al. 2000). Furthermore it is valid and applicable to virtually any sensor as long as only small signal changes are considered (Horvai 1997).

Table 6: Main analytical features obtained with the different electrochemical transducers.

Analytical Feature	Electrochemical Impedance Spectroscopy	Square-Wave Voltammetry	Potenti-ometry
Slope	-1.07[a)]	-2.08[b)]	-74.9[c)]
r^2	> 0.987	> 0.992	> 0.992
LOD, µg/mL	2.25	8.5	0.133
LLLR, µg/mL	9.0	9.0	0.348
Response time, s	< 90	< 30	< 15

a)log kΩ*/([Myo]/µg/mL);* b)*µA/ ([Myo]/µg/mL);* c) *mV/log([Myo]/µg/mL)*

The interfering species tested were selected among those that may be found in biological fluids, such as Crea, Hmg, BSA, Glt, and Urea. From these, only Hmg was able to promote a potential variation of 15.8 mV. The required concentration was about 333 mg/L, corresponding to a potentiometric selectivity coefficient of -0.77. For Crea, Glt, BSA, and Urea, the corresponding potential changes were only 10.3; 5.4; 0.3 and 4.8 mV, respectively. The corresponding concentrations were 5.84, 332, 10.2 and 3.23 mg/L, all below the reference levels for the intended samples. Overall, the selectivity study confirmed the high selectivity of the potentiometric device, suggesting its possible application under real samples.
The stereo-selectivity of the imprinted Au-SPE was also tested by checking the response of Myo in a NI device, fabricated by using only PBS buffer in the step C of protein binding (Figure 35). As may be seen in Figure 39, NI devices showed higher concentrations for linear ranges and detection limits with similar slope. Thus, the imprinting effect was observed only in the concentrations nearing the LOD. After that, Myo concentration starts being too high, leading to non-specific interactions at the membrane-solution interface. This may turn out especially relevant for Myo concentrations nearing cut-off levels.

6.3.5 Myo Assay

The standard addition method was applied to determine Myo in spiked urine samples, ranging from 0.48-0.96 µg/mL Myo. A good agreement was found between added and found amounts of Myo, with recoveries ranging 92.0-96.2%. Average relative standard deviations were 0.6%. These results pointed out the accuracy and the precision of the analytical data, suggesting that it may turn out a successful approach for screening AMI episodes in POC.

6.4 Conclusions

Surface imprinting of Myo was successfully established by merging self-assembled monolayer and molecular imprinting technologies on a single Au-

SPE device and applying it to Myo detection/determination in biological fluids. Potentiometric transduction offered the best analytical features compared to EIS and SWV, suitable selectivity features for practical application and quick responses.

Overall, the potentiometric method with the imprinted Au-SPE device is simple, of low cost, precise, accurate and inexpensive, and may turn out in a near future an alternative method for screening Myo in POC.

6.5 References

Arya, S.K., Solanki, P.R., Datta, M., Malhotra, B.D., 2009. Recent advances in self-assembled monolayers based biomolecular electronic devices. *Biosensors & Bioelectronics* 24(9), 2810-2817.

Brunori, M., Bourgeois, D., Vallone, B., 2004. The structural dynamics of myoglobin. *Journal of Structural Biology* 147(3), 223-234.

Horvai, G., 1997. The matched potential method, a generic approach to characterize the differential selectivity of chemical sensors. *Sensors and Actuators B-Chemical* 43(1-3), 94-98.

Lin, H.-Y., Rick, J., Chou, T.-C., 2007. Optimizing the formulation of a myoglobin molecularly imprinted thin-film polymer-formed using a micro-contact imprinting method. *Biosensors & Bioelectronics* 22(12).

Panagopoulou, M.A., Stergiou, D.V., Roussis, I.G., Prodromidis, M.I., 2010. Impedimetric Biosensor for the Assessment of the Clotting Activity of Rennet. *Analytical Chemistry* 82(20), 8629-8636.

Ronkainen, N.J., Halsall, H.B., Heineman, W.R., 2010. Electrochemical biosensors. *Chemical Society Reviews* 39(5), 1747-1763.

Silva, B.V.M., Cavalcanti, I.T., Mattos, A.B., Moura, P., Sotomayor, M.D.P.T., Dutra, R.F., 2010. Disposable immunosensor for human cardiac troponin T based on streptavidin-microsphere modified screen-printed electrode. *Biosensors & Bioelectronics* 26(3), 1062-1067.

Soper, S.A., Brown, K., Ellington, A., Frazier, B., Garcia-Manero, G., Gau, V., Gutman, S.I., Hayes, D.F., Korte, B., Landers, J.L., Larson, D., Ligler, F., Majumdar, A., Mascini, M., Nolte, D., Rosenzweig, Z., Wang, J., Wilson, D.,

2006. Point-of-care biosensor systems for cancer diagnostics/prognostics. *Biosensors & Bioelectronics* 21(10), 1932-1942.

Suni, I.I., 2008. Impedance methods for electrochemical sensors using nanomaterials. *Trac-Trends in Analytical Chemistry* 27(7), 604-611.

Umezawa, Y., Buhlmann, P., Umezawa, K., Tohda, K., Amemiya, S., 2000. Potentiometric selectivity coefficients of ion-selective electrodes Part I. Inorganic cations - (Technical report). *Pure and Applied Chemistry* 72(10), 1851-2082.

7

Smart Plastic Antibody Material (SPAM) tailored on disposable screen printed electrodes for protein recognition: application to Myoglobin detection

7.1 Introduction

Several strategies for surface imprinting have been described in the literature. Most of these report the use of immobilized template, initiation on the supporting matrix, and combined surface imprinting with controlled/living free radical polymerization (Bossi et al. 2007; Chen et al. 2011b; Shi et al. 1999), (Piletsky et al. 2000; Shiomi et al. 2005). In general, the covalent immobilization of the template molecules at the surface of solid substrates offers some advantages: it enables imprinting templates that are insoluble in the pre-polymerization mixture and minimizes the template aggregation, thus leading to more homogeneous binding sites (Chen et al. 2011b).

But the monomers selected for creating the surface imprinted binding sites are at the core of the success of the plastic antibody operation (Andersson 2000; Kriz et al. 1997; Shi et al. 1999). Due to the multiple-charge nature of proteins and to their

multiple surface features, different monomers have been employed, neutral or negatively/positively charged. In essence, they are expected to interact strongly with several points at the outer surface of the protein, thus favouring more specific template rebinding. However, as far as we are aware, the area surrounding the binding site has always been composed of the same material as the binding site, itself, which has contributed to non-specific interactions.

In order to create Smart Plastic Antibody Materials (SPAM) of enhanced specific binding, this work introduces for the first time charged monomers on the binding sites combined with neutral monomers in the rest of the polymeric matrix.

This concept formed the basis for the design of Myo plastic antibodies over the gold surface of commercial Au-SPE. The charged monomers used for this purpose were 2-Acrylamido-2-methyl-1-propanesulfonic acid (AMPSA) sodium salt and 2-Aminoethyl methacrylate (AEMA) hydrochloride. The neutral-surrounding material was obtained by co-polymerizing AAM and NNMBA. NIM was produced by removing the template from the procedure and measured the ability of the polymer to interact non-specifically with the template. The resulting biosensor was evaluated by several electrochemical techniques and further applied to the analysis of biological samples.

7.2. Experimental section

7.2.1 Apparatus

The electrochemical measurements were conducted with a potentiostat/galvanostat from Metrohm Autolab and a PGSTAT302N, impedimetric module and controlled by Ivium software. Au-SPEs were purchased from DROPSENS (DRP-C220AT), having working and CE made of gold and pseudo - reference electrode and electrical contacts made of silver. The diameter of the WE was 4 mm and the Au-SPEs were placed in a switch box (DROPSENS), interfacing the electrical contacts of the Au-SPE with the electrical connections of the potentiostat/galvanostat.

7.2.2 Reagents

All chemicals were of analytical grade and water was de-ionized or ultrapure Milli-Q laboratory grade $K_3[Fe(CN)_6]$ and $K_4[Fe(CN)_6]$ trihydrate were obtained from Riedel-deHaen; AAM, NNMBA, TnT, BSA, urea, and NaCl from Fluka; AMPSA, thiomalic acid (TMA) and AEMA from Aldrich; and Myo, NHS , EDAC and BPO from Himedia.

7.2.3 Solutions

Stock solutions of 5.0×10^{-6} mol/L Myo were prepared in MES buffer (1.0×10^{-2} mol/L, pH 4.5). Less concentrated standards were obtained by accurate dilution of the previous solution in the same buffer. Electrochemical assays were performed with 5.0×10^{-3} mol/L $K_3[Fe(CN)_6]$ and $K_4[Fe(CN)_6]$ in MES 1.0×10^{-3} mol/L, pH 4.5. The selectivity study used 2.0×10^{-7} mol/L Myo solutions prepared in buffer and solutions of possible interfering species, TnT (2.0×10^{-7} mol/L), BSA (2.0×10^{-7} mol/L), and urea (2.0×10^{-7} mol/L), prepared in the same buffer.

7.2.4 Design of the plastic antibody on the Au-screen printed electrode

The gold surface of the WE was thoroughly washed with de-ionized water and incubated in 10 mmol/L solutions of TMA for 20 h, at 25 °C, previously. After this stage, all modifying solutions were applied subsequently and only at the WE area, by placing on it a 5 µL drop of the corresponding solution.

The carboxylic acid groups on the gold surface (Au-SPE/TMA) were activated by reaction with EDAC 50 mmol/L and 25 mmol/L NHS, and washed after with deionized water. The modified electrode was then incubated in Myo solution 1.0×10^{-4} mol/L, prepared in PBS buffer, pH 7.0, for 2.5 h, at 4 °C. The SPE modified with Au/TMA/Myo was then thoroughly washed again with PBS buffer and ultrapure water to remove adsorbed Myo.

The imprinting stage started by incubating overnight the Au-SPE/TMA/Myo electrode in 5.0×10^{-4} mol/L AMPSA and 5.0×10^{-4} mol/L AEMA. This was followed by the addition of 5.0×10^{-4} mol/L AAM (monomer), 5.0×10^{-5} mol/L NNMBA (cross-linker) and 5.0×10^{-4}mol/L BPO (initiator) solutions. The polymerization was carried out at 25 ^{o}C, for 5 h. The resulting material, Au-SPE/TMA/Myo/polymer was thoroughly washed with deionized water and incubated overnight in Protease K, 400 µg/mL, prepared in PBS buffer, pH 7.4, in the dark, to remove the protein template. The resulting material without template, Au-SPE/TMA/SPAM, was then washed several times in PBS buffer to remove protein fragments and proteinase K, and finally rinsed with water MQ (Zayats et al. 2011).

Blank materials of SPAM were produced in parallel, where the protein was removed from the synthetic pathway. These were named NIM and were used to evaluate the imprinting effect, because no specific binding sites should exist on it.

7.2.5 Atomic force microscopy analysis

The SPAM/NIM surfaces were characterised using AFM. Two different modes of AFM were tried to characterise the surface of the electrodes. These were tapping mode (Veeco Metrology Multimode / Nanoscope IVA) and contact mode (Nanoink NScriptor based AFM with A type tips). AFM images from tapping mode were found better and Image J software was used to analyse these.

7.2.6 Electrochemical procedures

CV and SWV measurements were conducted in 5.0 mmol/L of $[Fe(CN)_6]^{3-}$ and 5.0 mmol/L of $[Fe(CN)_6]^{4-}$, prepared in MES buffer, pH 4.5. For CV assays, the potential was scanned from -0.6 to +0.7 V, at 50 mV/s. In SWV studies potentials were changed from -0.6 to +0.6 V, at a frequency of 50 Hz with a step height of 150 mV. All assays were conducted in triplicate.

EIS assays were also conducted in triplicate with the same redox couple $[Fe(CN)_6]^{3-/4-}$ at a standard potential of +0.12 V, using a sinusoidal potential perturbation with amplitude of 0.01 V and a number of frequencies equal to 50, logarithmically distributed over a frequency range of 0.1-100 kHz. The impedance data were fitted to a Randles equivalent circuit using the implemented Ivium software.

Calibration curves were determined for Myo concentrations between 0.0250 and 41.1 µg/mL. The time given for SPAM/Myo interaction was set to 5 minutes. The response of the sensor was reversed after cleaning with proteinase K for 12 h and subsequent washing with PBS and water.

Selectivity studies were conducted by competitive assay between Myo, with a 2.0×10^{-7} mol/L concentration, and TnT, BSA, or Urea, solutions of the same concentration. All these were prepared in MES buffer pH 4.5.

The standard addition method was applied to determine Myo in spiked serum samples with a BSA concentration. Myo concentration was set to 45 µg/mL. This solution was further diluted to achieve Myo levels from 0.59 to 18.77 µg/mL, lying within the linear range of the device.

7.2.7 Binding Isotherm

The rebinding properties of Au-SPE/TMA/SPAM biosensor were measured by calculating the K_D through SWV assays. K_D was the protein concentration required to give half of the maximum response produced by the device. This was

done by fitting to the Langmuir isotherm (Equation 28) where IS was the normalized current-density (in Acm^{-2}), S the concentration of Myo (in mol/L) and I_{max} the maximum current density observed (in Acm^{-2}).

$$I_S = \frac{I_{max}}{1 + K_D / [S]} \qquad \textbf{Equation 28}$$

7.3 Results and discussion

7.3.1 SPAM Design

The preparation of SPAM involved a bottom-up approach of 4 stages, as indicated in Figure 40. It started by assembling a carboxylic layer on top of the gold WE of the SPE. This layer was activated for covalently binding Myo. The imprinting stage started by positioning the charged-monomers on the pre-polymerization mixture and polymerizing the vacant sites around the protein with neutral monomer and cross-linker species. The imprinted sites were finally obtained once the protein was removed.

In detail, the carboxylic layer was formed first by incubating the Au-SPE in TMA (Figure 40A). The contact of TMA with a clean gold substrate lead to the spontaneous formation of a closely packed monolayer via a strong gold-sulfur interaction between the thiol group (-SH) and Au. The carboxylic groups pointing outside were then activated, aiming at binding the protein afterwards under near-to-physiological conditions. This was done by EDAC/NHS chemistry. This reaction is well known, forming a highly reactive *O*-acylisourea intermediate that reacts quickly with NHS to produce a more stable succinimidylester intermediate (Jiang et al. 2004). This ester undergoes nucleophilic substitution with any readily available amine group (on Myo), resulting in the formation of an amide bond between the ester and protein (Figure 40B).

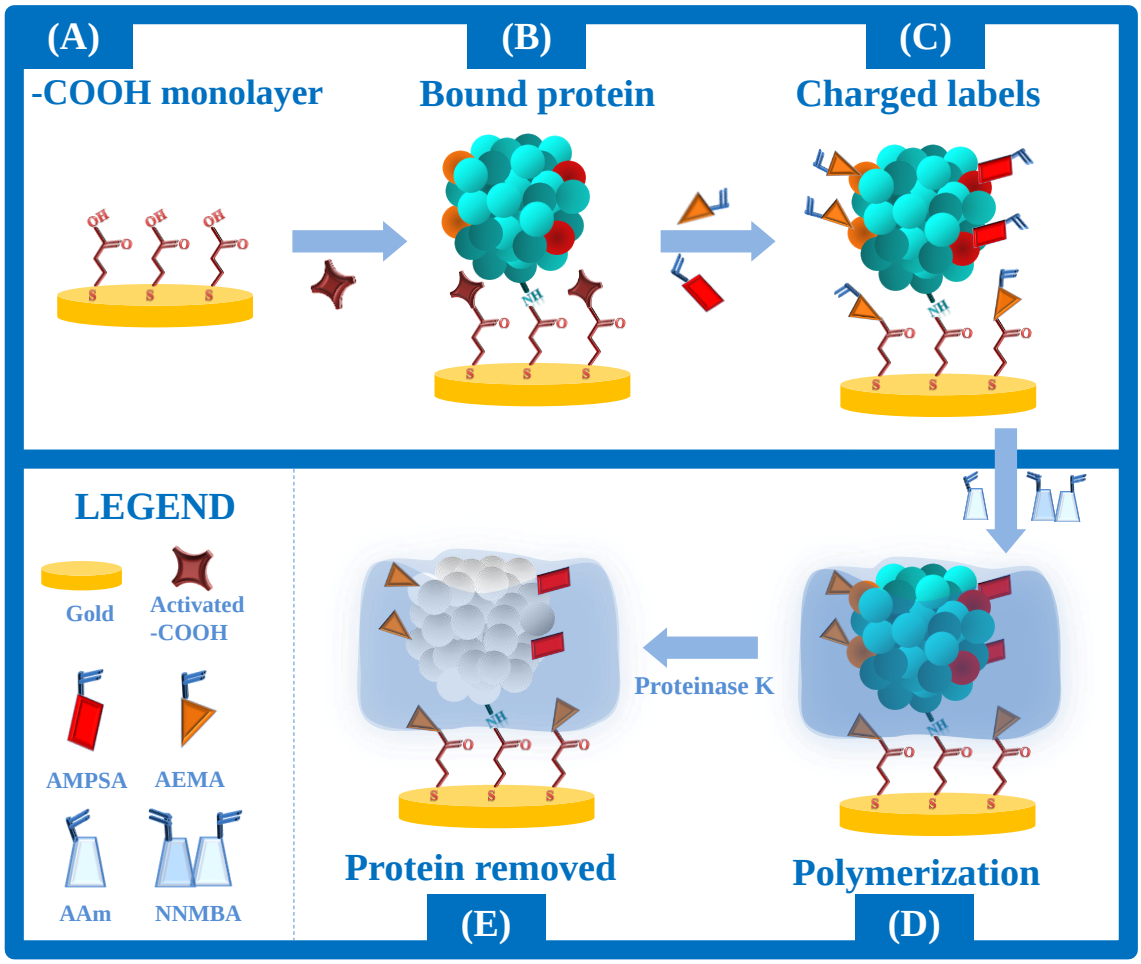

Figure 40: Schematic representation of the synthetic process of SPAM. A: Au-SPE modified with TMA and producing a carboxylic layer; B: Myo immobilized on the activated carboxylic groups of Au-SPE/TMA; C: charged-monomers in position and blocked carboxylic functions that remained active; D: polymerization with neutral monomer structures around the template; E: and binding site formation by template removal with proteinase K.

The rebinding cavities expected to display a similar-to-antibody behaviour started being formed by self-organizing the charged-monomers around the protein. Each charged monomer would be bound by ionic interaction to a Myo residue of opposite charge located on the protein surface. By taking part in the subsequent polymerization stage, these monomers would remain in position within

the final SPAM structure (Figure 40C). The selection of the most suitable monomers for this purpose depended on the nature of the organic functions of Myo pointing towards the surrounding environment. Myo has many kinds of amino acid residues along its polypeptide chain of 153 amino acids, distributed over a globular and compact form (45 × 35 × 25 Å). The exact amount and nature of the residues on the outer surface are however difficult to predict because proteins are not rigid objects and their biological function is controlled by conformational changes of different magnitudes (Brunori et al. 2004). So, one may say that both charged and uncharged polar amino acid side-chains are expected to be directed towards the external surface of the protein. Consequently, both positively and negatively charged-monomers were used, contributing to an increasing number of interactions, and thus to a more accurate stereochemical recognition of the protein template.

Monomers with amine (AEMA) and sulphonic acid (AMPSA) based functions were selected (Figure 40C). Although they are not completely ionized in solution, they ensure physiological compatibility with the target protein, granting that its conformation is kept. Only the ionized fraction of these monomers interacting with Myo is expected to contribute to the imprinted site because weakly bound monomers were removed by washing the material with water after positioning the monomers. This was indeed an essential condition to ensure that only neutral monomers would take part of the subsequent polymerization stage (thus avoiding any polymerizable charged species outside the binding site area). In addition, the non-ionized fraction of the amine function also blocked the carboxylic functions remaining active after protein binding, thus avoiding side-reactions with the material and ensuring that the subsequent polymeric fraction would remain attached to the modified gold surface.

The position of the charged groups was set firm by polymerizing the vacant area around the protein (Figure 40D). This was done by an addition reaction where all vinyl groups from monomer and cross-linker species gave rise to long branched carbon chains. Only amide functions were present in the final reticulated material because this was the only organic function in AAM and NNMBA monomers. A radical initiation of the polymerization was preferred (by using

BPO) to cationic or anionic ones, because these would introduce a lower number of charged species inside the polymeric matrix. This matrix was firstly designed to be neutral outside the binding sites, and this was an essential condition to reduce non-specific-binding.

The SPAM material was ready after removing the template from its imprinted site (Figure 40D). Many different approaches have been used for this purpose (Whitcombe et al. 2011; Zdyrko et al. 2009) and the use of a proteolytic enzyme is unique in this regard. This procedure was aimed at ensuring the complete removal of the protein and keeping mild conditions to avoid any disturbance around the SPAM network. Proteinase K was the enzyme selected for this purpose. It cleaved peptide bonds, converting each accessible single polypeptide from Myo into smaller peptide fragments. These fragments were removed from the cavity by rinsing the material with buffer.

7.3.2 Control of the surface modification by impedance and voltammetry measurements

The modification of metal surfaces with organic films produces global modifications in its electrical features. These can be measured by monitoring the changes in the electron transfer properties of well-known redox systems, such as $[Fe(CN)_6]^{4-}/[Fe(CN)_6]^{3-}$. Indirect ways of measuring such alterations include EIS and CV assays.

EIS studies were used to follow the Au-SPE modification after each chemical change. Randle's equivalent circuit was adopted to model the physiochemical process occurring at the gold electrode surface as it is frequently used to interpret simple electrochemical systems. R_S, the C_{dl}, R_{ct} which is inversely proportional to the rate of electron transfer, and the W, accounting for the diffusion of ions from bulk electrolyte to the electrode interface.

The obtained EIS spectra are presented as Nyquist plots in Figure 41A. In general, the semicircle was observed at high frequency range and indicated a charge-

transfer controlled process. The diameter of this semicircle equalled R_{ct}, controlling the electron transfer kinetics of the redox-probe at the electrode interface (Panagopoulou et al. 2010). The linear arm was seen in the low frequency range and showed diffusion-controlled mass-transfer.

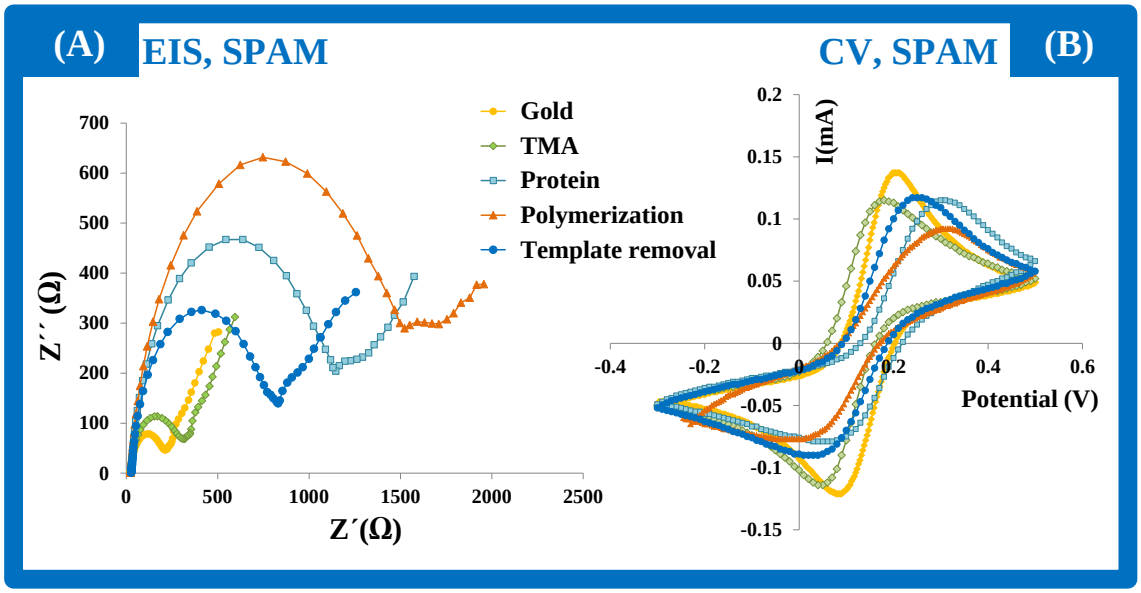

Figure 41: Electrochemical study over the subsequent modification steps of the Au-SPE in 5.0 mmol/L $[Fe(CN)_6]^{3-}$ and 5.0 mmol/L $[Fe(CN)_6]^{4-}$, in MES buffer pH 4.5, carried out by EIS (A, Nyquist plots) and CV (B, cyclic voltammograms) assays for SPAM.

The bare gold surface showed a very small semicircle domain, suggesting a very fast electron-transfer process with a diffusional limiting step (Figure 41A). Modification with the TMA monolayer gave rise to subsequent increases in the electron transfer resistance, resulting in increases in the semi-circular section of the Nyquist plot. For SPAM polymer (Figure 41A), further linkage of Myo followed by the polymerization stage produced additional barriers for the redox probe access to the Au-SPE modified electrode. This resulted in an extra increase in the electron transfer resistance, reflected by further substantial increase in R_{ct}. The final step of the artificial antibody synthesis was the template removal with proteinase K. In this step the resistance decreased (Figure 41A), suggesting that Myo

was successfully extracted from the polymer. No resistance decrease was observed on NIM after proteinase K treatment (**Figure 42**) which accounted the stability of the polymer network against the enzyme. The R_{ct} of the NIM materials (Figure 42A) was close to that of SPAM material without template, thus suggesting that the template removal step was efficient.

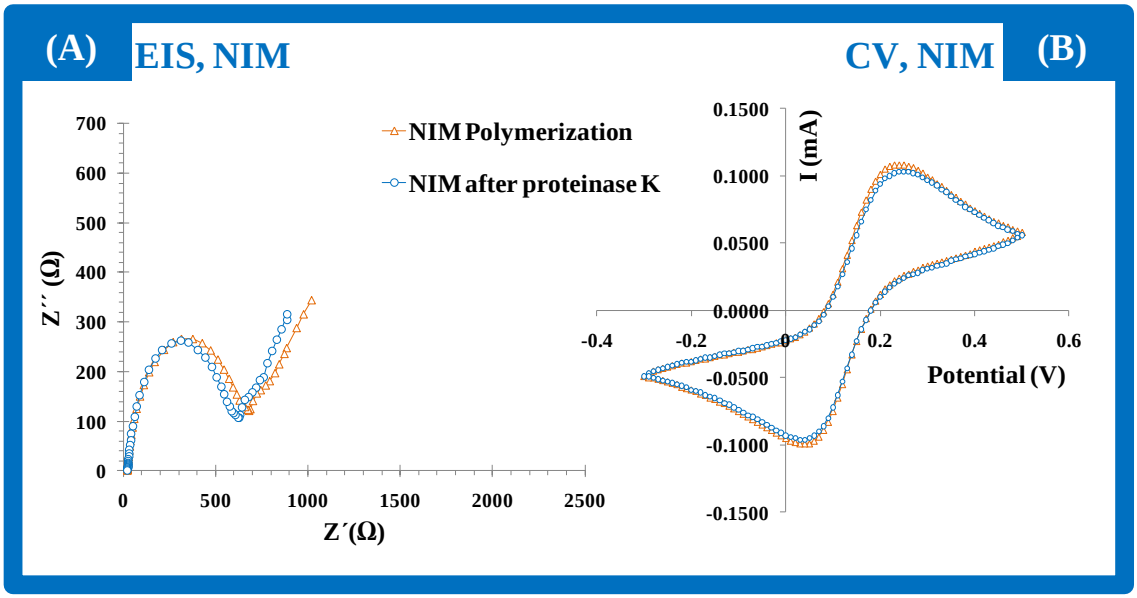

Figure 42: Electrochemical EIS spectra (A) and CV voltammograms (B) of the NIM-surfaces after polymerization and Proteinase K treatment stages (evaluated in 5.0 mmol/L $[Fe(CN)_6]^{3-}$ and 5.0 mmol/L $[Fe(CN)_6]^{4-}$, in MES buffer pH 4.5).

CV assays shown in Figure (Figure 41B and Figure 42B) supported the previous studies of EIS. The modifications of the bare gold up to the polymerization stage increased the peak-to-peak potential separation and decreased the peak height of the redox probe in the voltammograms, thus accounting for the increased R_{ct}. This behaviour was reversed after the template removal, accounting for the absence of the protein and the polymer porosity.

7.3.3 AFM analysis

Although electrical characterization was done on SPEs, surface characterization studies were conducted only on planar gold surfaces employed in regular surface SPR measurements. SPAM and NIM materials were assembled on the SPR planar gold chips following the same procedure as that described for the SPEs.

Clear differences were observed between the images of NIM and SPAM structures (Figure 43). Only SPAM material showed cavities (these were never present in the NIM material), attributed to the plastic antibodies. About 90% of these cavities ranged between 3.5 and 10 nm. Considering that a single Myo molecule is 4.5 nm × 3.5 nm × 2.5 nm (Lin et al. 2007a) , this indicated that under the imprinting conditions Myo existed both in monomeric and dimeric states. In addition, the pores of the acrylamide gels range between 21 to 200 nm (Stellwagen 1998) which indicated that the AFM images obtained from tapping modes were in fact cavities in the template. A good correlation with the electrochemistry data further confirms this observation.

7.3.4 Analytical performance of the sensor

The analytical performance of Myo sensory materials was evaluated by recording calibration curves in EIS and SWV measurements (Figure 35) Among other voltammetric methods, SWV offers the advantages of high sensitivity to surface-confined electrode reactions, along with suitable detection capabilities and rapidity. EIS readings may be straightforward for low cost and on-site analysis.

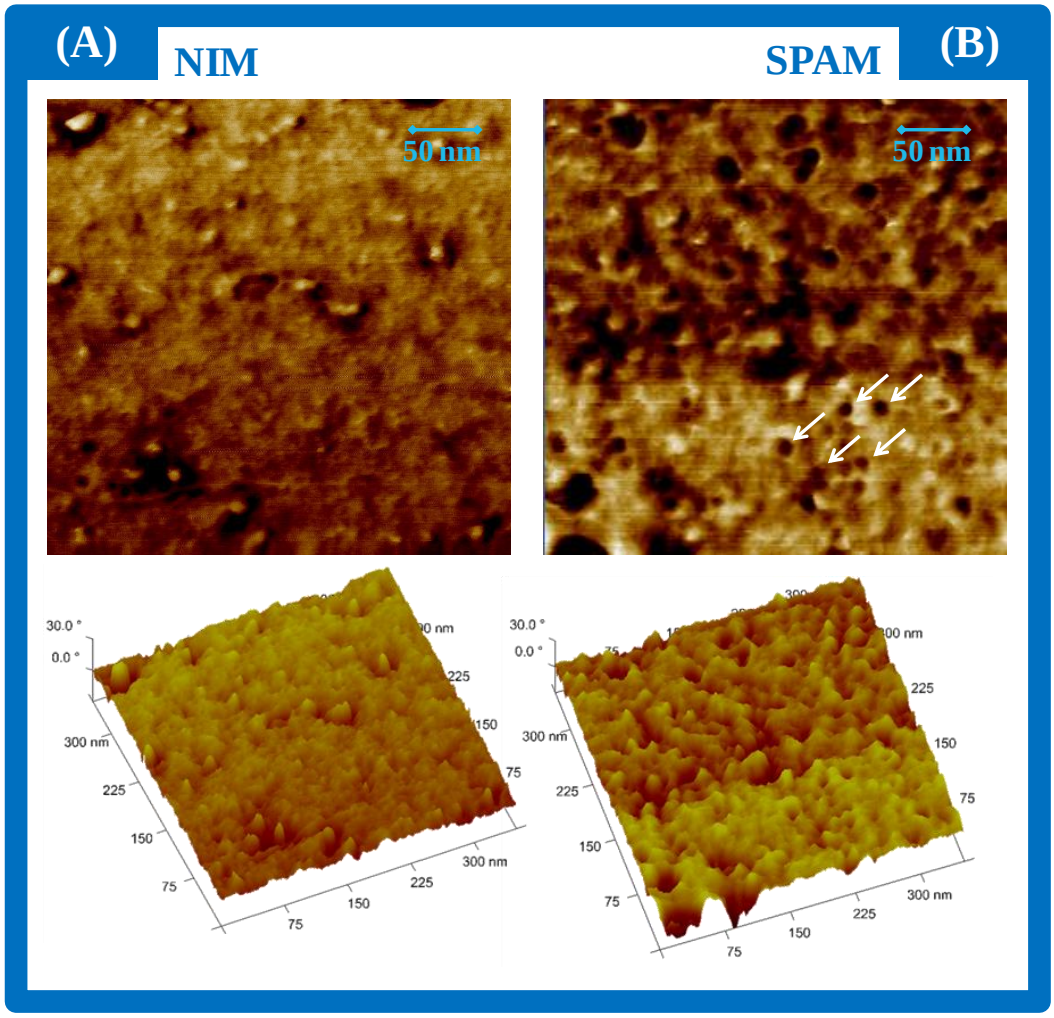

Figure 43: AFM tapping mode images showing 300 nm × 300 nm scan after proteinase K treatment of (A) NIM and (B) SPAM surfaces. AFM images processed using Nanorule program to show the 3-dimensional topography.

.

EIS calibration curves plotted the R_{ct} of SPAM or NIM Au-SPE sensors against logarithm Myo concentration (Figure 44). Increasing concentrations of Myo increased the diameter of the semicircles in the Nyquist plots, indicating that Myo bound to the sensory layer increased the charge-transfer resistance of the probe. This was as expected from the previous EIS studies, accounting for an increased R_{ct} when Myo was bound to the sensing material and a decreased R_{ct} when Myo

was removed from it. The typical calibration plot of SPAM sensors show linear behaviour down to 3.5 µg/mL, with average slope of 461.4 Ω/decade [Myo, µg/mL] and squared correlation coefficients > 0.999. The LOD was 1.5 µg/mL, corresponding to the concentration of the cross-section of the two linear parts of the response. The average and the relative standard deviation of the blank were 300 and 14 Ω, respectively. The standard deviation of repeated assays was < 5%.

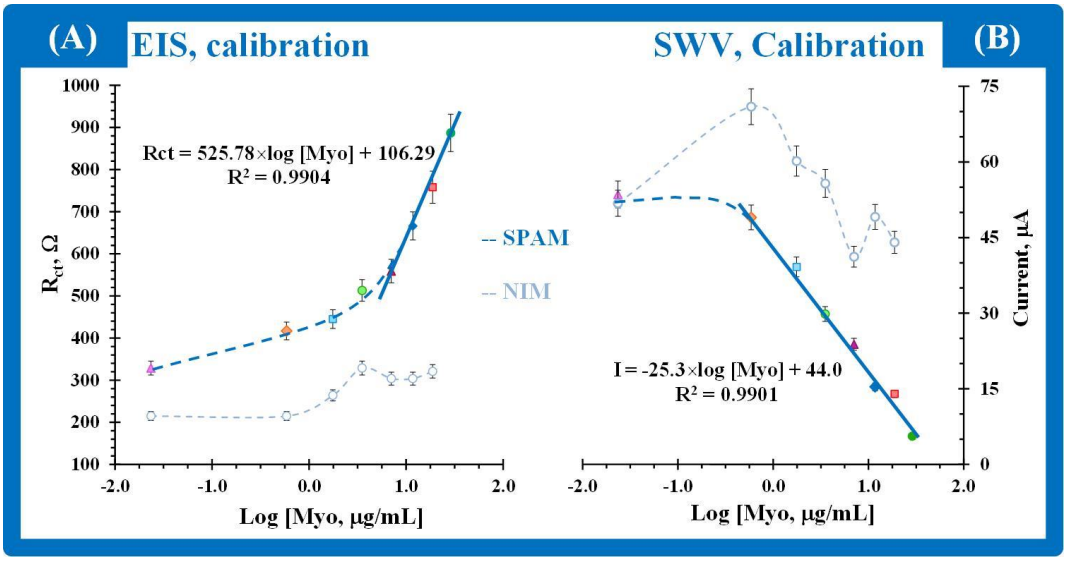

Figure 44: Calibration curves of SPAM and NIM based Au-SPE biosensors obtained by EIS (A) and SWV (B) measurements in 5.0 mmol/L $[Fe(CN)_6]^{3-}$ and 5.0 mmol/L $[Fe(CN)_6]^{4-}$, in MES buffer pH 4.5, with different concentrations of Myo (in ×g/mL). Coefficient of variation of presented data < 5%.

In SWV assays, Myo binding was revealed by a decrease in the typical anodic peak current of redox probe solutions. Higher Myo concentrations yielded smaller peaks. A linear pattern against log[Myo] was observed for concentrations down to 0.58 µg/mL (Figure 44B), a value that lies within the physiological levels expected by the first hour after cardiac damage. This linear behaviour was observed up to 0.58 µg/mL. The limit of detection was calculated similarly to EIS studies, and was equal to 0.28 µg/mL. The average and the standard deviation of the blank were 74.0 and 3.7 µA, respectively. The relative standard deviation of repeated assays was < 5%.

The NIM sensor displayed an inconsistent response over the range of the calibration curves, both in EIS and SWV assays (Figure 44A an B).These results indicated that the non-specific interaction (the only kind existing in NIM surfaces) between template and polymer did not control the electrochemical response. Only monomers polymerized in the presence of a template should have imprinted sites, and these sites are clearly controlling the interaction between Myo and SPAM.

7.3.5 Binding Isotherm

The calibration of the SPAM biosensor in SWV follows a hyperbolic response (Figure 45A) approaching the typical behaviour of antibody/antigen interactions (Yildirim et al. 2012). The parametric data over the Langmuir equation (I_{max} and K_D in Equation 30) assess the biosensor performance in terms of template rebinding. I_{max} reflects the differences in the amount of Myo bound to the sensor surface and K_D shows the concentration of template providing half of maximum response (I_{max}), thus measuring how well Myo complexes with the plastic antibody material and the affinity with which it occurs. If the K_D is low it indicates a large binding affinity, as the reaction will approach the maximum response more rapidly. On the contrary, a high K_D indicates that the plastic antibody does not bind as efficiently with the Myo, and only higher concentrations of Myo are able to saturate the response of the plastic antibody surface. In general, changes in K_D are sensitive to variations in protein access/binding (Rothwell et al. 2010; Sasso et al. 1990) and may be interpreted here in terms of barriers to antigen/artificial antibody access.

Fitting the data to a hyperbolic function (Langmuir), where (I*-I) represents the binding adsorption for each concentration value of Myo and I* the maximum current observed in all range of concentration studied, gave values of K_D = 3±0.5 µM and I_{max} = 44±2 nA with a chi squared of 26.5 for the SPAM (Figure 6A). The NIM binding data did not fit to the Langmuir model, since a chi squared of 556 was obtained. Overall, these results showed that the SPAM sensor displayed much higher affinity to Myo than NIM, showing a controlled/predictable response against Myo concentration. Since the differences between NIM and SPAM

are only the absence/presence of Myo tailored sites on the receptor structure, respectively, the above observations pointed out that the non-specific interaction has been majorly reduced by introducing the charged monomers upon the binding sites.

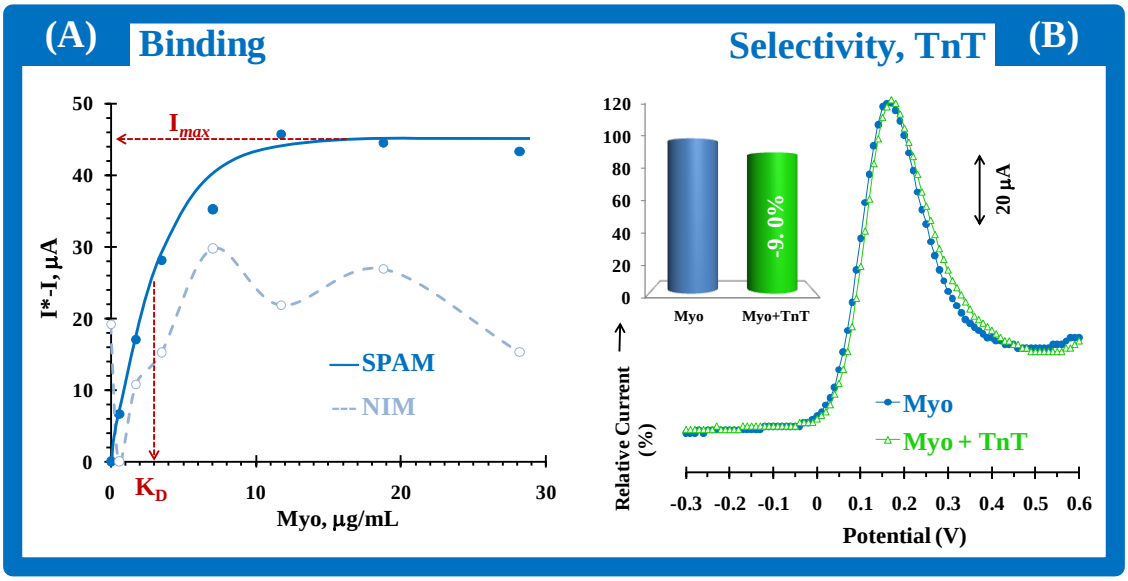

Figure 45: Graphical representation of the Langmuir isotherm plot (A) for SPAM (with I_{max} and K_D values) and NIM materials, and the selectivity data for TnT(B).

7.3.6 Selectivity study

The selectivity of the sensor is of main importance for a successful analytical application and was evaluated by SVW measurements. The interfering species tested were selected among those that may be found in biological fluids, such as TnT, BSA (serum) and Urea (urine).

A competitive assay was used to test their interference in a 2.0×10^{-7} mol/L Myo solution. For this purpose, the response of the SPAM sensors was checked for solutions having only Myo or Myo + interfering species, where a competition between Myo and interfering species for the same binding sites was established. A 5 minute contact between the SPAM surface and each solution was allowed.

Each assay was conducted in a different Au-SPE/SPAM sensor, in order not to avoid a cross contamination from previously adsorbed Myo or interfering compound.

The average % deviation produced by each interfering species in pure Myo solutions were 6.0 % for TnT, 10.9 % for BSA and 8.7 % for urea, respectively. A typical voltammogram with the corresponding average % deviation for TnT may be seen in Figure 46 and the others are shown as supplementary material. The relative standard deviation of repeated assays was < 5%.

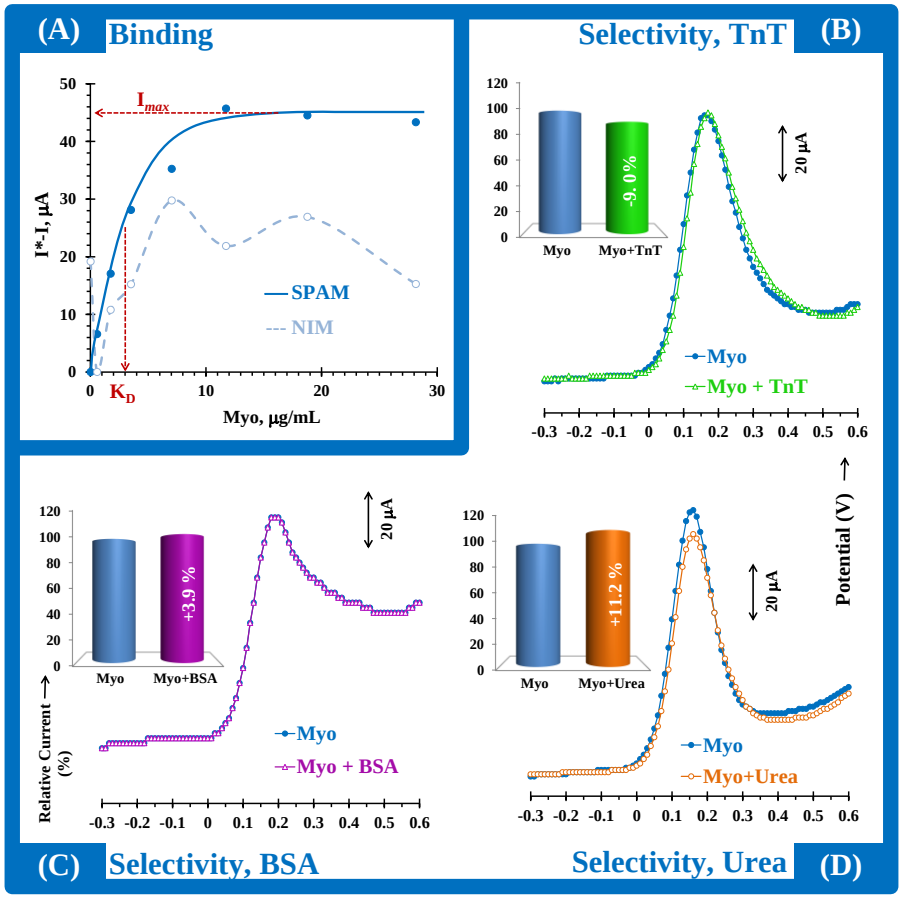

Figure 46: Selectivity study wit for TnT, BSA and urea.

7.3.7 Myo Assay

The standard addition method was applied to determine Myo in spiked diluted serum samples having Myo concentrations ranging from 0.59 to 18.77 µg/mL Myo. This was performed in triplicate by SWV measurements. A good agreement was found between added and found amounts of Myo, with recoveries lying within 94 and 97%. The relative standard deviation obtained for reproduced assays was < 5.8% and for repeated assays < 5%, thus confirming the good precision of this new analytical approach. These results show great expectations around this SPAM network, also acting as a promising tool for direct applications in POC context.

7.4. Conclusions

Comparing to previous Myo plastic antibodies described in the literature (Wang et al. 2008), this is the first time an imprinted material is able to recognize the target protein mostly by its specific binding sites. As far as we are aware this is the first time that a non NIP showed an absence of dose response behaviour with a target molecule protein, consistent with the non-specific binding to the polymer being minimal. Furthermore, we believe that it is the first time that the imprinted sites are seen in the AFM images, showing cavities of a comparable size to the imprinted protein or only small aggregates.

Overall, it seems that the SPAM approach proposed here concerning the using of charged-monomers offers a promising alternative to the design of new surface confined plastic antibodies for proteins. Although the LOD provides proof of concept for using the device in POC context, further developments will be necessary for practical application in a clinical setting.

7.5 References

http://www.alere.com/EN_US/products/alere-triage-cardiac-panel-poc-test/index.html, assessed 29th August 2012;.

Andersson, L.I., 2000. Molecular imprinting for drug bioanalysis - A review on the application of imprinted polymers to solid-phase extraction and binding assay. *Journal of Chromatography B* 739(1), 163-173.

Bossi, A., Bonini, F., Turner, A.P.F., Piletsky, S.A., 2007. Molecularly imprinted polymers for the recognition of proteins: The state of the art. *Biosensors & Bioelectronics* 22(6), 1131-1137.

Chen, L., Xu, S., Li, J., 2011. Recent advances in molecular imprinting technology: current status, challenges and highlighted applications. *Chemical Society Reviews* 40(5), 2922-2942.

Jiang, K.Y., Schadler, L.S., Siegel, R.W., Zhang, X.J., Zhang, H.F., Terrones, M., 2004. Protein immobilization on carbon nanotubes via a two-step process of diimide-activated amidation. *Journal of Materials Chemistry* 14(1), 37-39.

Kriz, D., Ramstrom, O., Mosbach, K., 1997. Molecular imprinting - New possibilities for sensor technology. *Analytical Chemistry* 69(11), A345-A349.

Lin, H.-Y., Rick, J., Chou, T.-C., 2007. Optimizing the formulation of a myoglobin molecularly imprinted thin-film polymer-formed using a micro-contact imprinting method. *Biosensors & Bioelectronics* 22(12), 3293-3301.

Panagopoulou, M.A., Stergiou, D.V., Roussis, I.G., Prodromidis, M.I., 2010. Impedimetric Biosensor for the Assessment of the Clotting Activity of Rennet. *Analytical Chemistry* 82(20), 8629-8636.

Piletsky, S.A., Piletska, E.V., Chen, B.N., Karim, K., Weston, D., Barrett, G., Lowe, P., Turner, A.P.F., 2000. Chemical grafting of molecularly imprinted homopolymers to the surface of microplates. Application of artificial adrenergic receptor in enzyme-linked assay for beta-agonists determination. *Analytical Chemistry* 72(18), 4381-4385.

Rothwell, S.A., Killoran, S.J., O'Neill, R.D., 2010. Enzyme Immobilization Strategies and Electropolymerization Conditions to Control Sensitivity and Selectivity Parameters of a Polymer-Enzyme Composite Glucose Biosensor. *Sensors* 10(7), 6439-6462.

Sasso, S.V., Pierce, R.J., Walla, R., Yacynych, A.M., 1990. Electropolymerized 1,2-diaminobenzene as a means to prevent interferences and fouling and to stabilize immobilized enzyme in electrochemical biosensors. *Analytical Chemistry* 62(11), 1111-1117.

Shi, H.Q., Tsai, W.B., Garrison, M.D., Ferrari, S., Ratner, B.D., 1999. Template-imprinted nanostructured surfaces for protein recognition. *Nature* 398(6728), 593-597.

Shiomi, T., Matsui, M., Mizukami, F., Sakaguchi, K., 2005. A method for the molecular imprinting of hemoglobin on silica surfaces using silanes. *Biomaterials* 26(27), 5564-5571.

Stellwagen, N.C., 1998. Apparent pore size of polyacrylamide gels: Comparison of gels cast and run in Tris-acetate-EDTA and Tris-borate-EDTA buffers. *Electrophoresis* 19(10), 1542-1547.

Wang, Y., Zhou, Y., Sokolov, J., Rigas, B., Levon, K., Rafailovich, M., 2008. A potentiometric protein sensor built with surface molecular imprinting method. *Biosensors & Bioelectronics* 24(1), 162-166.

Whitcombe, M.J., Chianella, I., Larcombe, L., Piletsky, S.A., Noble, J., Porter, R., Horgan, A., 2011. The rational development of molecularly imprinted polymer-based sensors for protein detection. *Chemical Society Reviews* 40(3), 1547-1571.

Yildirim, E., Turan, E., Caykara, T., 2012. Construction of myoglobin imprinted polymer films by grafting from silicon surface. *Journal of Materials Chemistry* 22(2), 636-642.

Zayats, M., Kanwar, M., Ostermeier, M., Searson, P.C., 2011. Molecular Imprinting of Maltose Binding Protein: Tuning Protein Recognition at the Molecular Level. *Macromolecules* 44(10), 3966-3972.

Zdyrko, B., Hoy, O., Luzinov, I., 2009. Toward protein imprinting with polymer brushes. *Biointerphases* 4(2), FA17-FA21 .

8

A Protein-responsive polymeric material for cardiac biomarker detection in point-of-care

8.1 Introduction

Electrogenerated polymers have concerned considerable attention in the development of biosensors and biochips, and are move forward rapidly (Cosnier 2003).

Electropolymerization is typically conducted by leaving the template within the monomer in solution and by applying electrical conditions to enable the formation of a thin film above the electrode surface. Electropolymerization is thus a very simple procedure, enabling the use of different conductive materials of different shape/size, and a close control of the polymer thickness by adjusting the electrical conditions under which the polymer is being formed (Lange et al. 2008; Malitesta et al. 1999). However, many of the protein structures, with little nm in size, are thus irreversibly entrapped inside the polymeric network and only few are at the outer surface of the newly formed film. The only specific work in this context is that of Qureshi et al., 2013, most

recently published (Karimian N 2013). The authors report a successful electropolymerised imprinted film for troponin, by mixing the cardiac biomarker in the solution with o-phenylenediamine, acting as monomeric parts of the film.

An alternative approach to this procedure, never tested before, as far as we know, would be adsorbing first the proteins to the electrode surface (that may even lead to multiple layers) and to control the thickness of the polymer under formation, to ensure that most of these proteins are not irreversibly covered and keep the ability of being removed. A high density of imprinting positions is thus expected. Thus, this new concept of electropolymerization for imprinting a protein cardiac biomarker is here described, using Myo as target protein. Myo is a heme protein responsible for the transport of oxygen within cardiac and skeletal muscle cells (Balk et al. 2001; Castaldo et al. 1994) that is early released to the blood in the course of cardiac muscle damage. The measure of Myo levels within the first few hours after symptom onset in acute events is crucial to dissipate cardiac injury diagnosis, with concentrations ranging from 95 to 472 µg/L (Dyan 2000) (Castaldo et al. 1994; Grand et al. 1994; Lee et al. 1994).

Overall, Myo imprinted films (MI) were prepared by electropolymerizing o-aminophenol above a protein layer previously absorbed to gold. The protein structures located at the outer surface of the film were removed by protease action. A non-imprinted (NI) film was also synthesized to act as control. This was done by removing the template from the overall process. The resulting biosensor was evaluated by CV, EIS and SWV techniques and further applied to the analysis of biological sample.

8.2 Experimental section

8.2.1 Apparatus

The electrochemical measurements were conducted with a potentiostat/galvanostat from Metrohm Autolab and a PGSTAT302N, equipped with a *Frequency Response Analysis* (FRA), module and controlled by Nova software. The Au-SPEs were purchased to DropSens, having working and CE made of gold and pseudo- reference electrode and electrical contacts made of silver. The diameter of the WE was 4 mm and the Au-SPEs. The SPEs were connected to a switch box, also from DropSens (DRP-DSC), allowing their interface with the potentiostat/galvanostat equipment.

FTIR measurements were performed using a Thermo Scientific Smart iTR Nicolet iS10, coupled to a SAGA smart accessory, also from Thermo Scientific. Raman measurements were performed using a Thermo Scientific DXR Raman microscope system with a 100 mW 532 nm excitation laser, and spectra were made for 5 mW power and 50 µm pinhole aperture. AFM analysis was made in a contact mode (Nanoink NScriptor based AFM with A type tips).

8.2.2 Reagents

All chemicals were of analytical grade and water was de-ionized or ultrapure Milli-Q laboratory grade. ($K_3[Fe(CN)_6]$) and ($K_4[Fe(CN)_6]$) trihydrate, and sodium acetate anhydrous, were obtained from Riedel-deHaen; BSA, Urea, Myo, TnT, CK-MB, Proteinase K, PBS and NaCl from Fluka; AP 99%, MES from Alfa Aesar; and KCl from Merck.

8.2.3 Solutions

Stock solutions of 5.0×10^{-6} mol/L Myo were prepared in MES buffer (1.0×10^{-2} mol/L, pH 5.0). Less concentrated standards were obtained by accurate dilution of the previous solution, in the same buffer. Electrochemical

assays were performed with 5.0×10^{-3} mol/L $K_3[Fe(CN)_6]$ and 5.0×10^{-3} mol/L $K_4[Fe(CN)_6]$, prepared in MES 1.0×10^{-3} mol/L, pH 5.0. The selectivity study used 4.0 µg/mL Myo solutions prepared in buffer and solutions of possible interfering species, TnT (0.22 µg/mL), and CK-MB (0.5 µg/mL), prepared in the same buffer.

8.2.4 Electrosynthesis of Molecular imprinting /Non-imprinting film

Prior to electropolymerization, the Au-SPE electrodes were cleaned with ethanol following electrochemical cleaning with H_2SO_4 0.5 mol/L by cycling the potential between -0.2 and 1.2 V, along 15 cycles, at a scan-rate of 50 mV/s.

MI films were produced by covering the working area of the Au-SPE with Myo solution, 5.0×10^{-5}mol/L, prepared in acetate buffer pH 5.0, and let it stand there for 15 minutes. This solution was then replaced by a drop of 1.0×10^{-2} mol/L AP, in acetate buffer pH 5.0, covering the three-electrodes on the SPE. Polymerization was conducted by CV, between -0.2 and 0.8 V, at a scan rate 50 mV/s and for 15 cycles. The resulting film was thoroughly washed with deionized water and incubated overnight in Proteinase K (500 µg/mL, prepared in PBS buffer, pH 7.4), in the dark. The film was finally washed for several times in PBS buffer to remove protein fragments and proteinase K, and then rinsed with water MiliQ (Zayats et al. 2011). NI materials were produced in parallel in the same way, but without the protein incubation step. These were used blank of the imprinting effect.

8.2.5 Qualitative characterization of the films

All qualitative analysis was conducted directly over the SPE without any previous treatment. Films of MI with Myo, MI with Myo removed, and NI were analysed by AFM working in contact mode.

FTIR was also conducted directly over the thin-film layer deposited after electropolymerization. A SAGA accessory was employed in order to ensure that only tangential infrared beams would be collected, thus allowing superficial analysis. The number of scans was set to 256, the resolution to 8, anodization of Happ-Genzel, Mertz Phase correction, and background gain of 8, from 400 to 4000 cm^{-1} wavenumber.

Raman microscopy was carried out in a Thermo Scientific DXR Raman microscope, equipped with laser with 532 nm. The average signal-to-noise ratio (peak height/RMS noise) was measured using standard polystyrene, full-range grating, 15 seconds measurement time, 5 mW laser power at sample, and 25 µm slit aperture.

8.2.7 Binding Isotherm studies

The adsorptions dynamics of MI before and after electrochemical cleaning with PBS buffer and in NI assay was measured in SWV assays. This assay was conducted by adding Myo standards ranging from 0.053 to 53.33 µg/mL, prepared in buffer, to the above electrodes. A period of 5 minutes incubation was allowed before adding the redox probe for subsequent SWV readings.

Langmuir isotherm model (Equation 28) was applied to the experimental data. K_D and maximum binding capacity (B_{max}) were calculated after this. K_D was the protein concentration required to provide half of the maximum response produced by the device.

8.2.8 Electrochemical assays

All CV, SWV and EIS measurements were conducted in triplicate and used as redox probe 5.0 mmol/L $[Fe(CN)_6]^{3-}$ and 5.0 mmol/L $[Fe(CN)_6]^{4-}$, prepared in MES buffer of pH 5.0. In CV assays the potentials were scanned from -0.2 to +0.8 V, at 50 mV/s; in SWV potentials changed from -0.5 to +0.6 V, at a frequency of 50Hz and a step height of 150 mV; and in EIS a standard potential of +0.12 V was set, using a sinusoidal potential perturbation of 0.01 V amplitude and a number of frequencies equal to 50, logarithmically distributed over a frequency range of 0.1-100 kHz.

Calibration curves were performed by SWV and EIS measurements in Myo range between 0.05 and 53.3 µg/mL, in MES buffer pH5.

Selectivity studies were conducted by competitive assay between Myo, with a 4.0 ug/mL concentration, and other interfering species. The interfering species selected for this purpose were other cardiac biomarkers that may co-exist with Myo in biological fluids: TnT (0.22 µg/mL) and CKMB (0.5 µg/mL). All these were prepared in MES buffer pH 5.0.

Myo assay in sample was performed by SWV measurements. Myo was prepared in synthetic serum diluted 50 times in a range between 0.053 and 53.0 µg/mL.

8.3 Results and discussion

8.3.1 Assembly of the responsive polymer

Molecular imprinting was prepared by electropolymerization of AP monomer using Myo as a template molecule by CV (Figure 48). The overall process consisted in 3 different stages: (1) Myo adsorption on the Au surface of the WE; (2) imprinting stage by PAP thin film formation on the Au/Myo surface; (3) and Myo removal from the PAP film by protease activity (Figure 47). All these stages promoted changes in the electron transfer properties of receptor surface, and were therefore followed by EIS and CV assays.

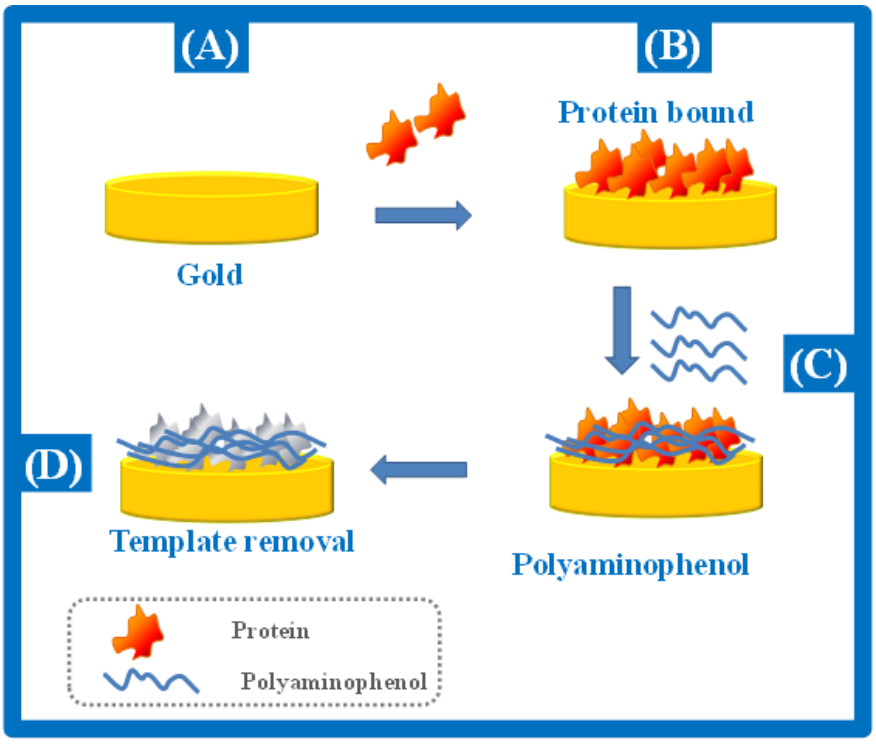

Figure 47: Schematic representation of the synthetic process of MI. A: Au-SPE; B: Myo adsorption on Au-SPE surface; C: Electropolymerization of AP; D: and binding site formation by template removal with proteinase K.

8.3.1.1 Protein adsorption

As to any other protein, the process of Myo binding to gold is a very complex and may be driven by different forces between the protein and the surface, including van-der-Waals, hydrophobic and electrostatic interactions. Overall, the adsorption of Myo to the solid support is expected to involve transport from the solution to the interface, binding to the surface and subsequent relaxation via conformational adaptations (Voros 2004). Adsorption occurs due to the energetically favourable expulsion of solute from solution into the interphase between bulk solid and solution phase, along with the reduction of interfacial energetics resulting from the replacing of water molecules by adsorbed solute at the solid surface (Vogler 1998). In addition, this interphase separating bulk

solution and surface phases may range from few to ~100 nm and proteins may apparently be adsorbed in multilayers at this interphase.

In the present study, Myo was adsorbed directly to the Au-SPE layer, just as indicated in Figure 47A. This was done by placing a drop of Myo, prepared in acetate buffer pH 5.0, in the WE area. The incubation period was set to 15 minutes, at 4°C. The adsorption of Myo to gold increases R_{ct} signals in the EIS spectra. The R_{ct} values increased up to a concentration of 5.0 $\times 10^{-5}$ mol/L and after that becames less. Thus, this Myo concentration was selected using a 15 minutes adsorption period, before the imprinting stage.

8.3.1.2 Imprinting Stage

The imprinting stage was conducted by electropolymerization on the Au-SPE/Myo in an AP solution of pH 5.0, by consecutive potential cycles in CV mode. The MI device is here identified as Au-SPE/Myo/PAP.

Many electrosynthesized polymers have been produced so far in MI-based materials (Alexander et al. 2006), but PAP films exhibit several advantages, including an easy control of the polymer thickness within 10-50 nm due to a self-limiting growth and an easy regeneration process after use (Sayyah et al. 2006 Tucceri R. 2012),. In addition, PAP is a permselective polymer with an interfering-free effect from some electroactive species present in biological fluids, such ascorbic and uric acid (Tucceri R. 2012).

In the course of electropolymerization, the current decreased, and when 15 cycles were reached, the current density of the oxidation peak was much smaller (Figure 48 A, left). No reduction peak was observed during electropolymerization, which also confirmed the growth of an insulator polymer layer on the Au-SPE electrode. Overall, these events confirmed the formation of the PAP film above Myo, because it displayed non-conductive proprieties (Levin et al. 2005; Mahjani et al. 2010; Sayyah et al. 2006). The obtained film was also evident to human eye, as the gold of the SPE became dark-brown. Its thickness is ex-

pected below 50 nm, due to the self-limiting effect, caused by the low polymer film conductivity (Levin et al. 2005).

In general, the EIS data obtained with Au-SPE/Myo/PAP was consistent with the formation of an insulating layer. The typically low R_{ct} from gold increased in a most evident way, reaching values of imaginary Z higher in Y axis higher than 60 kΩ (Figure 48 B, left). The typical Randles circuit circuit consisted of one resistor(solution resistance, R_s) in series with one parallel circuit comprising a resistor R_{ct} and a capacitor CPE (Daniels and Pourmand 2007; Ding et al. 2005a, b) was designated as the 1R//C model. A CPE was used instead of a pure capacitor to describe the heterogeneity on the electrode surface (Baur et al. 2010; Ding et al. 2005b).

In parallel, a negative control was also produced to create a NI film (Au-SPE/PAP). This was done by carrying out the electropolymerization stage over a clean Au-SPE support that did not contact with Myo (Figure 48, right). The CV record of such electropolymerization was quite similar to that observed in the production of the Au-SPE/Myo/PAP film, producing a continuous current decrease in subsequent cycles. Compared to the MI film, an additional oxidative peak was evident at about 0.5 V. This was probably a result of the absence of the Myo layer that acted as a barrier to electrical transfer in the MI film.

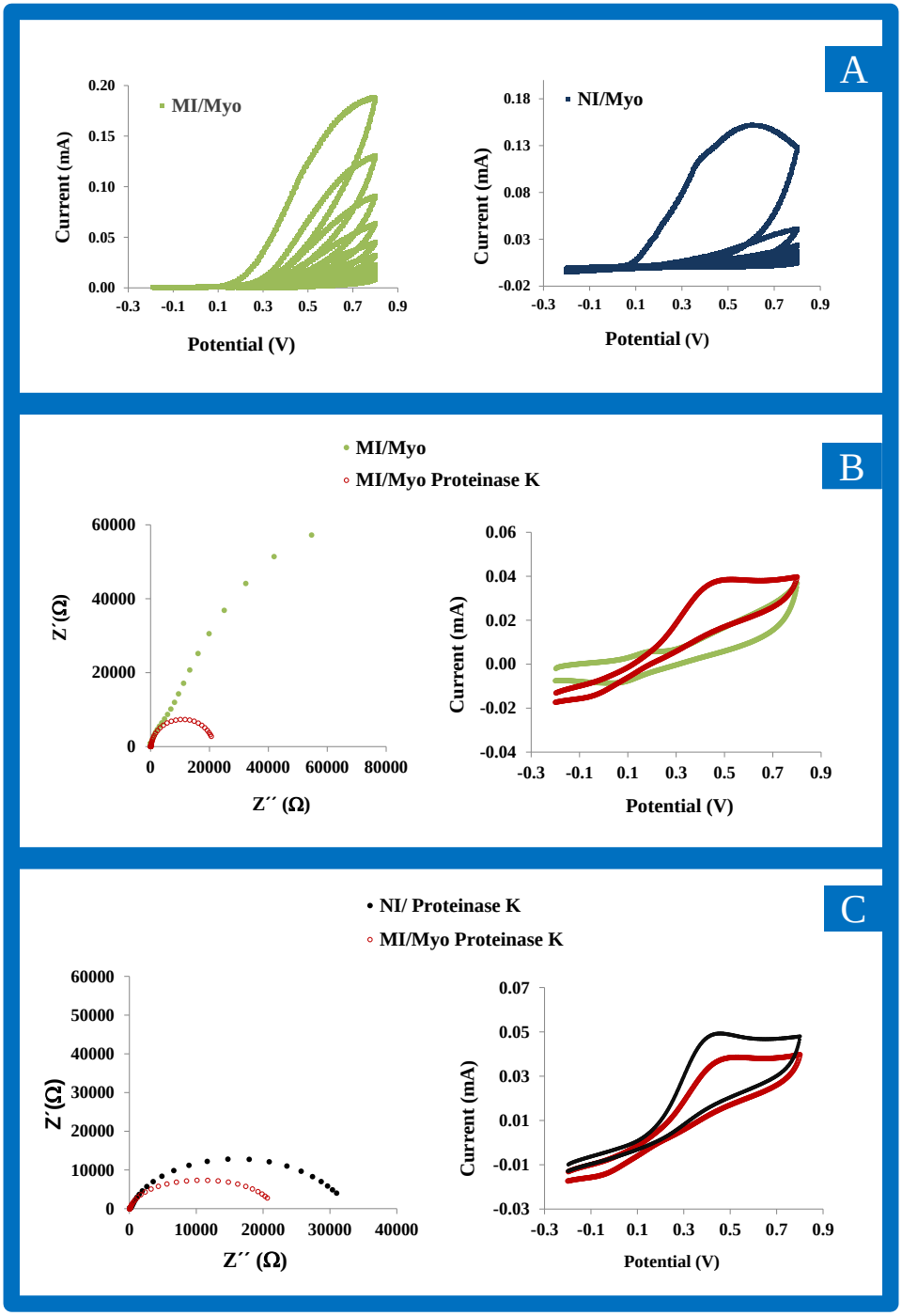

Figure 48: Electrochemical control of the subsequent modification steps of the Au-SPE in 5.0 mmol/L $[Fe(CN)_6]^{3-}$ and 5.0 mmol/L $[Fe(CN)_6]^{4-}$, in MES buffer pH 5, carried out by EIS (A, Nyquist plots), CV (B, cyclic voltammograms) and EIS and CV (C, after Proteinase K) assays for MI/NI.

8.3.1.3 Protein removal

Many strategies for removing protein form imprinted polymers have been described to date. These include mostly chemical treatments that look for protein denaturation and amide bond cleavage (Bonini et al. 2007; Bossi et al. 2001; Li et al. 2006; Lin et al. 2007; Turner et al. 2006). Most recently, we have proposed the use of enzymes displaying proteolytic activity capable of cleaving peptide bonds (Moreira et al. 2013). Enzymes are effective and act under mild conditions, thus preventing significant alterations at the polymeric network.

The Au-SPE/Myo/PAP film with Myo was therefore incubated overnight with Proteinase K 500 μg/mL. Proteinase K is a highly active and stable protease with low specificity regarding the peptide bond environment and high efficiency in cleaving the amide bond. The resulting peptide fragments from Myo, along with the free enzyme, were after removed by washing thoroughly the surface. This meant to ensure that the imprinted sites were free for Myo rebinding.

In general, part of the electron transfer ability of the MI film was recovered by protein removal (Au-SPE/–/PAP) (Figure 48B) thus indicating that Myo was successfully extracted from the PAP layer. This was also confirmed form a close look at EIS behavior of Au-SPE/–/PAP and Au-SPE/PAP films after protease action (Figure 48C, left). Their little difference in R_{ct} is probably confirming the presence of the binding sites that facilitated the electron transfer due to their smaller distance to the Au layer. CV data also confirmed a close behavior between Au-SPE/PAP and Au-SPE/–/PAP films after protease activity (Figure 48C, right). The oxidation peak observed at 0.5V after protein removal accounted possibly the absence of the protein and the polymer porosity.

8.3.2 Qualitative analysis

The chemical profile of the Au-SPE/PAP, Au-SPE/Myo/PAP and Au-SPE/–/PAP films was assessed by Raman analysis with Confocal microscopy (Figure 49), FTIR (Figure 50) and AFM (Figure 51).

8.3.2.1 Raman spectrometry

The PAP electropolymerization is expected to yield two main products: 3-aminophenoxazone (APZ) and 2,2′-dihydroxyazobenzene (DHAB). APZ is cyclic dimer, by the simultaneous N—C and O—C coupling of AP monomer units, obtained especially under acidic pH conditions. APZ can be oxidized further at the electrode forming the ladder structured polymer (Palys et al. 2010). DHAB is formed mostly in neutral and basic solutions. Considering this, the evidence of peaks at about 1400 and 1600 cm^{-1} Raman shift observed are assigned to quinoid groups of APZ and to the aromatic ring/–C=N– in quinonimine units, respectively (Li et al. 2009; Palys et al. 2010; Shah and Holze 2006), from the PAP films (Figure 49).

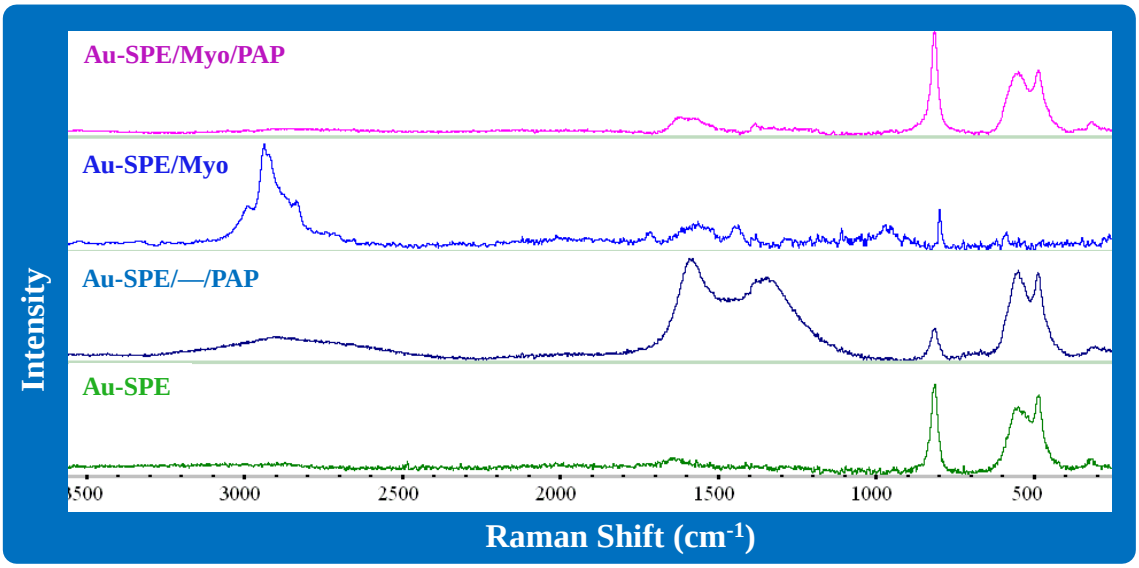

Figure 49: RAMAN spectra for: Au-SPE/Myo/PAP; Au-SPE/ Myo; Au-S PE/□/PAP and Au-SPE.

The presence of Myo on gold is confirmed by the large band ~3000 cm^{-1}. This is clearly an outcome of the presence of the protein, because the gold Raman spectrum has no absorption in this region. Similarly, the presence of Myo

in Au-SPE/Myo/PAP was confirmed by absorption in the same region. The absorption spectra of Au-SPE/–/PAP also indicated the presence of some Myo entrapped in the polymer.

8.3.2.2 Fourier Transformed Infrared Spectrometry

As in Raman assays, the FTIR analysis was conducted directly over the SPEs. When this analysis was conducted with an ATR accessory, the transmittance data was always showing the typical accounted Au layer in all kinds of SPE. So, a SAGA accessory as tried out because it enabled that the optical beam focused the electrode tangentially, thus allowing identifying small changes taking place at the outer surface of this active layer. The major drawback of such procedure was the decrease of the signal intensity, but this was compensated by an increased number of readings.

The FTIR data obtained with Au-SPE/PAP, Au-SPE/Myo/PAP, and Au-SPE/—/PAP electrodes is shown in (Figure 50). The common peaks at ~1600 cm^{-1} wavenumber were assigned to the carbonyl group and/or to the characteristic =C–C=O stretching in 3APZ, resulting from the PAP film. The common peaks located at ~850 cm^{-1} were assigned to –C–H bending vibration of aromatic ortho-substituted aromatic rings, also resulting from PAP. The absence of hydroxyl group absorption at 3500 cm^{-1} could be attributed to a low proportion of a linear chain polymer structure.

Overall, the differences within the three spectra are confined to two regions that seem to account the presence or removal of Myo (Figure 50). Comparing Au-SPE/PAP with Au-SPE/Myo/PAP, the presence of Myo in the later leads to an increased absorption at 1020 cm^{-1} and to a decreased absorption at 520 cm^{-1}. The removal of Myo from the film Au-SPE/Myo/PAP is detected by the recovery of the peak at 520 cm^{-1} in the FTIR spectra of Au-SPE/—/PAP. The presence of Myo inside the polymer was also evidenced by the presence of a small peak at 600 cm^{-1}, which was also present in Au-SPE/Myo/PAP film.

Overall, the combined information of the FTIR spectra confirmed the presence of the PAP film over the Au-SPE, the presence of Myo at the MI film and its partial removal after protease action.

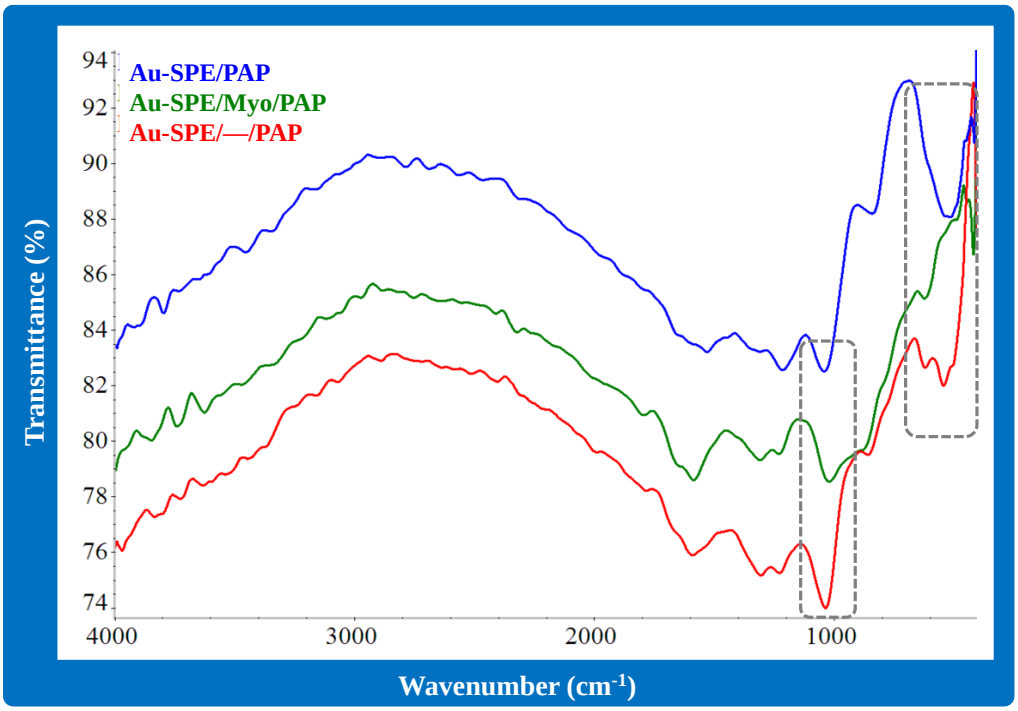

Figure 50: FTIR spectra for: Au-SPE/□/PAP; Au-SPE/Myo/PAP and Au-SPE/PAP.

8.3.2.3 Atomic Force Microscopy

The AFM analysis was also made directly over the surface of the modified Au-SPEs (Figure 51). The topographic images obtained seemed to suggest that Au-SPE/Myo/PAP films contained Myo inside the PAP film. This was observed from the higher roughness of the film, when compared to that of the Au-SPE/PAP. The Myo removal from Au-SPE/Myo/PAP also seemed to be effective because the images of the Au-SPE/—/PAP films point out a smother surface.

Although the images seem to corroborate the previous observations, and also FTIR and Raman studies, AFM tests should be confirmed with similar studies made on a flat gold-surface, since the natural roughness of the gold-layer of the SPE electrodes may turn out misleading.

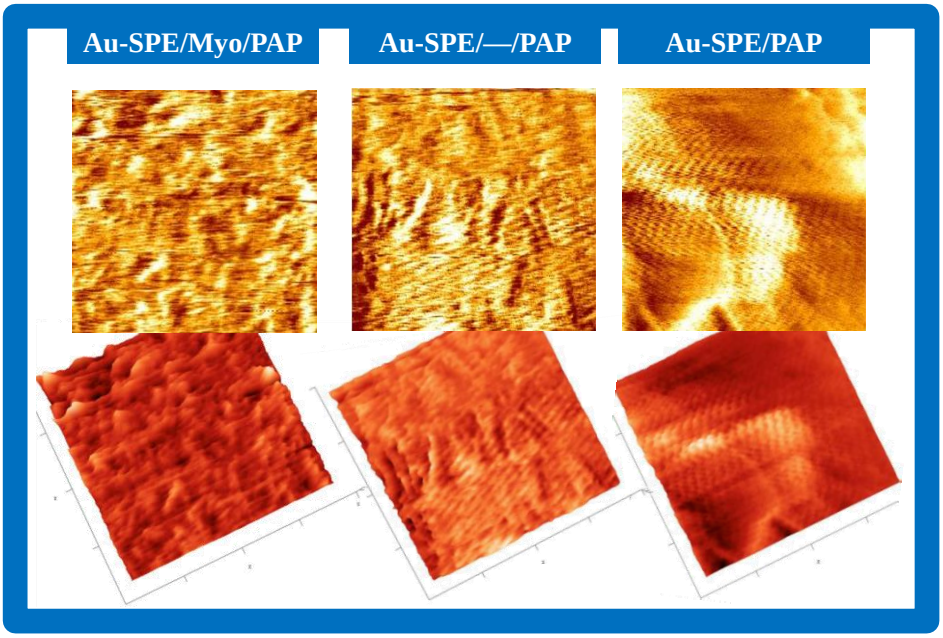

Figure 51: AFM images in contact mode from a 1 □m2 scan of Au-SPE/Myo/PAP, Au-SPE/—/PAP, and Au-SPE/PAP films, and processed using Nanoink program to show the 3-dimensional topography.

8.3.3 Analytical performance of the sensor

SWV and EIS calibration curves were recorded for Au-SPE/—/PAP and Au-SPE/PAP electrodes. The calibrations plotted current intensity (I, in SWV) or R_{ct} (in EIS) against logarithm Myo concentration, ranging from 0.05 to 53.3 μg/mL (Figure 52 A and B). In general, the presence of Myo in the redox probe concomitantly decreased the current of the typical anodic peak at ~0.4V, while increasing the resistance on Au-SPE surface.

Regarding EIS data, the R_{ct} values in the Nyquist plots, increased linearly with the increasing of the logarithm of Myo concentration after 4.0 µg/mL (Figure 52). The slope average was 11.0 kΩ/decade log[Myo, µg/mL] and the squared correlation coefficients > 0.988. The LOD was 3.53 µg/mL, corresponding to the concentration of the cross-section of the two linear parts of the response. In the NI sensor, R_{ct} increase with the increasing of the logarithm of Myo concentration after 16.0 µg/mL, but with squared correlation coefficients > 0.895. These results showed a random behaviour, showing that the imprinting recognition of Myo was governing the electrical response of the MI electrode.

In SWV assays, the Au-SPE/—/PAP sensor showed linear behaviour down to 2.22 µg/mL, with a slope of -0.0247 (± 0.003) µA/decade log[Myo, µg/mL] and squared correlation coefficients > 0.999. The LOD was equal to 0.827 µg/mL. The NI sensor, Au-SPE/PAP, displayed linear behaviour after 16 µg/mL, with the slope -0.0142 µA/decade log[Myo, µg/mL] and squared correlation coefficients > 0.995. The repeatability of the response was good, with standard deviations below than 5%.

Overall, SWV showed quicker, more sensitive and more selective responses to Myo, when compared to EIS assays. So, this electrochemical approach was selected for further studies.

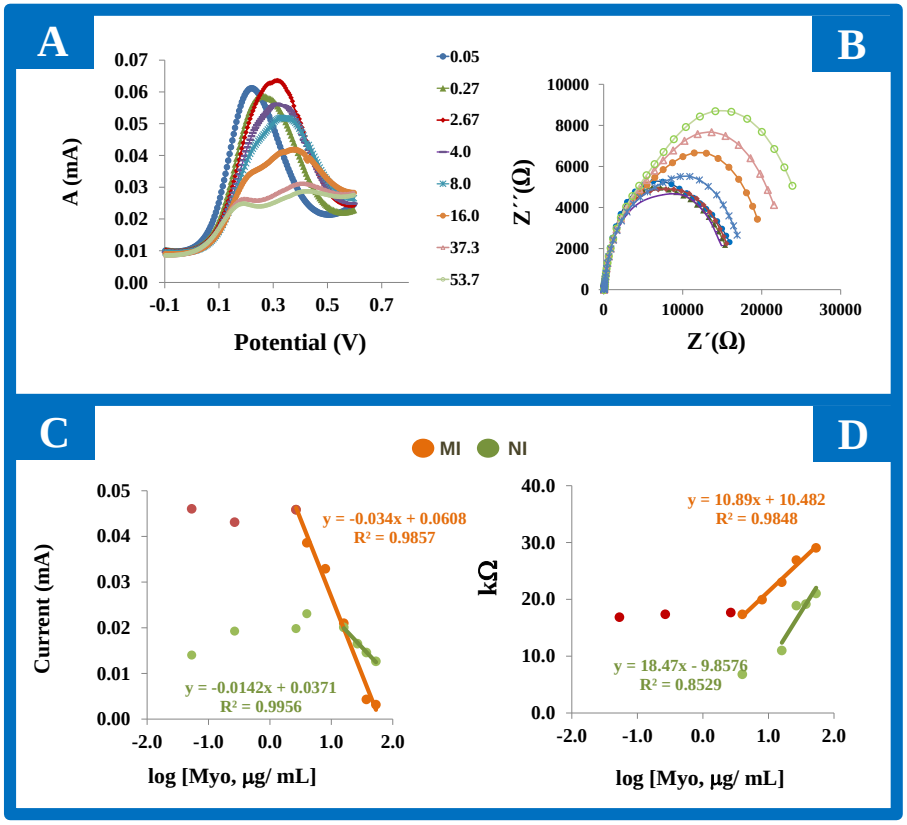

Figure 52: SWV (A) and EIS (B) measurements of MI based Au-SPE biosensor and the corresponding calibration curves (C and D) in 5.0 mmol/L $[Fe(CN)_6]^{3-}$ and 5.0 mmol/L $[Fe(CN)_6]^{4-}$, in MES buffer pH 5, with different concentrations of Myo. Calibration curves of NI based Au-SPE are also included de B and D.

8.3.4 Binding Isotherm

MI creates binding cavities that are expected to be complementary to the shape and functionality of the protein. The rebinding properties of the MI film after and before electrochemical cleaning with PBS were evaluated by the binding equilibrium experiments. NI films were also included in this study for comparison purposes.

The Langmuir isotherm model was used to fit the experimental data and the results are shown in **Figure 53**. The K_D indicates the necessary Myo concentration to reach one half of the maximal velocity for the reaction. This constant is thus a combination of the amount of Myo bound to the film and its affinity. A low K_D

indicates a large binding affinity, as the reaction will approach the maximum velocity (V_{max}) more rapidly, while a high K_D indicates that the sensor does not bind as efficiently to Myo, and the maximum binding capacity (B_{max}) will only be reached if the Myo concentration is high enough to saturate the binding sites in the film.

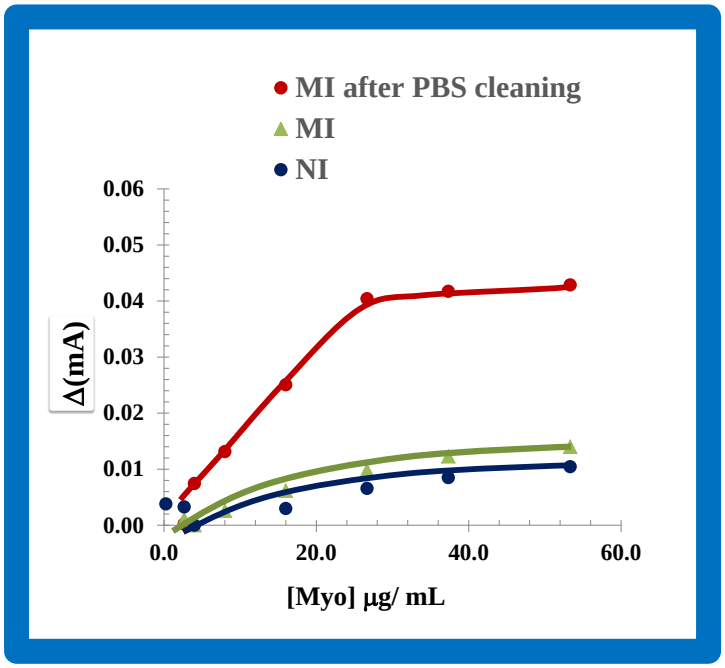

Figure 53: Graphical representation of the Langmuir isotherm plot, I_{max} and K_D values, for MI (before and after electrochemical surface cleaning) and NI materials.

In general, MI showed better features in terms B_{max} and K_D comparing with NI film. But, as may be seen in (Figure 52), the most important information regards the need of electrochemical cleaning after protease activity to ensure the good affinity of Myo to the Au-SPE/—/PAP film. This stage is required to ensure complete removal of unreacted organic compounds such as traces of monomers on its surface. These compounds shall promote a barrier, hindering the protein to reach its binding sites. The B_{max} and K_D values for this were 0.042 mA and 10 µg/ml respectively.

8.3.5 Selectivity study

Selectivity study used SWV measurements of the Au-SPE/—/PAP electrodes for solutions of only Myo or Myo + interfering species. The incubation period of the sensor with these solutions was set to 10 minutes, to ensure that equilibrium as always reached, even when interfering species were present. The interfering species tested were TnT and CK-MB. Their concentrations were set to their typical values in this biological fluid. The % deviation produced by each interfering species in pure Myo solutions were 12 % for TnT and 8 % for CK-MB respectively. The repeatability of the results accounts standard deviations below 5%.

Overall, the interference from the above proteins was considered negligible, meaning that the MI electrodes, Au-SPE/—/PAP, may provide accurate data under the analysis of real samples.

8.3.6 Sample analysis

Because no access to real samples was possible, synthetic serum samples were used to assess the possible application of the device. For this purpose, instead of a normal sample application, the calibration was made in a background of synthetic serum and compared to that made previously in buffer. The results obtained are presented in Figure 54.

In general, spiked serum samples showed good features in terms of lower concentration of the linear concentration range, LOD and slope (0.05 µg/mL, 0.01 µg/mL and -0.0308 µA/decade[Myo, µg/mL]) respectively. Comparing with the Myo calibration curve in MES buffer pH 5.0, the LOD is lower accounting a negligible interference of the serum matrix.

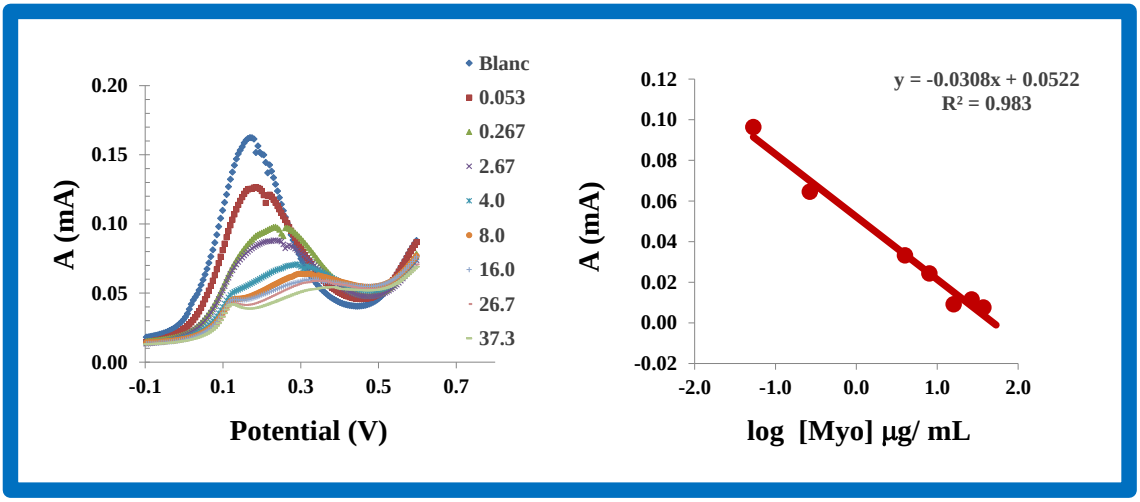

Figure 54: SWV measurements of MI based Au-SPE biosensor and the corresponding spiked serum samples with different concentrations of Myo.

8.4 Conclusions

The effective combination of electrochemistry and MI technology in an analytical device provided a promising tool for direct electrical detection of proteins. The adsorption of protein over the conductive layer promoting the electrosynthesis of the polymeric film seemed to be a successful imprinting approach. This new approach may lead to further improvements within the electropolymerization imprinted materials, by contributing with a new way of forming the imprinted film.

In general, the biosensor presented here showed simplicity in designing, short measuring time, reusability, high accuracy, low limit of detection and good selectivity. This approach seems a successful tool for screening cardiac biomarkers in POC.

8.5 References

Alexander, C., Andersson, H.S., Andersson, L.I., Ansell, R.J., Kirsch, N., Nicholls, I.A., O'Mahony, J., Whitcombe, M.J., 2006. Molecular imprinting science and technology: a survey of the literature for the years up to and including 2003. *Journal of Molecular Recognition* 19(2), 106-180.

Balk, E.M., Ioannidis, J.P.A., Salem, D., Chew, P.W., Lau, J., 2001. Accuracy of biomarkers to diagnose acute cardiac ischemia in the emergency department: A meta-analysis. *Annals of Emergency Medicine* 37(5), 478-494.

Baur, J., Holzinger, M., Gondran, C., Cosnier, S., 2010. Immobilization of biotinylated biomolecules onto electropolymerized poly(pyrrole-nitrilotriacetic acid)-Cu^{2+} film. *Electrochemistry Communications* 12(10), 1287-1290.

Bonini, F., Piletsky, S., Turner, A.P.F., Speghini, A., Bossi, A., 2007. Surface imprinted beads for the recognition of human serum albumin. *Biosensors & Bioelectronics* 22(9-10), 2322-2328.

Bossi, A., Piletsky, S.A., Piletska, E.V., Righetti, P.G., Turner, A.P.F., 2001. Surface-grafted molecularly imprinted polymers for protein recognition. *Analytical Chemistry* 73(21), 5281-5286.

Castaldo, A.M., Ercolini, P., Forino, F., Basevi, A., Vrenna, L., Castaldo, P., Ambrosio, V.D., Castaldo, A., 1994. Plasma myoglobin in the early diagnosis of acute myocardial-infarction. *European Journal of Clinical Chemistry and Clinical Biochemistry* 32(5), 349-353.

Cosnier, S., 2003. Biosensors based on electropolymerized films: new trends. *Analytical and Bioanalytical Chemistry* 377(3), 507-520.

Daniels, J.S., Pourmand, N., 2007. Label-free impedance biosensors: Opportunities and challenges. *Electroanalysis* 19(12), 1239-1257.

Ding, S.J., Chang, B.W., Wu, C.C., Lai, M.F., Chang, H.C., 2005a. Electrochemical evaluation of avidin-biotin interaction on self-assembled gold electrodes. *Electrochimica Acta* 50(18), 3660-3666.

Ding, S.J., Chang, B.W., Wu, C.C., Lai, M.F., Chang, H.C., 2005b. Impedance spectral studies of self-assembly of alkanethiols with different chain lengths using different immobilization strategies on Au electrodes. *Analytica Chimica Acta* 554(1-2), 43-51.

Dyan, H., 2000. Cardiac markers for acute myocardial infarction: When should we test? *Canadian Medical Association Journal* 163(9),1128-1129.

Grand, A., Laperche, T., Fruchaud, J., Fournis, Y., Benessiano, J., Sauser, E., 1994. Value of early serum myoglobin assay for the diagnosis of acute myocardial-infarction. *Archives Des Maladies Du Coeur Et Des Vaisseaux* 87(6), 729-735.

Karimian N, V.M., Zavar MH, Chamsaz M, Turner AP, Tiwari A, 2013. An ultrasensitive molecularly-imprinted human cardiac troponin sensor. *Biosensors and Bioelectronics* 50 C, 492-498.

Lange, U., Roznyatouskaya, N.V., Mirsky, V.M., 2008. Conducting polymers in chemical sensors and arrays. *Analytica Chimica Acta* 614(1), 1-26.

Lee, H.S., Cross, S.J., Garthwaite, P., Dickie, A., Ross, I., Walton, S., Jennings, K., 1994. Comparison of the value of novel rapid measurement of myoglobin, creatine-kinase, and creatine kinase-mb with the electrocardiogram for the diagnosis of acute myocardial-infarction. *British Heart Journal* 71(4), 311-315.

Levin, O., Kondratieva, V., Malev, V., 2005. Charge transfer processes at poly-o-phenylenediamine and poly-o-aminophenol films. *Electrochimica Acta* 50(7-8), 1573-1585.

Li, J., Zhao, J., Wei, X., 2009. A sensitive and selective sensor for dopamine determination based on a molecularly imprinted electropolymer of o-aminophenol. *Sensors and Actuators B-Chemical* 140(2), 663-669.

Li, Y., Yang, H.H., You, Q.H., Zhuang, Z.X., Wang, X.R., 2006. Protein recognition via surface molecularly imprinted polymer nanowires. *Analytical Chemistry* 78(1), 317-320.

Lin, H.-Y., Rick, J., Chou, T.-C., 2007. Optimizing the formulation of a myoglobin molecularly imprinted thin-film polymer-formed using a micro-contact imprinting method. *Biosensors & Bioelectronics* 22(12), 3293-3301.

Mahjani, M.G., Ehsani, A., Jafarian, M., 2010. Electrochemical study on the semiconductor properties and fractal dimension of poly ortho aminophenol modified graphite electrode in contact with different aqueous electrolytes. Synthetic Metals 160(11-12), 1252-1258.

Malitesta, C., Losito, I., Zambonin, P.G., 1999. Molecularly imprinted electrosynthesized polymers: New materials for biomimetic sensors. *Analytical Chemistry* 71(7), 1366-1370.

Moreira, F.T.C., Sharma, S., Dutra, R.A.F., Noronha, J.P.C., Cass, A.E.G., Sales, M.G.F., 2013. Smart plastic antibody material (SPAM) tailored on disposable screen printed electrodes for protein recognition: Application to myoglobin detection. *Biosensors & Bioelectronics* 45, 237-244.

Palys, B., Marzec, M., Rogalski, J., 2010. Poly-o-aminophenol as a laccase mediator and influence of the enzyme on the polymer electrodeposition. *Bioelectrochemistry* 80(1), 43-48.

Sayyah, S.M., El-Rabiey, M.M., Abd El-Rehim, S.S., Azooz, R.E., 2006. Electropolymerization kinetics of o-aminophenol and characterization of the obtained polymer films. *Journal of Applied Polymer Science* 99(6), 3093-3109.

Shah, A.-u.-H.A., Holze, R., 2006. Poly(o-aminophenol) with two redox processes: A spectroelectrochemical study. *Journal of Electroanalytical Chemistry* 597(2), 95-102.

Tucceri R., A.P., Scian A., 2012. Electrosynthesis and Spectroscopic Characterization of Poly(o-Aminophenol) Film Electrodes. *ISRN Polymer Science* 2012, 26 pages.

Turner, N.W., Jeans, C.W., Brain, K.R., Allender, C.J., Hlady, V., Britt, D.W., 2006. From 3D to 2D: A review of the molecular imprinting of proteins. *Biotechnology Progress* 22(6), 1474-1489.

Vogler, E.A., 1998. Structure and reactivity of water at biomaterial surfaces. *Advances in Colloid and Interface Science* 74, 69-117.

Voros, J., 2004. The density and refractive index of adsorbing protein layers. *Biophysical Journal* 87(1), 553-561.

Zayats, M., Kanwar, M., Ostermeier, M., Searson, P.C., 2011. Molecular Imprinting of Maltose Binding Protein: Tuning Protein Recognition at the Molecular Level. *Macromolecules* 44(10), 3966-3972.

9

Electrochemical biosensor for Creatine Kinase detection

9.1 Introduction

Enzymes are biological molecules capable of catalysing chemical reactions. They are used as selective biorecognition elements at the detection of various subtracts, which are converted into different molecules, entitled products. An enzymatic-based biosensor is a challenging and promising assay due to the high specificity and selectivity of enzymes. However, these biocatalysts are limited in the number of reactions they are evolved to catalyse, which limit the range of application. Additionally, enzymatic electrodes are instable in non-physiological conditions and high temperatures, thus contributing for restricted operating conditions. The immobilization of enzymes is also a crucial factor for the efficiency of the biosensor in terms of selectivity, reproducibility, sensitivity, response time and stability. It is vital that the immobilized biomolecule preserves its conformation and biological activity after covalent surface attachment (Sassolas et al. 2012), since changes affect directly the performance of the biosensor.

Different immobilization approaches of enzymes on the transducer surface have been reported so far, including: i) entrapment (Bossi et al. 2002; Sohail and Adeloju 2008); ii) adsorption (Mu and Xue 1996); iii) covalent immobilization and cross linking (Lin et al. 2009; Portaccio et al. 2007); and iv)

affinity and combination of these (Andreescu et al. 2003; Andreescu and Marty 2006). The choice of the most suitable technique is correlated with the enzyme nature, the transducer and the associated transduction method. Reproducibility, cost and difficulty of the immobilization process need to be considered (Sassolas et al. 2012). Sensitivity decreases if immobilization causes enzyme denaturation or conformational changes or if the enzyme has been modified, especially on its active site. Oriented immobilization on transducer surfaces allow better results in terms of sensitivity due the correct exposure of the active sites to the solution phase. Many immobilization techniques involve random distribution or poor orientation of enzyme molecules inducing a partial or a total loss of activity due to enzyme denaturation of the active site or hindered substrate accessibility (Sassolas et al. 2012). SAM covalent immobilization reduces the number of random orientations, generates uniform, reproducible and stable structures with high coverage (Sassolas et al. 2012).

Overall, enzymes are attached to a receptor surface as a selective and sensitive way to measure any substrate/product directly or indirectly involved in the catalytic reaction. The present case, however, is devoted to the determination of the enzyme, not substrate or product, because the enzyme is the one acting as cardiac biomarker. So, despite the major achievements within enzymatic biosensors, the present work must use a completely different approach.

In a complementary approach to that developed in enzyme biosensors, the substrate here immobilized in the biosensor, a very simple and completely new approach never presented before. In order to develop a POC biosensing device, this concept was tested over the gold surface of an Au-SPE modified by self-assembly. Crea was covalently linked over the Au-SPE film, previously treated with Cys. The resulting biosensor was evaluated by several electrochemical techniques and further applied to the analysis of biological samples.

9.2 Experimental section

9.2.1 Apparatus

Electrochemical measurements were conducted in a potentiostat/galvanostat from Metrohm Autolab/PGSTAT302N, impedimetric module and controlled by Nova software. Au-SPEs were purchased from DropSens (DRP-C220AT), having working and CE made of gold and reference electrode and electrical contacts made of silver. The diameter of the WE was 4 mm. For electrochemical assays the SPEs were place in a switch box from DropSens, interfacing the electrical contacts of the Au-SPE with the electrical connections of the potentiostat/galvanostat.

9.2.2. Reagents

All chemicals were of analytical grade and de-ionized water (conductivity <0.1 μS/cm) was employed. ($K_3[Fe(CN)_6]$, Riedel Haen, ($K_3[Fe(CN)_6]$, Riedel Haen), TnT, Fluka, CK-MB, Fluka, Cys, Fluka, BSA, Fluka Myo, Fluka, NHS, Acros, EDAC, Fluka, Creatine phosphate (Pcrea, Applichem) and Creatine monohydrate (Crea, Applichem.).

9.2.3 Solutions

Stock solutions of 50 μg/mL CK-MB were prepared in PBS buffer pH 7.0. Electrochemical assays were performed with 5.0×10^{-3} mol/L $K_3[Fe(CN)_6]^{4-}$ and $K_4[Fe(CN)_6]^{3-}$ in PBS buffer. The selectivity study used 1.67 μg/mL CK-MB solutions prepared in buffer and solutions of possible interfering species, TnT (0.70 ng/mL), Myo (0.80 μg/mL) and BSA (0.30 μg/mL) prepared in the same buffer.

9.2.4 Design of biosensor Au-SPE

The working area of the SPE (gold) was cleaned by washing three times with ethanol. The gold surface of the WE was incubated in 25 mmol/L solutions of Cys for 2 h, at 25 °C, washed with de-ionized water several times and kept in 5 x 10^{-3} mol/L of activated Pcrea prepared in PBS buffer, pH 7.0, for 2.5 h, at room temperature. The carboxylic acid groups were activated by EDAC 50 mmol/L. and 25 mmol/L The electrode was then rinsed thoroughly with distilled water to remove un-reacted species.

9.2.5 Electrochemical assays

CV and SWV measurements were conducted in 5.0 mmol/L of $[Fe(CN)_6]^{3-}$ and 5.0 mmol/L of $[Fe(CN)_6]^{4-}$, prepared in PBS buffer pH 7.4. For CV assays the potential was scanned from -0.7 to +0.7 V, at 50 mV/s. In SWV studies, potentials were changed from 0.0 to +0.8 V, corresponding to a frequency of 50 Hz and step height of 150 mV. EIS assays were conducted with the same redox couple $[Fe(CN)_6]^{3-/4-}$ at a standard potential of 0.12 V, using a with amplitude 0.01 V RMS and a number of frequencies equal to 50, logarithmically distributed over a frequency range of 0.1-100 kHz. The impedance data were fitted to a Randles equivalent circuit using the implemented Nova software. All assays were conducted in triplicate. When indicated, the LOD was calculated by using the equation $3\sigma/S$, where σ is standard deviation and S the slope of the linear range of the calibration curve.

9.2.6 Selectivity study

Selectivity studies were conducted by non-competitive assay. The interfering species tested were selected among those that may be found in biological fluids, such as TnT (0.7 ng/mL), Myo (0.8 µg/mL) and BSA (0.3 µg/mL). All assays were performed in triplicate.

9.2.8 Myo Assay

The performance of the sensor was checked in synthetic serum samples, spiked with CK-MB in a range between 0.07 and 6.67 µg/mL. The serum was 1:10 diluted in PBS buffer and the measurements were performed by SWV measurements. All assays were performed in triplicate.

.3 Results and discussion

9.3.1 Design of the biosensor

The WE of the Au-SPE was modified by following the scheme in Figure 55. It consisted of three different stages, starting with the formation of an amine layer, formed by incubating the gold surface in Cys. Its interaction with a gold substrate lead to the spontaneous formation of a closely packed monolayer via a strong gold-sulfur interaction between the -SH groups and gold.

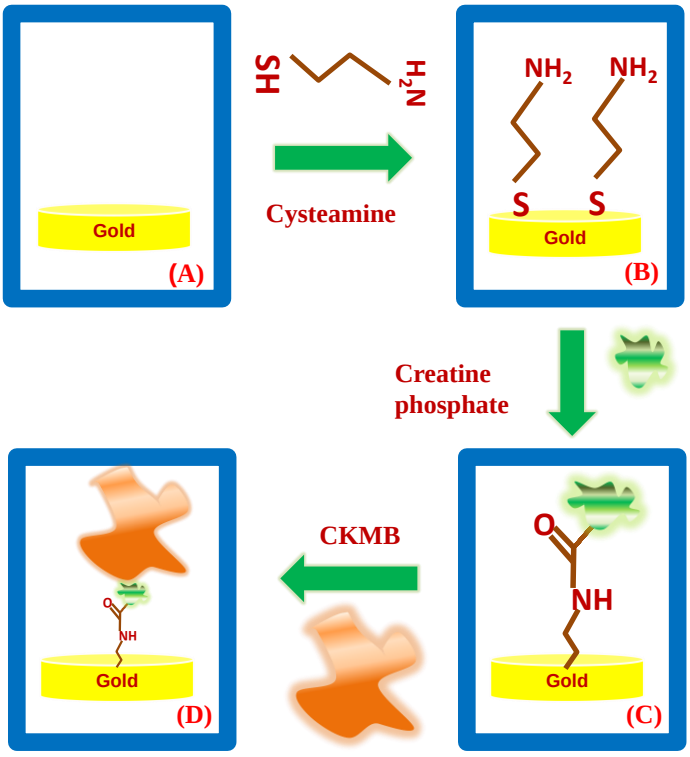

Figure 55: Schematic illustration of the stepwise preparation of the biosensor (A) bare gold SPE, (B) thiol imobilization, (C) creatine phosphate immobilization, and (D) creatine kinase immobilization.

The immobilization of the Pcrea on the modified surface was achieved by coupling its carboxylic acid group to a primary amine group at the modified gold electrode surface (Cys/Au-SPE). This was done via an amide linkage, formed after carboxylic acid activation by EDAC. This reaction forms a highly reactive *O*-acylisourea intermediate (Jiang et al. 2004) that reacts quickly with NHS to form a more stable ester (succinimidyl intermediate). This ester undergoes nucleophilic substitution with any readily available amine group (on Pcrea), resulting in the formation of an amide bond between the modified Au-SPE and Pcrea. Subsequently, the activated Pcrea solution was applied on the NH_2 functionalized Au electrode and left at room temperature, for 2 hours. The Pcrea/Cys/Au-SPE so-obtained was washed with PBS buffer to remove adsorbed Pcrea.

9.3.2 Control of the Surface modification

Electrochemical biosensors provide an attractive resource to analyze the content of a biological sample due to the direct conversion of a biological event to an electronic signal, provided that these are setup properly and reproducibly. Over the past decades several sensing concepts have been developed (Grieshaber et al. 2008), by immobilizing organic films on a suitable support and following the electrical/optical modifications occurring at the solid-state probe.

EIS study is an indirect way of measuring the electrical alterations produced at each stage of chemical modification. EIS assays were used to follow the Au-SPE modification after each chemical change. Randle's equivalent circuit was adopted to model the physiochemical process occurring at the gold electrode surface, as it is frequently used to interpret simple electrochemical systems. The elements of this circuit include R_S, C_{dl}, and R_{ct} which is inversely proportional to the rate of electron transfer, and the W, accounting for the diffusion of ions from bulk electrolyte to the electrode interface.

The EIS spectra of this Randle's equivalent circuit were recorded for every step of the Au-SPE surface modification and the results were presented as Nyquist plots. The semicircle was observed at high frequency range and

indicated a charge-transfer controlled process. The diameter of this semicircle equalled the R_{ct}, controlling the electron transfer kinetics of the redox-probe at the electrode interface (Panagopoulou et al. 2010). The linear range was given at the low frequency range and showed diffusion-controlled process from mass-transfer (Suni 2008).

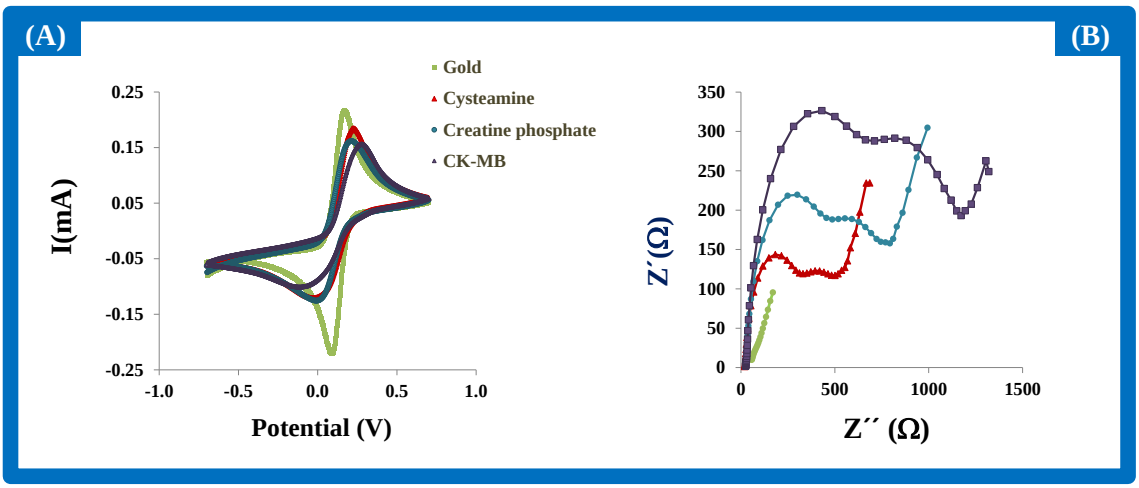

Figure 56: Electrochemical CV voltammograms (A) and EIS (B) of the biosensor immobilization stages evaluated $[Fe(CN)_6]^{3-/4-}$, in PBS buffer pH 7.4.

The bare gold electrode showed a very small semicircle area, suggesting a very fast electron-transfer process with a diffusional limiting step (Figure 56). Attachment of the Cys increased the electron transfer resistance, resulting in increases in the semicircular section of the Nyquist plot. The linkage of Pcrea produced an additional barrier for the redox probe access to the Au-SPE modified electrode. This resulted in an extra increase in the electron transfer resistance.

CV assays are shown in Figure 56 A. When compared to the redox probe in the bare gold, the consequent modification steps of the Au-SPE with Cys and Pcrea increased the peak-to-peak potential separation in the voltammograms, due the increased charge-transfer resistance. The cathodic and anodic peaks decreased with additional chemical modification (Figure 56 B).

9.3.3 Creatine phosphate versus creatine

The main purpose of the present sensing system was to generate electrical changes deriving from a reaction between Crea and CK-MB, provided that Crea is immobilized at the sensing layer. Considering that CK-MB is a phosphotransferase, it would be reasonable to think that phosphate was required at the reaction.

So, instead of adding an external source of phosphate, Pcrea could be immobilized instead of Crea. Furthermore, the current changes obtained after interaction of CK with Crea or Pcrea should be easily monitored. And finally, the peak reduction in the sensing element should be directly proportional to the CK-MB binding to its surface. The electro-activity of the modified Crea/Cys/Au/SPE and Pcrea/Cys/Au/SPE were evaluated in PBS buffer pH 7.4 by SWV assay (Figure 57).

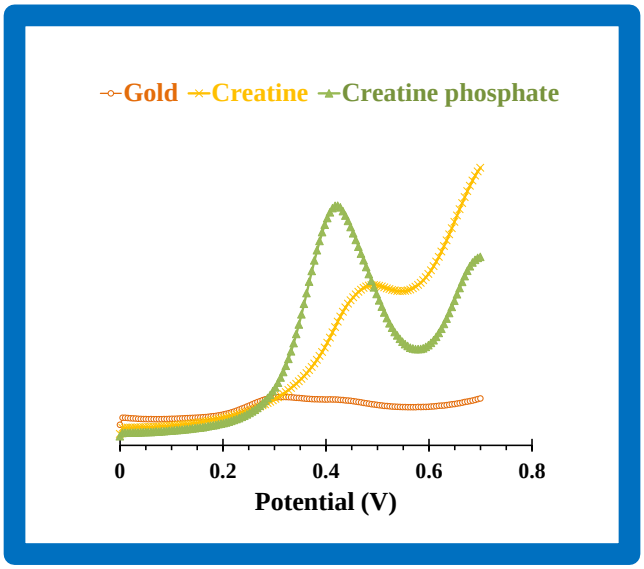

Figure 57: Peak potential obtained by SWV measurements in PBS buffer pH 7.4 for i) bare gold SPE (o) ii) creatine (×) and iii) creatine phosphate (Δ).

The modified Au-SPE with Pcrea showed an electrochemical peak with 0.0135 mA height, at 0.42 V. It was due to the presence of an electroactive phosphate compound, at practical potentials. The current peak obtained for Crea

was 0.00356 mA, at 0.46 V. The decrease in the peak height and potential shift are due to the absence of phosphate and the presence of a less-sensitive electroactive function. No peak was observed with the bare gold measurements.

Overall, the immobilization of Pcrea on Au/SPE was a simple and effective process. In addition, and as long as CK-MB further reacts with this substrate, using Pcrea would avoid the need for a second electroactive species ($[Fe(CN)_6]^{3-/4-}$), responsible for generating the electroanalytical signal. This feature is also advantageous, once the mediators can cause passivation on the electrode surface, reducing its life time (Gomes-Filho et al. 2013).

9.3.4 Analytical performance of the sensor

In this work, the analytical performance of the sensors was evaluated with an electrochemical approach by following typical calibration curve procedures. The concentration range of CK-MB was within 0.19 and 28.8 µg/mL, and the equilibration time for the interaction between CK-MB and Pcrea/Cys/Au-SPE was set to 10 minutes.

SWV was selected among other voltammetric methods due its excellent sensitivity, rejection of background currents and speed. In addition, SWV provides rapid diagnostic information that can help identify the reversibility of an electrochemically active reaction (Babauta et al. 2012). The excitation signal in SWV consists of a symmetrical square-wave pulse of amplitude superimposed on a staircase waveform of step height, where the forward pulse of the square wave coincides with the staircase step. The net current was obtained with the difference between the forward and reverse currents and is centred on the redox potential. The peak height is directly proportional to the concentration of the electroactive species (Settle 1997).

Overall, the presence of CK-MB decreased the typical cathodic peak current of Pcrea/Cys/Au-SPE, observed without CK-MB (Figure 58). Considering that this peak was correlated to the presence of phosphate on the sensory surface, a current decrease after contact with CK-MB could indicate a decrease in the phosphate group concentration and thus enzymatic activity at this surface. In terms of overall analytical performance, it was possible to observe that this effect

of CK-MB was consistent for all concentrations tested, ranging from 0.19 to 28.8 µg/mL. The sensor showed linear behaviour from 0.48 to 28.8 µg/mL, with a slope –0.0035 ± 0.0099 µA/(µg/mL), LOD 0.11 µg/mL and R2 0.978.

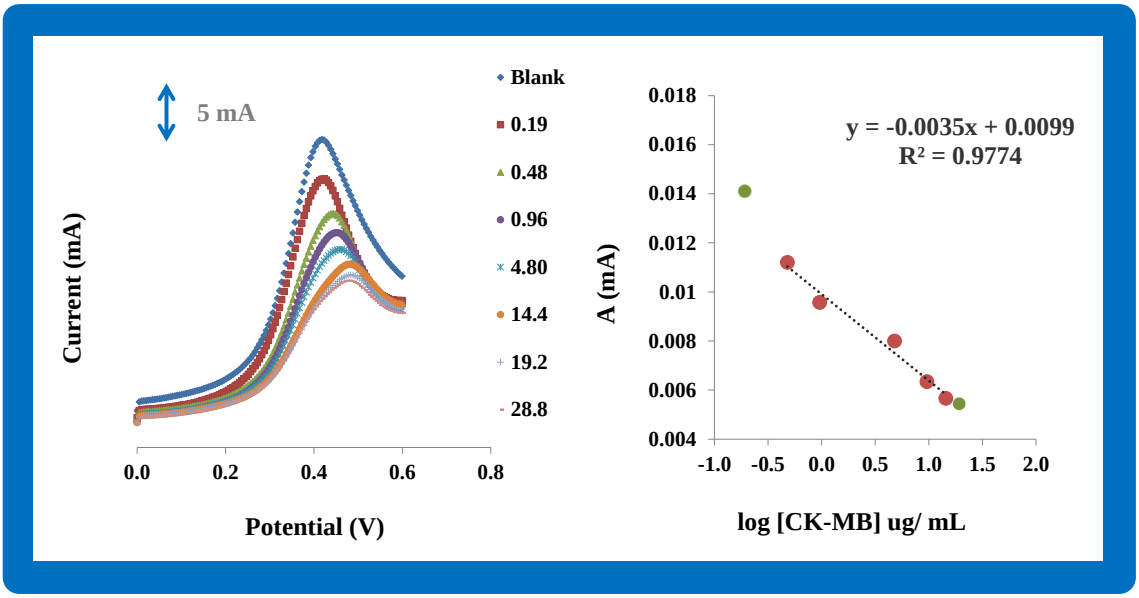

Figure 58: Calibration curve of CK-MB biosensor obtained by SWV measurements in PBS buffer pH 7.0.

Overall, this simple sensor, Pcrea/Cys/Au-SPE, showed high sensitive, in which the use of chemical mediators was not necessary for obtaining suitable electrochemical response.

9.3.5 Selectivity study

The selectivity of the sensor was evaluated in a non-competitive environment. The interfering species tested were selected among those that may be found in biological fluids, such as TnT, BSA, and Myo. The non-competitive assay was used with CK-MB (1.67 µg/mL), TnT (0.7 ng/mL), BSA (0.3 µg/mL) and Myo (0.8 µg/mL). The time given for CK-MB or interfering species to interact

was set to 10 minutes. After this, the peak current changed by+9.8% for BSA assays, -3.8% for TnT and +4.0% for Myo. The measurements were performed in triplicate using different gold SPE, to ensure good reproducibility (see Figure 59).

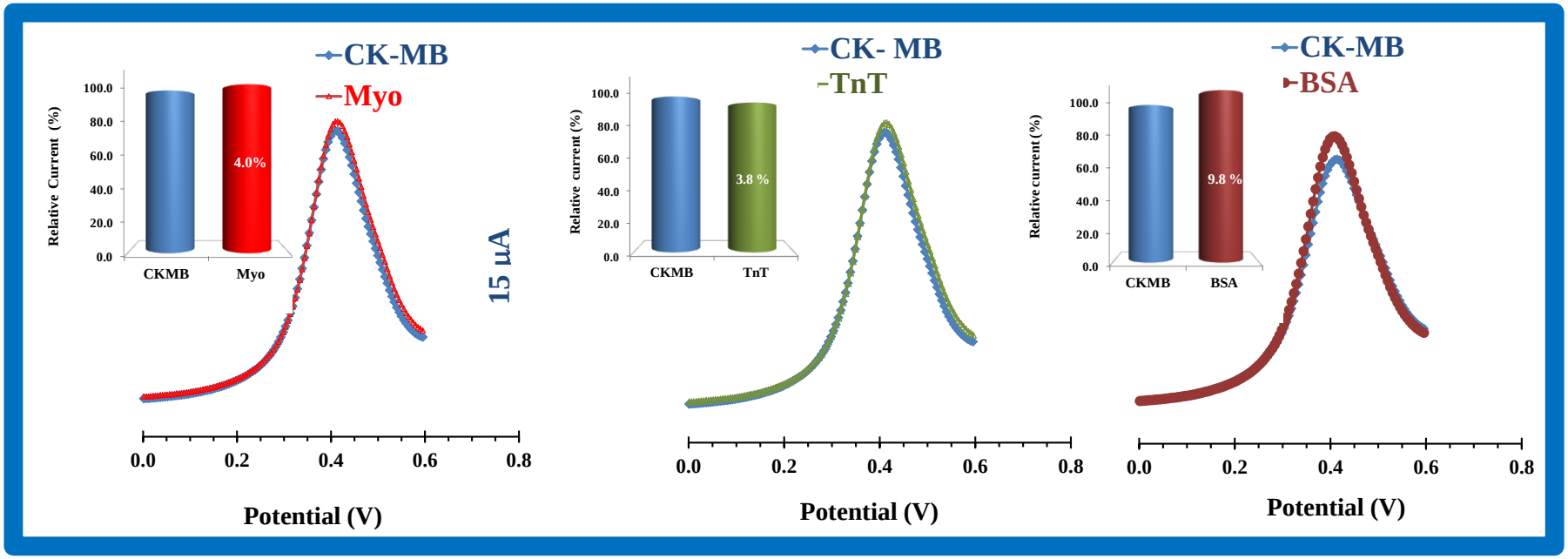

Figure 59: Selectivity data for Myo, TnT and BSA .

9.3.6 CK-MB Assay

The applicability of the sensor was tested by determining CK-MB in synthetic urine. For this purpose, calibration curves were recorded in standard solutions prepared in synthetic urine instead of buffer. The obtained calibration showed good analytical features, producing LLLR, LOD and slope values of 0.05 µg/mL, 0.48 µg/mL and -0.001 µA/decade [CK-MB, µg/mL], respectively. The slope was smaller than the calibration in buffer, but this is in agreement with the effect of high amounts of BSA on the sensor performance.

Synthetic serum samples spiked with different concentrations of CK-MB ranging 0.07 and 6.67 µg/mL were analysed by SWV. Overall, the results obtained suggested that the sensor could offer useful readings under real conditions.

9.4 Conclusions

A simple method fast for screening CK-MB in POC with electrochemical transduction was developed. The CK-MB determination has been achieved in mediator free-conditions due the redox proprieties of the Pcrea. Good performance in terms of selectivity and sensitivity were observed.

The biosensor was successfully applied to biological fluids, showing good stability at room temperature and excellent sensitivity and selectivity. This work opened new horizons at the production of cost-effective biosensors for cardiac biomarker detection in POC due its simplicity, robustness and feasibility and for other biosensors aiming at quantifying ptoteins with catalytic activity.

9.5 References

Andreescu, S., Fournier, D., Marty, J.L., 2003. Development of highly sensitive sensor based on bioengineered acetylcholinesterase immobilized by affinity method. *Analytical Letters* 36(9), 1865-1885.

Andreescu, S., Marty, J.L., 2006. Twenty years research in cholinesterase biosensors: From basic research to practical applications. *Biomolecular Engineering* 23(1), 1-15.

Babauta, J., Renslow, R., Lewandowski, Z., Beyenal, H., 2012. Electrochemically active biofilms: facts and fiction. *A review. Biofouling* 28(8), 789-812.

Bossi, A., Piletsky, S.A., Turner, A.P.F., Righetti, P.G., 2002. Repartition effect of aromatic polyaniline coatings on the separation of bioactive peptides in capillary electrophoresis. *Electrophoresis* 23(2), 203-208.

Gomes-Filho, S.L.R., Dias, A.C.M.S., Silva, M.M.S., Silva, B.V.M., Dutra, R.F., 2013. A carbon nanotube-based electrochemical immunosensor for cardiac troponin T. *Microchemical Journal* 109, 10-15.

Grieshaber, D., MacKenzie, R., Voeroes, J., Reimhult, E., 2008. Electrochemical biosensors. *Sensor principles and architectures*. Sensors 8(3), 1400-1458.

Lin, Z.A., Yang, F., He, X.W., Zhao, X.M., Zhang, Y.K., 2009. Preparation and evaluation of a macroporous molecularly imprinted hybrid silica monolithic column for recognition of proteins by high performance liquid chromatography. *Journal of Chromatography A* 1216(49), 8612-8622.

Mu, S.L., Xue, H.G., 1996. Bioelectrochemical characteristics of glucose oxidase immobilized in a polyaniline film. *Sensors and Actuators B-Chemical* 31(3), 155-160.

Panagopoulou, M.A., Stergiou, D.V., Roussis, I.G., Prodromidis, M.I., 2010. Impedimetric Biosensor for the Assessment of the Clotting Activity of Rennet. *Analytical Chemistry* 82(20), 8629-8636.

Portaccio, M., Durante, D., Viggiano, A., Di Martino, S., De Luca, P., Di Tuoro, D., Bencivenga, U., Rossi, S., Canciglia, P., De Luca, B., Mita, D.G., 2007. Amperometric glucose determination by means of glucose oxidase immobilized on a cellulose acetate film: Dependence on the immobilization procedures. *Electroanalysis* 19(17), 1787-1793.

Sasso, S.V., Pierce, R.J., Walla, R., Yacynych, A.M., 1990. Electropolymerized 1,2-diaminobenzene as a means to prevent interferences and fouling and to stabilize immobilized enzyme in electrochemical biosensors. *Analytical Chemistry* 62(11), 1111-1117.

Sassolas, A., Blum, L.J., Leca-Bouvier, B.D., 2012. Immobilization strategies to develop enzymatic biosensors. *Biotechnology Advances* 30(3), 489-511.

Settle, F.A., 1997. Handbook of Instrumental Techniques for Analytical Chemistry. Prentice Hall PTR.

Sohail, M., Adeloju, S.B., 2008. Electroimmobilization of nitrate reductase and nicotinamide adenine dinucleotide into polypyrrole films for potentiometric detection of nitrate. S*ensors and Actuators B-Chemical* 133(1), 333-339.

Suni, I.I., 2008. Impedance methods for electrochemical sensors using nanomaterials. *Trac-Trends in Analytical Chemistry* 27(7), 604-611.

10

Conclusion and future work

10.1 Conclusion

This thesis emerged new biosensing materials and platforms that may open new horizons on diagnostic, relying on non-invasive or minimally-invasive methods for the early screening of chronic diseases and fast-screening in POC of acute events. New synthetic receptors with affinity for cardiac biomarkers capable of resisting to more extreme conditions, such as high temperature, pressure, extreme pH, and organic solvents, were established successfully.

In surface imprinting the use of highly nanostructured supports seems necessary to achieve well imprinted material, leading to an effective signal generation. Of course this is not an isolated feature, but comparing the use of silica with MWCNTs, and even for different proteins, it seems that highly conductive supports seem the most suitable arrangement.

Regarding the transduction, it seems that EIS and SWV are suitable electrochemical approaches. In some conditions, SWV may lead to lower detection capability, but this is not consistent along all experiments involving this technique, mostly because the presence of any redox species in the sample may disturb the SWV signal but not the one in EIS. Eventually, potentiometry may turn out a suitable strategy due to low cost and portability feasibility which is easily achieved with low cost materials. The main issue of the ISE includes the use of a PVC mem-

brane, because it needs high volatile solvents and at the time of casting the membrane its composition is never controlled. The thickness of this membrane is also not controlled, which way account a reproducibility problem at the time of production.

Regarding the imprinting stage, new strategies for improving the binding affinity of the protein to its binding site were introduced successfully. The most important ones added specific modifications at the conventional imprinting process. A suitable approach includes creating imprinted sites with charged monomers, while the surrounding environment is tailored using neutral material. Furthermore the protein removal from its imprinted site using a protease, favours the preservation the polymeric network of the plastic antibody. This strategy enabling the production of NIM showing an absence of dose response behaviour with a target molecule protein, which is consistent with the non-specific binding to the polymer being minimal. Furthermore, we believe that it is the first time that the imprinted sites are seen in the AFM images, showing cavities of a comparable size to the imprinted protein or only small aggregates.

This work also introduced for the first time an inversed concept of enzyme detection. The enzyme is able to react with its substrate when it is immobilized on a nanostructured support. Of course this specific work combines the advantages of having an enzyme that is a phosphotransferase and its electrochemical response that is greatly linked to the phosphate level. Overall, the biosensing system is very simple, but it requires further studies because its reusability cannot be widely extended.

Overall, electrochemical techniques used along this thesis are easily adjusted for screening purposes, enabling simple and inexpensive procedures providing selective readings with low concentrations and low sample volumes. Furthermore, they may offer portable versions to carry out tests in POC.

Without question, this work introduced several technical innovations in the development of biosensors, both in terms of the assembly of the recognition element and chemical system configuration for screening cardiac biomarkers in POC. Further developments may however be achieved.

10.2 Future work

Enhancement of the selectivity of standard plastic antibodies may be tried out by imprinting biomarkers using chemical conditions and imprinting natural materials compatible with physiological conditions in order to preserve the appropriate protein conformation.

Furthermore, the set-up of biosensing devices offering good analytical response could be used to develop multi-analyte tests. The discrimination of analytical signals could be enhanced by suitable mathematical approaches and the results should be compared with clinical immunoassays whenever applicable.

Additionally, nanostructured control at the assembly of the device by employing analytical instruments that allow nanoscale studies, such as ellipsometry and additional microscope approaches, may also be introduced.

This page was intentionally left blank